

Microparticle-based biosensors for anthropogenic analytes

Von der Fakultät für Lebenswissenschaften

der Universität Leipzig

genehmigte

DISSERTATION

zur Erlangung des akademischen Grades

Doctor rerum naturalium

Dr. rer. nat.

vorgelegt

von

Master of Science Chemie

David Rettke

Geboren am 03.09.1986 in Annaberg-Buchholz

Dekan: Prof. Dr. Marc Schönwiesner

Gutachter: Prof. Dr. Tilo Pompe
Prof. Dr. Andreas Fery

Tag der Verteidigung: 18.03.2022

The work presented in this thesis was accomplished in the period between February 2017 and November 2021 at the Universität Leipzig, Faculty of Life Sciences, Institute of Biochemistry in the Department of Biophysical Chemistry under supervision of Prof. Dr. Tilo Pompe.

BIBLIOGRAPHY

David Rettke

Microparticle-based biosensors for anthropogenic analytes

Faculty of Life Sciences

Universität Leipzig

Dissertation

173 pages, 151 references, 7 figures, 5 publications

Anthropogenic pollution of water resources and the environment by various hazardous compounds and classes of substances raises concerns about public health impacts and environmental damage. Commercially available, portable and easy-to-use devices to detect and quantify these compounds are rather sparse, but would contribute to comprehensive monitoring and reliable risk assessment. The Soft Colloidal Probe (SCP) assay is a promising platform for the development of portable analytical devices and thus has a great potential for a transfer to industry. This assay is based on the differential deformation of an elastic particle, i.e., the SCP, as a function of analyte concentration, which affects the extent of interfacial interactions between the SCP and a biochip surface.

The objective of this work was to adapt this assay for the detection of anthropogenic pollutants. Biomimetic molecular recognition approaches were used based on naturally occurring target proteins that specifically bind the anthropogenic pollutants of interest. This adaptation included the elaboration of strategies for site-specific immobilization of the respective proteins and functionalization of SCPs. In this work, it is demonstrated that the SCP method can be employed for the highly specific and sensitive detection of the critically discussed pesticide glyphosate by using the target enzyme 5-enolpyruvylshikimate-3-phosphate synthase. Furthermore, a specific detection scheme for estrogens and compounds with estrogenic and antiestrogenic activity was developed by harnessing estrogen sulfotransferase as the biomimetic recognition element.

In the second part of the thesis, improvements of the SCP sensing methodology are described. These improvements were achieved by accelerating data analysis and developing a novel synthesis method for SCPs that ensures monodisperse particles with superior reproducibility. Rapid extraction of interaction energies is achieved by using a pattern matching algorithm that reduces the time required for data analysis to a fraction. The microfluidics-assisted synthesis of SCPs enables the production of highly monodisperse SCPs with adjustable size and mechanical properties. Various functionalization approaches have been developed that allow easy and modular introduction of functional groups and biomolecules for SCP-based sensing approaches.

Table of contents

Bibliography	I
---------------------	----------

Table of contents	II
--------------------------	-----------

Chapter I - Introduction

1. General Introduction to Biosensors	1
2. Components and classification of biosensors	3
3. Soft Colloidal Probe-based biosensors	4
4. Quantification of adhesion energy	6
5. SCP synthesis and characteristics	9
6. Biochips for SCP-based sensing approaches	14
7. Biomolecular recognition strategies	16
8. Aims of the study	19

Chapter II - Publications

Outline of publications	20
I. Surface functionalization by hydrophobin-EPSPS fusion protein allows for the fast and simple detection of glyphosate. Döring, J., Rettke, D. , Rödel, G., Pompe, T., Ostermann, K. Biosensors 2019; 9, 104.	21
II. Picomolar glyphosate sensitivity of an optical particle-based sensor utilizing biomimetic interaction principles. Rettke, D. , Döring, J., Martin, S., Venus, T., Estrela-Lopis, I., Schmidt, S., Ostermann, K., Pompe, T. Biosensors & bioelectronics, 2020; 165, 112262.	41
III. Biomimetic estrogen sensor based on soft colloidal probes. Rettke, D. , Seufert, F., Döring, J., Ostermann, K., Wilms, D., Schmidt, S., Pompe, T. Biosensors & bioelectronics 2021; 192, 113506.	50

IV.	Radial profile detection of multiple spherical particles in contact with interacting surfaces. Waschke, J., Pompe, T., Rettker, D. , Schmidt, S., Hlawitschka, M. PloS one, 2019; 14, e0214815.	64
V.	Microfluidics-assisted synthesis and functionalization of monodisperse colloidal hydrogel particles for optomechanical biosensors. Rettker, D. , Danneberg, C., Neuendorf, T.A., Kühn, S., Friedrichs, J., Hauck, N., Thiele, J., Werner, C., Pompe, T. submitted.	81

Chapter III - Conclusions & Outlook

Summary	135
Conclusions	138
Outlook	139

References	141
-------------------	-----

Appendix

Zusammenfassung	147
Curriculum vitae	152
Acknowledgements	155
Selbstständigkeitserklärung	156
Nachweis über die Anteile aller Co-autoren	157

Chapter I

-

Introduction

1. General introduction to biosensors

According to the International Union of Pure and Applied Chemistry, a biosensor is defined as “*a self-contained integrative device, which is capable of providing specific quantitative or semi-quantitative analytical information using a biological recognition element (biochemical receptor), which is retained in direct spatial contact with a transduction element*” (Renneberg et al. 2008). Such sensing approaches aim to deliver easy-to-use, portable and cost-efficient solutions for complex analytical problems by combining the sensitivity and specificity of biological recognition processes with transducers that convert these biological interactions or biochemical reactions into conveniently detectable and quantifiable signals.

The demonstration of amperometric glucose-sensing employing a Clark electrode with a glucose oxidase-decorated semipermeable membrane by Leland Clark Jr. and Champ Lyons in 1962 is considered the birth of biosensors and the translation of this electrode scheme by the Yellow Springs Instrument Company into the *YSI 23A biosensor* led to the first commercially successful biosensor (Clark and Lyons 1962; Juska and Pemble 2020; Wang 2008). The combination of optical transducers and antibody-based detection laid the foundation for affinity biosensors, which are, besides enzyme-based biosensors, regarded as a second eminent branch of biosensors (Turner 2013). Since the introduction of the first biosensor, a remarkable progress driven by integrating technological innovations like ion-sensitive field effect transistors, fiber-optics, surface plasmon resonance and many more, has been achieved and the field is nowadays a steadily emerging and highly interdisciplinary research area, that bridges natural sciences, engineering and medicine as well as environmental sciences (Bhalla et al. 2016).

Besides the well-established and well-accepted glucose and blood monitoring devices, which account for the major share of the biosensors market, the myriad applications, spanning environmental monitoring, disease detection, health monitoring, drug discovery, defense as well as food safety, opened up numerous perspectives for commercialization of several types of biosensors (see **Fig. 1**) ((Bhalla et al. 2016; Mehrotra 2016). This development is particularly fueled by opportunities for miniaturization and simplification of the respective technologies, a fact that results in affordable and easy-to-use home diagnostics as well as on-site analysis devices and rapid tests. Such devices allow for the decentralization of care systems as well as quality management, reduce costs and analysis time, and enable real-time data availability. Therefore, better decisions and results can be achieved, whether for clinical applications, environmental impact assessments or monitoring of specific parts of value chains, such as the food industry. In conjunction with a rising prevalence of chronic diseases, an increasing awareness of environmental concerns and a steadily mounting demand for portable analysis systems, the biosensors market is projected to grow at an annual growth rate of roughly 8 % per year (Grandview Research 2021). However, future breakthrough technological innovations could further accelerate this development.

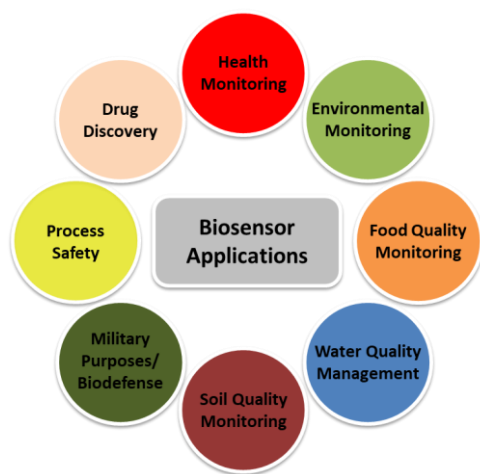


Figure 1: Fields of applications for biosensors (Bhalla et al. 2016; Mehrotra 2016).

Although biosensors are highly valued in routine laboratory applications such as drug discovery, life science research, and medical diagnostics, it is mainly techniques for on-site analytics that are driving the expansion of the biosensor market (Choi et al. 2017; Omidfar et al. 2020; Turner 2013). The latter are typically referred to as point-of-care (POC) tests and are routinely used, e.g., as home pregnancy tests or to determine blood glucose levels. Devices for the diagnosis and monitoring of cancer, cardiovascular and infectious diseases are also marketed (Ahmadi et al. 2020; Omidfar et al. 2020). Besides the advantage of decentralized testing, POC testing methods offer benefits such as easy function, low cost and high selectivity for the respective marker (da Silva et al. 2017). A prime example of the importance of POC testing for the detection of specific biomarkers is the global COVID-19 pandemic, where the appropriate antigen tests helped to prevent uncontrolled spreading of the virus.

POC is often associated with diagnostic applications, but many other systems have been developed to monitor environmental parameters such as water quality and endocrine disruptor exposure, or to ensure food quality by measuring contamination of animal products with antibiotics (Hossain and Mansour 2019; Kivirand et al. 2015). Further applications can be found in soil monitoring, e.g., quantification of heavy metals and pesticides, remediation of military contaminated sites, especially detection of explosives, or on-line monitoring of reactants and products in bioreactors, to name a few (Justino et al. 2017; Liu et al. 2019; Scheper 1992).

The required measuring range of the corresponding system depends strongly on the analytical problem at hand, with the lower limit of the measuring range in which a particular analyte can be quantified being referred to as the limit of quantification (LOQ) and the lower limit in which an analyte can be detected being referred to as the limit of detection (LOD). The necessary LOQ may be femtomolar or even zeptomolar for low abundance environmental contaminants and biomarkers, such as ethinylestradiol in agreement with the predicted no-effect concentration (PNEC), and microRNAs in the bloodstream (Caldwell et al. 2012; Parchekani et al. 2021). Although a superior LOQ is typically a hallmark of routine laboratory-based analytical systems, such as liquid-chromatography coupled tandem mass spectrometry,

reliable quantitation of low abundance analytes at physiologically and environmentally relevant concentrations remains a challenge (European Commission. Joint Research Centre. 2018). Intriguingly, the detection limits of biosensors are usually not limited to the limit inherent to the specific molecular recognition. Amplification mechanisms built into the sensors allow them to overcome this "binding reaction limit", providing interesting options to achieve relevant measurement ranges (Sevenler et al. 2019).

2. Components and classification of biosensors

Biosensing devices typically consist of a biological or biomimetic recognition element, a transducer as well as an electronic system and a display unit (see **Fig. 2**) (Bhalla et al. 2016). The recognition element enables the biosensor to selectively respond to one or more analytes present in a sample, and antibodies, receptors, enzymes, nucleic acids, tissues, whole-cells, molecularly imprinted polymers and many more structures can be used as recognition elements (Acha et al. 2010; Crapnell et al. 2020; Korotkaya 2014). The transducer converts the recognition of the analyte by the recognition element or the biochemical response into a measurable signal. Typical transducers are electrochemical, optical, mechanical, thermal, acoustic, etc. signal converters, and mixed forms have been described in the literature as well (Naresh and Lee 2021). The role of the electronics and the display is the processing, i.e., the conditioning, amplification, and conversion of the signal in order to transform the detected response into an interpretable output. Although there are many ways to categorize biosensors due to the multidisciplinary aspect of this research, biosensors are most commonly classified according to their recognition element (e.g., antibody-, receptor- or enzyme-based) or by their transducer technology (e.g., electrochemical, optical or mechanical biosensors) (Naresh and Lee 2021).

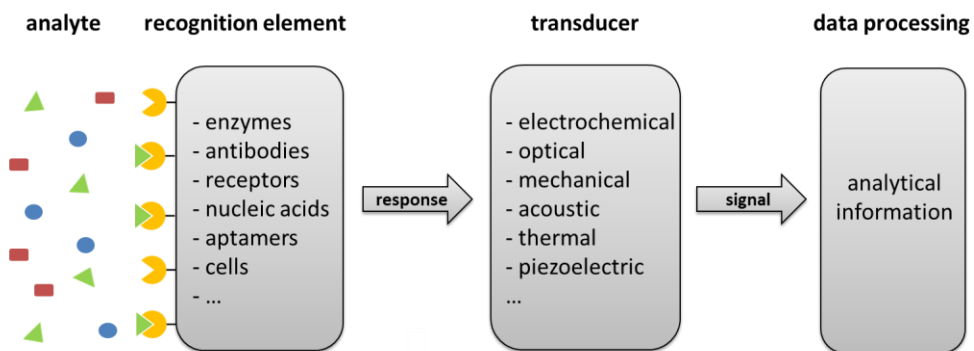


Figure 2: Principle of operation and major components of biosensors. Suitable recognition elements specifically bind the analyte, and the response is subsequently converted into a measurable signal by the transducer. Further processing provides qualitative, semi-quantitative or quantitative analytical information about the analyte.

3. Soft Colloidal Probe-based biosensors

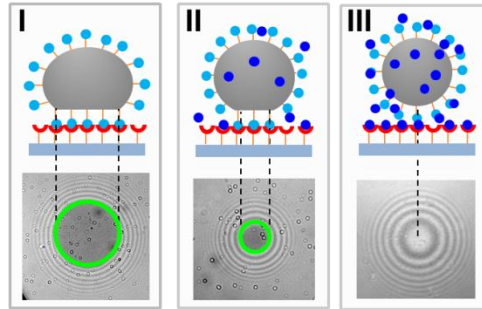
The Colloidal Probe methodology was independently introduced by Ducker et al. and Butt in order to enable the application of atomic force microscopy (AFM) for quantitative measurements of interaction forces between colloidal particles or colloidal particles and planar surfaces (Butt 1991; Ducker et al. 1991; Mark et al. 2019). The limitation of a poorly defined surface geometry of AFM tips was overcome by replacing the sharp tip by a hard, micrometer-sized sphere (colloidal probe), which meets the demand for a well-defined contact geometry. The use of soft elastomeric probes furthermore shifted the range of particle-surface contact radii R from the nanometer (hard particle – hard surface) to the micrometer regime (soft particle – hard surface), allowing precise in situ determination of R by optical interferometry (Erath et al. 2010). Accurate knowledge of the contact area allows the use of established models of contact mechanics to calculate the stored elastic energy from the deformation of the probe. In the absence of an applied load, this stored energy is exclusively related to the surface energy at the interface between probe and surface and can be determined using the Johnson-Kendall-Roberts (JKR) model of adhesive contact, without the necessity to detach the adherent surfaces. The JKR model is discussed in more detail in **section 4.1**.

The adaption of this optomechanical approach for the sensitive quantification of analytes is based on the idea of adhesion as the result of a specific interaction between a Soft Colloidal Probe (SCP) and a surface. The absence of non-specific interactions and the functionalizability of the glass surface and SCP with complementary binding partners, and thus chemical addressability, are prerequisites for the application of this technology. In the course of this adaption, polyethylene glycol was introduced as a precursor material for SCPs to avoid non-specific adsorption phenomena and to circumvent the drawbacks of the commonly used silicone-based chemistry (Fritz and Owen 1995; Görrn and Wagner 2010; Tóth et al. 1994). The strong hydration of the resulting hydrogel and the associated density, which is comparable to that of the surrounding aqueous medium, prevents deformation of the SCP in the absence of adhesion. Functionalization of SCPs is achieved by introducing carboxy groups, which serve as the basis for coupling the molecules of interest, and a lowered elastic modulus in the kPa range ensures sufficient deformation of the SCP for sensitive quantification of analytes (Pussak et al. 2012). The first biosensing approach relying on the SCP-methodology was developed by Pussak et al. for quantifying carbohydrates (Pussak et al. 2013).

General principles of analyte detection and quantification using SCP-based assays are either competitive binding or bridging assays (see **Fig. 3**). In both cases, a recognition element that binds the analyte with sufficient affinity is immobilized on the glass chip. In competitive binding assays, the number of binding sites for SCPs decreases with increasing analyte concentration, whereas the opposite is true for bridging assays. The SCP equipped with molecules complementary to the recognition element (competitive binding) or with recognition elements having affinity for the analyte (bridging), therefore adheres differentially to the functionalized glass surface, depending on the concentration of the analyte. Reflection interference contrast microscopy (RICM) allows the determination of the contact area between the SCP and the glass slide as well as the radius of the respective SCP. With this information,

adhesion energies are calculated using the JKR model of elastic contact and the concentration of the analyte is directly related to the calculated adhesion energy.

A, Competitive binding assay



B, Bridging assay

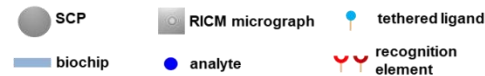
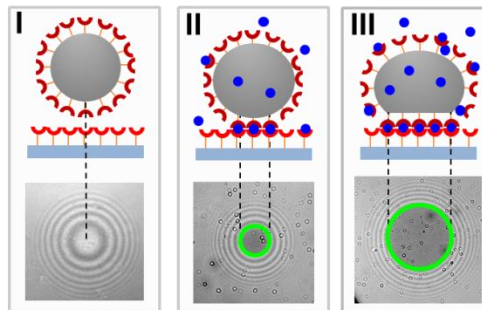


Figure 3: Schematic illustration of SCP-based biosensing assays. **A**, Competitive binding assay: **I**, An SCP equipped with ligands adheres to a transparent biochip bearing immobilized complementary receptors and forms an extended interfacial area as a result of biospecific interactions. **II**, Analytes present in the sample block binding sites for SCP tethered ligands. As a result, the contact area between SCP and biochip is markedly diminished. **III**, At high concentrations of analytes, the presented receptors are completely occupied, and the SCP cannot adhere to the biochip anymore. **B**, Bridging assay: SCP and biochip are decorated with receptors capable of binding to different domains of the analyte. **I**, In the absence of analytes, no biospecific interaction between SCP and biochip is observable, and no contact area is formed. **II** and **III**, Analytes within the sample to be analyzed cause a concentration-dependent increase in SCP-biochip interactions and contact area.

4. Quantification of adhesion energy

4.1 The Johnson-Kendall-Roberts model of elastic contact

Based on the Hertzian theory of elastic contact, Johnson, Kendall and Roberts postulated a theory relating the stored elastic energy, i.e., deformation of the elastic object, to the decrease of surface energy as a result of adhesion (Johnson et al. 1971). The theory describes the force distance relation between two homogeneous elastic spheres with contact pressure being present only within the contact area (Glaubitz et al. 2014). The corresponding adhesion energy can be calculated according to the following modified Hertz-equation:

$$a^3 = \frac{R}{E_{eff}} [F + 3W\pi R + \sqrt{6W\pi RF + [3W\pi R]^2}] \quad (1)$$

where a is the area of contact of the spheres, R the particle radius, $E_{eff} = 4E/3[1 - \nu^2]$ the effective elastic modulus, E the measured elastic modulus, ν the Poisson's ratio, F the applied external force and W the adhesion energy.

The JKR approach can also be applied to contact mechanics models for adhesive contacts between spherical and planar objects, and to interactions between an elastic and an inelastic object. This approach can be regarded as the Hertz-model with an offset due to surface forces. It is important to note that no external force is applied to the SCP in a typical assay. In the absence of applied external forces $F = 0$, equation 1 simplifies to:

$$a^3 = 6\pi \frac{W}{E_{eff}} R^2 \quad (2)$$

The SCP's adhesion and deformation proceeds under volume conservation, hence a Poisson's ratio of 0.5 is assumed and elastic moduli of SCPs are determined using force indentation measurements in the absence of adhesion between the SCP and the cantilever tip as well as the underlying surface (Glaubitz et al. 2014).

4.2 Reflection interference contrast microscopy (RICM)

To calculate the adhesion energy of an adhering particle using the JKR-model, knowledge of the contact area and particle radius is required. RICM with its ability to measure surface distances in aqueous media within milliseconds provides a straightforward basis for determining both variables. This method is known to provide vertical distance resolution in the low nanometer range by using optical interference (Limozin and Sengupta 2009; Stuart and Hlady 1999). Lateral resolutions are typically set by the limits of conventional optical microscopy.

RICM is a microinterferometric method that allows observing the adhesion behavior of colloidal particles, vesicles and cells (Contreras-Naranjo and Ugaz 2013; Kihm 2011; Monzel et al. 2009). RICM uses the interference of monochromatic light that is partly reflected on a planar and transparent surface and the surface of an object lying on or being in proximity to the surface. From the recorded two-dimensional intensity matrix, the distance of the object from the planar surface can be reconstructed (see **Fig. 4**) (Limozin and Sengupta 2009).

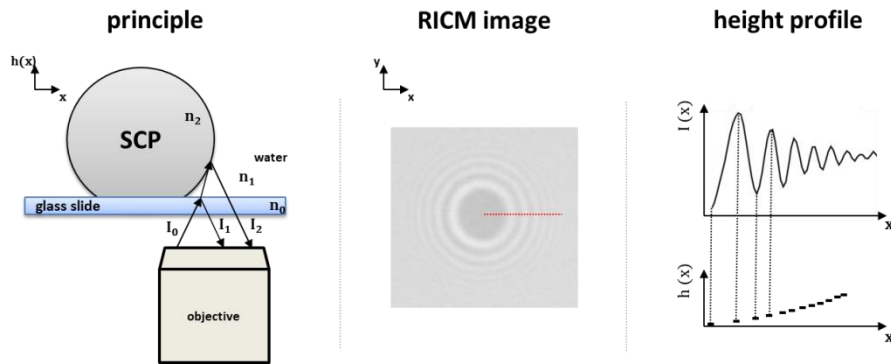


Figure 4: RICM principle, representative image, and height profile reconstruction of SCPs. A beam of monochromatic light is partially reflected at the glass-buffer interface and the SCP surface (left). Superposition of the reflected beams at each position within the xy -plane yields an interferogram with a center circular area of minimum intensity, representing the SCP-glass slide contact area, surrounded by circular Newtonian fringes (middle). The height difference is calculated from the difference of intensity of adjacent minima and maxima of the Newtonian fringes. A series of height positions (red dashed line) gives a portion of the contour of the SCP from which the SCP radius is determined (right).

The general setup of RICM as well as a representative RICM-micrograph and the principle of height reconstruction are depicted in **Figure 4**. Superposition of the reflected beams I_1 and I_2 leads to either constructive or destructive interference at each position within the xy -plane in dependence on the optical path difference. The resulting intensity distribution of the reflected superposed beams contains information about the local vertical distance $h(x, y)$ of the SCP and surface, with the intensity $I(x, y)$ at a certain position in the xy -plane:

$$I(x, y) = I_1 + I_2 + 2\sqrt{I_1 I_2} \cos [2kh(x, y) + \pi] \quad (3)$$

where $k = 2n_1/\lambda$ is the wave vector, with n_1 being the refractive index of water or the aqueous medium and λ the wavelength of the light beam and $h(x, y)$ the height difference between SCP and glass surface as a function of the lateral position (x, y) .

For adherent SCPs, the contact area of SCP and biochip appears as a dark disk in the center of the SCP and can therefore be read out directly from the image. The contact region where $h(x, y) = 0$ is the region with the lowest intensity according to the following equation:

$$I(x, y) = I_1 + I_2 - 2\sqrt{I_1 I_2} \quad (4)$$

For spherical objects such as SCPs, the contact area is surrounded by circular Newtonian fringes from which the curvature of the SCP can be reconstructed. Knowledge of the curvature, in turn, allows extrapolation to the SCP radius if the distortion of the curvature due to adhesion is negligible, which is true for SCP-based sensing approaches.

Reconstruction of the height profile, i.e., curvature, relies on the alternating minima and maxima of the intensity profile, as can be seen from **Figure 4**. The extrema contain information about the optical path difference between adjacent minima and maxima. A linear series of local vertical distances, starting at the center of the contact area, yields the contour line of the SCP from which the radius is calculated.

5. SCP synthesis and characteristics

Polymeric hydrogel microparticles, such as SCPs, are water-swelling colloidal particles with a diameter in the micrometer range, consisting of a crosslinked hydrophilic polymer scaffold (Suzuki et al. 2017). This class of particles attracted particular attention due to their large surface-to-volume ratio compared to bulk materials, softness and deformability, and biocompatibility along with broad tunability of material properties, including size, porosity, elasticity, charge, as well as responsiveness to stimuli. Polymeric hydrogel microparticles found applications in the use as templates, sensors, catalysts, coatings and drug carriers (Plamper and Richtering 2017; Saunders and Vincent 1999; Suzuki et al. 2017). Of particular interest for SCP-based biosensors is the fact that the deformability of the polymer network allows a defined response as a result of adhesion (Saxena et al. 2014). This deformability and defined response can in turn be controlled by manipulating the mechanical properties by varying the polymer content, the degree of polymerization, the molecular weight of the macromonomers, and the crosslink density of the polymer network.

5.1 Polyethylene glycol

Polyethylene glycols (PEGs) are linear or branched, liquid or solid polyethers of ethylene glycol of the general structure $\text{HO}-(\text{CH}_2\text{CH}_2\text{O})_n-\text{CH}_2\text{CH}_2-\text{OH}$. The polymers are uncharged, hydrophilic, soluble in polar as well as many apolar solvents, and neither toxic nor immunogenic or antigenic, and they exhibit protein repellent properties along with excellent biocompatibility (Gombotz et al. 1991; Kingshott and Griesser 1999; Llanos and Sefton 1993). The terminal functional groups also allow the molecules to be linked into insoluble networks, which mimic the physical properties of soft tissues due to their elasticity and high water content.

PEG is characterized by high conformational flexibility and functions as a hydrogen bond acceptor (Huang and Nishinari 2001; Maxfield and Shepherd 1975). The extensive hydration is explained by the geometric compatibility of ethylene glycol monomers and clusters of hydrogen-bridged water molecules, which force the polymer into a predominantly helical superstructure taking the trans-gauche-trans conformation (Blandamer et al. 1969). The diameter of the helix is 4.9 Å, which is within the range of the diameter of the backbone of an expanded water cluster, allowing the helix to be accommodated into the water structure (Begum and Hiroatsu Matsuura 1997; Wahab et al. 2006). Furthermore, the importance of the negative partial charges of the O-atoms as a basis of the high water solubility is highlighted in several research articles (Ensing et al. 2019; Wada et al. 2014; Wahab et al. 2006). Taking the gauche conformation around the C-C bond and trans conformation around the C-O bond leads to an increased dipole moment of the ether oxygen, which favors hydrogen bonding of PEG and water molecules. Hydration is a function of the degree of polymerization, with the number of bound water molecules per monomer increasing from 2 for a tetramer to 3-5 for a 45-mer (Branca et al. 2003).

PEG as a precursor molecule for SCPs has many advantageous properties, such as very low non-specific binding of most biological molecules, thus avoiding bias in the measurement of adhesion energies and preventing rapid ageing of the SCPs (Jeon et al. 1991; Jeon and Andrade 1991). In addition, the polyether structure of PEG is generally associated with extensive chemical inertness of the molecule, with reactive groups found only in the region of the α - as well as ω -termini in the form of hydroxy groups. The functional groups allow targeted chemical modification of the polymers, so that reactive derivatives such as amines, carboxylates, acrylates, maleimides and many more can be provided by esterification using acid chlorides or etherification using alkyl halides (Li and Kao 2003). The chemical inertness of PEG avoids undesired side reactions in the course of performed coupling reactions in later applications. On the downside, the inert nature of PEG and the corresponding hydrogels complicates conjugation (Pussak et al. 2013).

5.2 PEG-based hydrogels

Hydrogels are defined as gels consisting of a three-dimensional, insoluble polymer network (network component) and water, which fills the spaces between the chains (Ahmed 2015). The former component is composed of hydrophilic polymers, the insolubility being due to the crosslinking of the respective chains. The hydrophilicity of the macromolecules allows the binding of large amounts of aqueous fluids, so that the mass fraction of water is typically significantly higher than that of the polymer (Caló and Khutoryanskiy 2015). Hydrogels prepared exclusively from PEG usually have an equilibrium water content of about 80 - 90 %, although it should be noted that the water content depends on the degree of polymerization as well as on the architecture of the macromonomers used as precursors for gel preparation (Myung et al. 2007). Synthetic hydrogels, such as PEG-based gels, offer the perspective of control over structure, crosslinking, and function at the molecular level and, consequently, the design of systems with tailored characteristics in terms of mechanical properties, as well as bioreactivity and biofunctionality (Ahmed 2015).

PEG-based hydrogels can be prepared by chain-growth polymerization using vinyl-modified PEG macromonomers and a radical initiator. In addition, several strategies for preparing PEG-based hydrogels by a step-growth mechanism, leading to more homogeneous gels, were proposed and extensively exploited (Gao et al. 2021b). Chain-growth-polymerized PEG hydrogels are formed by propagation of active centers, i.e., free radicals, through unsaturated carbon-carbon bonds of the PEG macromonomers, whereas step-growth polymerized PEG hydrogels are formed by at least two mutually reactive multifunctional macromonomers with an average macromonomer functionality greater than two (Gao et al. 2021b; Lee et al. 2016; Lin and Anseth 2009). Hydrogels prepared by the latter method are characterized by better homogeneity, since the mechanism based on chain polymerization is more often associated with the occurrence of chain entanglements, intrachain loops and lower crosslinking efficiency due to the random nature of radical propagation and termination (Lee et al. 2016; Tibbitt et al. 2013; Wang et al. 2019; Yu and Chau 2015).

5.3 PEG-based polymeric hydrogel microparticles

Several solution-phase methods have been developed to prepare covalently crosslinked polymeric hydrogel particles, with precipitation, dispersion, suspension, and emulsion polymerization being the most commonly used methods (Zhang 2013). Hydrogel particles made exclusively from PEG with a diameter between 10 and 100 μm , preferably in the range of 20 – 50 μm , with a spherical shape and a smooth surface are needed for SCP-based biosensors, as the limited resolution of the optical instrumentation leads to increasingly imprecise results in the case of smaller particles. Very large particles or SCPs of irregular shape are prone to form non-circular contact areas, which means that simple physical models such as the JKR approach are no longer applicable. From the formerly mentioned synthesis methods, it can be concluded that precipitation polymerization is inapplicable because of the irregular shape of the particles obtained by this method (Arshady 1992; Pardeshi and Singh 2016). Other shortcomings include the inappropriate size of the particles, as is for example the case for emulsion polymerization, typically yielding particles in the nanometer range (Slomkowski et al. 2011). Additional potential problems highlighted in the literature are the necessity to include organic solvents, stabilizers, surfactants and other additives, which might be difficult to remove after synthesis or alter particle properties like surface roughness (Elbert 2011; Yuan et al. 1991). Furthermore, several methods relying on the addition of comonomers are described for the production of PEG-based microparticles. Addition of these compounds however might change the hydration of the gels or add charges, and is therefore assumed to modify the interaction between gel and surface of the SCP-based biosensor (Franssen and Hennink 1998; Leobandung et al. 2002).

Nichols et al. introduced a method based on phase separation of PEG in aqueous solution above its lower critical solution temperature (LCST), followed by coarsening and Ostwald-ripening of the PEG-rich domains (Nichols et al. 2009). A kosmotropic salt was used to lower the LCST and provide a salting-out effect below room temperature, and a Michael addition of PEG-vinylsulfones and PEG-amines was used for crosslinking (Bae et al. 1991; Bailey and Callard 1959). On this basis, a similar approach using photopolymerizable linear PEG-diacrylates was developed. Flake et al. investigated the effects of various parameters, such as the concentration of kosmotropic salts, the molecular weight of PEG, and the preincubation time, on the type of polymerization and thus on particle size, polydispersity, and aggregation, in detail (Flake et al. 2011). In this context, a distinction was made between the type of polymerization, i.e., precipitation polymerization with initiation of the reaction before phase separation, and phase inversion polymerization, i.e., initiation of the reaction after phase separation (Flake et al. 2011). Phase inversion polymerization is considered comparable to suspension polymerization, but differs in that coarsening is not prevented by stabilizers or rapid mixing (Flake et al. 2011). Depending on the ageing of the suspension, particles larger than one micrometer in diameter with a relatively broad size distribution can be produced. Pussak et al. adapted a similar approach based on photocrosslinkable linear PEGs for SCP-based sensors. By adjusting the salt concentration, PEG molecular weight and content, as well as agitating to form a more homogeneous suspension and avoid aggregation, particles with a size distribution of 10 – 100 μm in diameter and an elastic modulus of 20 – 60 kPa were prepared, which are well-suited for SCP-based sensing approaches (Pussak et al. 2012).

A brief summary of the typical synthesis procedure for SCPs is given in **Figure 5**. Unbranched PEG-diacrylamide is dissolved in an aqueous Na_2SO_4 solution. The kosmotrope increases the hydrophobic interactions of the PEG molecules, which drives aggregation and phase separation. The PEG-rich droplets are crosslinked into insoluble spherical gels by irradiating a photoinitiator, which initiates radical crosslinking of the PEG-diacrylamide end groups (Pussak et al. 2012). The spherical, micrometer sized gels can be separated from the supernatant by centrifugation and sedimentation.

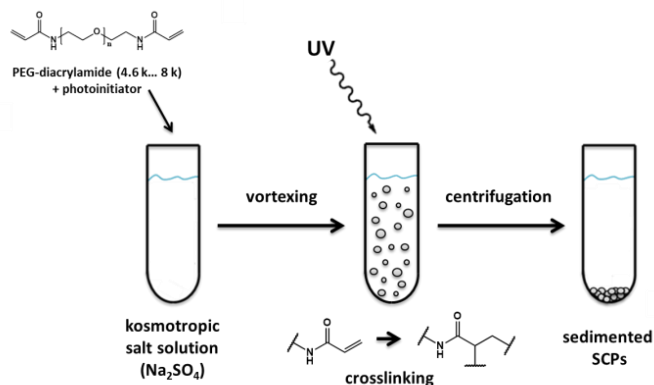


Figure 5: Illustration of SCP synthesis using phase inversion polymerization. A kosmotropic salt and vortexing triggers aggregation of PEG molecules. Decay of a photoinitiator after UV-irradiation generates radicals, initiating radical crosslinking of the acrylamide groups of the PEG molecules and formation of insoluble PEG networks. SCPs are isolated and purified by centrifugation.

As mentioned above, the absence of stabilizing agents in phase inversion polymerization leads to a relatively broad size distribution. As can be seen from equation 2, calculating adhesion energies requires knowledge of the individual SCP radius, and polydisperse particles could therefore limit the overall throughput of the method. Such obstacles can be overcome by microfluidic droplet generators that allow precise control of droplet size and generation of highly monodisperse SCPs (Guo et al. 2012; Moreira et al. 2021; Seiffert and Thiele 2019). Similar to inverse phase polymerization, preformed droplets containing the macromonomers and photoinitiator are dispersed and undergo bulk polymerization after initiation of the reaction. With this method, the diameter of the droplet, which serves as a template for the particle, can be precisely adjusted by manipulating the flow rates and viscosities as well as the surface tension between the dispersed and continuous phase (Seiffert and Thiele 2019). In addition, the droplets are sterically or electrostatically stabilized by surfactants, preventing coarsening and thus leading to a low dispersity of the resulting particles. However, it could be criticized that the scalability of this method is usually limited to parallelization and that organic solvents and relatively expensive instrumentation are required (Heida et al. 2017; Jeong et al. 2016).

5.4 Functionalization of PEG-based SCPs

Generally, functionalization of SCPs is conducted either during synthesis, e.g., in a copolymerization process, or by post-synthesis procedures (Lee et al. 2016; Zhu 2010). For synthesis of SCPs, it should be noted that copolymerization or introduction of recognition sites during synthesis affects size and mechanical properties of the resulting SCPs and might require an individual adjustment of the synthesis conditions (Pussak et al. 2012). In addition, copolymerization might dramatically alter the hydration of the PEG network and therefore enhance unspecific interactions (Nolan et al. 2005).

Modification of SCPs prepared by phase inversion polymerization is complicated due to the inertness of PEG, and the quantitative conversion of acrylate or acrylamide functional groups. Therefore, a photoradical method for the homolytic cleavage of hydrogen from the PEG-backbones was introduced, allowing grafting of unsaturated organic molecules onto the polymer backbone (Pussak et al. 2012). Although this technique allows the introduction of different functional groups depending on the unsaturated compound, emphasis was placed on the use of carboxylic acids. The simplified mechanism is depicted in **Figure 6**. SCPs are suspended in an ethanolic solution of benzophenone and an α,β -unsaturated carboxylic acid. UV-irradiation excites the benzophenone electron to the excited singlet state. Subsequent intersystem crossing yields the triplet state T_1 , capable of abstracting hydrogen from the PEG-backbone, thereby leaving a semipinacol and a PEG radical (Schneider et al. 2011). The radical on the PEG-backbone enables addition to carbon-carbon double bonds and therefore covalent grafting of the α,β -unsaturated carboxylic acid. It is important to note that crotonic acid is preferred over related compounds, such as acrylic or methacrylic acid, as steric hindrance strongly limits homo-polymerization and therefore provides superior control over the number of attached functional groups (Schmidt et al. 2015). The resulting carboxy-functionalized SCPs can be further modified by means of active ester chemistry and solid phase methodologies, i.e., sequential coupling of linkers and molecules bearing recognition sites, or by direct coupling of amino group containing conjugates.

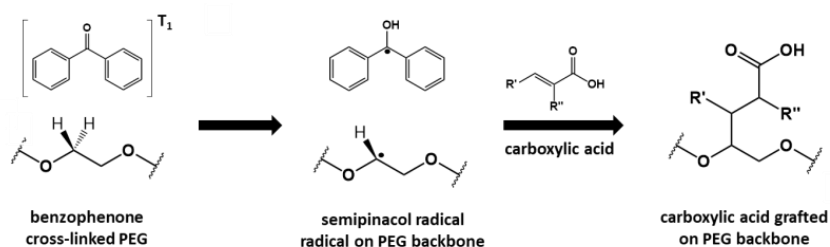


Figure 6: Simplified scheme of photoradical grafting of α,β -unsaturated carboxylic acids on PEG backbones. Benzophenone in the triplet state abstracts hydrogen from the PEG-backbone of PEG networks. The radical on the PEG-backbone attacks the double bond of an α,β -unsaturated carboxylic acid, resulting in a covalent bond between PEG and the carboxylic acid (Schmidt et al. 2015).

6. Biochips for SCP-based sensing approaches

The biochip presents a binding partner complementary to the analyte and, in the case of competitive binding assays, to the functionalized SCPs. As explained in more detail in **section 4.2**, optical transparency is prerequisite for the assay in order to allow for imaging of the adhering SCPs and for calculating the corresponding adhesion energies. Additionally, a smooth and non-porous surface with broad chemical addressability for the introduction of numerous functional groups and moieties is required. In a typical experimental setup, glass supports are used for adsorptive immobilization or covalent coupling of the respective molecules (Martin et al. 2016; Wang et al. 2017).

A simple approach to functionalize glass surfaces is the adsorption of proteins and lipids (Castellana and Cremer 2006; Messing 1975). Using this method, the chip surface is prepared by immersing or incubating the glass slide in a solution containing the respective compounds or structures (Duša et al. 2020; Jesionowski et al. 2014; Mohamad et al. 2015). Although it is a very simple method, the disadvantages are due to the weak interaction between the molecules to be immobilized and the glass surface. The low stability of the adsorbed layer, the strong dependence of the interactions between surface and immobilized molecule from the particular molecule used, the buffer solution, the present ions, as well as the random orientation of, e.g., the immobilized proteins are disadvantageous for SCP-based assays (Wu and Chen 1989). On the other hand, these weak interactions prevent denaturation of immobilized proteins. It has to be noted that the particular strength of interactions depends on the density of silanol groups on the surface and that contaminations with impurities can result in a pronounced hydrophobicity, along with structural distortions of the immobilized molecules and an inhomogeneous distribution.

Covalent coupling of the respective molecules to the surface is usually irreversible and leads to a stable coating of the surfaces. Non-specific coupling of proteins, i.e., immobilization without a favored orientation, is most frequently carried out using ϵ -amino groups of lysine, or the carboxy group of glutamic or aspartic acid in conjunction with active ester chemistry; the thiol-group of cysteine using thiol-Michael additions or oxidation to disulfides; or ϵ -amino groups of lysine using reductive amination (Rusmini et al. 2007). The random orientation of the immobilized proteins usually leads to a high fraction of molecules bearing inaccessible binding sites and coupling of multiple residues of the same protein can lead to denaturation and hence loss of activity as depicted in **Figure 7**.

Site-specific immobilization overcomes these obstacles by assuring optimal accessibility of the binding domains and recognition sites, but is at the same time more elaborate, as immobilization by this means requires the introduction of specific functional groups or functional domains at a defined position of the compound or protein to be immobilized (see **Fig. 7**). In the context of protein immobilization, fusion constructs consisting of the original protein and an additional domain for immobilization have to be expressed. A huge variety of methods to achieve oriented protein immobilization is described in the literature (Gao et al. 2021a; Kalecki et al. 2020; Liu and Yu 2016). Frequently applied methods include covalent coupling by chemoselective peptide ligation like native chemical ligation; the use of affinity tags

like site-specifically attached biotin in conjunction with the specific recognition of biotin by streptavidin; oligo-his-sequences in conjunction with the bidental complexation of nitrilotriacetic acid chelated divalent cations; as well as the introduction of unnatural amino acids carrying functional groups not present in the protein; and the site-specific addition of moieties functioning as a surface anchor (Hennig et al. 2016; Muir et al. 1997; Muir et al. 1998; Serfling and Coin 2016; Young et al. 2012).

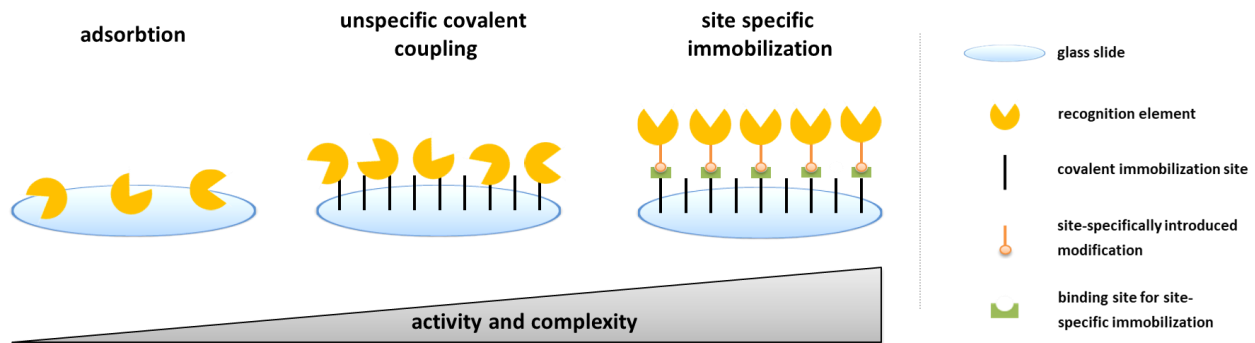


Figure 7: Illustration of immobilization strategies of recognition elements on glass surfaces. Immobilization of recognition elements by adsorption is convenient but yields randomly oriented recognition sites with low surface density. Covalent coupling increases the surface density and stability of recognition sites, but requires additional surface modification procedures. Site-specific immobilization allows detection elements to be immobilized with a uniform orientation and high surface density. As a compromise, the glass substrate usually has to be functionalized in a multi-step process and the recognition element has to be modified at a specific position. The modification ensures selective and oriented binding of the recognition element on the surface.

With the exception of adsorptive immobilization, protein immobilization requires functionalization of the biochip surface in order to introduce reactive functional groups. The most prominent process with particular emphasis on the functionalization of glass surfaces is silanization, although numerous methods of surface modification based on catechols, plasma treatment etc., which might suffer from limitations like a low density of functional groups on the surface or extensive cross-reactivity, have been reported (Fischer et al. 2020; Jonkheijm et al. 2008; Kim et al. 2003). Silanization is a simple and cost-efficient method to functionalize surfaces bearing a high density of hydroxy-groups by formation of Si-O-Si-bonds. Both alkoxy silane-based and chlorosilane-based approaches are widely used and a large number of commercially available silanes allow the covalent introduction of amine, thiol, carboxy as well as epoxy groups and the adjustment of surface wettability (Jonkheijm et al. 2008; Marques et al. 2013). These functional groups can be used for immobilizing recognition elements or for further functionalization steps, like the introduction of moieties that enable site specific attachment of the binding partners. However, it should be noted that these silane coatings are often prone to hydrolysis in aqueous solutions and may require additional stabilization, and ageing may limit the reproducibility of the functionalization due to the moisture sensitivity of the respective precursors (Park et al. 2011; Zhu et al. 2012).

7. Biomolecular recognition strategies

The biomolecular recognition strategies used in biosensing approaches are diverse, and the SCP assay is a platform technology that enables the use of different molecular binding partners. The choice of binding partners, i.e., the analyte and the appropriate recognition element, in turn determines the specific application of the sensor. Besides analyte binding, molecular recognition can be applied for site specific immobilization of the recognition elements, as mentioned in **section 6**. The detection elements greatly impact the sensitivity as well as selectivity and hence the overall performance of the biosensor. The most prominent recognition elements include enzymes, antibodies, receptors, nucleic acids and molecularly imprinted polymers (Chambers et al. 2008; Morales and Halpern 2018). In dependence on the particular recognition element, affinity and specificity is achieved by three-dimensional geometrical matching and by specific interactions between recognition site and analyte, including hydrogen bonding, hydrophobic effects, electrostatics and van der Waals forces.

Enzymes typically have a pocket or cleft-like structure that represents the catalytic center and substrate binding site, with the sequence and arrangement of the amino acids determining specificity and selectivity for the substrate through the formation of temporary bonds (Morales and Halpern 2018). The active site typically accounts for a comparatively small fraction of about 10 to 20 % of the total protein, while the remaining parts of the enzyme stabilize the active site structure, present allosteric modulation, posttranslational modification and multimerization sites, or are involved in binding to other molecules and ions, and the formation of molecular assemblies (Bugg 2008; Oue et al. 1999). In most enzyme-based biosensors, the catalytic conversion of the substrate to a measurable product is used for the quantification of the analyte (Gaudin 2017). Enzymatic activity and substrate binding is sensitive to many physical and chemical parameters like temperature, ionic strength as well as pH and maximum performance of the corresponding sensor requires identification and application of the ideal conditions (Blumenthal and Stull 1982; Bosco et al. 2002).

Receptor-based systems typically use non-catalytic and non-immune proteins that are usually membrane-bound or embedded or, to a lesser extent, found as soluble receptors in the cytosol (Féger et al. 1994). These receptors most commonly bind low molecular weight ligands, which activate or inhibit the corresponding receptor-associated pathway. The binding site of receptors is, similarly to enzymes, formed by a three-dimensional arrangement of amino acids with usually reversible and non-covalent binding of ligands (Alfonso-Prieto et al. 2019; Nadal et al. 2017; Puthenkalam et al. 2016). Binding of agonists to the binding pocket induces a conformational change, whereas binding of antagonists blocks the binding sites. Therefore the direct binding of analytes to the binding site as well as the signal resulting from receptor activation can be used for the detection of analytes (Gaudin 2019). Commonly applied methods for preparing receptor decorated surfaces include the use of tissue preparations, membrane preparations and nano-discs, all of which contain the respective receptors. Common approaches for immobilizing membrane preparations include adsorptive immobilization by the formation of solid-supported or polymer cushioned lipid bilayers or the covalent coupling of certain moieties of the bilayer with the resulting immobilized structure termed tethered lipid bilayer (Castellana

and Cremer 2006; Liszewski 2015). The literature also contains many biosensing approaches that rely on the use of a ligand-binding domain (LBD) rather than entire and complex proteins, which often comprise hydrophobic domains with a strong tendency for aggregation and denaturation (Murata et al. 2001; Suh et al. 2021). These LBDs can be immobilized with random alignment or by immobilization tags as described in **section 6**.

With the exception of glucose biosensors, the vast majority of biosensors employ antibodies as recognition elements, which is why the corresponding sensors are also referred to as immunosensors (Chambers et al. 2008). Antibodies, i.e., immunoglobulins (Ig), are categorized into IgG, IgA, IgM, IgD and IgE, with IgG being the most frequently used subtype for sensing approaches (Hoffmann et al. 2018; Sharma et al. 2016). IgGs are glycoproteins with a molecular weight of roughly 150 kDa and a Y-shaped structure consisting of two identical heavy and light chains (Chiu et al. 2019). Each tip of the antigen-binding fragment (Fab) presents a binding site, referred to as paratope, that specifically binds a structure of the analyte, called epitope, taking advantage of the sensitivity and specificity of antibody antigen interactions (Akbar et al. 2021). Antibodies are particularly useful for the detection of proteins as well as small molecules (Marsden et al. 2014). The fragment crystallizable (Fc) region of IgG is frequently used for site specific immobilization by protein A or protein G. N-glycans bound to the glycosylation sites of the Fc region are also commonly used for immobilization by carbohydrate chemistry (Shen et al. 2017). Antibodies are raised by immunization of suitable animals, and monoclonal antibodies are produced using the hybridoma technology, which is a comparatively costly and time-consuming process with reproducibility issues being frequently encountered (Groff et al. 2015; Milstein 1999). However, several alternative approaches like the generation of recombinant antibodies and affibodies were developed to overcome these and other obstacles of conventional antibodies (Ahmad et al. 2012; Friedman et al. 2007).

Nucleic acid-based biosensors comprise genosensors as well as aptasensors. Genosensors make use of the complementary binding of two or more nucleic acids. Consequently, nucleic acid-based capture probes are usually used to detect nucleic acids (Li et al. 2012). The corresponding capture probes can be easily synthesized by means of the phosphoramidite solid-phase methodology and functional groups for site specific immobilization can be incorporated in the form of non-natural building blocks during synthesis, or by post-synthetic modifications (Glazier et al. 2020; Verma and Eckstein 1998). Instead of conventional DNAs or RNAs, locked nucleic acids (LNAs) and peptide nucleic acids (PNAs) are often used for biosensing applications (Briones and Moreno 2012). These derivatives have a modified backbone that improves binding to the analyte nucleic acids and thus increases the melting temperature, making these probes particularly suitable for detecting short oligonucleotides such as microRNAs (Karkare and Bhatnagar 2006). In addition, PNAs are resistant to degradation by nucleases. This facilitates handling and working with biological fluids.

Aptamers used for aptasensors are single-stranded nucleic acids of usually 20 - 60 nucleotides, and self-annealing of the strand leads to the formation a three-dimensional structure (Lakhin et al. 2013; Zhou et al. 2014). Aptamers are considered to recognize their target primarily by shape, i.e., conformation,

although electrostatic interactions, hydrogen bonding and van der Waals forces contribute to analyte binding (Lakhin et al. 2013; Zhou et al. 2014). Aptamers have been shown to be suitable recognition elements for ions, small molecules, proteins, virus particles and whole cells and are typically synthetically evolved by an in vitro selection termed *systematic evolution of ligands by exponential enrichment* (SELEX) (Zhou et al. 2014). Affinities comparable to those of antibodies have been reported, with a major advantage being that aptamer discovery and production can be conducted entirely in vitro (Groff et al. 2015). Immobilization of aptamers usually follows protocols similar to those for other nucleic acids (Balamurugan et al. 2008).

Molecularly imprinted polymers (MIPs) are artificial recognition elements prepared by copolymerizing functional monomers and crosslinkers around template molecules, with the template subsequently removed (Tse Sum Bui and Haupt 2010). Consequently, the formed cavities provide affinity towards the original molecules and structures with similar moieties based on complementary of shape, size and chemical functionality (Vasapollo et al. 2011). Variation of the analyte to be detected and adjustment of specificity and sensitivity is achieved by varying the functional monomer, crosslinker, template molecule, and solvent (Wackerlig and Schirhagl 2016). MIPs exhibit higher stability under measurement conditions as well as better durability than their natural counterparts and have been successfully used to mimic antibodies, enzymes, receptors and other biological molecules (Gao et al. 2020).

8. Aims of the study

Previous studies reported by Pussak et al., Martin et al. and Schmidt et al. have shown that the SCP assay is a suitable method for the detection and quantification of carbohydrates, protein-material interactions as well as antibodies (Fischer et al. 2020; Martin et al. 2015; Pussak et al. 2013; Strzelczyk et al. 2017). Such versatile and modular platforms, which can be readily adapted to specific analytical problems and show a great potential for use in commercial applications, are highly desirable. The goal of this work was to expand the repertoire of detectable compounds and classes of substances as well as expanding the toolbox for immobilization of recognition elements, and functionalization of SCPs and biochips for modularization of the sensor concept. In particular, the SCP-based sensing principle should be evaluated for its suitability for the detection and quantification of low molecular weight anthropogenic pollutants in the context of environmental monitoring and water quality management. In addition to demonstrating that the SCP technology is highly suitable for such applications, translating this technology into a robust, commercially available product requires rationalizing several aspects of the sensor design. The assay should be simplified and throughput as well as overall performance should be improved. In this context, a rapid method for data analysis as well as a method for producing homogeneous and reproducible SCPs with superior and compelling chemical addressability must be established.

This results in the following objectives for the realization of the project:

- (i) Development and validation of a specific and sensitive biomolecular recognition strategy for a typical contaminant of water resources and its integration into the SCP-based sensing methodology**
- (ii) Transfer of the SCP-based sensing concept to other substance classes relevant to health and environment**
- (iii) Optimization of the SCP-based assay. Improving overall assay performance, shorten analysis time and enhancing modularity**

Chapter II

-

Publications

Outline of publications

This thesis is made up of 5 publications

Aim I: Development and validation of a specific and sensitive biomolecular recognition strategy for a typical contaminant of water resources and its integration into the SCP-based sensing methodology

The first publication, **“Surface functionalization by hydrophobin-EPSPS fusion protein allows for the fast and simple detection of glyphosate”**, describes a novel colorimetric approach for quantifying glyphosate in aqueous media, with the recognition based on the interaction between glyphosate and glyphosate’s target enzyme 5-enolpyruvylshikimate-3-phosphate synthase.

In the second publication, **“Picomolar glyphosate sensitivity of an optical particle-based sensor utilizing biomimetic interaction principles”**, this biomolecular recognition is used for affinity-based sensing of glyphosate employing functionalized SCPs in conjunction with a competitive binding assay.

Aim II: Transfer of the SCP-based sensing concept to other substance classes relevant to health and environment

The third publication, **“Biomimetic estrogen sensor based on soft colloidal probes”**, addresses the adaptation of the SCP method used for glyphosate detection to other small molecules of concern, in particular estrogenic compounds. Therefore, the estrogen-metabolizing enzyme estrogen sulfotransferase 1E1 was site-specifically immobilized and estrogens were coupled to SCPs to apply the same detection principle as used for the SCP-based glyphosate sensor.

Aim III: Optimization of the SCP-based assay. Improving overall assay performance, shorten analysis time and enhancing modularity

The fourth publication, **“Radial profile detection of multiple spherical particles in contact with interacting surfaces”**, describes the software-aided analysis of RICM images using pattern matching algorithms and GPU-driven parallel computing to enable automatic localization of adhesion contacts, detection of SCP and contact radii, and calculation of adhesion energies.

The fifth publication, **“Microfluidics-assisted synthesis and functionalization of monodisperse colloidal hydrogel particles for optomechanical biosensors based on reflection interference contrast microscopy”**, focuses on the use of microfluidic droplet generators for producing SCPs with narrow size distribution and excellent reproducibility, as well as developing various functionalization strategies for superior modularity in future SCP-based sensing approaches.

Publication I

Surface functionalization by hydrophobin-EPSPS fusion protein allows for the fast and simple detection of glyphosate

Julia Döring, **David Rettke**, Gerhard Rödel, Tilo Pompe, Kai Ostermann

Biosensors **2019**, 9, 104

Doi: [10.3390/bios9030104](https://doi.org/10.3390/bios9030104)

ISI Impact Factor 2020: 5.519



Article

Surface Functionalization by Hydrophobin-EPSPS Fusion Protein Allows for the Fast and Simple Detection of Glyphosate

Julia Döring ^{1,*} , David Rettke ², Gerhard Rödel ¹, Tilo Pompe ² and Kai Ostermann ¹¹ Institute of Genetics, Technische Universität Dresden, Zellescher Weg 20b, 01217 Dresden, Germany² Institute of Biochemistry, Leipzig University, Johannisallee 21-23, 04103 Leipzig, Germany

* Correspondence: julia.doering1@tu-dresden.de

Received: 12 July 2019; Accepted: 26 August 2019; Published: 29 August 2019



Abstract: Glyphosate, the most widely used pesticide worldwide, is under debate due to its potentially cancerogenic effects and harmful influence on biodiversity and environment. Therefore, the detection of glyphosate in water, food or environmental probes is of high interest. Currently detection of glyphosate usually requires specialized, costly instruments, is labor intensive and time consuming. Here we present a fast and simple method to detect glyphosate in the nanomolar range based on the surface immobilization of glyphosate's target enzyme 5-enolpyruvylshikimate-3-phosphate synthase (EPSPS) via fusion to the hydrophobin Cg2 and determination of enzyme activity with a malachite green assay, which is a common photometric technique to measure inorganic phosphate (Pi). The assay demonstrates a new approach for a fast and simple detection of pesticides.

Keywords: glyphosate; malachite green assay; hydrophobin; EPSPS; immobilization

1. Introduction

Glyphosate is a potent post-emergent total herbicide. It belongs to the group of organophosphonate-pesticides and is one of the most widely used herbicides worldwide. There is an ongoing discussion about its impact on human health [1–3] and on environment [4–6]. In 2014, an accredited but not peer-reviewed study was published reporting on the detection of glyphosate in breast milk of American mothers [7]. Glyphosate was also found in beer [8] and urine samples [9,10]. However, these findings could not be confirmed by some other studies [11–13]. Furthermore, there are studies showing an effect of glyphosate or its formulations for example on human placental cells and aromatase [14] or on cell adhesion properties [15]. Different results in several studies on glyphosate and its assessment of the International Agency for Research on Cancer (IARC) [16] as a probably carcinogenic compound raised the debate about the hazardous risks and the approval of glyphosate in the European Union. Glyphosate detection is therefore of great importance to reveal detailed information about its distribution. Because of its physicochemical properties, i.e., its small size, its polarity and the high water solubility, the detection of glyphosate is difficult. Furthermore, it is non-volatile and zwitterionic [17,18]. Most available methods for detection of glyphosate are costly in terms of sample preparation, technical equipment and time consumption. Moreover, they require qualified personnel as detection mostly relies on ELISA techniques or chromatography methods coupled with mass spectrometry [10,19–21].

Some approaches have been developed to detect glyphosate using colorimetric techniques. In general, they are based on the reaction of glyphosate with carbon dioxide or another substrate to form a dithiocarbamic acid intermediate which can be detected by different read out systems [22–24].

None of these techniques exploits the specific target of glyphosate, the 5-enolpyruvylshikimate-3-phosphate synthase (EPSPS) [25–27]. This enzyme is part of the shikimate pathway, which is

present in plants and some microorganisms and is responsible for the formation of aromatic amino acids [28]. It uses shikimate-3-phosphate (S3P) and phosphoenolpyruvate (PEP) as substrates to produce 5-enolpyruvylshikimate-3-phosphate (EPSP) and inorganic phosphate (Pi) [29]. Several studies suggest that glyphosate occupies the binding site for PEP keeping the enzyme inactive in an EPSPS-S3P-glyphosate intermediate ternary complex [30–32].

As described above, EPSPS enzymatic activity is accompanied by the formation of Pi. An option to detect and quantify Pi in the nanomolar range is the malachite green assay [33,34]. Therefore it might be suited to measure the enzymatic activity of EPSPS and its inhibition by glyphosate. Compared to other assays for Pi quantification, e.g., the molybdenum blue method, the malachite green assay is easier to handle and exhibits a higher sensitivity [33,35]. The assay is based on the formation of a complex of phosphomolybdate malachite green, which has a greenish blue color and absorbs in the range between 620 to 660 nm [33]. Baykov et al. [36] were able to simplify the procedure by increasing the amount of sulfuric acid in the malachite green solution so that filtration of the dye solution is no longer necessary.

To develop a fast, easy to handle, robust and compact detection assay, it might be advantageous to immobilize the detection unit (here: EPSPS) to create a ready-to-use chip. Furthermore, protein immobilization often can increase protein stability [37] and improve substrate accessibility [38]. On the other hand, protein immobilization can also lead to a decreased enzymatic activity due to poorer substrate accessibility [39,40]. Different strategies for protein immobilization on a surface have been described, e.g., the use of hydrogels, biopolymers or cross-linking [41].

Another method exploits the self-assembling property of hydrophobins. Hydrophobins are small, cysteine rich, amphiphilic proteins derived from fungi [42,43]. They are responsible for the water repellent surface of fungi and well-known for their ability to self-assemble at hydrophobic-hydrophilic interfaces [44,45]. Hydrophobins are divided into two classes based on their hydrophathy patterns [44]. Class I hydrophobins form very stable, rodlet shaped monolayers at interfaces that can only be dissociated with strong acids [46], whereas class II aggregates can be dissolved much easier and do not form rodlet shaped aggregates [47,48]. By exploiting their ability to self-assemble, hydrophobins have already successfully been used to immobilize proteins and peptides on a surface [49,50]. Hydrophobin-mediated surface functionalization allows for the development of a stable and highly ordered surface presenting a target molecule.

For this work, we have chosen the hydrophobin Ccg2 from *Neurospora (N.) crassa* also known as EAS [51]. Ccg2 is a class I hydrophobin that forms a robust amphipathic rodlet layer on interfaces [52,53]. It contains eight cysteine residues, typical for hydrophobins that form four disulfide bridges [51,54]. The 3D-structure of Ccg2, first described by Kwan et al. [54], revealed that the protein consists of a well ordered β -barrel core, while the other protein regions appeared quite unstructured. Surface-exposed amino acids are well-separated in charged and uncharged areas, presenting a clear segregation of hydrophobic and hydrophilic regions.

By utilizing a hydrophobin functionalized surface presenting EPSPS, this work provides a proof of principle for the fast and simple detection of glyphosate in the nanomolar range. It is based on the specific inhibition of enzymatic EPSPS activity by glyphosate, which leads to a decrease in formed Pi, which is measured with the malachite green assay. Furthermore, we present a simple strategy to increase the robustness of the assay by elimination of unspecific Pi in the analyte solution.

2. Materials and Methods

2.1. Chemicals

Chemicals used were purchased from VWR International (Radnor, PA, USA) or Merck KGaA (Darmstadt, Germany). The substrates for the EPSPS enzymatic reaction, shikimate-3-phosphate trisodium salt (S3P) and phosphoenolpyruvate-monopotassium salt (PEP) as well as the pesticides

chlorpyrifos, glufosinate and glyphosate's primary degradation product aminomethyl-phosphonic acid (AMPA) were purchased from Merck KGaA. Glyphosate was obtained from Molekula (Darlington, UK).

2.2. Molecular Cloning of *Ccg2* and *Ccg2_GS_EcEPSPS*

Cloning of constructs was done using standard cloning techniques including PCR, restriction and ligation. The open reading frame (ORF) of *Ccg2* was synthesized without its signal peptide. The ORF of *aroA* coding for *Escherichia (E.) coli* EPSPS (EcEPSPS, gene ID: 945528, UniProt: P0A6D3) was PCR-amplified from *E. coli* DH10 α (New England Biolabs GmbH, Frankfurt am Main, Germany). To create the fusion gene *Ccg2_GS_EcEPSPS* a glycine-serine linker sequence (G₄S)₃ was adhered to the 5'-region of the EcEPSPS using a modified primer. Cloning was done using *E. coli* Top10F' (Merck KGaA) and the desired PCR products were integrated via restriction and ligation into the pET28b vector (Merck KGaA) 3' to the (His)₆-tag sequence, resulting in constructs pET28b-*Ccg2* and pET28b-*Ccg2_GS_EcEPSPS*.

2.3. Protein Expression and Purification

The plasmids pET28b-*Ccg2* and pET28b-*Ccg2_GS_EcEPSPS* were transformed into the expression strain *E. coli* SHuffle[®] T7 express lysY (New England Biolabs). Transformed bacteria were grown in LB_{MOPS} medium (5 g/L yeast extract, 10 g/L peptone, 5 g/L sodium chloride, 10.5 g/L 3-(*N*-morpholino)propanesulfonic acid (MOPS), pH 7.4) with 60 mg/mL kanamycin as selective antibiotic. Protein expression was induced by adding 1 mM isopropyl- β -D-thiogalactoside (IPTG) to the culture medium at an OD₆₀₀ of >0.4. Cultures were grown for 4 h at 30 °C, 180 rpm, harvested by centrifugation (15,000 \times g, 10 min, 4 °C) and washed twice with Tris/HCl (pH 7.5). Cells were disrupted by incubation with lysozyme, DNase, RNase and benzonase for 30 min at 37 °C under shaking followed by ultrasonic treatment.

The fusion protein *Ccg2_GS_EcEPSPS*, found in the soluble fraction, was purified under native conditions via the N-terminal (His)₆-tag by Ni²⁺-affinity chromatography according to the manufacturer's instructions (His-Bind[®] resin, Merck KGaA). The eluted protein fractions were dialyzed twice against 1.5 L dialysis buffer (10 mM MOPS, 0.5 mM ethylenediaminetetraacetic acid (EDTA), 5% (*v/v*) 99% glycerin, 1 mM dithiothreitol (DTT), [55]) for 12 h in a dialysis cassette (Slide-A-Lyzer[®], 10,000 MWCO, Thermo Fisher Scientific, Waltham, MA, USA).

The hydrophobin *Ccg2* was mainly detected in the insoluble fraction and purified as described [50,54]. Briefly, the insoluble pellet was incubated three times on a rotating wheel for 30 min in lysis buffer (8 M urea, 50 mM potassium phosphate, 50 mM sodium phosphate, 10 mM Tris, pH 8.0). Solubilized proteins were purified using the N-terminal (His)₆-tag by Ni²⁺-affinity chromatography (His-Bind[®] resin, Merck KGaA) according to the manufacturer's instructions for denaturing purification. Subsequently, the proteins were concentrated by ultrafiltration using a Vivaspinn20 column (5000 MWCO, Sartorius AG, Göttingen, Germany) and finally dialyzed twice for 24 h against 2 L redox-refolding dialysis buffer (10 mM glutathione reduced, 1 mM glutathione oxidized, pH 5.4, [54]). Protein concentration was determined using the Bradford method [56]. Bovine serum albumin (BSA) was used as the standard protein. Protein purification was examined by running a tricine-SDS-PAGE [57] or glycine-SDS-PAGE [58] for hydrophobins and *Ccg2_GS_EcEPSPS*, respectively. Proteins were blotted after electrophoresis on a polyvinylidene fluoride (PVDF) membrane and detected with 6xHis monoclonal antibody (TaKaRa Bio Inc., Kusatsu, Japan) via immunodetection or stained with colloidal Coomassie brilliant blue.

2.4. Surface Functionalization and Contact Angle Measurement

For surface functionalization of 96-well plates (non-treated polystyrene or glass), protein solution was pipetted on the surface and incubated for 30 min at room temperature. Next, the protein solution was removed, followed by a further incubation step for 5 min. The functionalized surface was washed at least 10 times with dialysis buffer.

For water contact angle measurements, polystyrene or glass surfaces were cleaned with pure ethanol and distilled water. Surfaces were air-dried and protein solution was carefully pipetted on the surface and incubated overnight. On the next day, surfaces were washed thoroughly with distilled water and air-dried. The contact angle of a 2 μ L distilled water drop was determined using the OCA20 device (Dataphysics, Filderstadt, Germany). Measurements were performed for at least 7 drops.

2.5. Measurement of Enzyme Activity in Solution

To determine whether the heterologous expressed enzyme derivative is active, activity measurement using the EnzCheck[®] phosphate assay kit (Thermo Fisher Scientific, Waltham, MA, USA) was performed. The assay was carried out with 0.5 μ g of purified fusion protein (Ccg2_GS_EcEPSPS) according to the manufacturer's instructions. Substrate concentrations of 100 μ M S3P and 80 μ M PEP were used.

2.6. Measurement of Enzyme Activity of the Immobilized Proteins

Surfaces of 96-well plates were functionalized as described above (see Section 2.4). Enzyme activity was determined with the malachite green assay according to Baykov et al. [36]. After washing of the surface, glyphosate (or another analyte) in appropriate concentrations and substrates were added to final concentrations of 100 μ M S3P and 20 μ M PEP and filled up to a final volume of 160 μ L with dialysis buffer. The reaction was stopped after a 45 min incubation at room temperature by adding 40 μ L of malachite green working solution (5 mL malachite green solution (125 mL ddH₂O, 25 mL sulfuric acid (concentrated), 183 mg malachite green), 1.25 mL 7.5% ammonium molybdate solution, 0.1 mL 11% Tween20). Malachite green working solution was incubated for 20 min in the dark (RT) and absorbance was measured using a microplate reader device (Infinite 200, Tecan Group Ltd., Männedorf, Switzerland) at a wavelength of 630 nm. Unless otherwise stated, assays were performed in triplicates and repeated independently 3 times. Error bars show standard deviations. A blank value with all reagents in the absence of a protein-coated surface was subtracted from each sample as background control.

2.7. Statistics

Data were analyzed for significance using a one-sided student's T-Test using Microsoft Excel 2010.

3. Results

3.1. Cloning of Fusion Genes and Protein Purification

To prepare a functionalized surface presenting the *E. coli* enzyme 5-enolpyruvyl-shikimate-3-phosphate synthase (EcEPSPS) to detect glyphosate, we investigated two different variants of fusion proteins between the hydrophobin Ccg2 and the enzyme EcEPSPS, both separated by a flexible glycine-serine-linker (G₄S)₃. This strategy was used to figure out which fusion protein better meets the criteria for our approach. One of the constructs carries the hydrophobin Ccg2 at the N-terminal and the EcEPSPS at the C-terminal end of the linker, while the other construct was designed vice versa (see Figure 1a). Both constructs were cloned into the pET28b vector, providing a N-terminal (His)₆-tag, expressed in *E. coli* SHuffle[®] T7 express lysY and purified by native Ni²⁺-affinity purification. Furthermore, we expressed the hydrophobin Ccg2 lacking a fusion partner. The SHuffle[®] T7 express lysY strain was chosen due to its disulfide isomerase activity, which should support the formation of disulfide-bridges in the cytoplasm to keep the hydrophobins in a soluble form [59,60]. Nevertheless, the hydrophobins were almost exclusively found in the pellet fraction and had to be purified via denaturing purification. By contrast, the fusion proteins were found in the soluble fraction and thus purified via native Ni²⁺-affinity purification.

In Figure 1b the results of the Western blot analysis with 6xHis monoclonal-antibody and Coomassie staining of the electrophoretically separated proteins are shown. Expression and purification of the

different proteins were successful. The fusion protein Ccg2_GS_EcEPSPS is visible as a dominant band at a molecular mass of ca. 58 kDa (Figure 1b). In case of the EcEPSPS_GS_Ccg2 fusion protein, two neighboring bands of around 58 kDa are seen, which may reflect isomeric forms resulting from incomplete reduction of disulfide bridges prior to SDS-PAGE [61]. In case of Ccg2, a strong signal at ca. 11 kDa indicates the successful expression and purification of the hydrophobin. Protein bands with a lower molecular mass might reflect degradation products of the fusion proteins, while signals at higher molecular masses probably are due to protein multimerization [50].

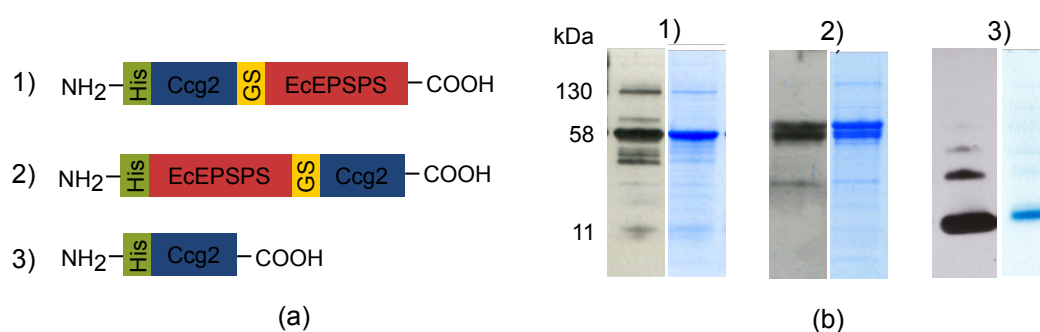


Figure 1. Utilized proteins for this study. (a) Schematic representation of Ccg2 and Ccg2-EPSPS fusion proteins; (b) Western blots (left lanes) and Coomassie stained gel strips (right lanes) after expression and purification of the proteins. For Western blot analysis the samples were electrophoretically separated, subsequently transferred to a PVDF membrane and probed with 6xHis monoclonal-antibody. Molecular masses (kDa) are indicated on the left. The molecular masses of the fusion proteins (1 + 2) and Ccg2 (3) are ca. 58 kDa and 11 kDa, respectively.

The purified proteins were applied for surface functionalization.

3.2. Self-Assembling Properties and Activity Measurement in Solution

After purification the proteins were tested for their functionality, i.e., the ability for self-assembly due to the hydrophobin and for enzymatic activity due to the EcEPSPS. Preliminary tests revealed a higher enzymatic activity of the fusion protein with the N-terminal Ccg2 (Figure 1a, construct 1, see Figure S1). Only this fusion protein was used for further experiments.

Self-assembly properties were tested using water contact angle measurement. The amphiphilic hydrophobins self-assemble at interfaces and change surface properties regarding their wettability with water. In the case of successful hydrophobin-layer formation a hydrophilic glass surface will turn hydrophobic, whereas a hydrophobic polystyrene surface will become hydrophilic. Respective surfaces were functionalized as described (see Section 2.4) and subjected to water contact angle measurements.

Figure 2 shows the results of the contact angle measurements on glass and polystyrene surfaces for the immobilization of fusion protein Ccg2_GS_EcEPSPS and the hydrophobin Ccg2. As a control, a surface treated with dialysis buffer was used.

The glass surface shows a contact angle after dialysis buffer treatment of $31^\circ \pm 2.4^\circ$, which is defined as hydrophilic [62]. Glass surfaces incubated with Ccg2_GS_EcEPSPS or Ccg2 are more hydrophobic with a contact angle of $\sim 61^\circ$ indicating a successful functionalization.

On a polystyrene surface, dialysis buffer shows a contact angle of $96^\circ \pm 2.5^\circ$ which is commonly denoted as hydrophobic [62]. Upon functionalization the polystyrene surface became more hydrophilic: With the fusion protein and hydrophobin, the contact angle decreases to 66° and to 63° , respectively.

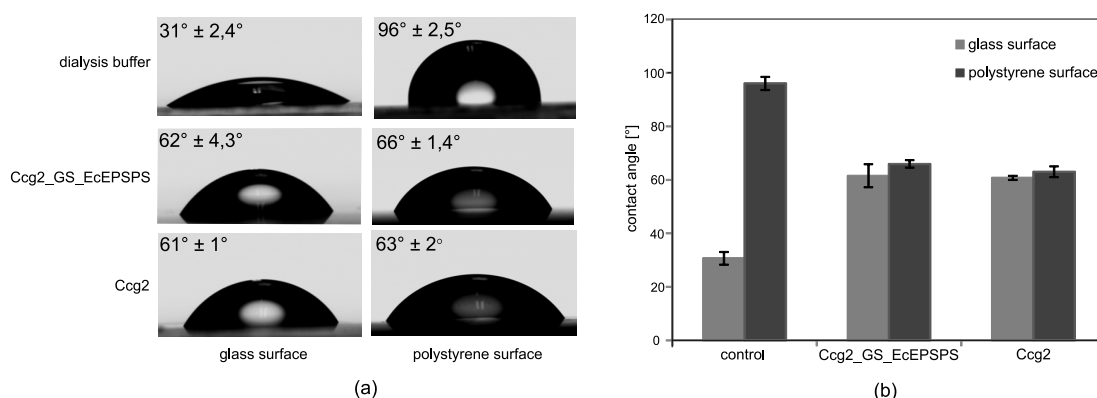


Figure 2. Water contact angle measurements on glass and polystyrene surfaces. The respective surface was treated with protein solution and then washed thoroughly with distilled water. Contact angle of a 2 μ L water droplet was determined using the OCA20 (Dataphysics) contact angle measuring instrument. (a) Representative drop shapes of surfaces functionalized with dialysis buffer (control), fusion protein (Ccg2_GS_EcEPSPS)-and hydrophobin (Ccg2)-solution. Mean values of measured contact angles are depicted in the upper left corner. (b) Bar graph of measured contact angles with standard deviation for 7 different drops (except Ccg2_GS_EcEPSPS (glass) = 6 drops).

The results of the contact angle measurement indicate the self-assembly properties of both, the purified hydrophobin and the fusion protein. This is in line with former reports showing that the self-assembling properties of hydrophobins are not influenced by modification of their N- or C-termini [49,63–65]. However, contact angle measurements only hint at a successful functionalization via hydrophobin self-assembly because proteins can also change the wettability of surfaces with water in an unspecific manner, e.g., through binding mediated by hydrophobic patches. In contrast, self-assembled hydrophobin monolayers are very stable and can only be removed with strong acids [47,66–68]. Nevertheless, our results indicate that both the purified hydrophobin and the hydrophobin-EcEPSPS fusion protein self-assemble at interfaces and can be used to functionalize glass and polystyrene surfaces.

Next, we tested the enzymatic activity of Ccg2_GS_EcEPSPS in solution. Reaction of EPSPS with its substrates S3P and PEP leads to the formation of Pi, which can be measured by photometry at a wavelength of 360 nm using the EnzCheck™ Phosphate Assay kit. The formation of Pi for 14 min was determined with different glyphosate concentrations for 0.05 μ M fusion protein in solution (Figure 3).

After one minute, the absorbance at a wavelength of 360 nm increased due to the enzymatic activity. Already a concentration of 2.5 μ M glyphosate leads to a decrease in enzymatic activity compared to the control without glyphosate. The results suggest that the fusion protein Ccg2_GS_EcEPSPS exhibits an enzymatic activity that is inhibited by glyphosate, which was a prerequisite for the aimed assay.

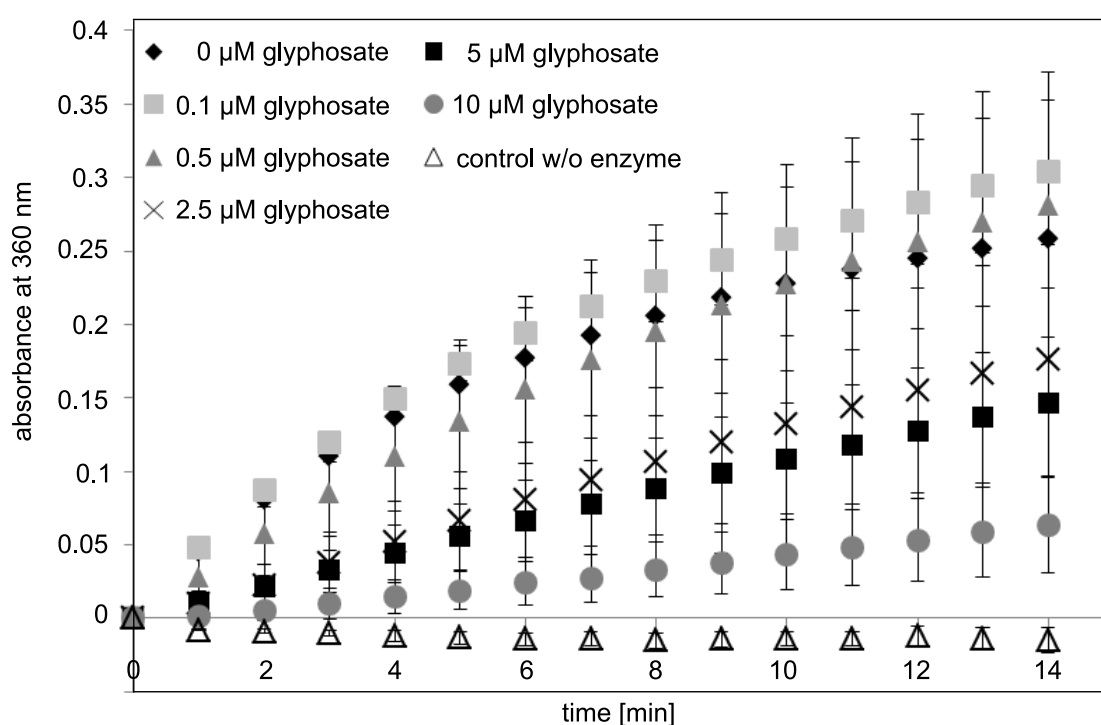


Figure 3. Activity measurement of Ccg2_GS_EcEPSPS (0.05 μM) in solution by detecting the formation of inorganic phosphate (Pi) using the EnzCheck™ Phosphate Assay Kit using photometry at a wavelength of 360 nm. Different glyphosate concentrations were added to the reaction, and the activity was measured over 14 min. Standard deviations derived from mean values of 2 independent measurements.

3.3. Surface Functionalization and Determination of Occupancy Ratio

The malachite green assay, an alternative method for the detection of Pi, is cheaper than the EnzCheck™ Phosphate Assay kit and proved to be more suitable for activity measurement of functionalized surfaces in initial experiments (data not shown). Functionalization of 96-well plates and the malachite green assay were performed as described (see Sections 2.4 and 2.6). As the molecular mass of the enzyme is about 4 times larger than that of the hydrophobin, it is possible that steric hindrance interferes with the fusion protein's ability to self-assemble. Therefore, we tested different molar ratios of fusion protein to hydrophobin to find an appropriate ratio for the surface functionalization. The necessity for an optimization of respective ratios has recently been reported for sensor applications [50].

Figure 4 shows the result of the malachite green assay with polystyrene surfaces functionalized with different ratios of Ccg2_GS_EcEPSPS to Ccg2. Functionalization of polystyrene surfaces with only 1 μM of the fusion protein leads to a low enzymatic activity, and inhibition by 0.5 μM glyphosate cannot be detected. Interestingly, raising the concentration of Ccg2 from 0 μM to 10 μM at constant fusion protein concentration results in an increase in the enzymatic activity. Beginning at a 1:1 ratio of hydrophobin to fusion protein, an inhibition of enzymatic activity by 0.5 μM glyphosate is detectable. Functionalization of the surface with hydrophobin yields no detectable signal at 630 nm, documenting that the measured absorbance is due to EcEPSPS activity on the surface. For the further experiments, we chose a ratio of 1 μM Ccg2_GS_EcEPSPS to 5 μM Ccg2, combining appropriate self-assembly property with the possibility for detection of the inhibition of the enzymatic activity by 0.5 μM glyphosate.

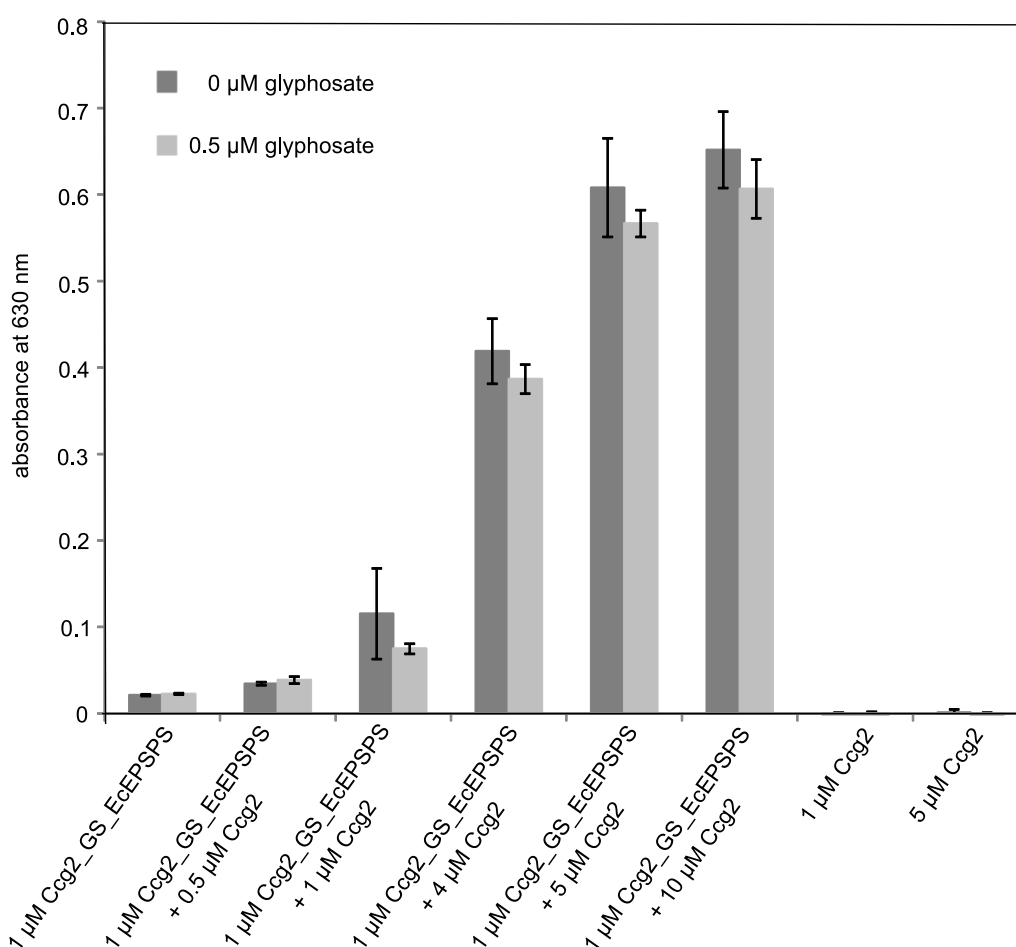


Figure 4. Activity measurements using the malachite green assay with polystyrene surfaces functionalized with Ccg2_GS_EcEPSPS and Ccg2 in different ratios (triplicate measurement). Absorbance at a wavelength of 630 nm was determined using photometry.

3.4. Concentration-Dependent Inhibition of EPSPS Enzymatic Activity by Glyphosate

Next, we tested functionalized surfaces for the detection of different glyphosate concentrations ranging from 0 to 1 μM and aimed at optimization of the assay. For this purpose, we used a 96-well plate with glass bottom and a reaction buffer with pH 10. The rationale is that glyphosate is deprotonated at basic pH values, and inhibition of EPSPS activity is more efficient in this form [69,70].

In order to show that the assay is not restricted to polystyrene, a glass plate was used herein. Regarding future applications, this information is important as different materials can be used to prepare ready-to-use chips. The results on polystyrene surface were similar but with slightly higher standard deviations (see Figure S2). Thus both materials are appropriate to generate robust results with the self-assembled layers.

Figure 5 shows the inhibition of immobilized EcEPSPS with different glyphosate concentrations. Results were normalized to the sample without glyphosate (0 μM). Low glyphosate concentrations of 0.005 and 0.01 μM cannot be detected, as impairment of the enzymatic activity by glyphosate cannot be seen. However, starting from 0.05 μM glyphosate a nearly linear decrease in the absorption at 630 nm compared to the control without glyphosate can be observed. These data document that a concentration-dependent inhibition of the enzymatic activity by glyphosate and in turn detection of the pesticide by the functionalized surfaces and the malachite green assay is feasible.

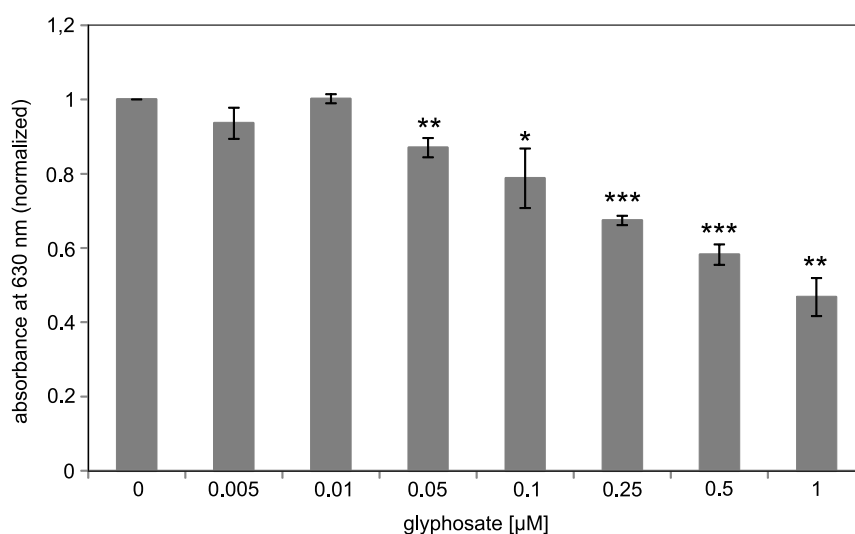


Figure 5. Inhibition of immobilized Ccg2_GS_EcEPSPS by glyphosate. Measurement of EcEPSPS activity using the malachite green assay with a glass surface functionalized with 1 µM Ccg2_GS_EcEPSPS:5 µM Ccg2. Results were normalized to the sample without glyphosate (0 µM). The detection limit is 50 nM glyphosate. *** $p \leq 0.001$; ** $p \leq 0.01$; * $p \leq 0.05$. Absorbance at a wavelength of 630 nm was determined using photometry.

3.5. Cross Reactivity of the Assay

We next investigated the specificity of the assay. Glyphosate is, amongst many others, an organophosphonate pesticide. To determine cross reactivity, another organophosphonate pesticide, glufosinate, an organophosphate, chlorpyrifos, and the first main degradation product of glyphosate, AMPA, were tested.

None of the three tested substances showed any influence on the enzymatic activity of immobilized EcEPSPS in a concentration range between 0 µM and 5 µM (Figure 6a–c). This holds even true for glufosinate, which is structurally quite similar to glyphosate (Figure 6d). Given that, to our knowledge, no other pesticide targets the EPSPS, the assay provides a highly specific detection system for glyphosate. However, the robustness of the assay to parameters like salt and metal ions has still to be determined.

3.6. Pre-Incubation of the Functionalized Surface with Glyphosate Solution

As the assay is based on the detection of Pi it is important that the analyte solution is free of phosphate. When testing the removal of phosphate with different phosphate-binding substances like magnetite or calcium peroxide, we noticed that this treatment also partially removed glyphosate out of solutions (data not shown). To circumvent this problem, we used a different approach.

Enzymatic reactions are equilibrium reactions. It is known that glyphosate inhibits the EPSPS in a slowly reversible manner [32]. Commonly, it is supposed that binding of glyphosate to the open form of EPSPS mainly occurs after binding of S3P [71]. Nevertheless, we pre-incubated the functionalized surfaces with a glyphosate containing solution, removed it carefully after 15 min incubation and measured the enzymatic activity with the malachite green assay. To test whether phosphate residues in the analyte solution will influence the results, we spiked the glyphosate solution with different concentrations of potassium phosphate.

Pre-incubation with 0.5 µM glyphosate led to a significantly reduced absorbance at 630 nm compared to the control without glyphosate (Figure 7). Interestingly, increasing phosphate concentrations in the pre-incubation solution had only a slight effect on the assay. Thus, the complete removal of phosphate from the analyte solution appears not to be essential for the pre-incubation method.

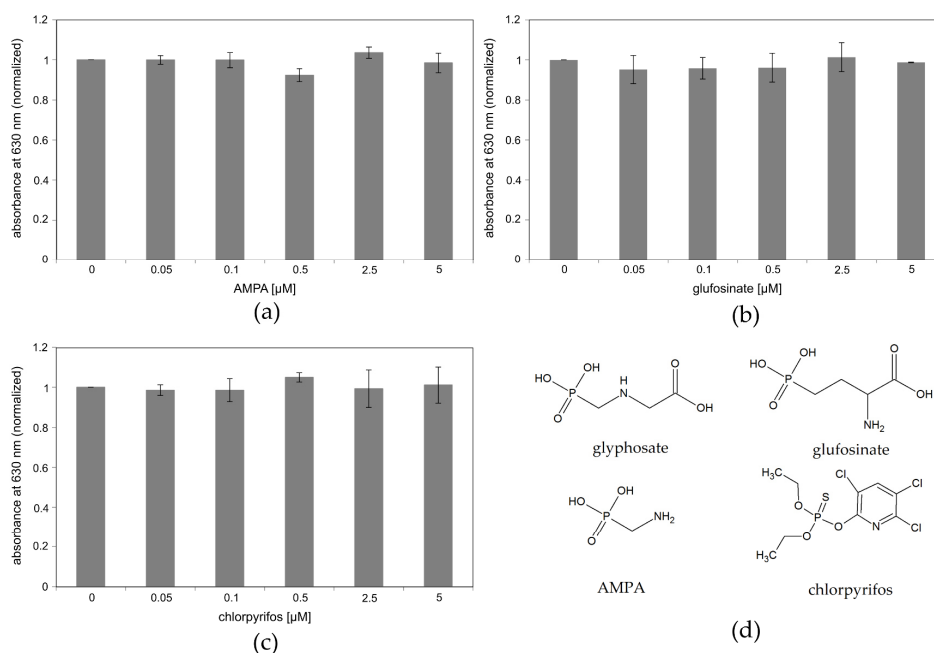


Figure 6. Measurement of cross-reactivity of the functionalized surface (1 μM Ccg2_GS_EcEPS:5 μM Ccg2, polystyrene) with the malachite green assay towards other pesticides. Results were normalized to the sample without glyphosate (0 μM). Absorbance at a wavelength of 630 nm was determined using photometry. (a) Cross-reactivity for AMPA (aminomethylphosphonic acid), the primary degradation product of glyphosate. (b) Cross-reactivity for glufosinate, a member of amino acid-derived organophosphonate pesticides. (c) Cross-reactivity for the insecticide chlorpyrifos, belonging to the group of organophosphate pesticides. (d) Chemical structure of glyphosate and the three tested chemicals.

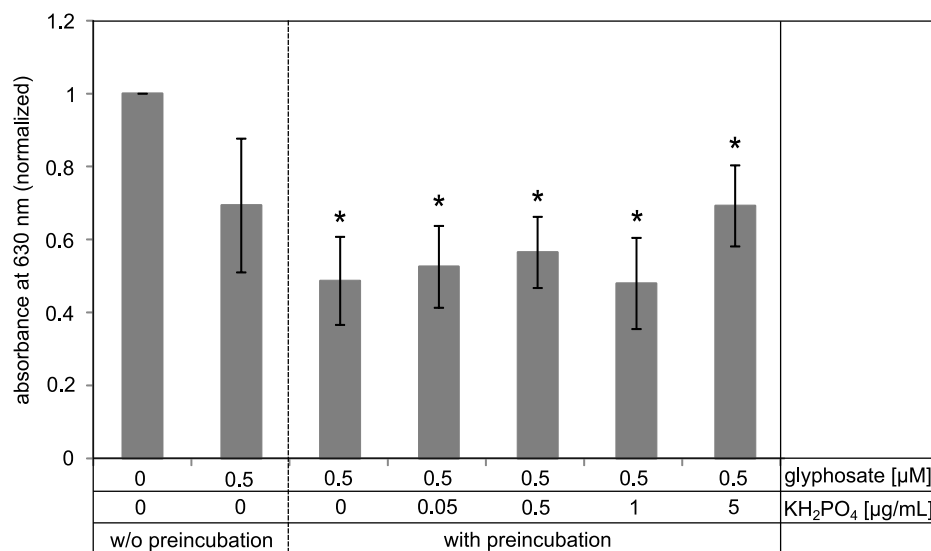


Figure 7. Malachite green assay with preincubation of the surface for 15 min with a solution containing 0.5 μM glyphosate and different phosphate concentrations. After removal of preincubation solution, the assay was performed as described. Samples with 0 and 0.5 μM glyphosate without preincubation were used as positive controls. Results were normalized to the sample without glyphosate (0 μM). Absorbance at a wavelength of 630 nm was determined using photometry. * *p*-value ≤ 0.05 compared to sample 0 μM glyphosate w/o preincubation.

Based on these findings, we developed a workflow for the proposed assay based on the functionalized surfaces and the malachite green assay as a fast and simple detection system for glyphosate (Figure 8).

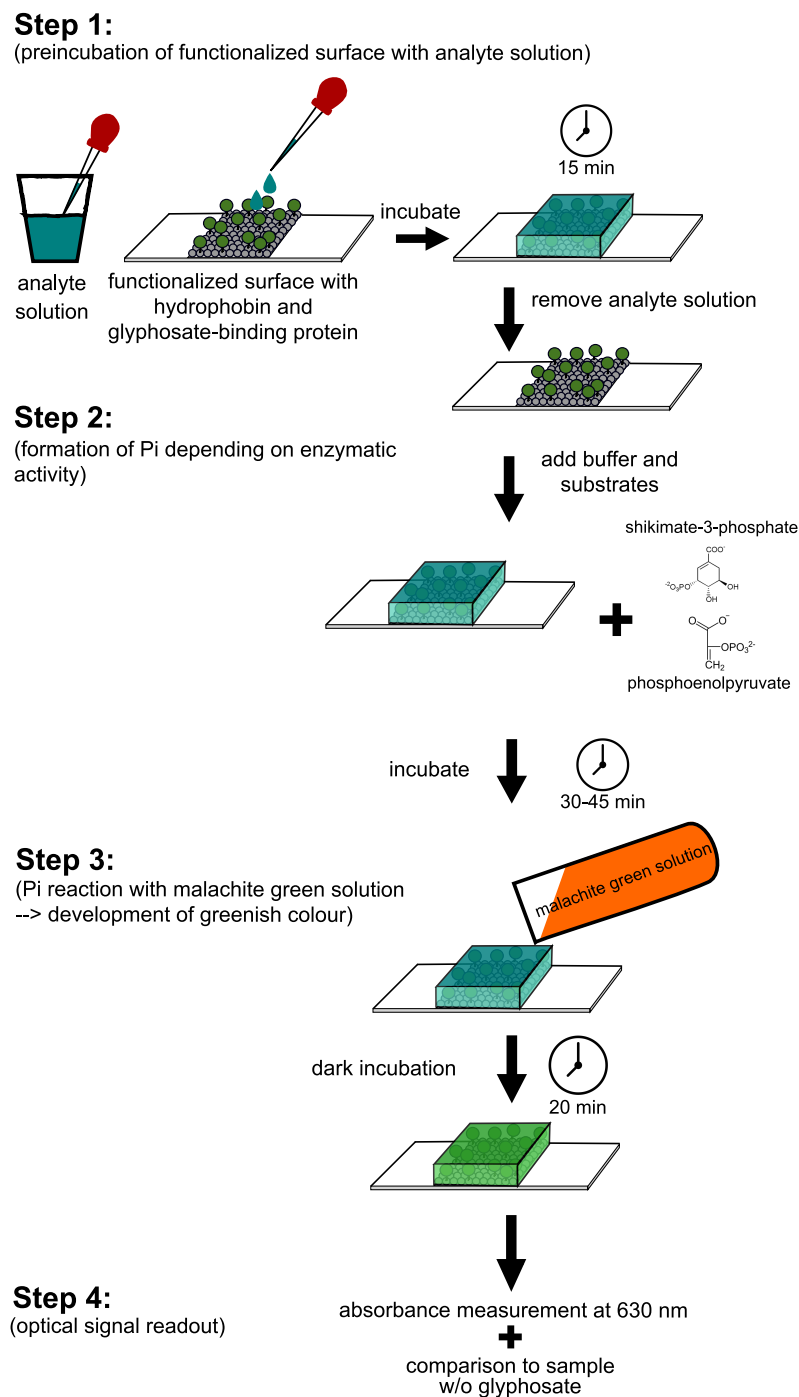


Figure 8. Workflow scheme of the glyphosate detection assay. For details see text.

In that, our assay consists of 4 steps. In the first step the “ready-to-use” functionalized surface is pre-incubated with the analyte solution for 1 min. After careful removal of the analyte solution, the buffer and the two substrates necessary for the enzymatic activity, PEP and S3P, respectively, are added in step 2, followed by incubation for 30 to 45 min at room temperature. In step 3 the reaction is

stopped by adding the malachite green working solution, followed by incubation for 10 to 20 min at room temperature, preferably in the dark. Step 4 comprises the signal read out using a photometer or a spectrophotometer. Absorbance can be measured between 620 and 660 nm [33,36] and has to be compared to a control sample without glyphosate.

The ready-to-use surface allows for a fast and easy assay. It takes about 60 min and requires only a pipette with tips, the reagents and a photometer. By using a hand-held photometer, the assay will also be applicable for in-place measurements in the field.

4. Discussion

The aim of our study was to provide an assay for the detection of glyphosate, which is easy to handle, fast and needs affordable equipment. To this end, we functionalized surfaces with a fusion protein consisting of the Ccg2 hydrophobin and EcEPSPS as the specific pesticide target protein [31]. Impairment of the enzymatic function leads to a decreased production of Pi, which is detected via a malachite green assay.

4.1. Contact Angle Measurements

Using contact angle measurements, we were able to show that the purified recombinant proteins keep their ability for self-assembly. Functionalization of either glass or polystyrene surfaces with the fusion protein or hydrophobin leads to the expected change in the water contact angle compared to the corresponding control. Water contact angles were reduced by about 30° on hydrophobic polystyrene and increased by about 30° on hydrophilic glass. This is in line with previously reported findings [50,72].

4.2. Activity Measurement and Glyphosate Inhibition

The fusion of two proteins can lead to functional loss, e.g., if one partner protein covers the active center of the other protein. To determine whether the recombinant Ccg2_GS_EcEPSPS fusion protein is enzymatically active, we measured its activity in solution by detection of Pi generated by the enzyme. We used the EnzCheck™ Phosphate Assay kit to record the enzyme kinetics. As can be seen in Figure 3, the enzyme shows the typical substrate-saturation curve of an enzymatic reaction, proving that the enzymatic function of EcEPSPS is not markedly affected by the fusion to the hydrophobin. Inhibition by glyphosate can be detected at concentrations exceeding 2.5 µM of the pesticide.

Immobilization of an enzyme in an active manner requires correct orientation of the protein on the surface, so that the active center is accessible for substrate binding. To avoid steric hindrance between enzyme molecules at the surface, we tested different molar ratios of fusion proteins to hydrophobins. Mixing of the fusion protein with hydrophobin for surface functionalization leads to an increased signal to noise ratio and allows detecting the inhibition by glyphosate. Fokina et al. [65] recently tested different molar ratios of a DewA-LaccaseC fusion protein to pure DewA hydrophobin. In contrast to our results the best laccase activity was obtained by coating the surface only with fusion proteins. In line with our results Takatsuji et al. [64] reported that a 1:1 to 1:19 mixture of a glucose oxidase-hydrophobin fusion protein and the respective hydrophobin HFBI exhibits the highest enzymatic activity. We found that a mixture of 1 µM Ccg2_GS_EcEPSPS to 5 µM Ccg2 is a suitable ratio to perform the surface associated malachite green assay, but other ratios might be applicable as well.

Using different glyphosate concentrations we could show that immobilization of the EcEPSPS via fusion with a hydrophobin is advantageous and, under the tested conditions, leads to a 10 times lower detection limit for glyphosate compared to measurement in solution (Figures 3 and 5). Our assay exhibits a detection limit of 50 nM (8.45 ng/mL) glyphosate. ELISA tests for glyphosate gain a detection limit of 0.6 ng/mL [17], which is around 15 times more sensitive than our assay. Nevertheless, glyphosate concentrations reported in beer and wine are in the range of our detection limit [8,73]. Furthermore, it is possible to concentrate the analyte solutions as it was done for ELISA [74].

We used chemically related and unrelated substances to test the specificity of our assay. AMPA, the main degradation product of glyphosate, shares a highly similar molecular structure and has been reported to cross-react with glyphosate detection methods [24,74]. This may falsify data as AMPA is not only a degradation product of glyphosate but also of some detergents and other amino-polyphosphonates [75–77]. As expected because AMPA is no active inhibitor of EPSPS, our assay shows no cross-reactivity in the tested concentration range for AMPA. The same holds true for glufosinate, which is like glyphosate an amino-acid derived phosphonate, and the insecticide chlorpyrifos, which was included in the test as a chemically unrelated substance. These results show that our assay benefits from the use of the natural target enzyme of glyphosate. To our knowledge, no other pesticide is known that inhibits EPSPS except for an artificial S3P-derivative which was used in studies on glyphosate's mode of action [78] and some glyphosate derivatives [79].

4.3. Practicability of the Assay

The proposed assay relies on the detection of phosphate from the enzymatic reaction using the malachite green assay. The use of phosphate binding substances to remove phosphate from the analyte solution prior to the enzymatic activity testing led to a partial removal of glyphosate from the solution. This removal can occur due to the chelating properties of glyphosate [80,81] as metal salts were used as phosphate binding substances. In an alternative approach, we removed the analyte solution from the EPSPS immobilized surface after 15 min thoroughly before performing the malachite green assay. This approach allowed to monitor the glyphosate-dependent enzyme inhibition, even in the presence of phosphate-spiked glyphosate solution. While phosphate concentrations up to 1 µg/mL did not disturb the assay, a slight increase in absorption was observed for higher phosphate concentrations (5 µg/mL).

It has to be noted that pre-incubation of the chip surface with analyte solutions containing glyphosate provided reliable results. This finding is interesting as it is commonly accepted that binding of glyphosate to EPSPS is dependent on the presence of an S3P-enzyme complex [32,71,82]. We argue that glyphosate interaction with EPSPS occurs already strong enough in the open enzyme form, resulting in an enzymatic inhibition even after removal of analyte solution during the timeframe of our developed assay. A previous report supports such a hypothesis as glyphosate binding to EPSPS without S3P was reported with lower affinity [83]. However, using our pre-incubation approach, the robustness of the assay has to be further investigated.

Moreover, detailed experiments also have to be done to test other robustness parameters of the proposed assay including salt and metal ion content, as well as pH of the analyte.

5. Conclusions

In this paper we describe a fast and easy detection assay for glyphosate by taking advantage of surfaces functionalized with a hydrophobin-EcEPSPS fusion protein together with the malachite green assay to determine inorganic phosphate concentrations. The assay shows excellent selectivity comparable or even superior to known ELISA tests. The assay's detection limit is higher than that of commercially available ELISA kits, but it is very easy to handle and to apply. Notwithstanding this aspect and tests of robustness at different solution parameters, the strengths of the described assay are the short assay time, its easy workability and the affordable lab equipment needed.

6. Patents

This work is part of a patent application "Verfahren zur Detektion von Analyten auf Basis immobilisierter Proteine" (application number: DE 10 2018 130 133.2).

Supplementary Materials: The following are available online at <http://www.mdpi.com/2079-6374/9/3/104/s1>, Figure S1: Activity measurement for different proteins after immobilization, Figure S2: Inhibition of immobilized Ccg2_GS_EcEPSPS by glyphosate on polystyrene.

Author Contributions: Conceptualization, J.D. and K.O.; methodology, J.D. and K.O.; validation, K.O., G.R., D.R. and T.P.; formal analysis, J.D.; investigation, J.D.; resources, K.O. and G.R.; writing—original draft preparation,

J.D.; writing—review and editing, K.O., G.R., D.R. and T.P.; visualization, J.D. and K.O.; supervision, K.O.; project administration, K.O.; funding acquisition, K.O.

Funding: This work was funded by grants of the Federal Ministry of Education and Research of Germany to K.O. and T.P. (grant no.: 13N13798, 13N13799) within the collaborative research project ‘Particle-based optical sensors for in-place analytics in quality control of drinking water and food’ (PARTOS) with the industrial partners Umex GmbH (Dresden, Germany), IfU GmbH Privates Institut für Umweltanalysen (Lichtenau, Germany) and Gebr. Heyl Vertriebsgesellschaft für innovative Wasseraufbereitung mbH (Hildesheim, Germany).

Acknowledgments: We thank the Institute of Electronic Packaging Technology and Center for Microtechnical Manufacturing (TU Dresden, Germany) for support with contact angle measurements.

Conflicts of Interest: The authors declare no conflict of interest.

References

1. Benachour, N.; Séralini, G.-E. Glyphosate Formulations Induce Apoptosis and Necrosis in Human Umbilical, Embryonic, and Placental Cells. *Chem. Res. Toxicol.* **2009**, *22*, 97–105. [[CrossRef](#)] [[PubMed](#)]
2. Guyton, K.Z.; Loomis, D.; Grosse, Y.; El Ghissassi, F.; Benbrahim-Tallaa, L.; Guha, N.; Scocciati, C.; Mattock, H.; Straif, K. Carcinogenicity of tetrachlorvinphos, parathion, malathion, diazinon, and glyphosate. *Lancet Oncol.* **2015**, *16*, 490–491. [[CrossRef](#)]
3. Tarazona, J.V.; Court-Marques, D.; Tiramani, M.; Reich, H.; Pfeil, R.; Istace, F.; Crivellente, F. Glyphosate toxicity and carcinogenicity: A review of the scientific basis of the European Union assessment and its differences with IARC. *Arch. Toxicol.* **2017**, *91*, 2723–2743. [[CrossRef](#)] [[PubMed](#)]
4. Giesy, J.P.; Dobson, S.; Solomon, K.R. Ecotoxicological risk assessment for Roundup herbicide. In *Reviews of Environmental Contamination and Toxicology*; Ware, G.W., Ed.; Springer Verlag: New York, NY, USA, 2000; Volume 167, pp. 35–120.
5. Zaller, J.G.; Heigl, F.; Ruess, L.; Grabmaier, A. Glyphosate herbicide affects belowground interactions between earthworms and symbiotic mycorrhizal fungi in a model ecosystem. *Sci. Rep.* **2014**, *4*, 1–8. [[CrossRef](#)] [[PubMed](#)]
6. Annett, R.; Habibi, H.R.; Hontela, A. Impact of glyphosate and glyphosate-based herbicides on the freshwater environment. *J. Appl. Toxicol.* **2014**, *34*, 458–479. [[CrossRef](#)] [[PubMed](#)]
7. Glyphosate Testing Report: Findings in American Mothers’ Breast Milk, Urine and Water. Available online: https://www.momsacrossamerica.com/glyphosate_testing_results (accessed on 20 February 2019).
8. Jansons, M.; Pugajeva, I.; Bartkevics, V. Occurrence of glyphosate in beer from the Latvian market. *Food Addit. Contam. Part A* **2018**, *35*, 1–9. [[CrossRef](#)] [[PubMed](#)]
9. Krüger, M.; Schledorn, P.; Schrödl, W.; Hoppe, H.-W.; Lutz, W.; Shehata, A.A. Detection of Glyphosate residues in animals and humans. *Environ. Anal. Toxicol.* **2014**, *4*, 1–5.
10. Jensen, P.K.; Wujcik, C.E.; McGuire, M.K.; McGuire, M.A. Validation of reliable and selective methods for direct determination of glyphosate and aminomethylphosphonic acid in milk and urine using LC-MS/MS. *J. Environ. Sci. Health Part B* **2016**, *51*, 254–259. [[CrossRef](#)]
11. Ehling, S.; Reddy, T.M. Analysis of Glyphosate and Aminomethylphosphonic Acid in Nutritional Ingredients and Milk by Derivatization with Fluorenylmethyloxycarbonyl Chloride and Liquid Chromatography–Mass Spectrometry. *J. Agric. Food Chem.* **2015**, *63*, 10562–10568. [[CrossRef](#)]
12. Steinborn, A.; Alder, L.; Michalski, B.; Zomer, P.; Bendig, P.; Martinez, S.A.; Class, T.J.; Pinheiro, N.C.; Mol, H.G.J. Determination of Glyphosate Levels in Breast Milk Samples from Germany by LC-MS/MS and GC-MS/MS. *J. Agric. Food Chem.* **2016**, *64*, 1414–1421. [[CrossRef](#)]
13. McGuire, M.K.; Price, W.J.; Shafii, B.; Carrothers, J.M.; A Lackey, K.; A Goldstein, D.; Jensen, P.K.; Vicini, J.L. Glyphosate and aminomethylphosphonic acid are not detectable in human milk. *Am. J. Clin. Nutr.* **2016**, *103*, 1285–1290. [[CrossRef](#)] [[PubMed](#)]
14. Richard, S.; Moslemi, S.; Sipahutar, H.; Benachour, N.; Séralini, G.-E. Differential Effects of Glyphosate and Roundup on Human Placental Cells and Aromatase. *Environ. Health Perspect.* **2005**, *113*, 716–720. [[CrossRef](#)] [[PubMed](#)]
15. Szekacs, I.; Farkas, E.; Gemes, B.L.; Takacs, E.; Szekacs, A.; Horvath, R. Integrin targeting of glyphosate and its cell adhesion modulation effects on osteoblastic MC3T3-E1 cells revealed by label-free optical biosensing. *Sci. Rep.* **2018**, *8*, 17401. [[CrossRef](#)] [[PubMed](#)]

16. IARC Monographs Volume 112: Evaluation of Five Organophosphate Insecticides and Herbicides. Available online: <https://www.iarc.fr/wp-content/uploads/2018/07/MonographVolume112-1.pdf> (accessed on 29 July 2019).
17. Sanchís, J.; Kantiani, L.; Llorca, M.; Rubio, F.; Ginebreda, A.; Fraile, J.; Garrido, T.; Farré, M. Determination of glyphosate in groundwater samples using an ultrasensitive immunoassay and confirmation by on-line solid-phase extraction followed by liquid chromatography coupled to tandem mass spectrometry. *Anal. Bioanal. Chem.* **2012**, *402*, 2335–2345. [[CrossRef](#)] [[PubMed](#)]
18. Okada, E.; Coggan, T.; Anumol, T.; Clarke, B.; Allinson, G. A simple and rapid direct injection method for the determination of glyphosate and AMPA in environmental water samples. *Anal. Bioanal. Chem.* **2019**, *411*, 715–724. [[CrossRef](#)] [[PubMed](#)]
19. Eberbach, P.L.; Douglas, L.A. Method for the determination of glyphosate and (aminomethyl)phosphonic acid in soil using electron capture gas chromatography. *J. Agric. Food Chem.* **1991**, *39*, 1776–1780. [[CrossRef](#)]
20. Rubio, F.; Veldhuis, L.J.; Clegg, B.S.; Fleeker, J.R.; Hall, J.C. Comparison of a Direct ELISA and an HPLC Method for Glyphosate Determinations in Water. *J. Agric. Food Chem.* **2003**, *51*, 691–696. [[CrossRef](#)]
21. Reynoso, E.C.; Torres, E.; Bettazzi, F.; Palchetti, I. Trends and Perspectives in Immunosensors for Determination of Currently-Used Pesticides: The Case of Glyphosate, Organophosphates, and Neonicotinoids. *Biosensors* **2019**, *9*, 20. [[CrossRef](#)]
22. Jan, M.R.; Shah, J.; Muhammad, M.; Ara, B.; Muhammad, D.M. Glyphosate herbicide residue determination in samples of environmental importance using spectrophotometric method. *J. Hazard. Mater.* **2009**, *169*, 742–745. [[CrossRef](#)]
23. Sharma, M.; Schmid, M.; Rothballer, M.; Hause, G.; Zuccaro, A.; Imani, J.; Kampfer, P.; Domann, E.; Schafer, P.; Hartmann, A.; et al. Detection and identification of bacteria intimately associated with fungi of the order Sebaciales. *Cell. Microbiol.* **2008**, *10*, 2235–2246. [[CrossRef](#)]
24. De Almeida, L.; Chigome, S.; Torto, N.; Frost, C.; Pletschke, B. A novel colorimetric sensor strip for the detection of glyphosate in water. *Sens. Actuators B Chem.* **2015**, *206*, 357–363. [[CrossRef](#)]
25. Steinrücken, H.; Amrhein, N. The herbicide glyphosate is a potent inhibitor of 5-enolpyruvylshikimic acid-3-phosphate synthase. *Biochem. Biophys. Res. Commun.* **1980**, *94*, 1207–1212. [[CrossRef](#)]
26. Amrhein, N.; Schab, J.; Steinrücken, H.C. The mode of action of the herbicide glyphosate. *Naturwissenschaften* **1980**, *67*, 356–357. [[CrossRef](#)]
27. Rogers, S.G.; A Brand, L.; Holder, S.B.; Sharps, E.S.; Brackin, M.J. Amplification of the *aroA* gene from *Escherichia coli* results in tolerance to the herbicide glyphosate. *Appl. Environ. Microbiol.* **1983**, *46*, 37–43. [[PubMed](#)]
28. Herrmann, K.M.; Weaver, L.M. The shikimate pathway. *Annu. Rev. Plant. Biol.* **1999**, *50*, 473–503. [[CrossRef](#)] [[PubMed](#)]
29. Levin, J.G.; Sprinson, D.B. The enzymatic formation and isolation of 3-enolpyruvylshikimate 5-phosphate. *J. Biol. Chem.* **1964**, *239*, 1142–1151. [[PubMed](#)]
30. Steinrücken, H.; Amrhein, N. 5-Enolpyruvylshikimate-3-phosphate synthase of *Klebsiella pneumoniae*. 1. Purification and properties. *Eur. J. Biochem.* **1984**, *143*, 341–349. [[CrossRef](#)]
31. Alibhai, M.F.; Stallings, W.C. Closing down on glyphosate inhibition—With a new structure for drug discovery. *Proc. Natl. Acad. Sci. USA* **2001**, *98*, 2944–2946. [[CrossRef](#)]
32. Schönbrunn, E.; Eschenburg, S.; Shuttleworth, W.A.; Schloss, J.V.; Amrhein, N.; Evans, J.N.S.; Kabsch, W. Interaction of the herbicide glyphosate with its target enzyme 5-enolpyruvylshikimate 3-phosphate synthase in atomic detail. *Proc. Natl. Acad. Sci. USA* **2001**, *98*, 1376–1380. [[CrossRef](#)]
33. Itaya, K.; Ui, M. A new micromethod for the colorimetric determination of inorganic phosphate. *Clin. Chim. Acta* **1966**, *14*, 361–366. [[CrossRef](#)]
34. Van Veldhoven, P.P.; Mannaerts, G.P. Inorganic and organic phosphate measurements in the nanomolar range. *Anal. Biochem.* **1987**, *161*, 45–48. [[CrossRef](#)]
35. Milin, S. Comparaison de deux méthodes spectrophotométriques de dosage de l'acide phosphorique. Application à des sols et des végétaux. *Cah. Tech. INRA* **2012**, *77*, 1–15.
36. Baykov, A.; Evtushenko, O.; Aვაeva, S. A malachite green procedure for orthophosphate determination and its use in alkaline phosphatase-based enzyme immunoassay. *Anal. Biochem.* **1988**, *171*, 266–270. [[CrossRef](#)]
37. Aguiar-Oliveira, E.; Maugeri, F. Thermal stability of the immobilized fructosyltransferase from *Rhodotorula* sp. *Braz. J. Chem. Eng.* **2011**, *28*, 363–372. [[CrossRef](#)]

38. Hanefeld, U.; Gardossi, L.; Magner, E. Understanding enzyme immobilisation. *Chem. Soc. Rev.* **2009**, *38*, 453–468. [[CrossRef](#)] [[PubMed](#)]
39. Boundy, J.A.; Smiley, K.L.; Swanson, C.L.; Hofreiter, B.T. Exoenzymic activity of alpha-amylase immobilized on a phenol-formaldehyde resin. *Carbohydr. Res.* **1976**, *48*, 239–244. [[CrossRef](#)]
40. Brena, B.; González-Pombo, P.; Batista-Viera, F. Chapter 2 Immobilization of Enzymes: A Literature Survey. In *Immobilization of Enzymes and Cells*, 3rd ed.; Guisan, J.M., Ed.; Springer Science+Business: New York, NY, USA, 2013; Volume 1051, pp. 15–31.
41. Sheldon, R.A. Enzyme Immobilization: The Quest for Optimum Performance. *Adv. Synth. Catal.* **2007**, *349*, 1289–1307. [[CrossRef](#)]
42. Hektor, H.J.; Scholtmeijer, K. Hydrophobins: Proteins with potential. *Curr. Opin. Biotechnol.* **2005**, *16*, 434–439. [[CrossRef](#)] [[PubMed](#)]
43. Bayry, J.; Amanianda, V.; Guijarro, J.I.; Sunde, M.; Latgé, J.-P. Hydrophobins—Unique Fungal Proteins. *PLoS Pathog.* **2012**, *8*, e1002700. [[CrossRef](#)]
44. Wessels, J.G.H. Developmental Regulation of Fungal Cell Wall Formation. *Annu. Rev. Phytopathol.* **1994**, *32*, 413–437. [[CrossRef](#)]
45. Wösten, H.A.B.; de Vocht, M.L. Hydrophobins, the fungal coat unravelled. *Biochim. Biophys. Acta.* **2000**, *1469*, 79–86. [[CrossRef](#)]
46. Wosten, H.; De Vries, O.; Wessels, J. Interfacial Self-Assembly of a Fungal Hydrophobin into a Hydrophobic Rodlet Layer. *Plant Cell* **1993**, *5*, 1567–1574. [[CrossRef](#)] [[PubMed](#)]
47. Linder, M.B. Hydrophobins: Proteins that self assemble at interfaces. *Curr. Opin. Colloid Interface Sci.* **2009**, *14*, 356–363. [[CrossRef](#)]
48. Lo, V.C.; Ren, Q.; Pham, C.L.L.; Morris, V.K.; Kwan, A.H.; Sunde, M. Fungal Hydrophobin Proteins Produce Self-Assembling Protein Films with Diverse Structure and Chemical Stability. *Nanomaterials* **2014**, *4*, 827–843. [[CrossRef](#)] [[PubMed](#)]
49. Soikkeli, M.; Kurppa, K.; Kainlauri, M.; Arpiainen, S.; Paananen, A.; Gunnarsson, D.; Joensuu, J.J.; Laaksonen, P.; Prunnila, M.; Linder, M.B.; et al. Graphene Biosensor Programming with Genetically Engineered Fusion Protein Monolayers. *ACS Appl. Mater. Interfaces* **2016**, *8*, 8257–8264. [[CrossRef](#)] [[PubMed](#)]
50. Hennig, S.; Rödel, G.; Ostermann, K. Hydrophobin-Based Surface Engineering for Sensitive and Robust Quantification of Yeast Pheromones. *Sensors* **2016**, *16*, 602. [[CrossRef](#)] [[PubMed](#)]
51. Bell-Pedersen, D.; Loros, J.J.; Dunlap, J.C. The *Neurospora* circadian clock-controlled gene, *cgc-2*, is allelic to *eas* and encodes a fungal hydrophobin required for formation of the conidial rodlet layer. *Genes Dev.* **1992**, *6*, 2382–2394. [[CrossRef](#)] [[PubMed](#)]
52. Lauter, F.R.; E Russo, V.; Yanofsky, C. Developmental and light regulation of *eas*, the structural gene for the rodlet protein of *Neurospora*. *Genes Dev.* **1992**, *6*, 2373–2381. [[CrossRef](#)] [[PubMed](#)]
53. MacIndoe, I.; Kwan, A.H.; Ren, Q.; Morris, V.K.; Yang, W.; Mackay, J.P.; Sunde, M. Self-assembly of functional, amphipathic amyloid monolayers by the fungal hydrophobin EAS. *Proc. Natl. Acad. Sci. USA* **2012**, *109*, E804–E811. [[CrossRef](#)]
54. Kwan, A.H.Y.; Winefield, R.D.; Sunde, M.; Matthews, J.M.; Haverkamp, R.G.; Templeton, M.D.; Mackay, J.P. Structural basis for rodlet assembly in fungal hydrophobins. *Proc. Natl. Acad. Sci. USA* **2006**, *103*, 3621–3626. [[CrossRef](#)] [[PubMed](#)]
55. Sammons, R.D.; Meyer, J.; Hall, E.; Ostrander, E.; Schrader, S. A Simple Continuous Assay for EPSP Synthase in Plant Tissue. 2007 (Poster). Available online: <https://www.cottoninc.com/wp-content/uploads/2017/03/11a-Industry-Sammons-NCWSS07-poster.pdf> (accessed on 28 June 2016).
56. Bradford, M.M. A rapid and sensitive method for the quantitation of microgram quantities of protein utilizing the principle of protein-dye binding. *Anal. Biochem.* **1976**, *72*, 248–254. [[CrossRef](#)]
57. Haider, S.R.; Reid, H.J.; Sharp, B.L. Tricine-SDS-PAGE. In *Protein Electrophoresis: Methods and Protocols*; Kurien, B.T., Scofield, R.H., Eds.; Humana Press: Totowa, NJ, USA, 2012; Volume 869, pp. 81–91.
58. Laemmli, U.K. Cleavage of structural proteins during assembly of the head of bacteriophage T4. *Nature* **1970**, *227*, 680–685. [[CrossRef](#)] [[PubMed](#)]
59. De Vocht, M.L.; Reviakine, I.; Wösten, H.A.B.; Brisson, A.; Wessels, J.G.H.; Robillard, G.T. Structural and Functional Role of the Disulfide Bridges in the Hydrophobin SC3. *J. Boil. Chem.* **2000**, *275*, 28428–28432. [[CrossRef](#)] [[PubMed](#)]

60. Kershaw, M.J.; Thornton, C.R.; Wakley, G.E.; Talbot, N.J. Four conserved intramolecular disulphide linkages are required for secretion and cell wall localization of a hydrophobin during fungal morphogenesis. *Mol. Microbiol.* **2005**, *56*, 117–125. [CrossRef] [PubMed]
61. Schägger, H. Tricine-SDS-PAGE. *Nat. Protoc.* **2006**, *1*, 16–23. [CrossRef] [PubMed]
62. Law, K.-Y. Definitions for Hydrophilicity, Hydrophobicity, and Superhydrophobicity: Getting the Basics Right. *J. Phys. Chem. Lett.* **2014**, *5*, 686–688. [CrossRef] [PubMed]
63. Boeuf, S.; Throm, T.; Gutt, B.; Strunk, T.; Hoffmann, M.; Seebach, E.; Mühlberg, L.; Brocher, J.; Gotterbarm, T.; Wenzel, W.; et al. Engineering hydrophobin DewA to generate surfaces that enhance adhesion of human but not bacterial cells. *Acta Biomater.* **2012**, *8*, 1037–1047. [CrossRef]
64. Takatsuji, Y.; Yamasaki, R.; Iwanaga, A.; Lienemann, M.; Linder, M.B.; Haruyama, T. Solid-support immobilization of a “swing” fusion protein for enhanced glucose oxidase catalytic activity. *Colloids Surf. B Biointerfaces* **2013**, *112*, 186–191. [CrossRef] [PubMed]
65. Fokina, O.; Fenchel, A.; Winandy, L.; Fischer, R. Immobilization of LccC Laccase from *Aspergillus nidulans* on Hard Surfaces via Fungal Hydrophobins. *Appl. Environ. Microbiol.* **2016**, *82*, 6395–6402. [CrossRef] [PubMed]
66. Wessels, J.G.H.; De Vries, O.M.H.; Ásgeirsdóttir, S.; Springer, J. The thn mutation of *Schizophyllum commune*, which suppresses formation of aerial hyphae, affects expression of the Sc3 hydrophobin gene. *J. Gen. Microbiol.* **1991**, *137*, 2439–2445. [CrossRef] [PubMed]
67. De Vries, O.M.H.; Fekkes, M.P.; Wösten, H.A.B.; Wessels, J.G.H. Insoluble hydrophobin complexes in the walls of *Schizophyllum commune* and other filamentous fungi. *Arch. Microbiol.* **1993**, *159*, 330–335. [CrossRef]
68. Wösten, H.A.B. Hydrophobins: Multipurpose Proteins. *Annu. Rev. Microbiol.* **2001**, *55*, 625–646. [CrossRef]
69. Rubin, J.L.; Gaines, C.G.; Jensen, R.A. Glyphosate Inhibition of 5-Enolpyruvylshikimate 3-Phosphate Synthase from Suspension-Cultured Cells of *Nicotiana glauca*. *Plant Physiol.* **1984**, *75*, 839–845. [CrossRef]
70. Steinrücken, H.C.; Amrhein, N. 5-Enolpyruvylshikimate-3-phosphate synthase of *Klebsiella pneumoniae*. 2. Inhibition by glyphosate [N-(phosphonomethyl)glycine]. *J. Biol. Chem.* **1984**, *259*, 351–357. [CrossRef]
71. Boocock, M.R.; Coggins, J.R. Kinetics of 5-enolpyruvylshikimate-3-phosphate synthase inhibition by glyphosate. *FEBS Lett.* **1983**, *154*, 127–133. [CrossRef]
72. Kwan, A.H.; MacIndoe, I.; Vukašin, P.V.; Morris, V.K.; Kass, I.; Gupte, R.; Mark, A.E.; Templeton, M.D.; Mackay, J.P.; Sunde, M. The Cys3–Cys4 Loop of the Hydrophobin EAS Is Not Required for Rodlet Formation and Surface Activity. *J. Mol. Biol.* **2008**, *382*, 708–720. [CrossRef]
73. Rubio, F.; Glaze, T.; Lance, J.; Hutchinson, Z. Survey of Glyphosate in Domestic and Imported Beer and Wine. 2016 (Poster). Available online: <https://www.abraxiskits.com/wp-content/uploads/2016/08/glyphosateinbeerwine.pdf> (accessed on 22 February 2019).
74. Clegg, B.S.; Stephenson, G.R.; Hall, J.C. Development of an Enzyme-Linked Immunosorbent Assay for the Detection of Glyphosate. *J. Agric. Food Chem.* **1999**, *47*, 5031–5037. [CrossRef]
75. Lesueur, C.; Pfeffer, M.; Fuerhacker, M. Photodegradation of phosphonates in water. *Chemosphere* **2005**, *59*, 685–691. [CrossRef]
76. Jaworski, E.G. Mode of action of N-phosphonomethylglycine. Inhibition of aromatic amino acid biosynthesis. *J. Agric. Food Chem.* **1972**, *20*, 1195–1198. [CrossRef]
77. Grandcoin, A.; Piel, S.; Baurès, E. AminoMethylPhosphonic acid (AMPA) in natural waters: Its sources, behavior and environmental fate. *Water Res.* **2017**, *117*, 187–197. [CrossRef]
78. Marzabadi, M.R.; Gruys, K.J.; Pansegrau, P.D.; Walker, M.C.; Yuen, H.K.; Sikorski, J.A. An EPSP Synthase Inhibitor Joining Shikimate 3-Phosphate with Glyphosate: Synthesis and Ligand Binding Studies. *Biochemistry* **1996**, *35*, 4199–4210. [CrossRef]
79. Priestman, M.A.; Healy, M.L.; Becker, A.; Alberg, D.G.; Bartlett, P.A.; Lushington, G.H.; Schönbrunn, E. Interaction of phosphonate analogues of the tetrahedral reaction intermediate with 5-enolpyruvylshikimate-3-phosphate synthase in atomic detail. *Biochemistry* **2005**, *44*, 3241–3248. [CrossRef]
80. Toy, A.D.F.; Uhing, E.H. Aminomethylenephosphinic acids, salts thereof, and process for their production. U.S. Patent 3,160,632, 8 December 1964.
81. Mertens, M.; Höss, S.; Neumann, G.; Afzal, J.; Reichenbecher, W. Glyphosate, a chelating agent—Relevant for ecological risk assessment? *Environ. Sci. Pollut. Res.* **2018**, *25*, 5298–5317. [CrossRef]

82. Anderson, K.S.; Sikorski, J.A.; Johnson, K.A. Evaluation of 5-enolpyruvylshikimate-3-phosphate synthase substrate and inhibitor binding by stopped-flow and equilibrium fluorescence measurements. *Biochemistry* **1988**, *27*, 1604–1610. [[CrossRef](#)]
83. Ream, J.E.; Yuen, H.K.; Frazier, R.B.; Sikorski, J.A. EPSP synthase: Binding studies using isothermal titration microcalorimetry and equilibrium dialysis and their implications for ligand recognition and kinetic mechanism. *Biochemistry* **1992**, *31*, 5528–5534. [[CrossRef](#)]



© 2019 by the authors. Licensee MDPI, Basel, Switzerland. This article is an open access article distributed under the terms and conditions of the Creative Commons Attribution (CC BY) license (<http://creativecommons.org/licenses/by/4.0/>).

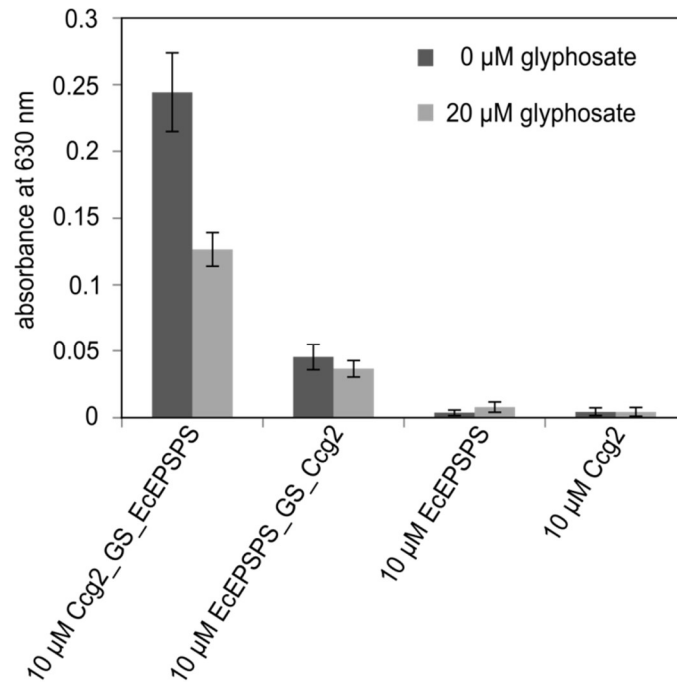


Figure S1. Activity measurement for different proteins after immobilization. Proteinsolutions were incubated for 15 min in a polystyrene 96-well plate. Malachite green assay was performed as described in materials and methods (see Section 2.6). Substrate concentrations were 100 and 80 μM for S3P and PEP, respectively.

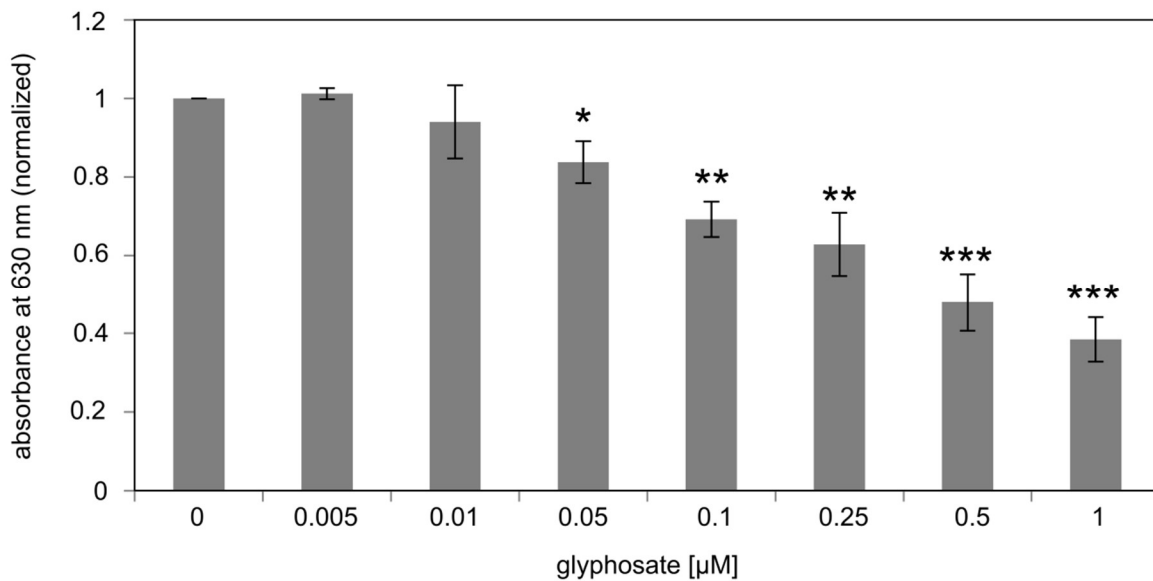


Figure S2. Inhibition of immobilized Ccg2_GS_EcEPSPS by glyphosate. Measurement of EcEPSPS activity using the malachite green assay with a polystyrene surface functionalized with 1 μM Ccg2_GS_EcEPSPS:5 μM Ccg2. Results were normalized to the sample without glyphosate (0 μM). The detection limit is 50 nM glyphosate. *** p ≤ 0.001; ** p ≤ 0.01; * p ≤ 0.05. Absorbance at a wavelength of 630 nm was determined using photometry.

Publication II

Picomolar glyphosate sensitivity of an optical particle-based sensor utilizing biomimetic interaction principles

David Rettke, Julia Döring, Steve Martin, Tom Venus, Irina Estrela-Lopis, Stephan Schmidt, Kai Ostermann, Tilo Pompe

Biosensors and Bioelectronics 165 (2020) 112262

Doi: [10.1016/j.bios.2020.112262](https://doi.org/10.1016/j.bios.2020.112262)

ISI Impact Factor 2020: 10.618



Picomolar glyphosate sensitivity of an optical particle-based sensor utilizing biomimetic interaction principles

David Rettke¹, Julia Döring², Steve Martin¹, Tom Venus³, Irina Estrela-Lopis³, Stephan Schmidt⁴, Kai Ostermann², Tilo Pompe^{1,*}

¹ Institute of Biochemistry, Leipzig University, Johannisallee 21–23, 04103, Leipzig, Germany

² Institute of Genetics, Technische Universität Dresden, Zellescher Weg 20b, 01217, Dresden, Germany

³ Institute of Medical Physics and Biophysics, Leipzig University, Härtelstraße 16-18, 04107, Leipzig, Germany

⁴ Institute of Organic Chemistry and Macromolecular Chemistry, Heinrich Heine Universität Düsseldorf, Universitätsstraße 1, 40225, Düsseldorf, Germany

ARTICLE INFO

Keywords:

Enzyme-based biosensors
Glyphosate
Reflection interference contrast microscopy
Soft colloidal probes
Immobilization technology
Hydrophobins

ABSTRACT

The continually growing use of glyphosate and its critically discussed health and biodiversity risks ask for fast, low cost, on-site sensing technologies for food and water. To address this problem, we designed a highly sensitive sensor built on the remarkably specific recognition of glyphosate by its physiological target enzyme 5-enolpyruvyl-shikimate-3-phosphate synthase (EPSPs). This principle is implemented in an interferometric sensor by using the recently established soft colloidal probe (SCP) technique. EPSPs was site-specifically immobilized on a transparent surface utilizing the self-assembling properties of circadian clock gene 2 hydrophobin chimera and homogeneity of the layer was evidenced by atomic force microscopy. Exposure of the enzyme decorated biochip to glyphosate containing samples causes formation of enzyme-analyte complexes and a competitive loss of available binding sites for glyphosate-functionalized poly(ethylene glycol) SCPs. Functionalization of the SCPs with different types of linker molecules and glyphosate was assessed employing confocal laser scanning microscopy as well as confocal Raman microspectroscopy. Overall, reflection interference contrast microscopy analysis of SCP-biochip interactions revealed a strong influence of linker length and glyphosate coupling position on the sensitivity of the sensor. In employing a combination of pentaglycine linker and tethering glyphosate via its secondary amino group, concentrations in aqueous solutions down to 100 pM could be measured by the differential adhesion between SCP and biochip surface, supported by automated image analysis algorithms. This sensing concept could even prove its exceptional pM sensitivity in combination with a superior discrimination against structurally related compounds.

1. Introduction

Since its market launch in the mid-70s, the overall use of glyphosate (N-(phosphonomethyl)glycine) has grown to dominate the herbicide market. Especially the introduction of “Roundup Ready” crops in 1996 boosted sales volumes considerably to a nearly 15-fold increase until 2014, not least due to a steadily mounting number of resistant weeds (Benbrook, 2016; Duke, 2018; Green, 2018). The glyphosate safety profile and possibly underestimated environmental ramifications are discussed controversially for decades. Particularly the unexpected classification of the France-based International Agency for Research on Cancer (IARC) as “probably carcinogenic to humans” brought glyphosate into the center of a public debate and triggered a flurry of lawsuits

against the manufacturer Monsanto in the US (International Agency for Research on Cancer, 2017). In the European Union the debate on glyphosate reached its preliminary climax with a long lasting political dispute on the renewal of the approval of glyphosate for another 15 years, which ended up in a shortened approval period of 5 years (Clausing et al., 2018; European Food Safety Authority, 2016; Székács and Darvas, 2018).

Despite the aforementioned concerns and widespread use, water resources, raw materials as well as final food products are almost never tested for glyphosate contaminations, owing to rather prohibitive cost and labor intensive methods (Reynoso et al., 2019; Rubio et al., 2003; Xu et al., 2019). Commercially available rapid tests on the other hand suffer from insufficient sensitivity or inadequate selectivity, accompanied by

* Corresponding author.

E-mail address: tilo.pompe@uni-leipzig.de (T. Pompe).

<https://doi.org/10.1016/j.bios.2020.112262>

Received 30 March 2020; Received in revised form 27 April 2020; Accepted 29 April 2020

Available online 11 May 2020

0956-5663/© 2020 Elsevier B.V. All rights reserved.

false positive or negative results (Clegg et al., 1999; Selvi et al., 2011; Tittlemier et al., 2017). We therefore sought to combine, in a new biosensing principle, the superior specificity of molecular glyphosate recognition by its target 5-enolpyruvyl-shikimate-3-phosphate synthase (EPSPs) with the recently established soft colloidal probe (SCP) technique, known to detect weak binding energies (Martin et al., 2016; Pussak et al., 2013; Schmidt et al., 2015).

Colloidal probe techniques have been extensively used to study a variety of processes, including particle aggregation and deposition as well as adhesion phenomena, typically in conjunction with hard spheres and atomic force microscopy (AFM) (Borkovec et al., 2012; Butt et al., 2005; Ralston et al., 2005). The advantage of using soft, elastomeric probes in the SCP technique lies in the much larger contact area between the probe and surface, higher adhesion energies, simplifying readout and improving sensitivity (Buzio et al., 2007; Pussak et al., 2012, 2014). Besides these advantages, SCPs can be easily equipped with molecules of interest and binding can be fine-tuned by variation of particle elasticity as well as linker type and length (Wang et al., 2017). The spherical probe geometry furthermore allows for data analysis by straightforward physical models. Adhesion energies of a soft spherical probe and a hard surface W can be extracted according to the Johnson - Kendall - Roberts - model of elastic contact (Wang et al., 2017):

$$a^3 = 6\pi \frac{W}{E_{eff}} R^2 \quad (1)$$

where a is the radius of contact, R the radius of the SCP and E_{eff} the effective elastic modulus of the probe ($E_{eff} = 4E/(3(1-\nu^2))$), E ...Young's modulus, ν ...Poisson ratio). Reflection interference contrast microscopy (RICM) allows for convenient, low-cost readout of contact area and SCP radius.

Based in this status, we set of in our new approach to use SCPs in a binding assay to detect glyphosate. Adhesion energies are directly related to biospecific interactions between SCP-tethered ligands, in this case glyphosate, and the respective recognition element immobilized on the biochip, here EPSPs (Fig. 1, left side). We apply a competitive binding assay as a straightforward approach to quantify analytes in aqueous samples. The presence of soluble glyphosate causes a concentration dependent loss of available binding sites, presented by immobilized EPSPs, for SCP-tethered ligands and thus the analyte is directly quantified by differential reduction of the SCP-biochip interfacial area (Fig. 1, middle and right panels).

2. Materials and methods

2.1. Particle preparation

SCP particles were synthesized as described previously (Wang et al., 2017). Briefly, 50 mg poly(ethylene glycol) diacrylate (Mn 6000 Da, Sigma Aldrich, Germany) and 1 mg of the photoinitiator Irgacure 2959 (Sigma Aldrich) were added to 10 ml 1M sodium sulfate solution and vortexed until microscopic droplets were formed. The dispersion was photopolymerized using a Heraeus HiLite UV curing unit (Heraeus Kulzer, Germany) for 90 s. Next, the PEG SCPs were grafted with crotonic acid (Sigma Aldrich) as described earlier (Schmidt et al., 2015). In short, water was exchanged by 10 ml ethanol, then 250 mg benzophenone (Sigma Aldrich) and 1.5 g crotonic acid were added. Subsequently, the mixture was flushed with nitrogen for 30 s before irradiating with UV light for 900 s. The resulting SCP particles were then washed with ethanol and PBS three times each.

2.2. Post-functionalization of SCPs

In order to enable specific interactions between EPSPs functionalized biochip surfaces and hydrogel probes, SCPs were first coated with the respective linker molecules and subsequently functionalized with

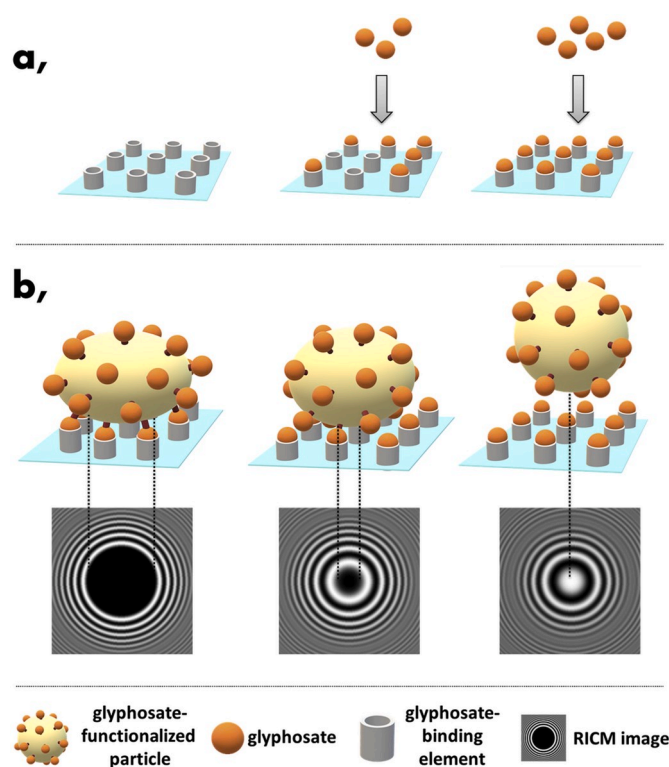


Fig. 1. General principle: a) a transparent biochip is competent of binding glyphosate (orange spheres) and the number of residual binding sites (EPSPs, grey cylinders) declines with increasing analyte concentrations. b) A glyphosate functionalized SCP approaches the biochip and forms a distinct contact area with the underlying surface. Left: The SCP strongly adheres to the unoccupied surface, resulting in an elastic SCP deformation and an extended contact area. Middle: Addition of analyte decreases SCP deformation until the SCP cannot bind to the surface anymore (right). The lowest panel indicates examples of RICM images of respective adhering SCPs. (For interpretation of the references to color in this figure legend, the reader is referred to the Web version of this article.)

glyphosate. The linker molecule permits coupling of glyphosate either *via* carboxy or secondary amino group, allowing shifting sensitivity of the sensor. Furthermore, length and degree of polymerization of the linker molecules can be varied; resulting in altered affinity of the immobilized competitor for the enzyme (EPSPs) and thus the working range of the sensor can be adjusted. The coupling steps were carried out using active ester chemistry.

Ethylene diamine, the short linker variant, was coupled to the SCPs by means of benzotriazol-1-yl-oxytri-pyrrolidinophosphonium hexafluorophosphate (PyBOP, ApexBio US) and 1-hydroxybenzotriazole (HOBt, Sigma Aldrich). For this, the SCPs were suspended and water was replaced by dimethylformamide (DMF, Carl Roth, Germany) in several washing steps. The particles were left in 2 ml DMF. Subsequently, 146 mg (280 μ mol) of PyBOP, 18 mg (140 μ mol) of HOBt and 39 μ l (280 μ mol) of triethylamine (Sigma Aldrich) were added to activate the carboxy groups and the suspension was shaken for 1 h at room temperature. After addition of 20 μ l (300 μ mol) of ethylene diamine (Alfa Aesar, US) and 3 h of reaction, the SCPs were centrifuged at 1844 x g for 10 min and washed 3 times each with DMF, a 1:1 mixture of DMF and water and pure water. For further coating, 4 mg (24 μ mol) of glyphosate (Sigma Aldrich, Germany) in 2 ml of 100 mM Hepes buffer (pH = 7.0) were dissolved in an ultrasonic bath and 46 mg (240 μ mol) of 1-ethyl-3-(3-dimethylaminopropyl) carbodiimide hydrochloride (EDC, Carbolution Chemicals, Germany) and 52 mg (240 μ mol) of N-hydroxysulfosuccinimide sodium salt (s-NHS, Carbolution Chemicals) were added and the carboxy groups were activated for 15 min. The coupling

of glyphosate to the amine-functionalized SCPs was carried out by combining suspension and solution. After reaction over a period of 1 h, the SCPs were washed 3 times with a 100 mM Hepes buffer solution (pH = 7.0).

Poly(ethylene glycol)-diamine (Mn = 3000, Sigma Aldrich) served as a long linker molecule. 2 ml of the SCP suspension was centrifuged and the SCPs were washed 3 times in Hepes buffer (pH = 7.0). 1 ml of a solution containing 23 mg (120 μ mol) EDC, 26 mg (120 μ mol) of s-NHS and 15 mg (5 μ mol) PEG-diamine was added to the SCPs and the mixture was allowed to react overnight. Finally the SCPs were washed 3 times in Hepes-buffer (100 mM, pH = 7.0). Glyphosate coupling was conducted as described for ethylene diamine functionalized SCPs.

Alternatively, the SCPs were functionalized with a pentaglycine linker (Sigma Aldrich). For this purpose, the SCPs were washed 3 times with 2 ml of 100 mM MES buffer (pH = 5.3) and the supernatant was discarded after centrifugation (10 min, 1844 g). 23 mg (120 μ mol) of EDC and 26 mg (120 μ mol) of s-NHS were dissolved in 1 ml of 100 mM MES buffer (pH = 5.3) and the SCPs were subsequently suspended in the solution. After 1 h of activation of the carboxyl groups, 10 μ l (143 μ mol) of mercaptoethanol was added to inactivate the excess unreacted EDC and the suspension was left at room temperature for an additional 15 min while agitating. After centrifugation (10 min, 1844 x g) the supernatant was discarded and 0.2 mg (660 nmol) of the peptide, dissolved in 1 ml of Hepes buffer (100 mM; pH = 7.0), was added and the coupling reaction was allowed to proceed overnight. Next, SCPs were washed 3 times (100 mM Hepes buffer; pH = 7.0) and the carboxy groups of the immobilized pentaglycine linkers were again converted into s-NHS esters according to the procedure described above. Subsequently excess EDC was inactivated by means of mercaptoethanol, the suspension was centrifuged and the supernatant was discarded. After addition of a 1 mg/ml 100 mM, pH = 7.0 Hepes-buffered glyphosate solution (6 μ mol), the reaction mixture was left overnight at room temperature with continuous agitation. Finally, the SCPs were washed 3 times with 100 mM Hepes buffer solution (pH = 7.0).

2.3. Protein expression

For the production of a functionalized surface, fusion proteins from the circadian clock gene 2 hydrophobin (Ccg2) from *Neurospora (N.) crassa* and the 5-enolpyruvylshikimate-3-phosphate synthase from *Escherichia (E.) coli* (EPSPS) were needed. Details of the protein expression methods are given in (Döring et al., 2019). For this purpose, the coding regions of the respective genes, linked via the sequence for a flexible glycine-serine linker, were transferred into the expression vector pET28b (Novagen, Germany). In this case, the sequence of the hydrophobin (SEQ ID No. 2) is on the 5' side and that of the EPSPS (SEQ ID No. 1) on the 3' side of the linker sequence. In addition, 5'-side of the sequence for the fusion protein, the sequence for a (His)₆-tag, which is required for the detection and purification of the fusion protein. Furthermore, hydrophobin without EPSPS was needed for the surface. The gene sequence was accordingly transferred without the linker and the EPSPS sequence into the vector pET28b. The vectors modified in this manner were transferred to the *E. coli* expression strain SHuffle T7 Express lysY (New England Biolabs, USA) after complete sequencing of the introduced sequences. This expression strain is advantageous for the expression of the hydrophobins, since it additionally codes for a protein disulfide isomerase, which favors the correct formation of the disulfide bridges of the hydrophobins. They play an essential role in the correct folding of the protein.

Protein expression was initiated by adding 1 mM isopropyl- β -D-thiogalactoside (IPTG) to *E. coli* cells in the exponential growth phase. After induction, the cells were incubated for 4 h at 30 °C and 180 revolutions per min. The cells were then pelleted and washed for further use. The cleaning method used depends on the solubility of the proteins. The soluble fusion proteins were purified by nickel affinity chromatography under native conditions according to the manufacturer's instructions,

while the insoluble hydrophobins were purified by means of denaturing nickel affinity chromatography according to the manufacturer's instructions. The hydrophobins were concentrated by ultrafiltration prior to dialysis, this approach was not necessary for the fusion proteins. After purification, the hydrophobins were dialyzed against redox refolding buffer (10 mM glutathione, 1 mM glutathione oxidized, pH 5.4) and the fusion proteins against Monsanto dialysis buffer (10 mM MOPS, 0.5 mM EDTA, 5% (v/v) 99.9% glycerol, 1 mM DTT, pH 7). The purified proteins were stored in a refrigerator and used for functionalization of glass surfaces.

2.4. Coating of glass surfaces

For preparation of biochip surfaces, glass coverslips (\varnothing 32 mm, Thermo Scientific, Germany) were placed in a Teflon rack and cleaned by sonication in double deionized water and ethanol (AppliChem, Germany) for 30 min each. Afterwards, chemical cleaning was performed to remove organic as well as particle contaminants from the surfaces. Therefore a mixture of 50 ml H₂O₂, 35% (Grüssing, Germany), 50 ml 25% NH₃ aqueous solution (Merck, Germany) and 250 ml double deionized water was heated to 60 °C on a hot plate and coverslips were left in the solution for 10 min. After rinsing twice with double deionized water, the coverslips were dried in a nitrogen stream. Coating of the glass surfaces was carried out by slowly pipetting up the protein solution followed by 60-min incubation at room temperature. Subsequently, the surfaces were thoroughly washed with distilled water and blown dry using a nitrogen flow. The two protein variants were needed to find an optimal ratio between the fusion protein (able to bind glyphosate) and hydrophobin (to stabilize the surface). For this purpose, the proteins were mixed in ratios of 25%, 50%, 75% and 100% fusion protein plus the respective complementary amount of Ccg2.

2.5. Reflection interference contrast microscopy (RICM) measurements

EPSPs coated cover glasses were adhered to a sticky-slide 16 well (Grace Biolabs, US) and each surface was covered with 200 μ l of HEPES-buffer pH = 7.0 as a positive control or the respective analyte solution for 10 min. For initial specificity testing of SCPs functionalized with the respective linker and glyphosate, 10 mM solutions of glyphosate or glufosinate were prepared. Assessment of cross-reactivity was conducted in 1 mM pesticide or glycine solutions. In case of atrazine, chlorpyrifos and phosmet, saturated solutions were prepared (atrazine: 153 μ M, chlorpyrifos: 4 μ M, phosmet: 79 μ M). Afterwards, 20 μ l of a suspension containing linker- or glyphosate-functionalized SCPs were added dropwise. After a period of 15 min, sedimentation of the SCPs was completed and the probes and their corresponding radial profiles were imaged using an inverted microscope (Olympus IX73, Germany) with an integrated halogen lamp for bright-field microscopy. To obtain the respective interference reflection patterns, samples were illuminated by a monochromatic 530 nm collimated LED (M530L2-C1, Thorlabs, Germany). An Olympus 60x, NA (numerical aperture) 1.35 oil-immersion objective (UPlanSApo 60x 1.35 oil, Olympus, Germany) was used in concert with a quarter waveplate (WPMQ05M-532, Thorlabs GmbH, Germany), placed on the microscope's breadboard between objective and sample, as well as additional polarizers to avoid internal reflections (Limozin and Sengupta, 2009). Images were captured with a monochrome CCD camera (DMK 23U274, ImagingSource, Germany) using μ Manager microscopy software. All datasets were recorded applying an exposure time of 50 ms and stored in tagged image file format (tiff).

2.6. Data analysis of RICM measurements

Obtained images of radial profiles resulting from the respective adhering or non-adhering SCPs were analyzed by the home-built software based on pattern matching (Waschke et al., 2019). Adhesion energies were calculated by the software. Due to the strongly different

adhesion energies of glyphosate-functionalized SCPs in dependence of selected linker molecules, the respective adhesion energies were normalized to values of adhering glyphosate-coated SCPs in the absence of soluble pesticides for better comparability of the results.

Detailed information of procedures for determination of elastic modulus of SCPs, confocal fluorescence microscopy and confocal Raman microspectroscopy of functionalized SCPs as well as surface roughness determination of protein-coated biochips is given in the ESI.

3. Results and discussion

In our experimental setup, SCPs were prepared by dispersion polymerization using photo-crosslinking of linear PEG₆₀₀₀ diacrylamide and subsequent functionalization with carboxy groups by photoradical grafting of crotonic acid on the PEG meshwork according to the procedure introduced by Pussak et al. (2012). Poly(ethylene glycol) (PEG) as an SCP scaffold suppresses nonspecific interactions between the SCP and biochip surface to achieve highly sensitive and specific measurements in combination with low-cost synthesis and straightforward methods for ligand tethering (Ogi et al., 2009; Pussak et al., 2012).

The quantification of analytes in this setup necessitates covalent coupling of the target analyte glyphosate (or analogous binding molecules for the specific EPSP binding site) to the SCPs. Glyphosate coupling using reactive functional groups (carboxy, amino or phosphono group) can be expected to result in altered interactions with the EPSPs binding domain and possibly a shift of affinities in an undesirable manner due to the small size of glyphosate and the different groups involved in the biospecific EPSPs binding. Therefore we investigated glyphosate binding via different linkers to the SCP and tested the effect on the selectivity of EPSPs binding. Carboxy groups allow for post-functionalization of the SCPs by active ester chemistry to tether linker molecules of different characteristics, namely ethylene diamine (EDA), PEG₃₀₀₀ diamine (PEG₃₀₀₀-DA) and pentaglycine (gly₅). The two diamine linkers have different lengths and couple to the carboxylic acid moiety of glyphosate (Fig. 2). The pentaglycine linker binds glyphosate via its secondary amino group to the SCP.

For diamine linkers success of each functionalization step and homogeneous distribution of the reactive groups, linker molecules and glyphosate were assessed by means of confocal laser scanning microscopy (cLSM) using FITC labelling of amino groups either after linker-tethering to SCPs or glyphosate coupling to the linkers. For the pentaglycine linker, glyphosate coupling was verified using more elaborate confocal Raman microscopy (CRM) as other labelling strategies like staining of COOH groups are inappropriate due the presence of this

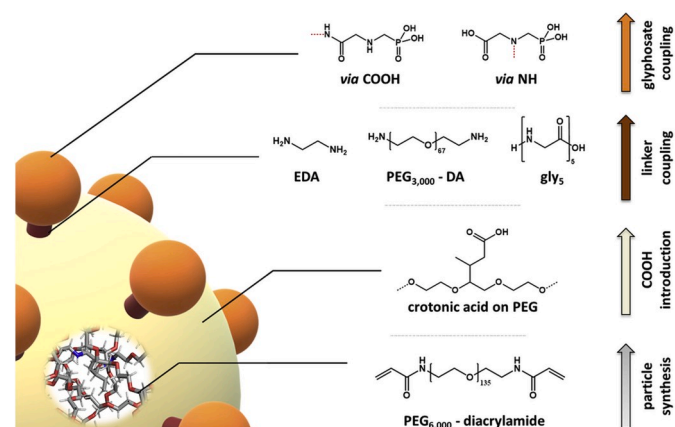


Fig. 2. Schematic representation of SCP components. A spherical PEG meshwork is functionalized with crotonic acid to introduce COOH groups, facilitating coupling of the linker molecules ethylene diamine, PEG₃₀₀₀ diamine or pentaglycine. Depending on the linker type, i.e. diamine or pentaglycine, glyphosate is coupled via carboxy or amino group.

moiety on COOH- as well as pentaglycine- and glyphosate-functionalized SCPs.

cLSM analysis of at least 50 FITC labelled SCPs per condition revealed a maximum fluorescence intensity of the respective amine-functionalized SCPs (ethylene diamine and PEG diamine). The decrease in fluorescence intensities of roughly 50% after glyphosate (GPS) functionalization indicated amino group consumption accompanied by amide bond formation (Fig. 3).

Successful glyphosate coupling was additionally visualized and verified for pentaglycine functionalized probes using CRM. The spectra of PEG and GPS differ strongly from each other, especially in the spectral region of CH₂ vibration modes. An appearance of the vibration at 2960 cm⁻¹, which is originated from CH₂ stretching mode of glyphosate, may serve as an indicator of efficacy of glyphosate coupling to SCPs. Spectra extracted from each pixel in the scanned area were decomposed to glyphosate and PEG ones. The recalculated de-mixed images show the distribution of PEG and glyphosate molecules in one SCP revealing core/shell structure (Fig. 4, top). The analysis of the CH₂ stretching and bending regions in spectra extracted from core and shell of single SCP shows specific spectral characteristics of both, PEG and GPS molecules (Fig. 4, bottom). While the shell spectrum resembles the GPS one, the core spectrum is composed of GPS and PEG spectra. The cross-section concentration profile of GPS indicated glyphosate to be homogeneously distributed in the core of the SCP with enrichment at the surface (Fig. 4, bottom).

Young's elastic modulus of SCPs was determined by force-indentation measurements. No impact of the different linker and glyphosate functionalizations on elasticity was found as moduli of all probes were in the range of 47 ± 11 kPa.

The second component of the biosensing approach encompasses a transparent glass surface that presents the glyphosate recognition element EPSPs and thus allows evaluating SCP-biochip surface binding events. Controlling the orientation of binding sites on a biochip is mandatory for high sensitivity and selectivity, but also difficult to achieve. We used fusion constructs of EPSPs and self-assembling fungal surface proteins, more precisely the class I hydrophobin Ccg2 from *Neurospora Crassa* (see Fig. 5). Hydrophobins are low molecular weight proteins secreted by filamentous fungi, which, owing to their ability to assemble into amphiphilic rodlets at materials surfaces, allow versatile and robust surface engineering applications (Hennig et al., 2016). Using

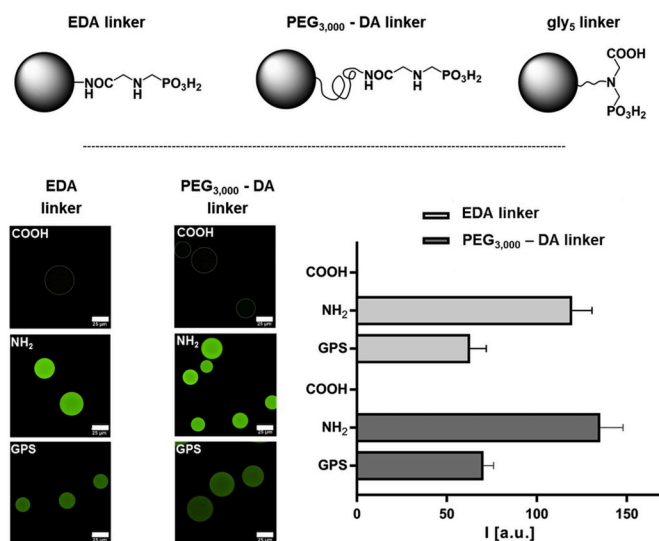


Fig. 3. SCP functionalization: COOH-, diamine-linker- (ethylene diamine, PEG_{3,000} diamine) and glyphosate (GPS)-functionalized SCPs were stained for free amino groups using FITC. Fluorescence intensities increase after diamine coating and drop as a result of covalent glyphosate coupling. COOH-functionalized SCPs are accentuated by white dashed lines. Scale bar: 25 μm.

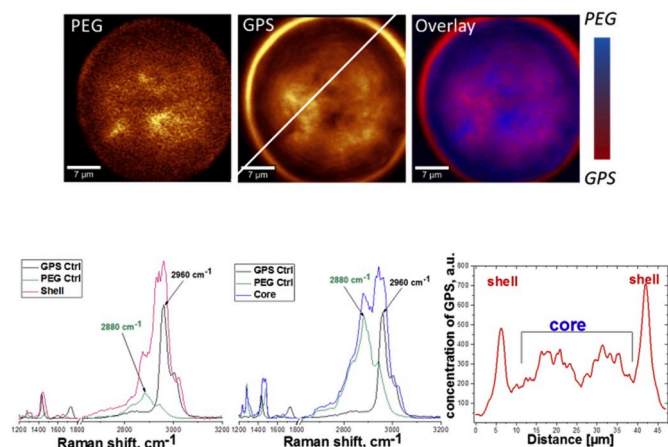


Fig. 4. SCP functionalization: SCPs bearing glyphosate tethered to a pentaglycine linker were assessed by means of CRM. Distribution of PEG and GPS were visualized by de-mixing (top), exploiting characteristic vibrations at 2880 cm^{-1} and 2960 cm^{-1} of the spectra (bottom), respectively. Glyphosate was found in the core but is particularly enriched at the surface, as seen by the cross-section concentration profile (bottom) along the white line in GPS image. Scale bar: $7\text{ }\mu\text{m}$.

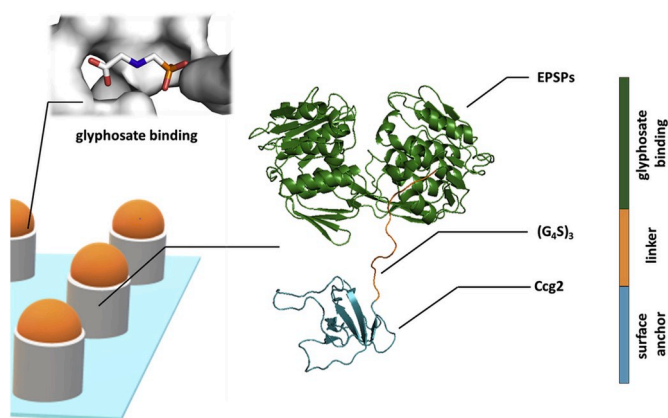


Fig. 5. Schematic representation of biochip components. A transparent glass slide is decorated with a fusion protein comprising the glyphosate binding enzyme EPSPs. The hydrophobin Ccg2 functions as surface anchor and is linked to EPSPs by a glycin-serine linker ((G₄S)₃) to assure favourable orientation of the enzyme's active site. Protein structures were modified from PDB IDs: 1G6S (Schönbrunn et al., 2001), 2GG4 (Funke et al., 2006) and 2FMC (Kwan et al., 2006).

this approach, biochips can be stably decorated with EPSPs in a one-step procedure by simply pipetting the corresponding EPSPs-Ccg2 chimera on a glass slide.

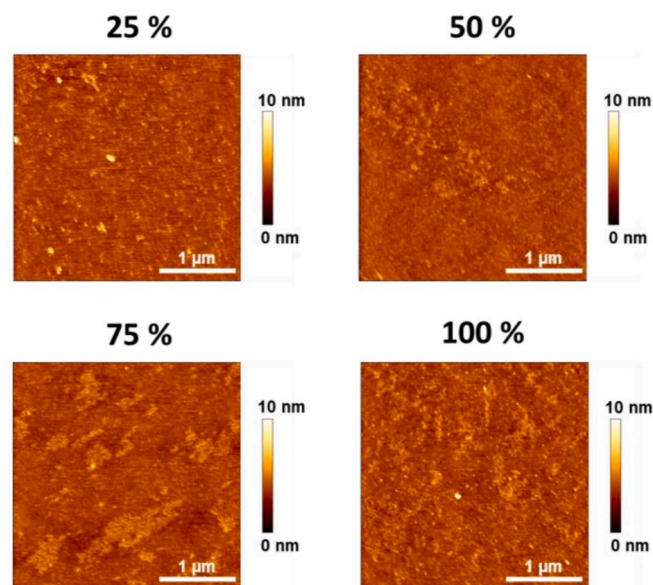
The general procedure of fusion gene cloning and protein expression were recently reported in connection with a colorimetric rapid test for on-site glyphosate quantification based on the release of inorganic phosphate with μM sensitivity (Döring et al., 2019). Adaption of the surface for our setup required adjustment of the ratio between fusion protein (EPSPs-Ccg2) and Ccg2 lacking a fusion partner, as a strong influence of this parameter on enzymatic activity was reported earlier (Döring et al., 2019). These findings can be accounted to modulations of the surface topography in dependence of EPSPs-Ccg2 – Ccg2 ratio of the coating solution, which are most likely driven by geometric inequalities between the comparatively large EPSPs and lower molecular weight Ccg2 domains of the chimera. Studies on these effects were performed using 25%, 50%, 75% (w/w) and mere fusion protein coating solutions comprising the respective complementary amount of Ccg2. Surface

topographies were analyzed by AFM and root mean square (RMS) roughness served as an indicator for surface homogeneity.

Fig. 6 clearly demonstrates the impact of EPSPs-Ccg2 – Ccg2 ratios. A low fusion protein content causes formation of protein clusters that adversely affects surface roughness. A high fusion protein content ($\geq 75\%$ w/w) also affects this parameter in an undesirable manner, most likely due to excessive clustering of the EPSPs-Ccg2. A 50% w/w mixture was identified to yield lowest RMS roughness values and best homogeneity of the biochip, in consistency with studies on the enzymatic activity of these surfaces (Döring et al., 2019). Follow-up RISM experiments were therefore conducted employing 50% (w/w) mixture coatings.

Having generated glyphosate tethered SCPs and EPSPs functionalized biochips, we scrutinized the specific interaction of the glyphosate conjugated SCPs with the different linkers using RISM. The acquired images displaying the respective interference patterns were analyzed by a home-built software to extract adhesion energies of the SCPs by measuring their radius and radii of contact, see equation (1). A detailed description of the image pattern-matching algorithm was recently published (Waschke et al., 2019).

The initial experiments were carried out in absence and presence of 10 mM glyphosate. Additionally, the structurally related glufosinate was used as a negative control to ascertain whether the requisite specificity for fail-safe glyphosate identification were met. As can be seen from Fig. 7, all types of glyphosate bearing SCPs reveal a strong increase in adhesion energy when compared to the SCPs lacking glyphosate. Importantly, adhesion energies are markedly diminished in presence of 10 mM glyphosate solutions in all cases, confirming glyphosate EPSP binding. However, glyphosate-tethering via the long PEG_{3,000} diamine



fusion protein	25%	50%	75%	100%
RMS	910 pm	495 pm	575 pm	850 pm

Fig. 6. AFM images and RMS roughness of EPSPs-Ccg2 – Ccg2-coated glass surfaces. Percentages given indicate the amount of fusion protein in a mixture with Ccg2. Colour scale on the right of the image indicates height difference. (For interpretation of the references to color in this figure legend, the reader is referred to the Web version of this article.)

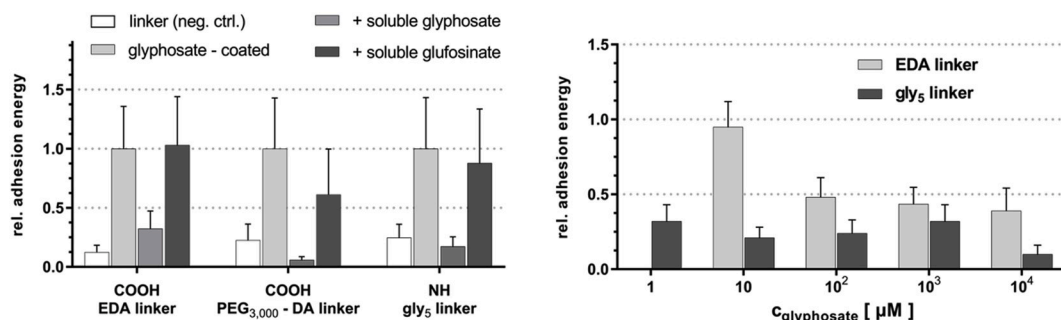


Fig. 7. Comparison of relative adhesion energies concerning glyphosate sensitivity and specificity of the respective SCP linker types and controls. Adhesion energies are normalized to values of adhering glyphosate-coated SCPs in the absence of soluble pesticides. Left: Relative adhesion energies of linker and glyphosate-functionalized SCPs in the absence and presence of soluble glyphosate. Unspecific response was assessed using glufosinate. Right: Relative adhesion energies of SCPs with glyphosate coupled *via* ethylene diamine and pentaglycine linker in dependence of glyphosate concentration (soluble).

linker showed a strong response to both, glyphosate as well as the negative control glufosinate and hence fall short in terms of specificity. The binding of the short ethylene diamine linker and the pentaglycine linker were not significantly biased by glufosinate and were thus selected for detailed inhibition competition assays.

The concentration dependence of the ethylene diamine and pentaglycine linker on the SCP adhesion energies is illustrated in Fig. 7. It can be concluded that the sensitivity for the detection of soluble glyphosate is above 10 μM for the ethylene diamine linker. In contrast, the pentaglycine linker showed a clearly improved sensitivity below 10 μM . Though adjustment of ligand densities on the probes might shift the sensitivity to lower concentrations, ethylene diamine linker SCPs were not further investigated. A detailed measurement using the pentaglycine linker SCPs revealed a pM sensitivity to glyphosate, covering an operating range of 10^{-11} M - 10^{-8} M (Fig. 8, left panel). This sensitivity range is highly remarkable, as it meets the 0.1 $\mu\text{g}/\text{l}$ threshold for pesticide impurities in German tap water.

Lastly, we examined the robustness and specificity of the glyphosate sensor. Cross-sensitivity was assessed by testing structurally related compounds, non-glyphosate organophosphorus, and frequently applied pesticides as analytes. Importantly, the only compound that exhibits a small but measurable effect on SCP adhesion is glufosinate (Fig. 8, right panel), confirming the ability to specifically detect glyphosate, even in a cocktail of other pesticides as well as in the presence of compounds bearing structural elements of glyphosate.

4. Conclusions

In sum, a novel method for quantification of glyphosate in aqueous samples was established. The strength of this assay is particularly based

on the interplay between SCP technique and EPSPs-decorated biochip, respectively conducive to sensitivity and selectivity. In adjusting linker type and coupling position, i.e. employing a pentaglycine linker and coupling glyphosate to SCPs *via* the amino group, analyte concentrations down to the pM range could be detected, which is comparable to liquid chromatography-based detection schemes considered as the “gold standard” for glyphosate quantification (Valle et al., 2019). In contrast, SCP-based detection does not require derivatization of the sample or high-end equipment, thereby reducing the level of complexity of the procedure and allowing for real-time detection. Screening for potentially cross-reactive compounds did not reveal any interference of structurally related compounds, proving the robustness the sensing concept. In spite of these qualities our prospective research addresses essential parameter testing, as for example ionic strength, pH as well as the presence of di- or trivalent metal ions and adjuvants within the specimen might limit practicability in terms of real-sample analysis, especially in complex environmental matrices. Aside from the demonstrated accurate, low-cost and on-site detection procedure for glyphosate, it is noteworthy to also emphasize the modularity of this approach as well as its adaptability to numerous analytical problems.

Declaration of competing interest

D.R., J.D., K.O., T.P. declare competing financial interests. A provisional patent has been filed on behalf of Universität Leipzig and the Technische Universität Dresden.

CRediT authorship contribution statement

David Rettke: Methodology, Investigation, Formal analysis,

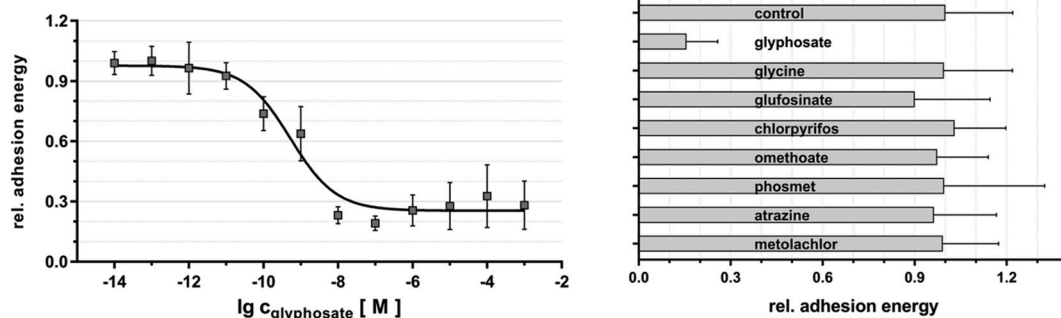


Fig. 8. Relative adhesion energies of SCPs with glyphosate tethered *via* pentaglycine linker in the presence of soluble glyphosate and other pesticides. Relative adhesion energies are normalized to values of adhering glyphosate-coated particles in the absence of soluble pesticides. Left: Dependence of adhesion energies from glyphosate concentrations. Right: Assessment of cross-reactivity of SCPs towards organophosphorus and commonly used pesticides as well as glycine as a structural element of glyphosate. Each compound was tested at 1 mM concentration with the exception of atrazine, chlorpyrifos and phosmet, with respective concentrations of 153 μM , 4 μM and 79 μM . Saturated solutions were prepared in case of the latter compounds.

Visualization, Writing - original draft. **Julia Döring**: Methodology, Resources, Writing - review & editing. **Steve Martin**: Investigation, Formal analysis. **Tom Venus**: Investigation, Formal analysis. **Irina Estrela-Lopis**: Methodology, Formal analysis, Writing - review & editing. **Stephan Schmidt**: Methodology, Resources, Writing - review & editing. **Kai Ostermann**: Conceptualization, Writing - review & editing, Supervision, Funding acquisition. **Tilo Pompe**: Conceptualization, Writing - original draft, Supervision, Funding acquisition.

Acknowledgements

This work was funded by grants of the Federal Ministry of Education and Research of Germany to K.O. and T.P. (grant no.: 13N13798, 13N13799) within the collaborative research project 'Particle-based optical sensors for in-place analytics in quality control of drinking water and food' (PARTOS) with the industrial partners Umex GmbH (Dresden, Germany), IfU GmbH Privates Institut für Umweltanalysen (Lichtenau, Germany) and Gebr. Heyl Vertriebsgesellschaft für innovative Wasseraufbereitung mbH (Hildesheim, Germany). The usage of the Bioluminescence Core Facility of the Faculty of Life Science of Leipzig University, supported by a grant from Deutsche Forschungsgemeinschaft INST 268/293-1 FUGG to T.P., is gratefully acknowledged.

Appendix A. Supplementary data

Supplementary data to this article can be found online at <https://doi.org/10.1016/j.bios.2020.112262>.

References

- Benbrook, C.M., 2016. *Environ. Sci. Eur.* 24, 24.
- Borkovec, M., Szilagyi, I., Popa, I., Finessi, M., Sinha, P., Maroni, P., Papastavrou, G., 2012. *Adv. Colloid Interface Sci.* 179–182, 85–98.
- Butt, H.J., Cappella, B., Kappell, M., 2005. *Surf. Sci. Rep.* 59, 1–152.
- Buzio, R., Bosca, A., Krol, S., Marchetto, D., Valeri, S., Valbusa, U., 2007. *Langmuir* 23, 9293–9302.
- Clausing, P., Robinson, C., Burtcher-Schaden, H., 2018. *J. Epidemiol. Community Health* 72, 668–672.
- Clegg, B.S., Stephenson, G.R., Hall, J.C., 1999. *J. Agric. Food Chem.* 47, 5031–5037.
- Döring, J., Rettke, D., Rödel, G., Pompe, T., Ostermann, K., 2019. *Biosensors* 9, 104.
- Duke, S.O., 2018. *Pest Manag. Sci.* 74, 1027–1034.
- European Food Safety Authority, 2016. *EFSA J* 13, 4302.
- Funke, T., Han, H., Healy-Fried, M.L., Fischer, M., Schönbrunn, E., 2006. *Proc. Natl. Acad. Sci. U. S. A* 103, 13010–13015.
- Green, J.M., 2018. *Pest Manag. Sci.* 74, 1035–1039.
- Hennig, S., Rödel, G., Ostermann, K., 2016. *Sensors* 16, 602.
- International Agency for Research on Cancer, 2017. *IARC Monographs* 112, 321–399.
- Kwan, A.H.Y., Winefield, R.D., Sunde, M., Matthews, J.M., Haverkamp, R.G., Templeton, M.D., Mackay, J.P., 2006. *Proc. Natl. Acad. Sci. U. S. A* 103, 3621–3626.
- Limozin, L., Sengupta, K., 2009. *ChemPhysChem* 10, 2752–2768.
- Martin, S., Wang, H., Rathke, T., Anderegg, U., Möller, S., Schnabelrauch, M., Pompe, T., Schmidt, S., 2016. *Polymer* 102, 342–349.
- Ogi, H., Fukunishi, Y., Nagai, H., Okamoto, K., Hirao, M., Nishiyama, M., 2009. *Biosens. Bioelectron.* 24, 3148–3152.
- Pussak, D., Behra, M., Schmidt, S., Hartmann, L., 2012. *Soft Matter* 8, 1664–1672.
- Pussak, D., Ponader, D., Mosca, S., Pompe, T., Hartmann, L., Schmidt, S., 2014. *Langmuir* 30, 6142–6150.
- Pussak, D., Ponader, D., Mosca, S., Ruiz, S.V., Hartmann, L., Schmidt, S., 2013. *Angew. Chem. Int. Ed.* 52, 6084–6087.
- Ralston, J., Larson, I., Rutland, M.W., Feiler, A.A., Kleijn, M., 2005. *Pure Appl. Chem.* 77, 2149–2170.
- Reynoso, E.C., Torres, E., Bettazzi, F., Palchetti, I., 2019. *Biosensors* 9, 20.
- Rubio, F., Veldhuis, L.J., Clegg, B.S., Fleeker, J.R., Hall, J.C., 2003. *J. Agric. Food Chem.* 51, 691–696.
- Schmidt, S., Wang, H., Pussak, D., Mosca, S., Hartmann, L., 2015. *Beilstein J. Org. Chem.* 11, 720–729.
- Schönbrunn, E., Eschenburg, S., Shuttleworth, W.A., Schloss, J.V., Amrhein, N., Evans, J.N.S., Kabsch, W., 2001. *Proc. Natl. Acad. Sci. U. S. A* 98, 1376–1380.
- Selvi, A.A., Sreenivasa, M.A., Manonmani, H.K., 2011. *Food Agric. Immunol.* 22, 217–228.
- Székács, A., Darvas, B., 2018. *Front. Environ. Sci.* 6, 78.
- Tittlemier, S.A., Drul, D., Lake, B., Zirdum, T., Hammond, E., Sobering, D., Lin, W.J., Tran, M., Roscoe, M., 2017. *Cereal Chem.* 94, 1028–2036.
- Valle, A.L., Mello, F.C.C., Alves-Balvedi, R.P., Rodrigues, L.P., Goulart, L.R., 2019. *Environ. Chem. Lett.* 17, 291–317.
- Wang, H., Jacobi, F., Waschke, J., Hartmann, L., Löwen, H., Schmidt, S., 2017. *Adv. Funct. Mater.* 27, 1702040.
- Waschke, J., Pompe, T., Rettke, D., Schmidt, S., Hlawitschka, M., 2019. *PLoS One* 14, e0214815.
- Xu, J., Smith, S., Smith, G., Wang, W., Li, Y., 2019. *Food Contr.* 106, 106710.

Supplemental Information

Picomolar glyphosate sensitivity of an optical particle-based sensor utilizing biomimetic interaction principles

David Rettke, Julia Döring, Steve Martin, Tom Venus, Irina Estrela-Lopis, Stephan Schmidt, Kai Ostermann, Tilo Pompe

Determination of elastic modulus: Young's modulus of functionalized and glyphosate decorated SCPs was determined by means of scanning force microscopy using a NanoWizard 3 system (JPK instruments, Germany). Silica beads (Kisker, Germany) with a diameter of 10 μm were glued onto a tip-less cantilever (spring constant 0.03 N/m, CSC 38, μMasch , Bulgaria) and served as a probe for force indentation experiments. Several force curves were recorded for each sample of SCP and elastic moduli were calculated using a model of non-adhesive elastic contact developed by Glaubitz et al. (2014).

Fluorescence microscopy of functionalized SCPs: Successful coupling of linker molecules and glyphosate was assessed employing confocal laser scanning microscopy. In order to fluorescently label the SCPs, 500 μg of fluorescein isothiocyanate (1.28 μmol , Sigma Aldrich) was dissolved in 20 ml of 100 mM borate buffer (pH = 9.0, Sigma Aldrich) and 10 ml of the stock solution was added to each sample of the respective diamine linker or glyphosate functionalized SCPs. The reaction tubes were covered with aluminum foil and agitated for 2 h at room temperature. The excess solution was centrifuged and the SCPs were washed with water several times. The resulting SCPs were measured in Hepes buffer, pH 7.0 on a confocal laser scanning microscope (LSM 700, Zeiss, Germany).

Surface roughness determination: Root-mean-square roughness (RMS) of protein-coated glass slides was determined using a NanoWizard 3 system (JPK instruments). Images were acquired in Quantitative Imaging™ mode employing a Multi 75E-G cantilever (Budget Sensors, Bulgaria) and RMS-roughness was calculated by JPK Data Processing Software Version 4.2. applying the following equation, N being the number of pixels, z_i being the measured height at each pixel and \bar{z} being the average height of all pixels.

$$RMS = \sqrt{\frac{1}{N} * \sum_{i=1}^N (z_i - \bar{z})^2}$$

Confocal Raman microspectroscopy (CRM) analysis: SCPs functionalized with pentaglycine and glyphosate were dried on glass and subsequently analyzed by means of CRM using an Alpha300 R microscope (WITec GmbH, Ulm, Germany) equipped with a piezo-scanner (P-500, Physik Instrumente, Karlsruhe, Germany), multi-mode fiber (50 μm diameter) and a charge-coupled device (CCD) cooled down to -61°C . All measurements were conducted using laser wavelength of 532nm, 50x objective (Zeiss, EC "Epiplan-neofluar", NA (numerical aperture) = 0.8) and a 600 g mm^{-1} grating. The samples were scanned pixel-wise in x-y direction and processed using the Project FOUR PLUS software (WITec GmbH, Ulm, Germany). The chemical imaging of samples including different treatment steps, as a background subtraction, the de-mixture of recorded spectra and the decomposition of a data set into images of different components, is described elsewhere in detail (Blucher et al., 2019; Coelho et al., 2019; Ganassin et al., 2018).

References

- Glaubitz M., Medvedev N., Pussak D., Hartmann L., Schmidt S., Helm C. A., Delcea M., 2014. *Soft Matter*. 10, 6732-6741.
- Blucher C., Zilberfain C., Venus T., Spindler N., Dietrich A., Burkhardt R., Stadler S.C., Estrela-Lopis I., 2019., *Analyst*. 144, 5558-5570.
- Coelho J.M., Camargo N.S., Ganassin R., Rocha M.C.O., Merker C., Böttner J., Estrela-Lopis I., Py-Daniel K.R., Jardim K.V., Sousa M.H., Ombredane A.S., Joanitti G.A., Silva R.C., Azevedo R.B., Longo J.P.F., Muehlmann L.A., 2019. *J Mater Chem B*, 7, 6390-6398.
- Ganassin R., Merker C., Rodrigues M.C., Guimaraes N.F., Sodre C.S.C., Ferreira Q.D.S., da Silva S.W., Ombredane A.S., Joanitti G.A., Py-Daniel K.R., Zhang J., Jiang C.S., de Moraes P.C., Mosiniewicz-Szablewska E., Suchocki P., Longo J.P.F., Meijer J., Estrela-Lopis I., de Azevedo R.B., Muehlmann L.A., 2018. *Artif Cells Nanomed Biotechnol*, 46, 2002-2012.

Publication III

Biomimetic estrogen sensor based on soft colloidal probes

David Rettke, Florian Seufert, Julia Döring, Kai Ostermann, Dimitri Wilms, Stephan Schmidt, Tilo Pompe

Biosensors and Bioelectronics 192 (2021) 113506

Doi: [10.1016/j.bios.2021.113506](https://doi.org/10.1016/j.bios.2021.113506)

ISI Impact Factor 2020: 10.618



Biomimetic estrogen sensor based on soft colloidal probes

David Rettke^{a,*}, Florian Seufert^a, Julia Döring^b, Kai Ostermann^b, Dimitri Wilms^c,
Stephan Schmidt^c, Tilo Pompe^a

^a Institute of Biochemistry, Leipzig University, Johannisallee 21 – 23, 04103, Leipzig, Germany

^b Institute of Genetics, Technische Universität Dresden, Zellescher Weg 20b, 01217, Dresden, Germany

^c Institute of Organic Chemistry and Macromolecular Chemistry, Heinrich Heine Universität Düsseldorf, Universitätsstraße 1, 40225, Düsseldorf, Germany

ARTICLE INFO

Keywords:

Xenohormones
Estrogen
Steroids
Molecular recognition
Reflection interference contrast microscopy (RICM)
Optomechanical biosensor

ABSTRACT

An increasing number of reports substantiate the link between emerging estrogenic pollutants and a variety of adverse effects including developmental disorders, infertility, cancer and neurological disorders, threatening public health as well as environment. The detection of the diverse classes of estrogenic and antiestrogenic substances is still challenging due to analytics which needs to cover the whole range of compounds acting on estrogen receptors and the complex estrogen pathways. In this proof-of-concept study, we report a novel biomimetic detection scheme based on the specific recognition of estrogenic ligands by estrogen sulfotransferase 1E1 (SULT1E1), which acts as one of the key enzymes in estrogen homeostasis. SULT1E1 was site-specifically immobilized on transparent glass slides via a hexahistidine-tag in a multi-step procedure. Soft colloidal probes (SCPs) covalently functionalized with ligands of SULT1E1, namely estrone and estradiol 17-(β -D-glucuronide), served as adhesion probes. The various functionalization steps were analyzed and optimized using epifluorescence, confocal laser scanning as well as reflection interference contrast microscopy (RICM). A competitive SCP binding assay probing the elastic SCP deformation driven by the specific interaction between SCPs and the SULT1E1 decorated glass slides was employed in conjunction with an optical readout by RICM and automated image analysis to detect estrogenic compounds by their inhibition of SCP adhesion. This sensing concept has demonstrated exceptional specificity for estrogenic steroid compounds compared to structurally related substance classes and provides promising options for multiplexed assays and incorporation of other proteins of the endocrine system to fully capture the whole ensemble of hormonally active substances.

1. Introduction

Anthropogenic immissions of estrogens and xenoestrogens into water, foods and environment raised increasing concerns about growing threats to public health and ecological systems. At existing pollutant levels, these exogenous estrogenic substances potentially cause alterations of the functions of endocrine systems and consequently affect reproductive development, cause precocious puberty, feminization as well as reproductive disorders and induce premature menopause (Aks-glaede et al., 2006; Aravindakshan et al., 2004; Bolong et al., 2009). Moreover, a cause-and-effect link between elevated environmental estrogen levels and increased incidences of breast cancer in women and prostate cancer in men is vigorously debated (Moore et al., 2016; Nelles et al., 2011).

Consequently, a comprehensive monitoring of estrogen, xenoestrogen and potentially hazardous estrogen metabolite and prohormone

levels in final food products and environment is a mandatory prerequisite to secure consumer health and to clearly identify causal relationships between exposure levels of estrogens and incidence of presumably endocrine-related disease patterns as well as environmental damage. Omnipresence along with the structural diversity of substances affecting the balance of endocrine systems however, poses a demanding challenge to nowadays analytics, effective monitoring and reliable risk assessment. The inherent problem is well-reflected in the European Union's effort to protect water quality. As monitoring data of emerging pollutants are generally too sparse to determine the risk they pose to, in this case, aquatic systems, a surface water watch list for EU-wide monitoring of these substances was established in 2015 (Carvalho et al., 2015). Notably, the number of substances, or substance groups including estrone (E₁), estradiol (E₂) and ethinylestradiol (EE₂), to be analyzed by liquid-chromatography coupled tandem mass spectrometry (LC-MS/MS), had to be limited to 10 in order to "maintain monitoring

* Corresponding author.

E-mail address: david.rettke@uni-leipzig.de (D. Rettke).

<https://doi.org/10.1016/j.bios.2021.113506>

Received 25 April 2021; Received in revised form 6 July 2021; Accepted 12 July 2021

Available online 15 July 2021

0956-5663/© 2021 Elsevier B.V. All rights reserved.

costs at reasonable levels' (European Union, 2013). Such statements underscore the cost-intensiveness of these procedures, concomitantly limiting a comprehensive monitoring of estrogen levels in countries with lower economic performance. It follows at the same time, that the tremendous range of estrogenic substances, spanning plasticizers, pharmaceuticals, pesticides and many others, cannot be covered by a monitoring program using sophisticated detection schemes, like LC-MS/MS, even in highly developed countries.

To overcome the significant limitations of pure chemical analysis, several bioassays as well as biosensors were developed to measure estrogenicity, mostly as a sum parameter rather than quantifying single compounds (Arnold et al., 1996; Soto et al., 1995; Wilson et al., 2004). In-vitro bioassays are generally based on activation, inhibition or binding to physiological targets, i.e. estrogen receptors. They therefore expediently include compounds that "mimic" the action of naturally occurring substances. These approaches on the other hand do not aim at the numerous effects of xenoestrogens on estrogen synthesis, metabolism and the presence of inactive prohormones or prodrugs (Kunz et al., 2015; Zacharewski, 1997). Hence, an integrated testing strategy for safety assessment is highly demanded, which cannot be covered by single target tests (Wang et al., 2014).

In this context, natural enzymes acting on estrogen substance classes, like sulfotransferases (SULTs), may serve as an attractive biomimetic tool. Cytosolic sulfotransferases (SULTs) are critical enzymes in steroid homeostasis and play a pivotal role in detoxification of xenobiotics by sulfate conjugation (Gamage et al., 2006). Amongst these proteins, estrogen sulfotransferase (SULT1E1) exhibits the highest affinity for estrogens ($K_M = 5$ nM) in concert with a broad overlapping specificity for substrates that interact with estrogen receptors (Cole et al., 2010; Falany et al., 1995; Zhang et al., 1998). The unique architecture of the binding pocket additionally allows for complexation of C-17 esters of steroidal estrogens, i.e. prodrugs, including frequently prescribed pharmaceuticals and environmental contaminants (Kuhl, 2005). Furthermore, ubiquitous chlorinated and brominated flame retardants majorly exert their endocrine disrupting effect through binding and inhibition of SULT1E1 rather than by direct interactions with estrogen receptors, underlining the importance of this enzyme for estrogenicity assessment (Dorosh et al., 2011; Gosavi et al., 2013).

Taken together, SULT1E1 might serve as an important complement to the aforementioned analytical methods for monitoring food and environmental estrogenic pollutants. We therefore set off to integrate this enzyme into the recently established soft colloidal probe (SCP) assay, employing soft elastomeric microparticles for sensitive quantification of adhesion energies between SCPs and interacting inelastic surfaces in combination with simple and fast interferometric optical readout technologies, like reflection interference contrast microscopy (RICM). With this novel tool, some major drawbacks of cell and chromatographic/mass spectrometric methods can be overcome, in particular the necessity of well-equipped laboratories, trained personnel and time-consuming analysis procedures. In conjunction with fine tunable parameters like particle elasticity, ligand density and linker architecture, the working range and sensitivity can be adjusted, making the SCP assay an attractive platform for precise and convenient on-site detection of diverse analytes (Fischer et al., 2020; Rettke et al., 2020; Wang et al., 2017). The feasibility of this highly specific and sensitive biosensing concept even in the pM range has been proven in the areas of carbohydrate, pesticide as well as antibody detection, deserving a translation into a detection assay of estrogenic substances (Pussak et al., 2013; Rettke et al., 2020; Strzelczyk et al., 2017).

2. Materials and methods

2.1. Particle preparation

SCP particles were synthesized as described previously (Pussak et al., 2012; Wang et al., 2017). Briefly, 50 mg poly(ethylene glycol) diacrylate

(Mn 6000 Da, Sigma Aldrich, Germany) and 1 mg of the photoinitiator Irigacure 2959 (Sigma Aldrich) were added to 10 ml 1M sodium sulfate and vortexed until microscopic droplets were formed. The dispersion was photopolymerized using a Heraeus HiLite UV curing unit (Heraeus Kulzer, Germany) for 90 s. Next, the PEG SCPs were grafted with crotonic acid (Sigma Aldrich) as described earlier (Pussak et al., 2012; Wang et al., 2017). In short, water was exchanged by 10 ml ethanol, then 250 mg benzophenone (Sigma Aldrich) and 1.5 g crotonic acid were added. Subsequently, the mixture was flushed with nitrogen for 30 s before irradiating with UV light for 900 s. The resulting SCP particles were then washed with ethanol and PBS three times each. Young's elastic modulus of SCPs is analyzed by means of colloid force spectroscopy. Suitable SCPs exhibit a modulus of elasticity of approx. 20–40 kPa (Glaubitz et al., 2014; Schmidt et al., 2015), see also ESI.

2.2. Post-functionalization of SCPs

In order to enable specific interactions between SULT1E1 functionalized biochip surfaces and hydrogel probes, SCPs were first coated with the mono-protected diamine linker 1-(9-fluorenylmethoxycarbonylamino)-4,7,10-trioxa-13-tridecanamine (Fmoc-TOTA, IRIS Biotech, Germany) for introduction of amino groups employing active ester chemistry. For this purpose, 2 ml of an SCP suspension were washed with 2 ml of 100 mM MES buffer (pH = 5.3) and the supernatant was discarded after centrifugation (10 min, 1844 g). 6.2 mg (40 μ mol) of 1-ethyl-3-(3-dimethylaminopropyl)carbodiimide (EDC, Carbolution Chemicals, Germany) and 11.5 mg (100 μ mol) of *N*-hydroxysuccinimide (NHS, Sigma Aldrich, US) were dissolved in 2 ml of 100 mM HEPES buffer (pH = 7.0) and the SCPs were subsequently suspended in the solution. After 15 min of activation of the carboxyl groups, 50 μ l of a Fmoc-TOTA solution (2.4 mg, 5 μ mol) in HEPES buffer was added and the reaction was allowed to proceed for 1 h while agitating. After centrifugation (10 min, 1844 \times g) the supernatant was discarded and replaced by a 20% piperidine (Sigma Aldrich, US)/double deionized water (ddH₂O) mixture to deprotect amino groups. The particles were left in the solution for 10 min. Subsequently, SCPs were washed 3 times with ddH₂O prior to coupling of E₁ (Sigma Aldrich, US) or estradiol 17 β -D-glucuronide (E₂17G, Cayman Chemical, US).

E₁ was coupled to the particles by means of reductive amination. Therefore, 1 ml of an ethanolic estrone solution (2.6 mg, 9.6 μ mol) was prepared and added to the particle pellet. Next, 20 μ l of a 1 M NaOH solution containing 6.3 mg (100 μ mol) sodium cyanoborohydride (Sigma Aldrich, US) was prepared and added to the suspension for reaction under alkaline conditions. Alternatively, 6.3 mg (100 μ mol) sodium cyanoborohydride was dissolved in the ethanolic particle suspension and 20 μ l of glacial acetic acid was added for reaction under acidic conditions. The suspensions were left to react for 120 min in a rotator. After centrifugation and discarding the supernatant, the SCPs were washed three times with ethanol.

E₂17G was coupled to SCPs employing active ester chemistry. 2 mg (4.5 μ mol) E₂17G were dissolved in 1 ml of a 14% v/v dimethyl sulfoxide (DMSO)/100 mM Hepes solution (pH = 7.0). Subsequently 3.8 mg (24 μ mol) EDC and 5.8 mg (50 μ mol) NHS were added directly to the solution and left to form the reactive NHS-ester with the glucuronide for 15 min at room temperature. The reaction mixture was added to the previously centrifuged and decanted amino-terminal SCPs and allowed to react for 2 h in a rotator. Finally, the SCPs were washed 3 times with 100 mM HEPES buffer.

The introduction of glycolic acid (Sigma Aldrich, US) was performed to block residual unreacted NH₂-moieties after the initial estrogen coupling steps. 750 μ l of a glycolic acid solution (2.9 mg, 38 μ mol), activated with 2.3 mg (15 μ mol) EDC/4.3 mg (37 μ mol) NHS for 15 min in 100 mM HEPES buffer, were added to the SCP pellet and left to react for 2 h in a rotator. SCPs were washed several times with 100 mM HEPES buffer prior to use for subsequent experiments.

Young's elastic modulus of SCPs after functionalization was assessed

by colloid force spectroscopy, see ESI and Fig. S2.

2.3. Chip surface preparation

To prepare biochip surfaces for specific interaction with SCPs, glass coverslips (\varnothing 32 mm, Thermo Scientific, Germany) were placed in a Teflon rack and cleaned by sonication in double deionized water and ethanol (AppliChem, Germany) for 30 min each. To remove organic and particle contaminants from the surfaces, a mixture of 50 ml H_2O_2 , 35% (Grüssing, Germany), 50 ml 25% NH_3 aqueous solution (Merck, Germany) and 250 ml ddH_2O was heated to 60 °C on a hot plate and coverslips were left in the solution for 10 min. After rinsing twice with ddH_2O , the coverslips were dried in a nitrogen stream. Subsequently, a solution of 20 mM APTES in a 9:1 (v/v) mixture of isopropanol (AppliChem, Germany)/ ddH_2O was prepared using 225 ml isopropanol, 25 ml ddH_2O and 1.16 ml (5 mmol) 3-aminopropyltriethoxysilane (Alfa Aesar, US). The cover glasses were left in the solution for 120 min, washed thoroughly with isopropanol and dried using a nitrogen flow prior to annealing for 60 min at 120 °C.

The amine functionalized coverslips were placed in a 60, 120, 180 or 240 mM solution of succinic anhydride (Merck, Germany) in 250 ml tetrahydrofuran (THF, AppliChem, Germany) respectively, left to react for 60 min at room temperature and washed twice with THF and ddH_2O . The COOH-groups were subsequently activated by addition of 2 ml of a solution containing 3.8 mg (40 μmol) EDC/21.7 mg (100 μmol) sulfo-NHS (Carbolution Chemicals, Germany) per slide and allowed to react for 30 min to form active esters. After washing twice with MES buffer and once with HEPES buffer, a 20 mM solution of N_α,N_α -bis(carboxymethyl)-L-lysine (NTA- NH_2 , Sigma Aldrich, US) in HEPES buffer was added to the surfaces and allowed to react for 2 h at room temperature. The supernatant was discarded and the coverslips were again washed twice with HEPES buffer. Subsequently, each of the coverslips was treated with 1.5 ml of a 20 mM (7.5 mg/ml) Na_2EDTA solution and left for 30 min to remove metal contaminations prior to Ni-chelation. The supernatant was discarded and the surfaces were rinsed with ddH_2O and 100 mM HEPES buffer containing 200 mM imidazole (Sigma Aldrich, US), pH = 7.0 several times before addition of 2 ml of a 20, 50 100, 150 or 200 mM NiSO_4 (Sigma Aldrich, US) solution to each slide. After 2h, the coverslips were rinsed with ddH_2O as well as HEPES buffer, dried using pressurized N_2 , and hexahistidine - green fluorescent protein (his₆-GFP; Sino Biological, PRC) or SULT1E1 - hexahistidine (SULT1E1-his₆; Prospec, Israel) was immobilized by means of the his₆-tag. Therefore, solutions of his₆-GFP (25 $\mu\text{g}/\text{ml}$) and SULT1E1-his₆ (5 $\mu\text{g}/\text{ml}$) in 1x PBS (VWR, US), 10 mM imidazole, pH = 7.4 were prepared and 2 ml were carefully pipetted onto each slide. After 2 h of incubation, the slides were finally washed 3 times with 1x PBS buffer containing 10 mM imidazole.

2.4. Fluorescence microscopy of functionalized SCPs and biochips

Successful coupling of linker molecules, estrone and estradiol 17 β -D-glucuronide as well as chip surface functionalization was assessed employing confocal laser scanning microscopy (cLSM, LSM700, Zeiss, Germany). In order to fluorescently label the SCPs and chip surfaces, 500 μg of fluorescein isothiocyanate (1.28 μmol , Sigma Aldrich) was dissolved in 20 ml of 100 mM borate buffer (pH = 9.0, Sigma Aldrich, US) and 1.5 ml of the stock solution was added to each sample of the functionalized SCPs or coverslips. The reaction tubes and coverslips were protected from light and reacted for 1 h at room temperature. Excess solution was discarded and the samples were washed with HEPES buffer 3 times.

For verification of functionalization of E₂17G-coated SCPs, a similar procedure was conducted. 500 μg carboxyfluorescein succinimidyl ester (FAM-SCM, Sigma Aldrich, US) was dissolved in 20 ml of 100 mM HEPES buffer (pH = 7.0, Sigma) and 1.5 ml of the stock solution was added to each sample of the functionalized SCPs, reacted for 1 h at room

temperature, washed thoroughly and finally analyzed via cLSM. The resulting fluorescently labelled SCPs and chip surfaces were analyzed in HEPES buffer at pH 7.0.

All stained samples were excited using a 488 nm laser line. FITC stained surfaces and SCPs were imaged using an LCI Plan-Neofluar 63x/1.3 oil immersion objective (Zeiss, Germany) and areas of 105.2 \times 105.2 μm (512 \times 512 pixel, 4.87 pixels/ μm) were recorded. To avoid rapid photobleaching of labelled samples, the pinhole was set to 10.8 airy units to allow for imaging with very low laser intensities. For evaluation of the data obtained, a fit was applied due to the dependence of fluorescence intensities on the SCP diameter. Detailed information is given in the ESI. For fluorescence intensity profiles of cross-sectional areas of FITC stained SULT1E1 coated surfaces, a 20 pixels median filter was applied and areas of 100 \times 14.4 μm in the center of the images ($y = 52.6 \mu\text{m}$) were analyzed to minimize the impact of noise on the analysis. Standard deviation of fluorescence intensities was calculated from the intensity distribution in x-direction of the cross-sectional areas.

For examinations of FAM-SCM stained SCPs via cLSM, a water immersion objective (C-Apochromat, Zeiss, Germany) with 40 \times magnification and a numerical aperture of 1.20 was used. The pinhole was set to 1 airy unit. In order to analyze sedimented SCPs, areas of 320.08 \times 320.08 μm (512 \times 512 pixels, 1.60 pixels/ μm) were recorded and the mean grey value (fluorescence intensity) of each particle was calculated based on the fluorescence intensity within the corresponding x-y plane. No fitting was necessary in the case of FAM-SCM stained SCPs.

2.5. Reflection interference contrast microscopy (RICM) measurements

RICM was used to examine surface homogeneity of functionalized coverslips, to investigate the effect of estrogen functionalization on the SCPs and for final estrogen detection assays. For analysis of coated coverslips, the coverslips were clamped into a Teflon rack, covered with 2 ml of ddH_2O and examined via RICM. SCP evaluation was conducted in 400 μl wells. Therefore untreated coverslips (\varnothing 32 mm, Thermo Scientific, Germany) were adhered to a sticky-slide 16 well (Grace Biolabs, US) and each surface was covered with 200 μl of 100 mM HEPES-buffer pH = 7.0. 20 μl of the respective SCP solution was carefully pipetted into the wells, allowed to sediment for 20 min and the particles were subsequently investigated. For estrogen specificity testing, SULT1E1 coated coverslips were adhered to sticky-slide 16 wells and each surface was incubated with 200 μl of HEPES-buffer as a positive control or the respective analyte solution for 30 min. Analyte solutions were prepared as saturated hormone solutions (progesterone: 28 μM , testosterone: 81 μM , ethinylestradiol: 38 μM) with the exception of estrone (100 μM). Afterwards, 20 μl of a suspension containing E₂17G functionalized SCPs were added dropwise. After 30 min, sedimentation of the SCPs was completed and interference patterns were imaged using an inverted microscope (Olympus IX73, Germany) with an integrated halogen lamp for bright-field microscopy. To obtain interference reflection patterns, samples were illuminated by a monochromatic 530 nm collimated LED (M530L2-C1, Thorlabs, Germany) in reflection mode using a 60x, NA (numerical aperture) 1.35 oil-immersion objective (UPlanSApo 60 \times 1.35 oil, Olympus, Germany). Images were captured with a monochrome CCD camera (DMK 23U274, ImagingSource, Germany) using μ Manager microscopy software. All datasets were recorded applying an exposure time of 50 ms and stored in tagged image file format (tiff).

2.6. Data analysis of RICM measurements

Obtained images of radial profiles resulting from the adhering or non-adhering SCPs were analyzed by a home-built software based on pattern matching using the routinely analyzed Young's elastic modulus of SCP of roughly 20 kPa (Waschke et al., 2019). Adhesion energies were calculated by the software.

3. Results and discussion

3.1. Experimental setup

In our experimental setup, as outlined in Fig. 1, a SULT1E1-his₆ fusion construct was immobilized on a transparent coverslip presenting Ni²⁺-NTA to generate the protein-functionalized biochip. Estrogenic ligands of the estrogen binding domain of SULT1E1 were conveniently coupled to amine-functionalized SCPs by either reductive amination or active ester chemistry. The so-equipped SCPs are able to specifically interact with the SULT1E1 decorated biochip and form a distinct contact area. A simple, low-cost optical readout of contact area and SCP size, realized by RICM, facilitates calculation of the related adhesion energies by means of the Johnson-Kendall-Roberts-model of elastic contact (Johnson et al., 1971):

$$a^3 = 6\pi \frac{W}{E_{eff}} R^2 \quad (1)$$

where a is the radius of contact, W the adhesion energy of an SCP and a hard surface, R the radius of the SCP and E_{eff} the effective elastic modulus of the probe ($E_{eff} = 4E/(3(1-\nu^2))$; E - Young's modulus, ν - Poisson ratio). Detection of estrogenic substances was carried out in a straightforward competitive binding assay. The presence of analytes within a sample solution causes a concentration dependent loss of accessible binding sites for SCP-tethered ligands, leading to a differential reduction of the SCP-biochip interfacial area. Thus, the concentration of an analyte in the solution is directly related to the adhesion energy. The general principle of analyte detection is depicted in Fig. 1.

At first, one has to consider the SULT1E1 binding principle of estrogens in order to functionally mimic this situation in the SCP assay. The structure of the used SULT1E1-his₆ and the binding pocket of SULT1E1 for estrogens and xenoestrogens are schematically illustrated in Fig. 2a. The C-terminal his₆-tag of SULT1E1-his₆ is approximately situated opposite to the estrogen binding pocket on a flexible C-terminal

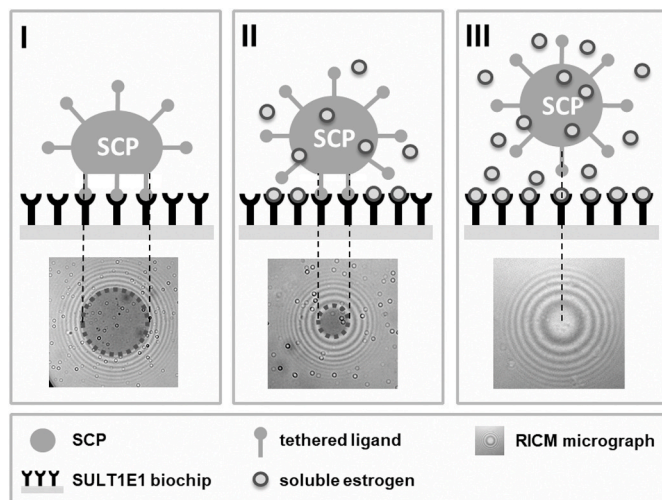


Fig. 1. General principle of estrogen detection using the SCP assay. A transparent biochip is coated with SULT1E1 (black symbols), capable of binding estrogens (pale grey spheres with black borders) and the number of residual binding sites declines with increasing analyte concentration. SCPs functionalized with ligands of SULT1E1 (grey spheres) approach the biochip and form a distinct contact area with the biochip surface. I) The SCP strongly adheres to the SULT1E1 binding sites, resulting in an elastic SCP deformation and an extended contact area. II) Increasing the analyte concentration decreases the number of available binding sites and the SCP adhesion and contact area declines, until the SCP cannot bind to the biochip surface anymore (III). The lowest panel indicates RCM model images of the respective adhering and non-adhering SCPs.

loop of SULT1E1, assuring optimum accessibility for estrogenic ligands. In contrast, the N-terminus is in close proximity to the ligand binding domain and N-terminal modifications are therefore expected to interfere with ligand binding by either shielding the binding site or causing an unfavorable orientation of the immobilized enzyme. The visualized estrogen-SULT1E1-complex shows the alignment of estradiol within the enzyme's binding pocket. As can be seen, the C-17 β -OH group of estradiol and C-17-keto group of estrone point outward the binding domain and can therefore be used for functional modifications, i.e. for coupling the molecules to SCPs without loss of affinity of the conjugated estrogen.

3.2. Biochip functionalization

For site-directed immobilization of proteins bearing a hexahistidine (his₆) sequence, a multistep procedure for generating surfaces presenting Ni²⁺ chelated by NTA was established, which is schematically outlined in Fig. 2b. Freshly oxidized glass coverslips were silanized to introduce amino groups, which were subsequently converted into carboxy groups via treatment with succinic anhydride in THF. These functional groups in turn allow for covalent coupling of NTA-NH₂ via the amino group using active ester chemistry. After charging NTA with Ni²⁺, the surfaces were loaded with the respective protein, which forms a stable complex by interaction of the his₆ sequence with the presented Ni²⁺-NTA.

To generate SULT1E1 biochips, amine functionalized surfaces were treated with 60, 120, 180 or 240 mM succinic anhydride to introduce carboxy groups. The 240 mM solution yields nearly complete conversion of amino groups and was therefore used for all follow up experiments (see ESI). Next, the carboxy terminated slides were functionalized with NTA-NH₂ using active ester chemistry. Subsequently, surfaces were charged with 20, 50, 100, 150 or 200 mM NiSO₄ solutions to closely examine the impact of Ni²⁺ concentrations on surface homogeneity, which is a key indicator for highly sensitive measurements of interfacial surface areas by the SCP assay. As can be seen from Fig. 3a, deposits of impurities are encountered with significantly higher frequency on surfaces treated with highly concentrated NiSO₄ solutions, hence coverslips charged with 150 and 200 mM solutions can be regarded inapplicable for the envisioned assay and were therefore not further investigated.

After the Ni²⁺ charging step, the biochip surface was functionalized with SULT1E1-his₆ and stained with FITC for assessment of protein immobilization capacity and homogeneity of the resulting protein layer in dependence on the NiSO₄ concentration. cLSM measurements of the stained biochips revealed only a minor correlation of fluorescence intensities of FITC-stained SULT1E1 coatings with the NiSO₄ concentration (see Fig. 2b and c), indicating saturation of the immobilized NTA moieties and saturated protein immobilization even at a NiSO₄ concentration of 20 mM. For verification of protein immobilization via his-tag, analogous experiments were conducted using his₆-GFP instead of SULT1E1-his₆ and FITC labelling. A bare NTA functionalized slide served as a control. Although his₆-GFP shows some unspecific binding to NTA slides, site-directed immobilization of the protein via his₆-tag could be validated by the clear increase of the fluorescence intensity after Ni²⁺ charging (20 mM NiSO₄). Additionally, the homogeneity of the FITC-stained SULT1E1 coated biochips was examined in more detail, as cLSM images showed irregular structures at a NiSO₄ concentration of 100 mM (Fig. 2b). Intensity profiles of cross-sectional areas for each slide were evaluated as well (Fig. 2d). The intensity variations positively correlated with the amount of NiSO₄ used for charging of NTA-coated slides. An analysis of the intensity standard deviation of these cross-sections showed the lowest variation and hence the most homogeneous surface for the 20 mM NiSO₄ condition (Fig. 2e). Taken together, these results indicate saturation of the immobilized NTA moieties even at low concentrations of NiSO₄. Concentrations above 20 mM of the charging solution led to formation of detrimental deposits on the surfaces. In the light of these findings and in view of potential risks that

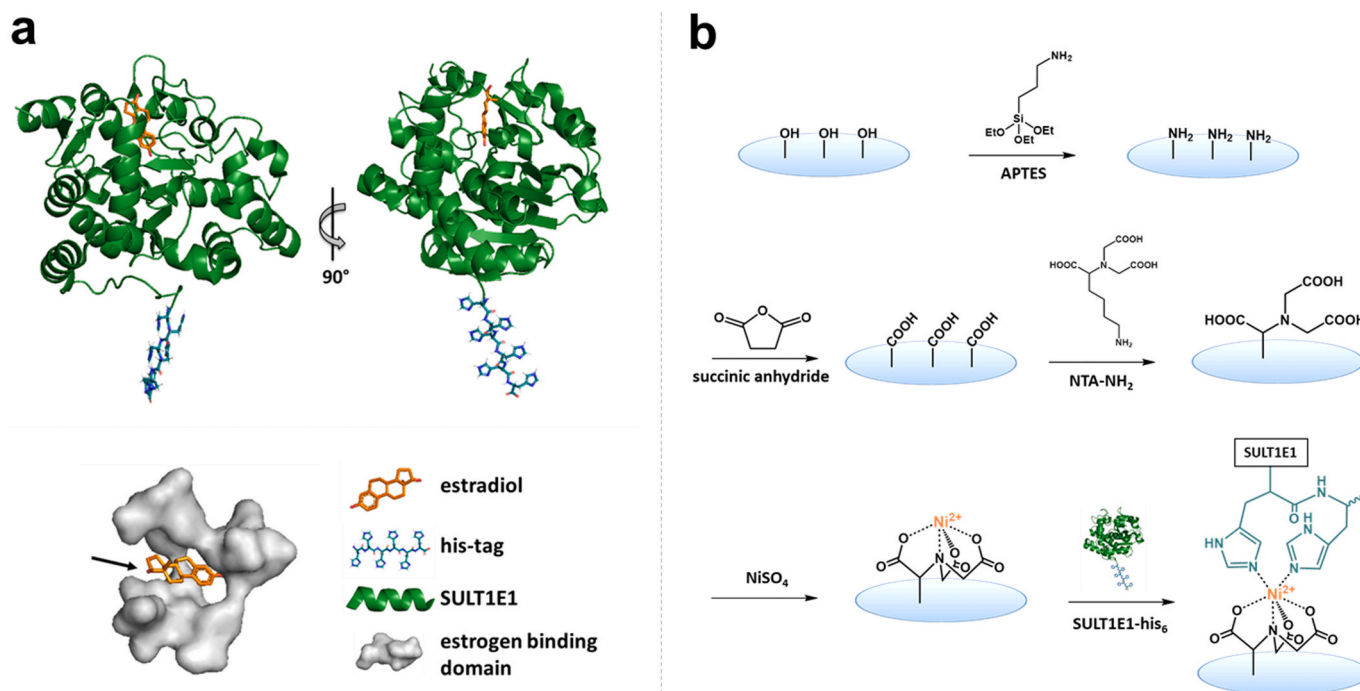


Fig. 2. Schematic representation of the used SULT1E1 - estradiol binding site and surface coating procedure for site-specific SULT1E1 immobilization on the transparent biochips. **a) Upper panel:** SULT1E1 (green) is expressed as a fusion construct, bearing a C-terminal his₆ sequence (blue) connected to a flexible loop of the enzyme. Estradiol (orange) is known to bind to the estrogen binding domain of SULT1E1, which is located approximately on the opposite site of the his₆ sequence. The his₆ sequence has no preferred secondary structure and is displayed in linear zigzag conformation for better visualization. **Lower panel:** Orientation of estradiol within the binding pocket shows functional groups of estrogens which are not involved in interactions with the enzyme, e.g. the C-17 β -OH group of estradiol and the C-17-keto group of estrone (black arrow). The estradiol-SULT1E1-his₆ complex was modified from PDB identification code 4JVL. SULT1E1 estrogen binding domain was modelled according to Cole et al. (2010). **b) Surface functionalization strategy:** Silanol groups of a glass coverslip are functionalized with NTA in a multistep procedure, including treatment with APTES, succinic anhydride and NTA-NH₂. Ni²⁺ charging of NTA functionalized glass slides allows for immobilization of proteins presenting a his₆ sequence. (For interpretation of the references to colour in this figure legend, the reader is referred to the Web version of this article.)

impurities and non-uniform coatings present for sensitive measurements of interfacial adhesion energies, all follow-up experiments were conducted using 20 mM NiSO₄ charged Ni²⁺-NTA surfaces.

3.3. SCP functionalization

The second component of the biosensor encompasses estrogen functionalized SCPs, capable of specifically interacting with SULT1E1 decorated biochips. E₁ as well as the estradiol metabolite E₂17G were selected for functionalization as both are substrates of SULT1E1 and bear functional groups or substituents at C-17 of the steroid scaffold that can be coupled to SCPs conveniently and under comparatively mild conditions (Sun et al., 2010). Tethering steroid estrogens via C-17 substituents is preferred for the envisioned assay, as these groups are not involved in interactions with SULT1E1.

Carboxy functionalized SCPs were prepared according to the procedure established by Pussak et al., (2012) and post-functionalized as depicted in Fig. 4. A diamine linker was coupled to the SCPs first to introduce amino groups, requisite for conjugating the selected estrogens to the SCPs. The Fmoc protecting group prevents SCP crosslinking during amine functionalization of the SCPs. NaBH₃CN was used for reduction of the Schiff base formed from SCP-amine and estrone-keto group. Alternatively, the carboxy group of the glucuronic acid moiety was utilized for coupling E₂17G by means of active ester chemistry.

Both coupling strategies were evaluated employing FITC staining of amino groups and analyzed by cLSM. The results shown in Fig. 5a indicate successful coupling of E₁ and E₂17G to SCPs, as these reactions are accompanied by consumption of amino groups. The decline of fluorescence intensities can be correlated to the number of estrogen molecules coupled to the respective SCP. It can be concluded that reductive amination is more efficient in the presence of NaOH (basic

than under acidic conditions. To prevent disturbances of subsequent RICM assays by charged residual amino groups, an additional coupling step was performed utilizing glycolic acid (gly) for conversion of these groups into hydroxyls. This quenching of remnant amino groups resulted in a low fluorescence signal, which is likely to be attributed to unspecific binding or entrapment of dye molecules in the SCP's polymer meshwork.

Eligibility of the respective estrogen functionalized SCPs was assessed by probing interfacial areas between SCP and glass surface by means of RICM (Fig. 5b and c). The resultant micrographs revealed that E₁ functionalization is steadily accompanied by irregularities of the interference patterns. Very bright as well as dark spots visible at the SCP-surface interface indicate areas of high reflectivity arising from a locally increased density. This effect might be a result of local deposits, aggregation of poorly soluble E₁ molecules during solvent exchange or degradation of the SCPs due to comparatively harsh pH conditions for both reductive amination protocols. Besides this, a considerable proportion of SCPs showed non-circular Newtonian fringes, detrimental to accurate quantification of contact areas as well as SCP radii. Additionally, SCPs coupled under acidic conditions showed a strong tendency to aggregate rather than being homogeneously suspended. Taken together these results led us to conclude to E₁-functionalized SCPs to be unsuitable for the envisioned assay. However, E₂17G functionalized SCPs showed none of these effects and were hence selected for follow-up experiments.

In a final step, the E₂17G functionalization strategy was validated employing cLSM analysis of carboxy fluorescein succinimidyl ester (FAM-SCM) stained SCPs. FAM-SCM is similarly utilized for staining of amino groups but shows better specificity compared to FITC. The results from the initial characterization (see above) could be validated as the fluorescence signal of the SCPs was markedly decreased after coupling

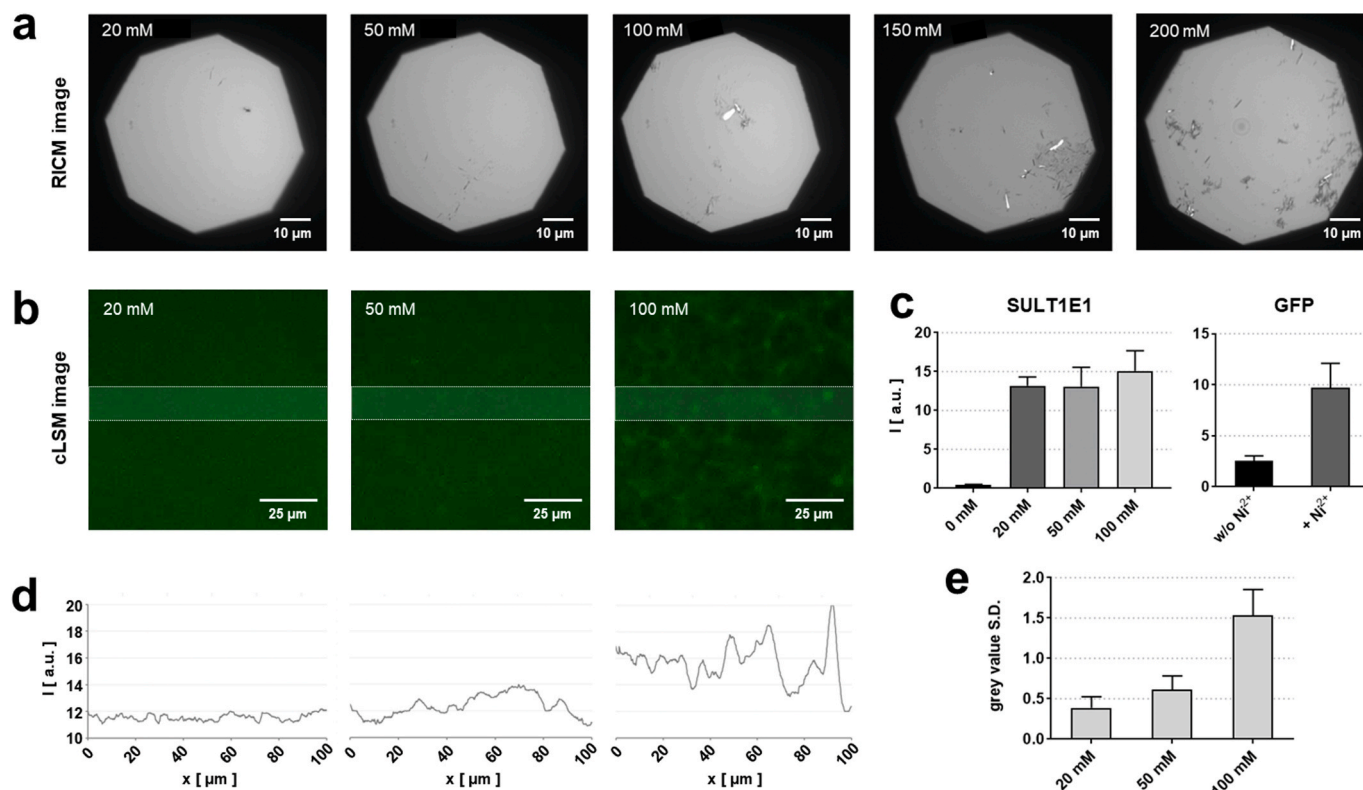


Fig. 3. RISM, cLSM and homogeneity assessment of Ni^{2+} -NTA functionalized and protein coated biochip surfaces. a) NTA-functionalized glass slides were charged with NiSO_4 at different concentrations and surfaces were examined by RISM. Increasing amounts of NiSO_4 progressively caused deposition of impurities onto surfaces. b) SUL1E1-coated and FITC stained surfaces were analyzed using cLSM to evaluate the impact of NTA-charging with 20, 50, 100, 150 and 200 mM NiSO_4 solutions on subsequent protein immobilization. c) Fluorescence intensity analysis of FITC-stained SUL1E1-coated surfaces with 9 cLSM images per slide (3 samples per condition) in dependence on NiSO_4 concentration (left). Protein immobilization was verified using his₆-GFP- and a NTA surface charged with 20 mM NiSO_4 (right). Error bars indicate S.D. d) Representative fluorescence intensity profiles of cross-sectional areas (semi-transparent overlay in b) of FITC-stained SUL1E1-coated surfaces. e) Averaged standard deviations of intensity profiles of cross-sectional areas (9 cross sections per sample, 3 samples per condition). Error bars indicate S.D.

E_2 17G to amine functionalized SCPs (Fig. 5d). The averaged fluorescence intensity of E_2 17G + gly functionalized SCPs was at a level comparable to the reference, i.e. unfunctionalized SCPs, which can be regarded as a measure of unspecific binding of dye molecules. This experiment shows a similar trend to Fig. 5a (right), supporting the reproducibility of SCP functionalization with E_2 17G + gly, although it should be noted that the experimental setups differ slightly.

3.4. SCP-based estrogen sensing assay

Having established and optimized biochip and SCPs for adhesion measurements, we finally tested our detection system, employing binding assays in the presence and absence of soluble ligands of immobilized SUL1E1. Estrone (E_1) and ethinylestradiol (EE_2) were selected as representative natural and synthetic estrogens. These compounds function as competitors of SCP tethered ligands, occupying available binding sites of SUL1E1 presented by the biochip. This blocking of the binding sites should result in a reduction of adhesion between SCP and chip surface, consequently decreasing adhesion energies and contact areas of SCPs. To show the specificity of the assay, the respective biochips were also incubated with testing solutions containing testosterone (T) and progesterone (P_4) representing the group of androgens and progestogens as negative controls. Estrogens, androgens and progestogens span all classes of gonadal steroids and were chosen because of the significant structural similarities and the associated complexity to distinguish between these compounds. The specificity of the interactions between SCP-tethered ligands and biochip was additionally addressed by comparing adhesion energies of SUL1E1-coated

chips and bare Ni^{2+} -NTA-functionalized surfaces without competitors.

Fig. 6 shows that E_2 17G-functionalized SCPs adhered strongly to SUL1E1 decorated biochips (reference), whereas without SUL1E1, a negligible adhesion to the surface was observed. This result indicates the general specificity of interactions between SCP-tethered ligands and biochip. Comparison of adhesion energies under reference conditions with biochips incubated with saturated solutions of P_4 and T do not reveal any impact of progestogen and androgen on SCP binding to immobilized SUL1E1. In sharp contrast, both estrogens, i.e., E_1 and EE_2 , markedly diminish adhesion energies by roughly 70%, demonstrating the selective occupation of estrogen binding sites of SUL1E1 by soluble as well as SCP tethered ligands. Taken together, these results confirm that estrogen analytes can be clearly distinguished from other structurally related substance classes, proving the general feasibility and adequate specificity of our sensing concept.

Identifying, detecting and quantifying estrogenic compounds is of vast importance for assessing and monitoring implications for public health and the environmental status. The requirements for the particular analytical method vary greatly depending on the field of application. In this proof-of-concept study, the ability of the assay to discriminate steroidal estrogens (E_1 and EE_2) from non-steroidal estrogens (T, P_4) was demonstrated using saturated hormone solutions (EE_2 : 38 μM , T: 81 μM , P_4 : 28 μM) and a 100 μM estrone solution, respectively.

In view of the ever-growing list of compounds potentially exerting estrogenic effects and the numerous physiological effects of estrogens, novel methods for rapid screening of this diverse group of substances, which includes industrial chemicals, natural products, pharmaceuticals, etc., are highly demanded. Because of the complexity of testing and

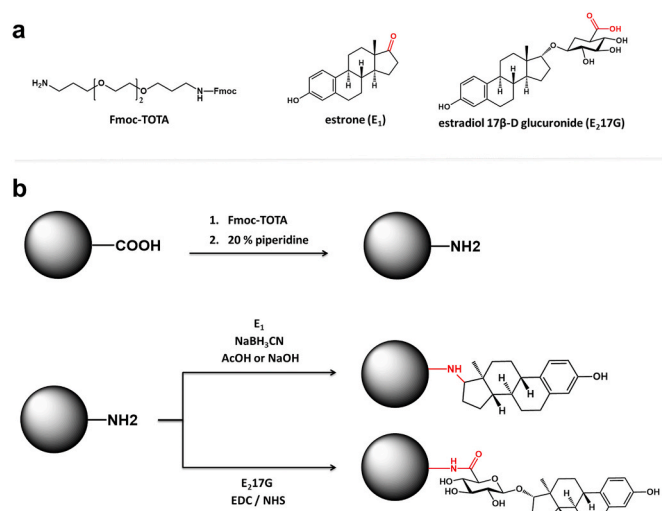


Fig. 4. Workflow for estrogen functionalization of SCPs. a) Compounds for the functionalization of SCPs. Fmoc-TOTA serves as a mono-protected linker for the introduction of amino groups. Estrone (E_1) as well as estradiol 17 β -D-glucuronide (E_217G) are coupled to the SCPs by either keto or carboxy groups. Functional groups employed for coupling are highlighted in red. b) General procedure of SCP functionalization. Amino groups are introduced to carboxy functionalized SCPs by Fmoc-TOTA and subsequent deprotection by treatment with piperidine. E_1 and E_217G are conjugated to the SCPs by reductive amination and active ester chemistry, respectively. E_1 is coupled via the keto group using cyanoborohydride under acidic (acetic acid, AcOH) or basic (sodium hydroxide, NaOH) conditions. As a second strategy, the carboxy group of the glucuronic acid moiety of E_217G is reacted with the presented amino groups employing active ester chemistry. (For interpretation of the references to colour in this figure legend, the reader is referred to the Web version of this article.)

identifying all of these compounds, establishing a single “gold standard” analytical method is unrealistic, and it is widely recognized that multiple in vitro and in vivo assays must be used together to comprehensively evaluate the effects of these compounds on estrogen homeostasis. The herein described new SCP-based assay, which uses immobilized SULT1E1 as a recognition element, can help identify and prioritize compounds that are overlooked by estrogen receptor-based assays but exert indirect effects by binding to SULT1E1. In this scenario, superior sensitivity of the assay compared to established methods is not a requirement, but special efforts should be made to establish a high-throughput and cost-effective platform. The United States Environmental Protection Agency published guidelines for competitive ligand binding assays within the framework of the Endocrine Disruptor Screening Program (United States Environmental Protection Agency, 2009). This Method employs rat uterine cytosol containing estrogen-receptors and radiolabeled estradiol. The disadvantages of this approach are the necessity of specialized laboratories and personnel to handle radioactivity and the necessity to sacrifice animals. These obstacles can be overcome by the proposed SCP-based assay, as the recognition elements are used in the form of recombinant proteins and this method does not require labelled molecules. However, for the envisioned application, additional validation is necessary and the implementation of additional recognition elements, such as recombinant estrogen receptors etc., might be a useful extension for a comprehensive identification of estrogen-like compounds.

Besides this application, the SCP-based assay can be a useful tool for diagnostic approaches in a clinical setting. Estrogen imbalance is associated with numerous adverse outcomes, including precocious or delayed puberty, menstrual problems and infertility. In addition, estrogen levels need to be monitored as part of fertility and menopause treatment, and abnormal estrogen levels can result from estrogen-producing tumors. Physiological serum estrone and estradiol levels

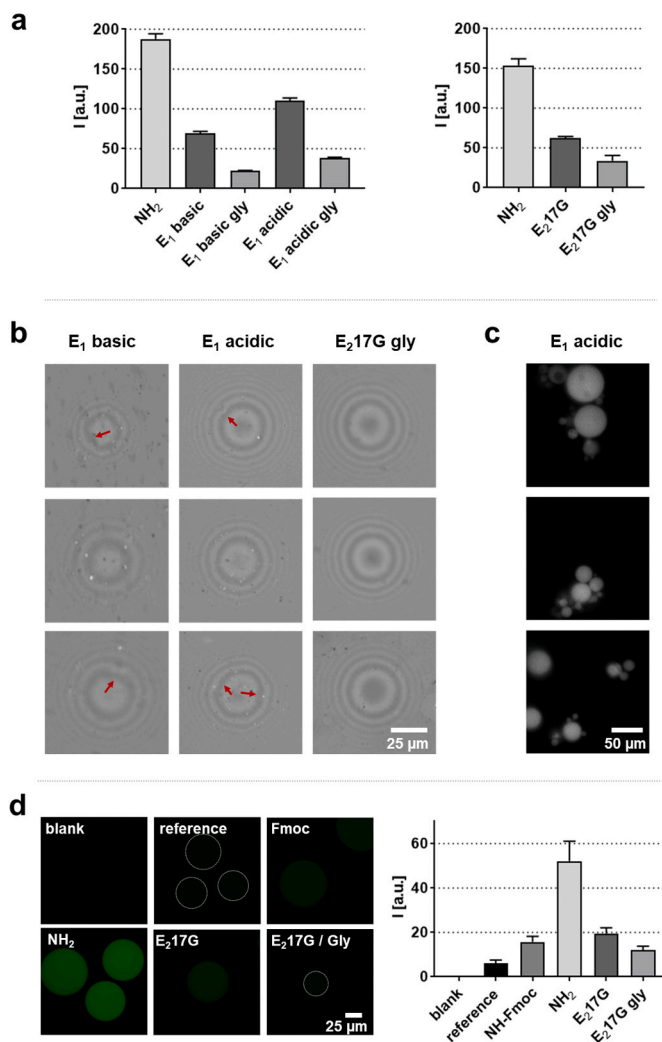


Fig. 5. Characterization of SCP functionalization using cLSM and RICM. a) cLSM images of FITC stained SCPs. Intensities after E_1 and E_217G coupling to amine functionalized SCPs using basic and acidic reductive amination and active ester chemistry as coupling strategies are shown. Quenching of remnant amino groups was achieved by reacting SCPs with glycolic acid (gly). At least 20 SCPs were measured per condition. Error bars indicate S.E. b) RICM images of estrogen coated SCPs. E_1 functionalized SCPs reveal irregular spots (white and grey dots) and non-circular Newtonian fringes, as indicated by red arrows. c) Representative fluorescence micrographs of SCPs treated with E_1 under acidic conditions. d) cLSM studies documenting all steps of E_217G SCP functionalization, employing carboxyfluorescein succinimidyl ester staining. Amine-functionalized SCPs reveal high fluorescence intensities after deprotection (NH_2), which drops stepwise in the course of E_217G and glycolic acid (quenching) coupling. Faintly visible SCPs (reference, E_217G /gly) are highlighted by dashed white circles. An averaged intensity value of 60 SCPs per condition is represented in the right plot with error bars indicating S.D.

(pregnancy not included) depend on gender, age and stage of the menstrual cycle and are typically in the pg/ml range (Stanczyk and Clarke, 2014). However, extremely low estradiol levels (<1 pg/ml) can be found in patients treated with aromatase inhibitors. Serum concentrations up to 10 ng/ml are typical during ovarian stimulation in women with infertility, and estrogen monitoring is particularly useful in assessing treatment response. In this proof-of-concept study, concentrations of estrogens (E_1 , EE_2) in the μ g/ml range were used. Therefore, further experiments are required to evaluate the suitability of the SCP-based assay in terms of the required sensitivity for such applications.

In the clinical setting, both immunoassays and mass spectroscopy

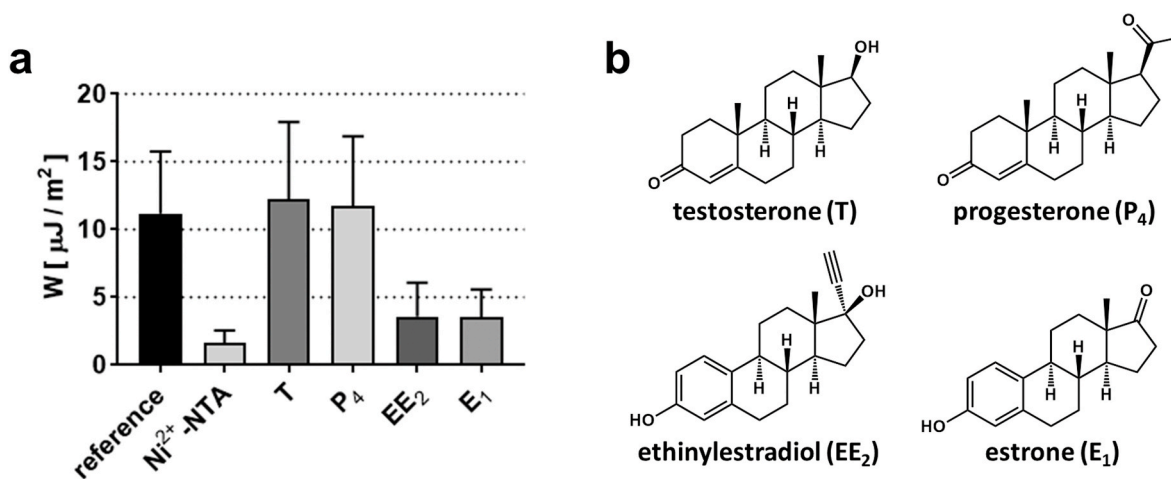


Fig. 6. Proof of concept for the specific detection of estrogens. a) The plot shows SCP adhesion energies determined by the SCP assay using RICM. E_2 17G-functionalized SCPs adhere strongly to the reference surface (SULT1E1-coated chip in absence of competitors), whereas SCPs show negligible interactions with the bare Ni^{2+} -NTA-coated chip. The adhesion energy is markedly diminished in presence of the estrogens ethinylestradiol (EE_2) and estrone (E_1) but is not affected by soluble testosterone (T) or progesterone (P_4). At least 40 SCPs are determined per condition and each individual particle is defined as a sample. Error bars indicate S.D. b) structures of tested estrogens and structurally related compounds.

methods are routinely used (Denver et al., 2019; Stanczyk and Clarke, 2014). Liquid chromatography-tandem mass spectroscopy (LC-MS/MS) is the superior method in terms of sensitivity, allows discrimination between different estrogens and their metabolites, and can be multiplexed for high throughput, but usually requires derivatization of the analytes and clinical implementation is often not cost and time efficient (Keski-Rahkonen et al., 2015; Wu and French, 2013). Direct (non-extraction) immunoassays are comparatively inexpensive and provide rapid results, but suffer from antibody cross-reactivity, matrix effects, and suboptimal sensitivity (Demers et al., 2015). The SULT1E1-based assay is capable of distinguishing estrogenic steroids from non-estrogenic steroids but not between E_1 , E_2 and EE_2 . Therefore, this assay provides a rapid testing platform for total estrogen levels, whereby immunoassays and LC-MS/MS are both capable of measuring the concentration of a particular estrogen. In addition, it should be noted that C-17 conjugated steroid estrogens contribute to cross-reactivity and overestimation of total estrogen levels, which calls into question the suitability of this assay for clinical applications (Gamage et al., 2006; Schrag et al., 2004). From a technical perspective, implementation of the current microscopy-based SCP assay readout for rapid and cost-efficient estrogen monitoring is not feasible, as this approach requires specialized optical instruments. However, current efforts are focused on transferring this technology to a portable optical device that allows convenient integration into clinical laboratory routines and environmental as well as process monitoring procedures.

4. Conclusions

We presented a novel approach for the detection of estrogenic small molecules employing the recently established SCP biosensing methodology in conjunction with the naturally occurring estrogen binding enzyme SULT1E1, which is a key enzyme for maintenance of estrogen balance. A transparent SULT1E1 biochip was generated by immobilizing the enzyme via his₆-sequence on Ni^{2+} -NTA functionalized glass coverslips. In this context, especially the NiSO_4 charging was optimized to avoid coarse sediments and microinhomogeneities on the surface, detrimental to the precise determinations of contact areas of adhering SCPs. Amine-coated SCPs were functionalized with E_1 and E_2 17G by means of reductive amination and active ester chemistry, respectively. The latter strategy yielded uniformly functionalized particles without affecting the SCPs integrity. In a proof-of-concept experiment using RICM to measure adhesion energies between E_2 17G functionalized SCPs

and SULT1E1 decorated biochips, a high specificity for the natural and synthetic estrogens E_1 and EE_2 as well as a strong discrimination of non-estrogenic steroids (progesterone P_4 and androgen T) was observed. This result demonstrates the feasibility of the new assay.

Besides the well-known impact and complexity of the estrogen metabolism on hormone levels and thus balance, this is, to our knowledge, the first approach explicitly implementing an estrogen metabolizing enzyme in a biosensor, enabling the detection of hormonally active estrogenic compounds that might not act on estrogen receptors. We specifically emphasize the modularity of implementing an estrogen metabolizing enzyme, as it is not restricted to SULT1E1 and allows for the use of the entire set of estrogen metabolizing- or estrogen binding proteins in a multiplexed assay. This may open new avenues to cover the whole complexity of estrogenicity assessment without animal testing.

CRedit authorship contribution statement

David Rettke: Conceptualization, Formal analysis, Investigation, Writing – original draft, Methodology, Supervision, Visualization. **Florian Seufert:** Formal analysis, Investigation, Validation, Writing – review & editing. **Julia Döring:** Formal analysis, Writing – review & editing. **Kai Ostermann:** Funding acquisition, Writing – review & editing. **Dimitri Wilms:** Formal analysis, Resources. **Stephan Schmidt:** Methodology, Resources, Writing – review & editing. **Tilo Pompe:** Funding acquisition, Methodology, Supervision, Writing – review & editing.

Declaration of competing interest

The authors declare the following financial interests/personal relationships which may be considered as potential competing interests: D. R., F.S., J.D., K.O., T.P. declare competing financial interests. A provisional patent has been filed on behalf of Universität Leipzig and the Technische Universität Dresden.

Acknowledgements

This work was funded by grants of the Federal Ministry of Education and Research of Germany to K.O. and T.P. (grant no.: 13N13798, 13N13799) within the collaborative research project 'Particle-based optical sensors for in-place analytics in quality control of drinking water and food' (PARTOS) with the industrial partners Umex GmbH (Dresden,

Germany), IfU GmbH Privates Institut für Umweltanalysen (Lichtenau, Germany) and Gebr. Heyl Vertriebsgesellschaft für innovative Wasseraufbereitung mbH (Hildesheim, Germany). The usage of the BioImaging Core Facility of the Faculty of Life Science of Leipzig University, supported by a grant from Deutsche Forschungsgemeinschaft INST 268/293-1 FUGG to T.P., is gratefully acknowledged.

Appendix A. Supplementary data

Supplementary data to this article can be found online at <https://doi.org/10.1016/j.bios.2021.113506>.

References

- Aksuglaede, L., Juul, A., Leffers, H., Skakkebaek, N.E., Andersson, A.-M., 2006. *Hum. Reprod. Update* 12 (4), 341–349.
- Aravindakshan, J., Gregory, M., Marcogliese, D.J., Fournier, M., Cyr, D.G., 2004. *Toxicol. Sci.* 81 (1), 179–189.
- Arnold, S.F., Robinson, M.K., Notides, A.C., Guillette, L.J., McLachlan, J.A., 1996. *Environ. Health Perspect.* 104 (5), 544–548.
- Bolong, N., Ismail, A.F., Salim, M.R., Matsuura, T., 2009. *Desalination* 239 (1–3), 229–246.
- Carvalho, R.N., Ceriani, L., Ippolito, A., Lettieri, T., 2015. JRC Technical Report. Report EUR 27142 EN.
- Cole, G.B., Keum, G., Liu, J., Small, G.W., Satyamurthy, N., Kepe, V., Barrio, J.R., 2010. *Proc. Natl. Acad. Sci. U.S.A.* 107 (14), 6222–6227.
- Demers, L.M., Hankinson, S.E., Haymond, S., Key, T., Rosner, W., Santen, R.J., Stanczyk, F.Z., Vesper, H.W., Ziegler, R.G., 2015. *J. Clin. Endocrinol. Metab.* 100 (6), 2165–2170.
- Denver, N., Khan, S., Homer, N.Z.M., MacLean, M.R., Andrew, R., 2019. *J. Steroid Biochem. Mol. Biol.* 192, 105373.
- Dorosh, A., Dèd, L., Elzeinová, F., Pěkníková, J., 2011. *Folia Biol.* 57 (1), 35–39.
- European Union, 2013. *Off. J. Eur. Union* 56. L:2013:226.
- Falany, C.N., Krasnykh, V., Falany, J.L., 1995. *J. Steroid Biochem. Mol. Biol.* 52 (6), 529–539.
- Fischer, L., Strzelczyk, A.K., Wedler, N., Kropf, C., Schmidt, S., Hartmann, L., 2020. *Chem. Sci.* 36 (11), 9919–9924.
- Gamage, N., Barnett, A., Hempel, N., Duggleby, R.G., Windmill, K.F., Martin, J.L., McManus, M.E., 2006. *Toxicol. Sci.* 90 (1), 5–22.
- Glaubit, M., Medvedev, N., Pussak, D., Hartmann, L., Schmidt, S., Helm, C.A., Delcea, M., 2014. *Soft Matter* 10 (35), 6732–6741.
- Gosavi, R.A., Knudsen, G.A., Birnbaum, L.S., Pedersen, L.C., 2013. *Environ. Health Perspect.* 121 (10), 1194–1199.
- Johnson, K.L., Kendall, K., Roberts, D.A., 1971. *Proc. Roy. Soc. Lond. A.* 324 (1558), 301–313.
- Keski-Rahkonen, P., Desai, R., Jimenez, M., Harwood, D.T., Handelsman, D.J., 2015. *Anal. Chem.* 87 (14), 7180–7186.
- Kuhl, H., 2005. *Climacteric* 8, 3–63.
- Kunz, P.Y., Kienle, C., Carere, M., Homazava, N., Kase, R., 2015. *J. Pharmaceut. Biomed. Anal.* 106, 107–115.
- Moore, S.C., Matthews, C.E., Ou Shu, X., Yu, K., Gail, M.H., Xu, X., Ji, B.-T., Chow, W.-H., Cai, Q., Li, H., Yang, G., Ruggieri, D., Boyd-Morin, J., Rothman, N., Hoover, R.N., Gao, Y.-T., Zheng, W., Ziegler, R.G., 2016. *J. Natl. Cancer Inst.* 108 (10).
- Nelles, J.L., Hu, W.-Y., Prins, G.S., 2011. *Expet Rev. Endocrinol. Metabol.* 6 (3), 437–451.
- Pussak, D., Behra, M., Schmidt, S., Hartmann, L., 2012. *Soft Matter* 8 (5), 1664–1672.
- Pussak, D., Ponader, D., Mosca, S., Ruiz, S.V., Hartmann, L., Schmidt, S., 2013. *Angew. Chem. Int. Ed.* 52 (23), 6084–6087.
- Rettke, D., Döring, J., Martin, S., Venus, T., Estrela-Lopis, I., Schmidt, S., Ostermann, K., Pompe, T., 2020. *Biosens. Bioelectron.* 165, 112262.
- Schmidt, S., Wang, H., Pussak, D., Mosca, S., Hartmann, L., 2015. *Beilstein J. Org. Chem.* 11, 720–729.
- Schrag, M.L., Cui, D., Rushmore, T.H., Shou, M., Ma, B., Rodrigues, A.D., 2004. *Drug Metab. Dispos.* 32 (11), 1299–1303.
- Soto, A.M., Sonnenschein, C., Chung, K.L., Fernandez, M.F., Olea, N., Serrano, F.O., 1995. *Environ. Health Perspect.* 103 (Suppl. 7), 113–122.
- Stanczyk, F.Z., Clarke, N.J., 2014. *J. Clin. Endocrinol. Metab.* 99 (1), 56–58.
- Strzelczyk, A.K., Wang, H., Lindhorst, A., Waschke, J., Pompe, T., Kropf, C., Luneau, B., Schmidt, S., 2017. *Gels (Basel, Switzerland)* 3 (3).
- Sun, H., Zeng, Y.-Y., Pang, K.S., 2010. *Drug Metab. Dispos.* 38 (5), 769–780.
- United States Environmental Protection Agency, 2009. *Endocrine Disruptor Screening Program Test Guidelines OPPTS 890.1250*. NSCEP Pubnumber: 740C09005.
- Wang, H., Jacobi, F., Waschke, J., Hartmann, L., Löwen, H., Schmidt, S., 2017. *Adv. Funct. Mater.* 27 (41), 1702040.
- Wang, S., Rijk, J.C.W., Besselink, H.T., Houtman, R., Peijnenburg, A.A.C.M., Brouwer, A., Rietjens, I.M.C.M., Bovee, T.F.H., 2014. *Toxicol. Sci.* 141 (1), 78–89.
- Waschke, J., Pompe, T., Rettke, D., Schmidt, S., Hlawitschka, M., 2019. *PLoS One* 14 (4), e0214815.
- Wilson, V.S., Bobseine, K., Gray, L.E., 2004. *Toxicol. Sci.* 81 (1), 69–77.
- Wu, A.H.B., French, D., 2013. *Clin. Chim. Acta* 420, 4–10.
- Zacharewski, 1997. *Environ. Sci. Technol.* 31 (3), 613–623.
- Zhang, H., Varlamova, O., Vargas, F.M., Falany, C.N., Leyh, T.S., Varmalova, O., 1998. *J. Biol. Chem.* 273 (18), 10888–10892.

Supplemental Information

Biomimetic Estrogen Sensor Based on Soft Colloidal Probes

David Rettke^{1*}, Florian Seufert¹, Julia Döring², Kai Ostermann², Dimitri Wilms³, Stephan Schmidt³, Tilo Pompe¹

1) Institute of Biochemistry, Leipzig University, Germany

2) Institute of Genetics, Technische Universität Dresden, Germany

3) Institute of Organic Chemistry and Macromolecular Chemistry, Heinrich Heine Universität Düsseldorf, Germany

Coating of amine functionalized coverslips with succinic anhydride: Amine functionalized coverslips (\varnothing 32 mm, see “*materials and methods*” section “*chip surface preparation*”) were placed in a 60, 120, 180 or 240 mM solution of succinic anhydride (Merck, Germany) in 250 mL tetrahydrofuran (THF, AppliChem, Germany) respectively and left to react for 60 min at room temperature. The coverslips were washed twice with THF and ddH₂O. In order to fluorescently label the chip surfaces, 500 μ g of fluorescein isothiocyanate (1.28 μ mol, Sigma Aldrich) was dissolved in 20 ml of 100 mM borate buffer (pH = 9.0) and 1.5 ml of the stock solution was added to each sample of the glass slides. The coverslips were protected from light and reacted with the FITC solution for 1 hour at room temperature. Excess solution was discarded and the samples were washed with HEPES buffer several times. The resulting fluorescence intensity of chip surfaces were measured in HEPES buffer at pH 7.0 on a confocal laser scanning microscope (LSM700, Zeiss, Germany) using a water immersion objective (C-Apochromat, Zeiss, Germany) with 40x magnification and a numerical aperture of 1.20 and the pinhole was set to 1 airy unit. Areas of 320.08 x 320.08 μ m (512 x 512 pixel, 1.60 pixels / μ m) were imaged and the mean grey value (fluorescence intensity) of 15 images per condition (3 samples per condition) were averaged for mean intensity analysis.

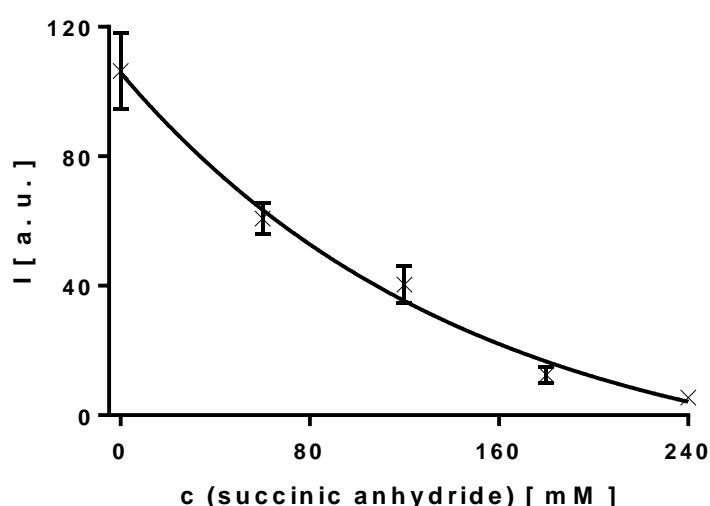


Figure S1: cLSM evaluation of succinic acid coupling to amine functionalized coverslips. Mean fluorescence intensities drop with increasing concentration of succinic anhydride for carboxy functionalization of amine coated surfaces. Error bars indicate S.D.. 15 images (3 samples, 5 images each) were analyzed per condition.

As can be seen from **Fig. S1**, functionalization using 60 or 120 mM succinic anhydride solutions results in incomplete conversion of amino to carboxy groups. Fluorescence of the amine reactive dye is on the other hand scarcely detectable on surfaces treated with 240 mM succinic anhydride solutions, indicating complete carboxy functionalization without remaining residual amino groups.

Determination of elastic modulus: Young's modulus of functionalized SCPs was determined by means of scanning force microscopy using a NanoWizard 3 system (JPK instruments, Germany). Silica beads (Kisker, Germany) with a diameter of 10 μm were glued onto a tip-less cantilever (spring constant 0.03 N/m, CSC 38, μMasch , Bulgaria) and served as a probe for force indentation experiments. Several force curves were recorded for each sample of SCP and elastic moduli were calculated using a model of non-adhesive elastic contact developed by Glaubitz et al. (2014).

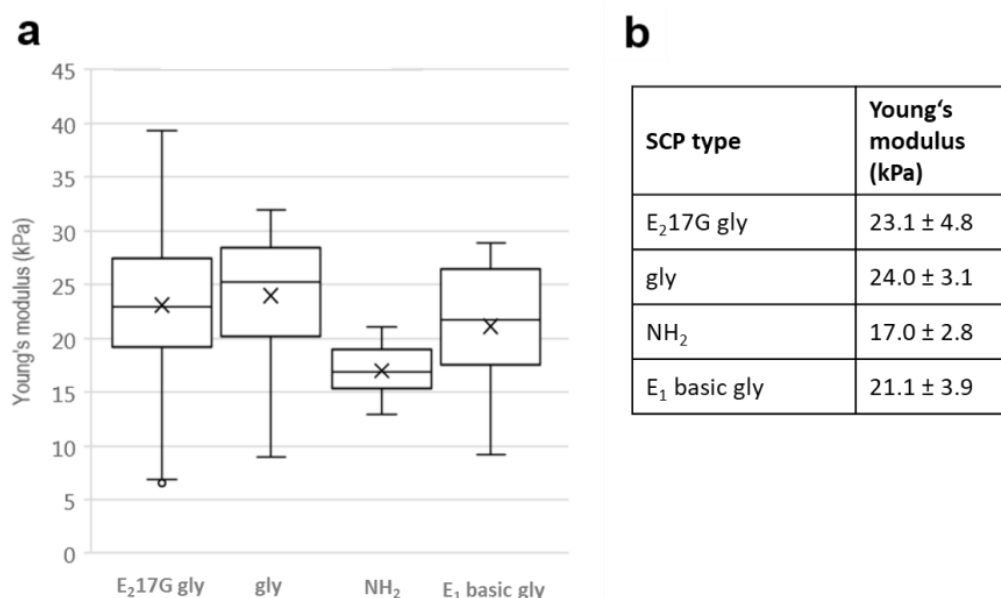


Figure S2: Force spectroscopy measurements of 4 types of SCPs: **a)** Boxplot showing the resulting Young's moduli of push-on scanning force spectroscopy measurements of functionalized SCPs. Upper and lower horizontal lines of the boxes correspond to the third respectively first quartile. Median values are depicted as horizontal line within the boxes. Whiskers represent the maximum and minimum values. Outliers are indicated by solid circles and are defined as values outside the upper and lower inner fence (possible minimum and maximum values referring to the default coefficient of 1.5.) **b)** Mean values of Young's moduli and standard error of mean is shown.

Force spectroscopy was exploited to determine Young's moduli of amine (NH₂), glycolic acid (gly), estradiol-17- β -D-glucuronide (E₂17G) and estradiol-17- β -D-glucuronide plus glycolic acid functionalized (E₂17G gly) SCPs as well as SCPs coated with estrone plus glycolic acid (E₁ basic gly). The SCPs showed no significant difference of Young's moduli with the exception of initial amine functionalized SCPs prior coupling of ligands and gly (**Fig. S2**). Stiffness increases after conjugating estrogenic compounds, i.e. E₂17G or E₁, as well as after coupling gly to the SCPs.

Fluorescence microscopy of FITC stained SCPs: Successful coupling of linker molecules and estrone as well as estradiol 17 β -D-glucuronide was assessed employing fluorescence laser scanning microscopy (LSM700, Zeiss, Germany) using an LCI Plan-Neofluar 63x/1.3 oil immersion objective (Zeiss, Germany). Areas of 105.2 x 105.2 μm (512 x 512 pixels, 4.87 pixels / μm) were recorded. To avoid rapid photobleaching of labelled samples and sensing low fluorescence intensities, the pinhole of the confocal laser scanning microscope remained fully opened (10.8 airy units) to allow for imaging with very low laser intensities. Labelling of SCPs was conducted as described in the “*materials and methods*” section.

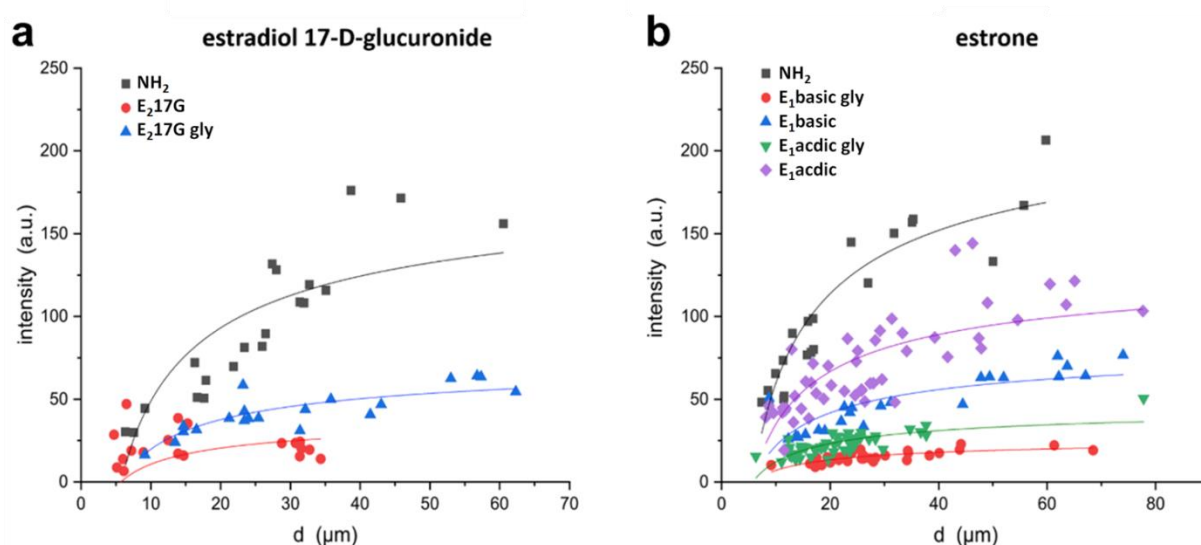


Figure S3: Fluorescence microscopy of FITC stained SCPs. **a)** SCP's diameter dependent fluorescence intensities (mean intensity at equatorial plane normalized by SCP cross-sectional area at equatorial plane) of amine (NH_2), estradiol-17- β -D-glucuronide (E_217G) and estradiol-17- β -D-glucuronide plus glycolic acid ($\text{E}_217\text{G gly}$) coated SCP. **b)** SCP's diameter dependent fluorescence intensities of amine, estrone (E_1) and estrone plus glycolic acid ($\text{E}_1 \text{ gly}$) coated SCPs. E_1 is coupled under either acidic or basic conditions. SCP fluorescence intensities of single SCPs were fitted with a SCP's diameter dependence (solid lines) caused by the low vertical resolution and extrafocal contributions of the microscopic setup (open pinhole) in the range of 1 μm , which affects intensity measurements of SCP with diameters in the range of some tens of micrometers, see also equation below.

The stained SCPs generally show increasing fluorescence intensities with increasing SCP diameter due to the large point spread function in vertical direction because of the opened pinhole (low vertical resolution) (**Fig. S3**). The diameter-dependent fluorescence intensities drop after coating the SCPs with estrogens and glycolic acid as a result of amino group consumption. The size-dependence of fluorescence analysis can be accounted by an approximate fit using the empirical equation for the intensity I : $I = I_{\text{SCP}} (h_z - h_z^3 \cdot d^{-0.5})$ ($h_z = 1.3$). This equation is reasoned by diameter dependent analyzed SCP volume of the SCP cross-section at its equatorial plane. The rather low vertical resolution with a long-ranged and complex point spread function in vertical direction in the range of 1 μm leads to a dependence of the analyzed cross-sectional volume of the SCP at the equatorial plane in dependence on SCP surface curvature in relation to cross-sectional area at the equatorial plane of SCP. For large SCP diameters this influence levels off, as observed in the data and modelled by the fitting equation. The intensity fit parameter I_{SCP} can be used to compare the resulting fluorescence intensities for the different conditions of functionalization, which are summarized in **Fig. 5a**.

References

Glaubitz M., Medvedev N., Pussak D., Hartmann L., Schmidt S., Helm C. A., Delcea M., 2014. *Soft Matter*. 10, 6732-6741.

Limozin L. and Sengupta K., 2009. *ChemPhysChem*. 10, 2752-2768.

Publication IV

Radial profile detection of multiple spherical particles in contact with interacting surfaces

Johannes Waschke, Tilo Pompe, **David Rettke**, Stephan Schmidt, Mario Hlawitschka

PLoS ONE 14(4): e0214815.

Doi: [10.1371/journal.pone.0214815](https://doi.org/10.1371/journal.pone.0214815)

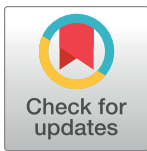
ISI Impact Factor 2020: 3.240

RESEARCH ARTICLE

Radial profile detection of multiple spherical particles in contact with interacting surfaces

Johannes Waschke^{1*}, Tilo Pompe², David Rettke², Stephan Schmidt³, Mario Hlawitschka⁴

1 Max Planck Institute for Human Cognitive and Brain Sciences, Stephanstr. 1a, Leipzig, Germany, **2** Institute of Biochemistry, Leipzig University, Johannisallee 21-23, Leipzig, Germany, **3** Department of Chemistry, Heinrich Heine University Düsseldorf, Düsseldorf, Germany, **4** Faculty of Computer Science, Mathematics and Natural Sciences, Leipzig University of Applied Sciences, Leipzig, Germany

* jowaschke@cbs.mpg.de

Abstract

Adhesive interactions of soft materials play an important role in nature and technology. Interaction energies can be quantified by determining contact areas of deformable microparticles with the help of reflection interference contrast microscopy (RICM). For high throughput screening of adhesive interactions, a method to automatically evaluate large amounts of interacting microparticles was developed. An image is taken which contains circular interference patterns with visual characteristics that depend on the probe's shape due to its surface interaction. We propose to automatically detect radial profiles in images, and to measure the contact radius and size of the spherical probe, allowing the determination of particle-surface interaction energy in a simple and fast imaging and image analysis setup. To achieve this, we analyze the image gradient and we perform template matching that utilizes the physical foundations of reflection interference contrast microscopy.

OPEN ACCESS

Citation: Waschke J, Pompe T, Rettke D, Schmidt S, Hlawitschka M (2019) Radial profile detection of multiple spherical particles in contact with interacting surfaces. PLoS ONE 14(4): e0214815. <https://doi.org/10.1371/journal.pone.0214815>

Editor: Victor M Ugaz, Texas A&M University College Station, UNITED STATES

Received: November 15, 2018

Accepted: March 20, 2019

Published: April 2, 2019

Copyright: © 2019 Waschke et al. This is an open access article distributed under the terms of the [Creative Commons Attribution License](https://creativecommons.org/licenses/by/4.0/), which permits unrestricted use, distribution, and reproduction in any medium, provided the original author and source are credited.

Data Availability Statement: All relevant data are within the manuscript and Supporting Information files. The presented software is available from our repository: <https://gitlab.imn.htwk-leipzig.de/jwaschke/particle-detector>.

Funding: J.W. received funding from the International Max Planck Research School on Neuroscience of Communication: Function, Structure, and Plasticity (Leipzig, Germany; <https://imprs-neurocom.mpg.de>). T.P. and D.R. acknowledge the support by a grant from Federal Ministry for Education and Research (BMBF) within

1 Introduction

Adhesive interactions between deformable materials play an important role in technology as well as in biological processes, e.g. when cells interact with surfaces. In order to shed light on the underlying principles, adhesion phenomena need to be precisely quantified.

Direct quantification of adhesion by means of a surface force apparatus or atomic force microscopy has provided valuable insights into the field of mechanobiology, bioadhesives and colloid science, to name just a few. While offering precise quantitative information on adhesive interactions down to the molecular level, these force-based techniques require considerable experimental effort. As a facile alternative, adhesion assays with soft polymer particles as probes (soft colloidal probes, SCPs) have been introduced to directly quantify adhesive interactions [1–3]. The method is based on determining the mechanical deformation of the SCP particles on a planar substrate by means of reflection interference contrast microscopy (RICM, see Fig 1). RICM as an imaging technique has long been successfully used to study the adhesion phenomena of cells, vesicles, and hard colloidal particles [4], since the underlying contacts can be visualized with nanometer-precision in the vertical direction using an optical

the program "Photonics in Life Sciences" (no. 13N13799). The remaining authors received no specific funding for this work. The funders had no role in study design, data collection and analysis, decision to publish, or preparation of the manuscript.

Competing interests: The authors have declared that no competing interests exist.

microscope. When observing the adhesive contacts of SCP-particles with well-defined elastic modulus, the underlying adhesion energy W_{adh} can be quantified using the Johnson-Kendall-Roberts (JKR) model [3, 5]:

$$W_{adh} = \frac{r_c^3 \cdot \frac{4E}{3(1-\nu^2)}}{6\pi p^2} \tag{1}$$

where p is the SCP radius, r_c the radius of the contact area, E the Young's modulus of the SCP and ν the Poisson ratio.

In order to advance this method further, in the current work we establish software-aided analysis of the RICM-images—i.e. automated localization of adhesive contacts, detection of SCP radius and radius of contact area from the fringe pattern. Quantitative image analysis was already introduced in the early days of RICM. For example, Rädler and Sackmann analyzed the fringe patterns in RICM images and developed a theory that regards spatial distance between a sphere and substrate [6]. Later, an improved approach, which also considered the slope of non-planar surfaces, was proposed by Wiegand et al. [7]. With such a model as a foundation and with knowledge of the relevant parameters, it is possible to accurately simulate RICM profiles. Using non-planar image formation theory and numerical profile reconstruction, Contreras-Naranjo et al. [8, 9] developed more advanced algorithms showing improved profile reconstruction of unknown convex particle shapes. Clack and Groves [10] utilized the model of Wiegand et al. to create a library of 1250 synthetic templates for automated analysis of RICM images. The authors generated templates for particle sizes at height levels between 0 nm and 250 nm. Then they analyzed the microscope image via correlation filter to detect image regions having a high similarity to any of the templates. Related, but technically more demanding, methods, e.g. combining dual-wavelength RICM and atomic force microscopy, have made use of automated analyses to simultaneously measure force and absolute distance, while additionally relying on existing knowledge of particle size [11].

A quantitative analysis of SCP-surface interactions in biomedical and biosensor approaches with increased throughput relies on a large number of analyzed particles, simple and robust imaging, and reliable detection of variable object shapes and disturbing features. Various

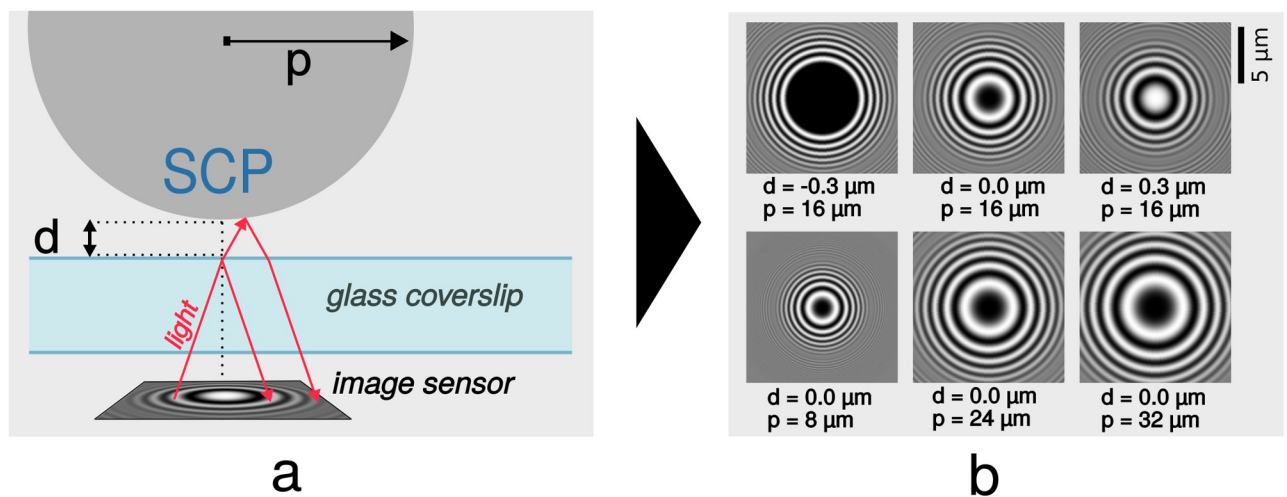


Fig 1. Image acquisition. Experimental setup (a), adapted from [6]. Light is emitted from behind the camera and light rays are reflected twice, leading to the characteristic interference patterns (b). Parameters d and p have a strong impact on the appearance of the ring-shaped patterns (simulation results).

<https://doi.org/10.1371/journal.pone.0214815.g001>

efficient image analysis algorithms have been developed for automated pattern detection in computer-aided image analysis. One such method is circle detection, which can be performed with the Circle Hough Transform [12]. More generally, many approaches exist to detect various kinds of objects in images. Common techniques include thresholding, edge-detection, watershed transformation, or region growing [13]. One quickly growing field is convolutional neural networks, which can be used for image classification and segmentation [14]. While the above-mentioned methods can detect the location of a profile, an analysis based on physical parameters (like radius, or spacing and number of peaks) is lacking. In addition, another major obstacle for automated profile detection is the variety of expressions of radial profiles, like in SCP-surface analysis. The shape of the profile depends on object size, object deformation, image scale, microscope setup, as well as the distance between probe and surface (Fig 1).

In this work, we aimed to develop a quick and efficient way to automatically process a high number of RICM images which should enable sampling of a large number of adhesive contacts, providing reliable quantification of adhesion energies by means of the JKR method. We considered the physical principles of the RICM image within the theory of Rädler and Sackmann [4] to reconstruct theoretical images and use them in an automated pattern matching algorithm. The experimental setup involves a glass coverslip with the adhered SCP placed on an inverted microscope setup, which can be functionalized in various ways for physiochemical, biomedical, or biosensing analysis [1, 15–18]. For high throughput, we use automated detection and profile analysis. Previous work demonstrated template matching as a means to detect the interaction of hard microparticles from RICM images [10]. Our method uses template matching as well, but we introduced a preliminary processing step that reduces the search space and thus vastly decreases the calculation time. Furthermore, we use a higher number of templates, which allows us to search for more heterogeneous expressions of fringe patterns (caused by varying SCP sizes and different contact radii due to deformation of the soft microparticles). Accordingly, our approach is able to detect SCPs and to intrinsically determine their size and contact radius in a highly efficient way involving GPU-accelerated calculation.

2 Materials and methods

2.1 Glass surface preparation

Sample interference patterns were obtained on hard glass surfaces. For the preparation of electrostatically repulsive and attractive model surfaces, glass coverslips ($\phi 32$ mm, Thermo Scientific, Germany) were placed in a Teflon rack and cleaned by sonication in double deionized water and ethanol (AppliChem, Germany) for 30 min each. Afterwards, chemical cleaning was performed to remove organic as well as particle contaminants from the surfaces. Therefore a mixture of 50 ml H_2O_2 , 35% (Grüssing, Germany), 50 ml 25% NH_3 aqueous solution (Merck, Germany) and 250 ml double deionized water was heated to 60°C on a hot plate and coverslips were left in the solution for 10 min. After rinsing twice with double deionized water, the coverslips were dried in a nitrogen stream and used as negatively charged (repulsive) surfaces.

Positively charged (attractive) surfaces were prepared by coating the clean glass slides with branched polyethylene imine (PEI) (average $M_w \sim 800$ by LS, Merck, Germany). Here, a 20 mM solution of 3-aminopropyl-triethoxysilane (VWR, Germany) in a 1% (v/v) double deionized water / isopropanol mixture (AppliChem, Germany) was used for the introduction of amino groups to the glass surfaces. After a reaction time of 10 min, surfaces were washed thoroughly with isopropanol, dried in a nitrogen stream and annealed in a pre-heated oven for 60 min at 120°C . Subsequently, the glass slides were hydrolyzed for 2 h in double deionized water to remove excess and loosely bound silane. For further functionalization and stabilization of the silane layer, the amine coated slides were placed in a 240 mM succinic anhydride solution

in THF (Grüssing, Germany) and allowed to react for 1 h. Following 2 washing steps, 1.5 ml of a 20 mM 1-Ethyl-3-(3-dimethylaminopropyl)carbodiimide (EDC) / 50 mM N-Hydroxysuccinimide (NHS) solution (Carbolution Chemicals, Germany; Merck, Germany) in HEPES buffer (Carl Roth, Germany) 100 mM, pH = 7.0 was pipetted on top of each glass slide. After 15 min of activation, 1.5 ml of a 4 mM PEI solution in the same buffer was added to the slides and the reaction was allowed to proceed for 1 h. Finally, the coated surfaces were rinsed three times in HEPES buffer.

2.2 Particle preparation

SCP particles were synthesized as described previously [17]. Briefly, 50 mg poly(ethylene glycol) diacrylate (Mn 6000 Da, Sigma Aldrich, Germany) and 1 mg of the photoinitiator Irgacure 2959 (Sigma Aldrich, Germany) were added to 10 ml 1M sodium sulfate and vortexed until microscopic droplets were formed. The dispersion was photopolymerized using a Heraeus HiLite UV curing unit (Heraeus Kulzer, Germany) for 90 s. Next, the PEG SCPs were grafted with crotonic acid (Sigma Aldrich, Germany) as described earlier [15]. In short, water was exchanged by 10 ml ethanol, then 250 mg benzophenone and 1.5 g crotonic acid were added. Subsequently, the mixture was flushed with nitrogen for 30 s before irradiating with UV light for 900 s. The resulting SCP particles were then washed with ethanol and PBS three times each. This synthesis resulted in SCPs with a Young's elastic modulus of approximately 40 kPa as characterized by scanning probe spectroscopy, for details see [17].

2.3 Reflection interference contrast microscopy and bright-field imaging

Cleaned or PEI-coated cover glasses were placed in a sealed PTFE-ring and each surface was covered with 1 ml of a 10% ethanol (AppliChem, Germany) HEPES-buffer mixture pH = 7.0. 100 μ l of a suspension containing COOH-functionalized particles (section 2.2) was added dropwise afterwards. After a period of 15 min, sedimentation of the particles was completed and the probes and their corresponding radial profiles were imaged using an inverted microscope (Olympus IX73, Germany) with an integrated halogen lamp for bright-field microscopy. To obtain the respective interference reflection patterns, samples were illuminated by a monochromatic 530 nm collimated LED (M530L2-C1, Thorlabs, Germany). An Olympus 60x, NA (numerical aperture) 1.35 oil-immersion objective (UPlanSApo 60x 1.35 oil, Olympus, Germany) was used in concert with a quarter waveplate (WPMQ05M-532, Thorlabs GmbH, Germany), placed on the microscope's breadboard between objective and sample, as well as additional polarizers to avoid internal reflections [19]. Images were captured with a monochrome CCD camera (DMK 23U274, ImagingSource, Germany) using μ Manager microscopy software. All datasets were recorded applying an exposure time of 50 ms and stored in tagged image file format (tiff). Besides the methods explained in the following sections, no image processing was performed.

2.4 RICM model

Reflection interference contrast microscopy (RICM) is suitable to measure nanoscale distances between a planar transparent surface and another object, like the aforementioned SCPs. The main idea is based on the fact that a light ray is reflected (at least) twice—once from the planar transparent glass surface, once from the particle—and the phase difference between the two interfering rays translates into increased or decreased intensity on the image sensor (Fig 1). The phase difference is basically a geometrical problem and a basic model concerning this experimental situation was established by [6], see also details to other model extensions and approaches in the introduction. The intensity along a profile's radius r of a spherical hydrogel

Table 1. Overview of parameters.

	Template Profile Parameters	Value
u	Pixel length [μm]	0.067
λ	Wavelength [μm]	0.53
INA	Numerical aperture of illumination	0.67
r_{max}	Radius of generated templates [pixel]	100
n	Refraction index	1.332
θ	Phase shift	π
dec	Decay	[0, 1, . . . , 10]
d	Particle height [μm]	[-0.45, -0.44, . . . , 0]
p	Particle radius [μm]	[10, 11, . . . , 30]
	Sampling and Detection Parameters	Value
m	Number of radial samples per position	90
c	Percentage of pixels to remain after pre-processing (in%)	1
a	Minimum amplitude of the local profile p_{mean}	0.05
t_1	Minimum correlation of p_{mean} to best template	0.9
t_2	Minimum average correlation between p_{mean} and the radial samples $p_i \forall i$	0.5

The upper part shows parameters for the template generation. Single values are constant for all templates; the values provided as ranges define the search space. The lower part contains parameters for the search process and the last three rows define constraints that every detected profile must fulfill.

<https://doi.org/10.1371/journal.pone.0214815.t001>

particle in an aqueous solution (with parameters from Table 1 and $h(r)$ from Eq 5) can be calculated by

$$p_{\text{template}}(r) = \frac{\sin y}{y} \cdot \cos\left(2kh(r) \cdot \left(1 - \sin^2 \frac{\alpha}{2}\right) + \theta\right) \tag{2}$$

$$\text{with } \alpha = \sin^{-1} \frac{INA}{n} \text{ and } k = \frac{2\pi n}{\lambda} \text{ and } y = 2kh(r) \cdot \sin^2 \frac{\alpha}{2} . \tag{3}$$

The applied basic RICM theory is known to exhibit certain deviations in exactly describing the intensity distribution, but, as we will show later in the validation section, is appropriate to provide a simple and fast approach to analyze SCP-surface interaction. Intensity deviations for outer peaks can be handled using an empirical exponential decay, as suggested in previous work [4]:

$$p_{\text{template}}(r)' = e^{\frac{-dec \cdot r^2}{r_{\text{max}}}} \cdot p_{\text{template}}(r) . \tag{4}$$

2.5 Implementation details

We implemented the algorithms as a standalone software tool with the Qt framework (C++). The calculation of the template correlation is pixel-wise independent and it involves many numerical computations, which is the reason why we utilized OpenCL for a GPU-driven parallel calculation. The evaluation was performed on a desktop computer (Intel Core i7 4770, AMD R9 280X Graphics Card, 16GB RAM).

3 Algorithm development and results

For automated RICM image analysis, the variety of profiles hampers the utilization of most detection algorithms, but since the profile shape follows physical laws, we can harness the physically predicted profiles to detect and analyze the shape of adhered objects. These template profiles are used to perform template matching over promising image regions. As an additional benefit, we can also derive the probe size and the contact radius from the best-matching template. However, template matching is a computationally expensive procedure and thus analyzing the full image would lead to relatively long calculation times. Prior to the template matching, we exclude image parts from the search space by analyzing their gradient orientation.

Based on these general considerations we developed an algorithm which follows three main steps:

- Pre-selection based gradient orientation
- Template matching
- Data extraction and calculation of results

The general workflow of the image analysis algorithm and the detailed workflow of the detection is additionally illustrated in Figs 2 and 3.

3.1 Object distance and particle size

Eq 2 requires knowledge about the distance between the surface and the SCP object at any radius position r . Though the particles are in general spheric, recent publications describe neck-like deformations along the border of the contact zone [20] or suggest a water meniscus [9] around the particle (Fig 4). These effects depend e.g. on the elasto-capillarity of the surfaces and result in image artifacts along the contact border. However, since the concrete shape of the artifacts is hard to predict, and because of their relatively little impact on only minor regions in the image, we assume the SCPs to be perfectly round and ignore any deformations of the probe. These assumptions are valid, as seen from the results below and earlier reports [1]. For touching surfaces ($d \leq 0$), we set $d := 0$ which crops the sphere. Thus, with parameters from Table 1 we calculate the height with

$$h(r) = \max(0, d + p - \sqrt{p^2 - r^2}) . \quad (5)$$

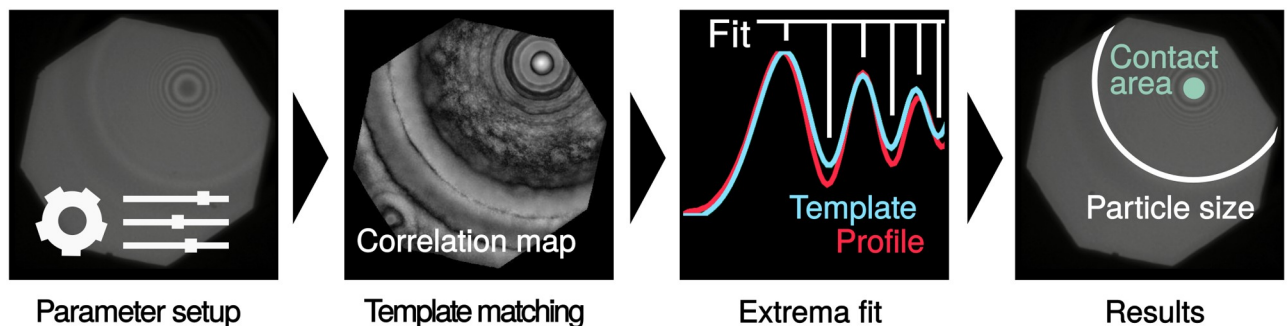


Fig 2. General workflow. Processing steps of an (experimental) image containing one particle. The result includes the particle position, particle size, and its contact area.

<https://doi.org/10.1371/journal.pone.0214815.g002>

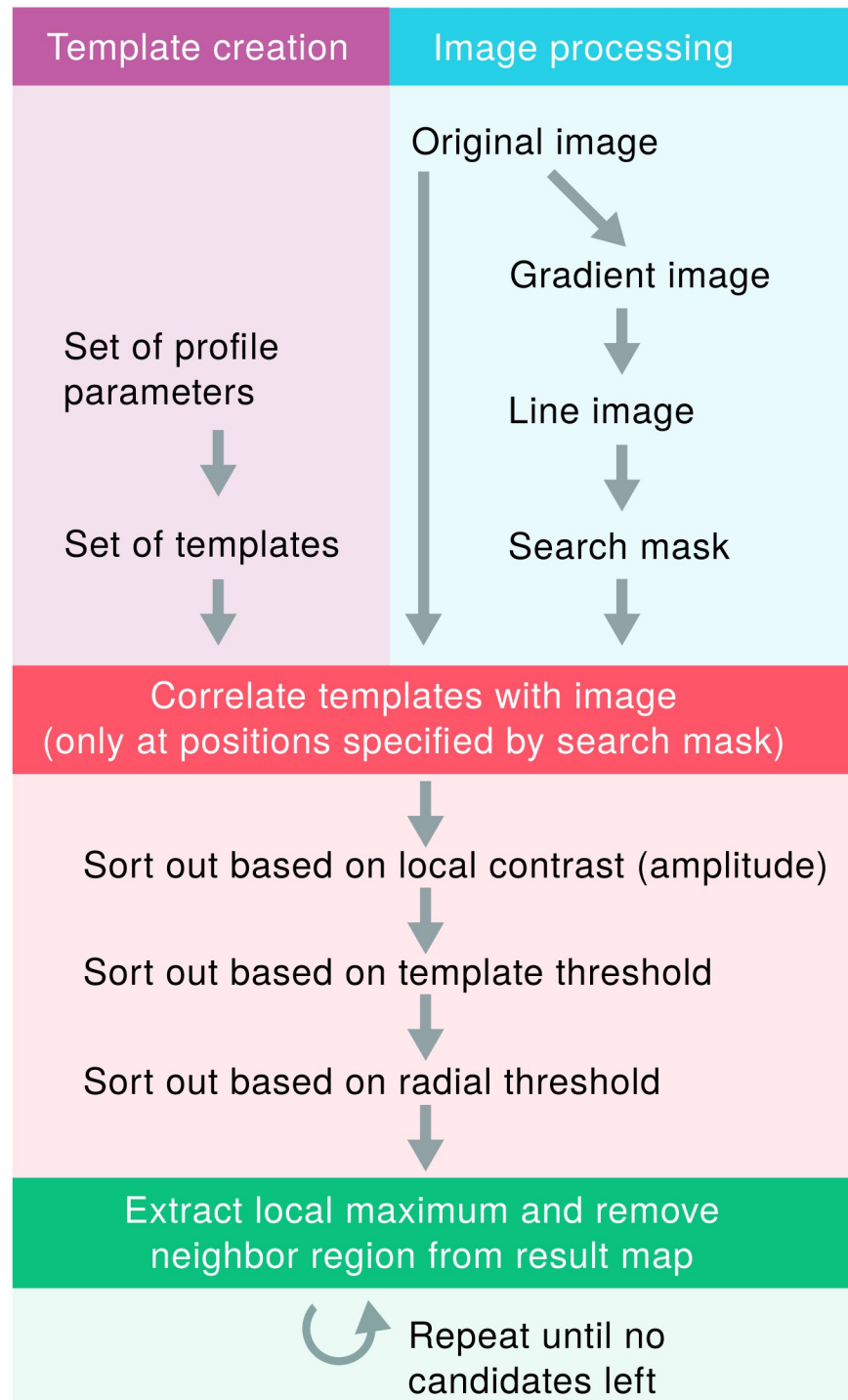


Fig 3. Workflow of the detection process. The processing steps of template creation and image processing.
<https://doi.org/10.1371/journal.pone.0214815.g003>

3.2 Pre-selection based on gradient orientation

To reduce the calculation time of the template matching (see next subsection), we attempt to exclude less interesting image parts from the search space. We utilize the Sobel operator to

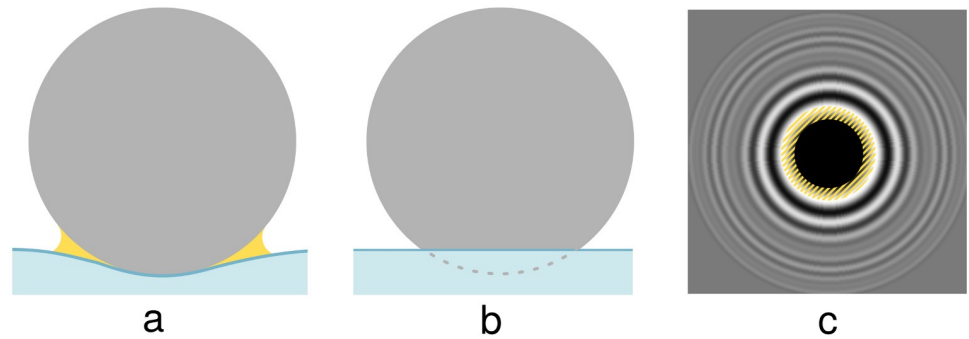


Fig 4. Geometric model assumptions. Deformations or menisci (yellow) can occur and vary depending on material properties (a). We assume a simpler geometric model (b), which is independent of such material properties but, however, could lead to deviations along the border of the contact area (hatched yellow area in the simulated image (c)).

<https://doi.org/10.1371/journal.pone.0214815.g004>

calculate the image gradient. For every image position with a non-zero gradient, we draw a straight line along the gradient orientation into a new image (*line image*, see Fig 5c and 5d). The length of the line is chosen according to the expected profile radius of r_{max} pixels. Caused by the circular shape of the profiles, lines will cluster in the center of profile positions. These clusters are visible as bright spots in the line image. We then select the brightest c percent of pixels and restrict the template matching to these positions (see Fig 5). Since the intensities at the center of spherical objects in the line image are more than exponentially higher than surrounding pixels, a high number of pixels can be omitted without losing coverage of important image regions around the profile centers. Consequently, the reduction of the search space to e.g. 1% of the image increases calculation speed up to a factor of 100.

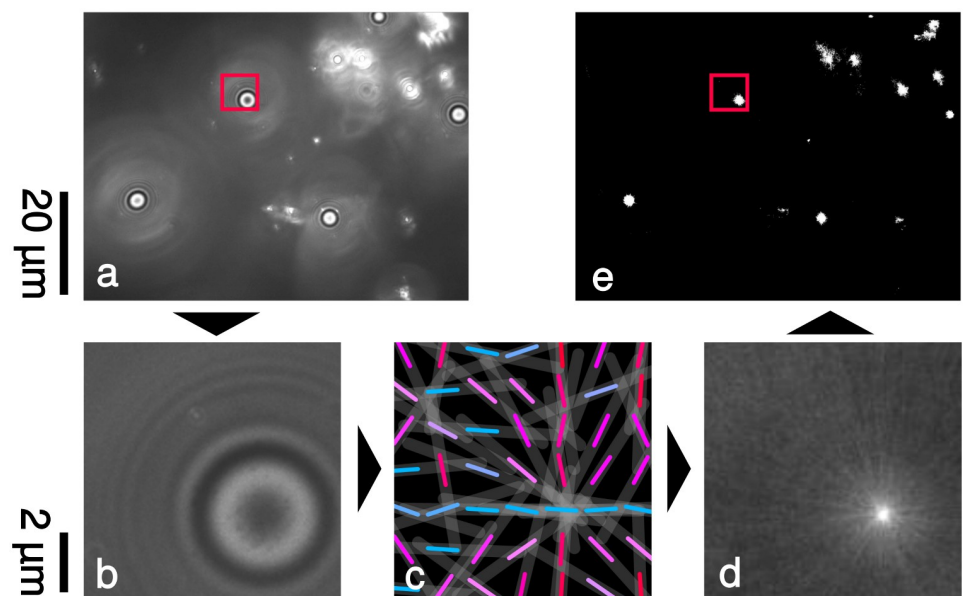


Fig 5. Increasing performance by reducing the search-space. A pre-processing step aims to reduce the search space. To achieve this, the gradient is calculated (glyphs in Fig c, with color-coding based on their orientation) and lines are drawn along the gradient for every pixel (line image). Overlapping lines lead to intensity peaks in the center of radial profiles (d). These peaks are extracted with thresholding and they form the search space for the template matching process (e). Images a and b are experimental results (acquired as described in section 2.3) and their contrast was enhanced for presentation purposes.

<https://doi.org/10.1371/journal.pone.0214815.g005>

3.3 Template matching

We create templates on basis of the model from Eq 2 and the distance function from Eq 5. The parameters are mostly constrained within an experiment and we can use these limits to define a minimum search space. We pre-calculate the profiles for a number (e.g. $\sim 8\,000$) of possible combinations.

For the actual detection process, we consider all candidate pixels provided by the pre-processing step. At each such pixel, we sample starting from a center position (x, y) along radius $r = 1 \dots r_{\max}$. We calculate the average (p_{mean}) of all profiles p_i . With this process, noise is reduced and image positions with radial symmetry are favored since their amplitude is maximum. With $I(x, y)$ being the intensity at image coordinates (x, y) , the sampling steps are defined by

$$p_i(r) = I\left(x + r \cdot \sin\left(\frac{2\pi i}{m}\right), y + r \cdot \cos\left(\frac{2\pi i}{m}\right)\right) \tag{6}$$

and the average profile is

$$p_{\text{mean}}(r) = \frac{1}{m} \sum_{i=1}^m p_i(r) \tag{7}$$

As the next step, we calculate the Pearson correlation coefficients between p_{mean} and all pre-calculated templates. We save the index of the template with the highest similarity and we also note the respective correlation in a map.

We also make use of additional constraints to reduce false positives. One problem is the fact that correlation as comparison metric ignores the amplitude. Our solution is to define a minimum amplitude a that a certain profile p_{mean} from Eq 7 should contain after it was sampled from the image (e.g. 5% of the whole intensity range). Profiles with lower contrast are omitted.

To further reduce false positives, we introduce a threshold for circular correlation (t_2). We only consider positions for which all samples p_i have at least a certain mean correlation t_2 to p_{mean} and thus we exclude asymmetrical image parts. This step is applicable thanks to the fact that our objects of interest always have a spherical shape.

3.4 Extraction of matches and contact radius

The result of the previous calculation is a map of correlations and information of the respective best-matching template. We search for the maximum value in the map. Next, we save the respective coordinates and we store the parameters of the best-matching template. Finally, we apply a consecutive template matching step at this position. This time we ignore the amplitude but we focus on a good matching of the extrema (Fig 6), since they directly relate to particle size. We define similarity by counting the number of positions with the same slope orientation as the sampled profile has (both simultaneously falling or rising) and normalize by r_{\max} . This metric holds the percentage of the template and the measured profile running in synchronism. After extraction, we set a neighborhood of radius r_{\max} around the current match to zero and we repeat the search process on the updated map. We stop the extraction when all positions of the correlation map contain a value less than t_1 (and thus no image position shows sufficient similarity to any of the templates), or when a maximum number of iterations is reached. The radius r_c of the contact area can be derived from the particle radius p and particle height d , which are associated with the respective best-matching template, by calculating the

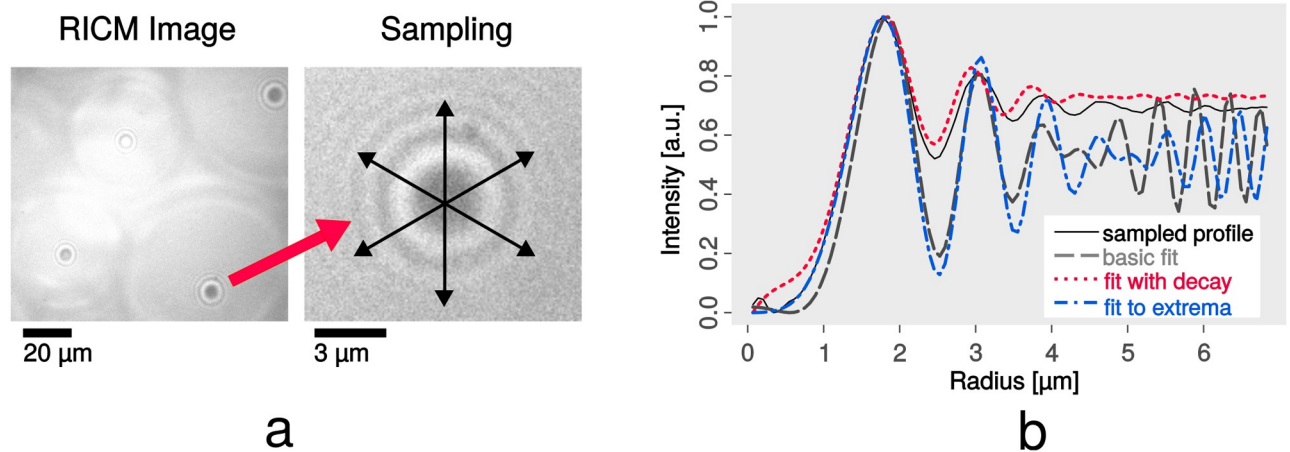


Fig 6. Sampling and fitting of profiles. Fig a shows a RICM image and sampling at an exemplary position (brightness increased for presentation). Fig b demonstrates the fitting procedure of the obtained profile. Our basic template fit for this example shows good Pearson correlation of 0.91, however, adding an exponential decay for higher radii improves correlation to 0.99. To determine particle size, we fit the template regarding optimized extrema overlap (note the better match especially of low peaks for radius positions 5 μm and higher).

<https://doi.org/10.1371/journal.pone.0214815.g006>

intersection of the sphere and the coverslip plane:

$$r_c = 2\sqrt{2pd - d^2} \quad (8)$$

Note, due to the periodicity of the cosine (right term of Eq 2), it is hardly possible to determine the absolute height of the particle. We can only compute the particle height relative to the phase of the light

$$d_{relative} = offset + i \frac{\lambda}{2n(1 - \sin^2 \frac{\alpha}{2})} \quad (9)$$

where *offset* equals the parameter *d* of the best-matching template and *i* is an integer. For all $i \geq 0$, the frequency of the rings is identical. The amplitude (left term of Eq 2), however, is dependent on the absolute height, but its effect on the image is relatively low. This makes it difficult to determine *i* (with our simple and cost-efficient experimental setup) and thus leads to an ambiguous solution for the absolute particle height. We could avoid this problem by an advanced experimental setup involving dual wavelengths [21]. However, we are only interested in touching surfaces of interacting functionalized SCPs and surfaces in physiochemical, biomedical and biosensing applications, hence we can assume $i \leq 0$. For negative heights, the profiles additionally show a distinct uniform center (the contact area) and, thus, there is no ambiguity in the appearance of the profiles.

3.5 Evaluation

We implemented the method in a software tool that allows the user to load a series of images, define suitable parameters (Table 1) and start batch processing of all images. We support the user by providing parameter estimations for manually defined sample positions and by providing presets. The calculation speed grows linearly with the number of templates, the image size, the radius of a profile, and the number of samples *m*. In addition, a constant time span is required to load data and to store results. The calculation speed for a full image—without pre-processing—is roughly 20s for one image (1 600 × 1 200 pixels) with a number of 8 000

templates and a maximum radius of 100 pixels. However, enabling pre-selection of image regions (as explained in section 3.2) leads to an overall calculation time of less than 2.5s per image (570s for a test stack of 265 images).

Starting the calculation with adequate search space usually results in a Pearson correlation of more than 0.95 at profile positions, which is in most cases notably higher than any other profile-free image part. For relatively complex profiles (e.g. involving intensity drops at inner and outer radius positions) the highest correlation might also decrease to 0.8. We used test data for which we initiated the detection process session-wise. For example, images with a constant microscope setup were analyzed in one batch. For proper sampling of the profiles, it is vital to know their accurate center position. To verify the localization of profiles, we used a test data stack of 265 images of SCPs and PEI-coated (attractive) surfaces. All profiles have been detected and the average distance to the manually defined reference position was 1.08 pixels (see Fig 7a). However, false positives are occasionally caused by round objects or air bubbles that are also present in the data. In our test case, 11 false positives have been detected, but they were never marked as the first choice since their template correlation was comparably low. Increasing the radial correlation threshold would reduce the number of false positives but also leads to false negatives. In summary, we prefer to use a tolerant threshold that reliably detects all present profiles. False positives can be quickly deleted in a manual review step.

To verify the particle size, which we derived from the parameters of the best-matching template, we acquired another test data of SCPs on PEI-coated (attractive) surfaces showing 47 particles. The test data includes bright-field data (as reference) in which we could manually measure the size of the SCPs. The validation of the particle diameter shows a mean absolute difference to the reference data of 2.6 μm for particle diameters from 11 μm to 62 μm (see Fig 7b for details).

Evaluation of the contact radius faces the problem of a missing direct measurement as reference. However, the contact radius can also be estimated from the size of the flat dark area in the center of a profile: we determined the contact radius in the average profile p_{mean} based on region growing. We started with the center position of the profile and iteratively selected neighbor positions that showed similar intensity to the center position. The stopping criterion for this process was an increase of the intensity by a certain percentage of the profile's overall amplitude. The concrete choice of the threshold is a trade-off between sensitivity towards noise (too strict threshold) and overestimation of the contact radius (too tolerant threshold), therefore we analyzed the result of 40 uniformly distributed thresholds in the range from 1% to 40%. We then manually reviewed the results and chose the lowest threshold for which region growing never failed, which was a value of 30%.

Our test data consists of 205 images containing in total 184 adhering particles (hence, for these particles the best-matching template implied $d \leq 0$). We describe the relationship between the result c_{model} of the model-based approach and the result $c_{intensity}$ of the intensity-based reference by the linear relationship

$$c_{model} = a \cdot c_{intensity} + b . \quad (10)$$

For the threshold of 30%, the function lm (linear model) in R Statistics determined $a = 1.0247$ and $b = -0.2890 \mu\text{m}$ (adjusted $R^2 = 0.9856$), which shows a strong linear relationship of our approach to the intensity-based reference data (see section 4.3 and Fig 7c and 7d for details).

4 Discussion

In this section we want to first discuss methodical aspects and explain the merits of the chosen techniques compared to possible alternatives. Subsequently, we provide justification for the simplifications and discuss the evaluation presented in section 3.5.

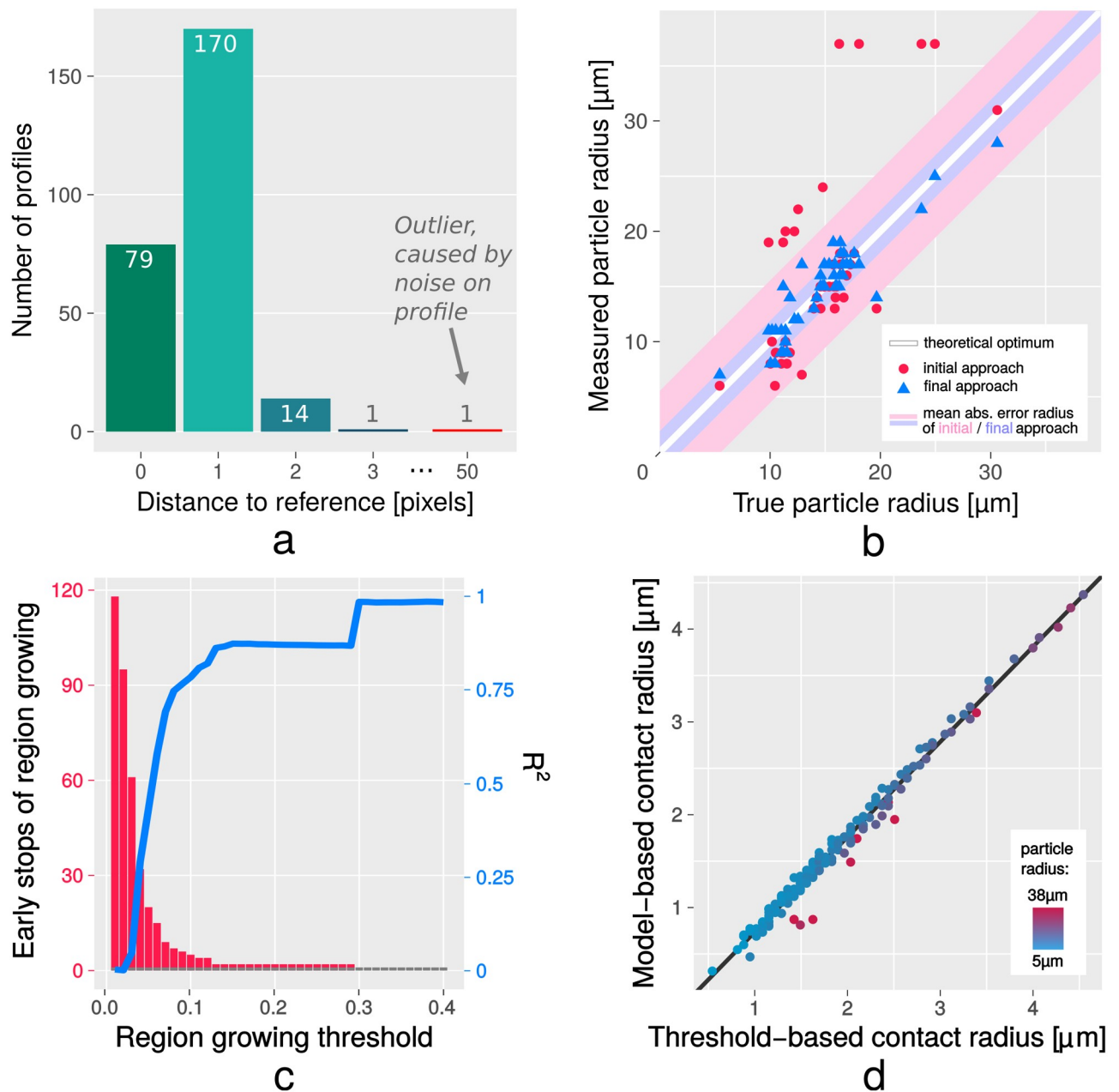


Fig 7. Evaluation of particle detection, particle radius and contact radius. The histogram (Fig a) displays the deviation for the location of the profiles compared to manually labeled reference data (total of 265 samples). The scatterplot (Fig b) shows results for particle radius determination compared to manually labeled reference data (total of 47 samples). It can be seen that the optimized version, in which particle size is determined on basis of a second extrema-focused matching, works notably better (mean absolute error 1.3 μm) than our naive approach (mean absolute error 3.8 μm). The bottom row shows the results for the comparison between the model-based contact radius and the reference data created by region growing. Plot c presents an evaluation for various region growing thresholds between 1% and 40% of the profile amplitude. Plot d shows detailed results for the lowest threshold (30%) that was free of erroneous stops during region growing, and the regression line ($R^2 = 0.9856$). The plot reveals an overestimation of the contact radius by the threshold-based approach, which is a consequence of the relatively high threshold. Lower thresholds would lead to earlier stops (and thus smaller radii) but also to erroneous stops (see Fig c). Further details are given in section 4.3.

<https://doi.org/10.1371/journal.pone.0214815.g007>

4.1 Methodological considerations

We have developed a method that generates templates based on an established physical model. We use a pre-processing step to accelerate the calculation and we apply Pearson correlation to

compare the templates with the microscope image. A consecutive fit based on the profile slope improves the estimation of the particle radius considerably.

The method we present relies on knowledge of a very specific use-case, but with a broad applicability in science and engineering. For example, the method may be applicable to physiochemical interactions of soft hydrogel particles and mimics of living cells with interacting surfaces [22], determination of protein adsorption energies on materials surfaces [23] or bio-sensing approaches [15, 16, 18]. Naturally, a solution based on a more general and re-usable approach would be preferred, however many such approaches we examined lead to noisy results or miss profile occurrences. For example, one technique we designed focused only on statistical properties of the set of profiles p_i ($i = 0 \dots m$) from Eq 6. We searched for positions of simultaneously low variance between all the sampled profiles p_i and high variance inside the averaged profile p_{mean} . This approach matched positions with high rotational symmetry and strong contrast. However, this simplified method produced less predictable special cases, and the problem of profile evaluation remained.

Our images contained brightness shifts (vignetting) and could be noisy or cluttered due to their application on biofunctionalized surfaces and high-throughput tasks, which impaired results obtained by thresholding or edge detection. The variety of frequencies of the rings and thus the strength of the edges made it particularly difficult to detect all rings of an image with a single edge detection setup. Usually, edge detection would only be able to detect thin or thick edges separately. Furthermore, we utilized Circle Hough Transform [12] to detect rings formed by intensity peaks of the profile, but the result was sensitively depending on the chosen parameters. Even in the best case only a few rings with high contrast could be found, which might be related to the above-mentioned difficulties in edge detection. This would lead to inaccurate results since the frequency and thus detection of every single ring is of high importance. While classical template matching with manually defined templates could be an option, the circular patterns differ strongly in appearance, and the variance in the frequency of intensity peaks makes it cumbersome to manually define a profile library. Another popular option has been machine learning, which we initially considered but we lacked sufficient training data. The number of parameters which affect the shape of the profile is comparably high and hence many combinations of training cases would be required. Furthermore, the evaluation of the detected profile would likely require for a second processing step and thus we rejected that approach.

Thus, while other promising techniques may exist, we reasoned that a positive outcome was more likely by trying to advance existing techniques that can already represent the issue with a physical model. With developing theories on reflection interference contrast microscopy, future updates of the model could be implemented with little effort.

4.2 Simplifications

The model we use as a basis for template calculation involves simplifications. We consider the SCP to be perfectly spheric (see Eq 5), even for the case of touching surfaces ($d \leq 0$), although deformations of the SCP have to be present [20]. This leads to minor artifacts on the boundary between contact area and non-contact area, since the transition is very sharp. These artifacts could be addressed by a more detailed model in the future, although the effects on the outcome are considered to be of minor impact, as our validation results show. Furthermore, Eq 2 ignores changes in the angle of the light rays that were reflected from the SCP surface. An analytical solution seems to be unknown [19].

4.3 Evaluation

An important metric is the correctness of the position of the detected templates. Wrong coordinates would lead to an asynchronous radial sampling. This causes increased variance between the samples p_i and eventually a distorted profile p_{mean} . Consequently, the parameters derived from this profile would be inaccurate as well. Clack and Groves [10] verified their precision by checking if their matches were precisely placed in the center of symmetry of the measured profile, and if they were stable for repeated measurements of immobile particles. We decided to use manually labeled reference data, since in several cases artifacts (e.g. bubbles) lead to asymmetric patterns. Our result shows a mean deviation of 1.08 pixels ($\sim 0.07 \mu\text{m}$), which seems to be very accurate.

The particle size is probably the most challenging parameter here (it suffers most from inaccurate templates), therefore the deviation of $1.3 \mu\text{m}$ to the reference data is relatively high. However, other methods only work with already known particle sizes from other analytical techniques [10], but with our method a separate measurement of the particle size can be omitted. The results for this parameter could probably be improved with models that allow a better fit to the underlying RICM image.

The contact radius is often visible in the RICM images as a flat dark area in the center of the profile, which makes it relatively easy to define by basic image processing. A challenge for region growing are the noisy center positions of p_{mean} . The radial averaging has only little effect for small radii, and most extreme, at radius position 0 all profiles p_i sample from the same pixel of the image. As expected, the number of failed region growing attempts was high for low thresholds. Therefore we chose a threshold of 30%, which resulted in valid region growing for all test samples. Nevertheless, all thresholds of at least 10% indicated a very strong similarity of our approach compared to the results of region growing. Due to the tolerant threshold, region growing usually stopped relatively late, which results in an overestimation of the contact radius (as can be seen in the offset $b = -0.2890 \mu\text{m}$ from the linear regression). An evaluation based on a lower threshold led to b closer to $0 \mu\text{m}$, but more outliers led to a worse R^2 . Our reference data contained particles from $5 \mu\text{m}$ to $38 \mu\text{m}$ (mean: $13.84 \mu\text{m}$). The absolute error between our results and the reference data (mean: $0.0643 \mu\text{m}$) depended moderately on the particle size (Pearson correlation of 0.5492, which means that deviations were higher for larger particles) but it was independent from the contact radius (Pearson correlation of -0.0296).

In summary, we attempted to validate the most important parameters of our approach to reference data (see further details in [S1 Dataset](#)). At this point a direct comparison to alternative approaches is hard, since previous work made no claims concerning the accuracy towards separate reference data. Furthermore, previous work neither aimed at determination of particle size nor at optimization of the calculation speed.

5 Conclusion

We demonstrated an efficient and accurate detection of multiple radial profiles in RICM images. The focus of the work lies on image analysis algorithm development (and its validation) using a gradient analysis of the image and template matching. We used theoretical templates based on basic physical foundations of RICM microscopy with minor adaptation for known deviations [4]. Our new method always chose the real template position as top match, but sometimes additional false positives were detected. The position is detected precisely (deviation of 1.08 pixels compared to reference data) and the determination of the particle diameter delivers results within a mean error of $2.6 \mu\text{m}$ for particles with an average diameter of $30 \mu\text{m}$. Although template matching is computationally expensive, we achieve relatively quick

processing times (<2.5 s per image) thanks to the pre-processing step. Our approach also delivers implicit data about the detected objects derived from the best-matching template. These values include particle radius and contact radius of the SCP and they are of importance for determining adhesion energies between the SCP and its underlying surface in physico-chemical, biomedical and biosensing applications.

Supporting information

S1 Dataset. Numerical data from the evaluation of the particle position, particle size, and contact area.

(ZIP)

Author Contributions

Data curation: Tilo Pompe, David Rettke, Stephan Schmidt.

Methodology: Johannes Waschke, Tilo Pompe.

Project administration: Tilo Pompe, Stephan Schmidt.

Software: Johannes Waschke.

Supervision: Tilo Pompe, Stephan Schmidt, Mario Hlawitschka.

Writing – original draft: Johannes Waschke.

Writing – review & editing: Tilo Pompe, David Rettke, Stephan Schmidt, Mario Hlawitschka.

References

1. Pussak D, Behra M, Schmidt S, Hartmann L. Synthesis and functionalization of poly (ethylene glycol) microparticles as soft colloidal probes for adhesion energy measurements. *Soft Matter*. 2012; 8(5):1664–1672. <https://doi.org/10.1039/C2SM06911C>
2. Erath J, Schmidt S, Fery A. Characterization of adhesion phenomena and contact of surfaces by soft colloidal probe AFM. *Soft Matter*. 2010; 6(7):1432–1437. <https://doi.org/10.1039/b923540j>
3. Moy VT, Jiao Y, Hillmann T, Lehmann H, Sano T. Adhesion energy of receptor-mediated interaction measured by elastic deformation. *Biophys J*. 1999; 76(3):1632–1638. [https://doi.org/10.1016/S0006-3495\(99\)77322-4](https://doi.org/10.1016/S0006-3495(99)77322-4) PMID: 10049343
4. Rädler J, Sackmann E. On the measurement of weak repulsive and frictional colloidal forces by reflection interference contrast microscopy. *Langmuir*. 1992; 8(3):848–853. <https://doi.org/10.1021/la00039a019>
5. Johnson KL, Kendall K, Roberts A. Surface energy and the contact of elastic solids. *Proc R Soc Lond A*. 1971; 324(1558):301–313. <https://doi.org/10.1098/rspa.1971.0141>
6. Rädler J, Sackmann E. Imaging optical thicknesses and separation distances of phospholipid vesicles at solid surfaces. *J Phys II*. 1993; 3(5):727–748. <https://doi.org/10.1051/jp2:1993163>
7. Wiegand G, Neumaier KR, Sackmann E. Microinterferometry: three-dimensional reconstruction of surface microtopography for thin-film and wetting studies by reflection interference contrast microscopy (RICM). *Appl Opt*. 1998; 37(29):6892–6905. <https://doi.org/10.1364/AO.37.006892> PMID: 18301506
8. Contreras-Naranjo JC, Silas JA, Ugaz VM. Reflection interference contrast microscopy of arbitrary convex surfaces. *Appl Opt*. 2010; 49(19):3701–3712. <https://doi.org/10.1364/AO.49.003701> PMID: 20648136
9. Contreras-Naranjo JC, Ugaz VM. A nanometre-scale resolution interference-based probe of interfacial phenomena between microscopic objects and surfaces. *Nat Commun*. 2013; 4:1919. <https://doi.org/10.1038/ncomms2865> PMID: 23715278
10. Clack NG, Groves JT. Many-particle tracking with nanometer resolution in three dimensions by reflection interference contrast microscopy. *Langmuir*. 2005; 21(14):6430–6435. <https://doi.org/10.1021/la050372r> PMID: 15982050

11. Attili S, Richter RP. Combining colloidal probe atomic force and reflection interference contrast microscopy to study the compressive mechanics of hyaluronan brushes. *Langmuir*. 2012; 28(6):3206–3216. <https://doi.org/10.1021/la204602n> PMID: 22216832
12. Kimme C, Ballard D, Sklansky J. Finding circles by an array of accumulators. *Commun ACM*. 1975; 18(2):120–122. <https://doi.org/10.1145/360666.360677>
13. Raut SA, Raghuwanshi M, Dharaskar R, Raut A. Image segmentation—a state-of-art survey for prediction. In: 2009 International Conference on Advanced Computer Control. IEEE; 2009. p. 420–424.
14. Russakovsky O, Deng J, Su H, Krause J, Satheesh S, Ma S, et al. Imagenet large scale visual recognition challenge. *Int J Comput Vis*. 2015; 115(3):211–252. <https://doi.org/10.1007/s11263-015-0816-y>
15. Schmidt S, Wang H, Pussak D, Mosca S, Hartmann L. Probing multivalency in ligand–receptor-mediated adhesion of soft, biomimetic interfaces. *Beilstein J Org Chem*. 2015; 11:720–729. <https://doi.org/10.3762/bjoc.11.82> PMID: 26124875
16. Strzelczyk AK, Wang H, Lindhorst A, Waschke J, Pompe T, Kropf C, et al. Hydrogel microparticles as sensors for specific adhesion: case studies on antibody detection and soil release polymers. *Gels*. 2017; 3(3):31. <https://doi.org/10.3390/gels3030031>
17. Wang H, Jacobi F, Waschke J, Hartmann L, Löwen H, Schmidt S. Elastic modulus dependence on the specific adhesion of hydrogels. *Adv Funct Mater*. 2017; 27(41):1702040. <https://doi.org/10.1002/adfm.201702040>
18. Pussak D, Ponader D, Mosca S, Ruiz SV, Hartmann L, Schmidt S. Mechanical carbohydrate sensors based on soft hydrogel particles. *Angew Chem Int Ed*. 2013; 52(23):6084–6087. <https://doi.org/10.1002/anie.201300469>
19. Limozin L, Sengupta K. Quantitative reflection interference contrast microscopy (RICM) in soft matter and cell adhesion. *ChemPhysChem*. 2009; 10(16):2752–2768. <https://doi.org/10.1002/cphc.200900601> PMID: 19816893
20. Butt HJ, Pham JT, Kappel M. Forces between a stiff and a soft surface. *Curr Opin Colloid Interface Sci*. 2017; 27:82–90. <https://doi.org/10.1016/j.cocis.2016.09.007>
21. Schilling J, Sengupta K, Goennenwein S, Bausch AR, Sackmann E. Absolute interfacial distance measurements by dual-wavelength reflection interference contrast microscopy. *Phys Rev E*. 2004; 69(2):021901. <https://doi.org/10.1103/PhysRevE.69.021901>
22. Martin S, Wang H, Rathke T, Anderegg U, Möller S, Schnabelrauch M, et al. Polymer hydrogel particles as biocompatible AFM probes to study CD44/hyaluronic acid interactions on cells. *Polymer*. 2016; 102:342–349. <https://doi.org/10.1016/j.polymer.2016.02.019>
23. Martin S, Wang H, Hartmann L, Pompe T, Schmidt S. Quantification of protein–materials interaction by soft colloidal probe spectroscopy. *Phys Chem Chem Phys*. 2015; 17(5):3014–3018. <https://doi.org/10.1039/c4cp05484a> PMID: 25560365

Publication V

Microfluidics-assisted synthesis and functionalization of monodisperse colloidal hydrogel particles for optomechanical biosensors based on reflection interference contrast microscopy

David Rettke, Christian Danneberg, Talika Alina Neuendorf, Sebastian Kühn, Jens Friedrichs, Nicolas Hauck, Carsten Werner, Julian Thiele, Tilo Pompe

submitted

Microfluidics-assisted synthesis and functionalization of monodisperse colloidal hydrogel particles for optomechanical biosensors based on reflection interference contrast microscopy

David Rettke¹, Christian Danneberg¹, Talika Alina Neuendorf², Sebastian Kühn³, Jens Friedrichs³, Nicolas Hauck², Carsten Werner³, Julian Thiele^{2,4}, Tilo Pompe^{1,3}

1) Institute of Biochemistry, Leipzig University, Johannisallee 21 – 23, 04103 Leipzig, Germany

2) Leibniz-Institut für Polymerforschung Dresden e.V., Hohe Strasse 6, 01069 Dresden, Germany

3) Leibniz-Institut für Polymerforschung Dresden e.V., Max Bergmann Center of Biomaterials, Hohe Strasse 6, 01069 Dresden, Germany

4) Dresden Center for Intelligent Materials (DCIM), Technische Universität Dresden, 01069 Dresden, Germany.

* Corresponding Author:

Institute of Biochemistry, Leipzig University, Johannisallee 21 – 23, 04103 Leipzig, Germany

E-mail: tilo.pompe@uni-leipzig.de

Abstract

The soft colloidal probe (SCP) assay is a highly versatile sensing principle employing micrometer-sized hydrogel particles as transducer elements. We report the synthesis, optimization, and conjugation of SCPs with defined narrow size distribution and specifically tailored mechanical properties and functionalities for integration into a microinterferometric optomechanical biosensor platform. Droplet-based microfluidics was used to crosslink polyethylene glycol (PEG) macromonomers by photocrosslinking and thiol-Michael addition. The effect of several synthesis parameters, i.e. PEG and radical initiator solid content, molecular weight and architecture of macromonomers, as well as UV exposure time and energy, were examined. SCPs were characterized with regard to the conversion of contained functional groups, morphology and mechanical properties by bright-field, confocal laser scanning and reflection interference contrast microscopy, as well as force spectroscopy. Functional groups were introduced during SCP synthesis and by several post-synthesis

procedures, based on photoradical grafting and thiol-Michael addition. Preparation of SCPs by thiol-Michael addition and subsequent coupling of maleimide derivatives to unreacted thiols proved to be the superior strategy, while other approaches were associated with changes in the properties of the SCP. The newly developed SCPs were tested for their sensing capabilities employing the biotin-streptavidin-system. Biotin detection in the range of 10^{-7} to 10^{-10} M verified the concept of the synthesis strategy and the advantage of using monodisperse SCPs for easier and faster sensing applications of the SCP assay.

Keywords

microfluidics, hydrogel, microparticles, optomechanical, biosensor, soft colloidal probes (SCP)

1 Introduction

Hydrogels are versatile materials due to their high degree of hydration in conjunction with non-fouling characteristics and broad tunability of mechanical, optical and volumetric properties. Consequently, in recent decades these materials have found numerous applications in a wide range of disciplines, from industrial to medical and environmental purposes [1–3].

By endowing hydrogels with different functionalities, a variety of "smart" materials could be produced that respond to environmentally and biologically relevant conditions. Thus, hydrogel-based systems provide an ideal platform for designing the interplay between biological recognition processes and associated detectable modulations of bulk material properties and have emerged as a relevant transducer element in biosensing and bioresponsive applications [4–7]. The variety of possibilities for mechanistically distinct strategies can be exemplified by affinity-based glucose detection: Hydrogel-based glucose measurements were achieved either by direct detection of volumetric changes or by coupled changes of refractive indices and diffraction wavelengths, respectively, osmotic balance, dielectric constants and electrical conductance, each as a result of enzyme-catalyzed glucose oxidation, or binding of glucose to suitable capture molecules immobilized on the polymer scaffold [8–12].

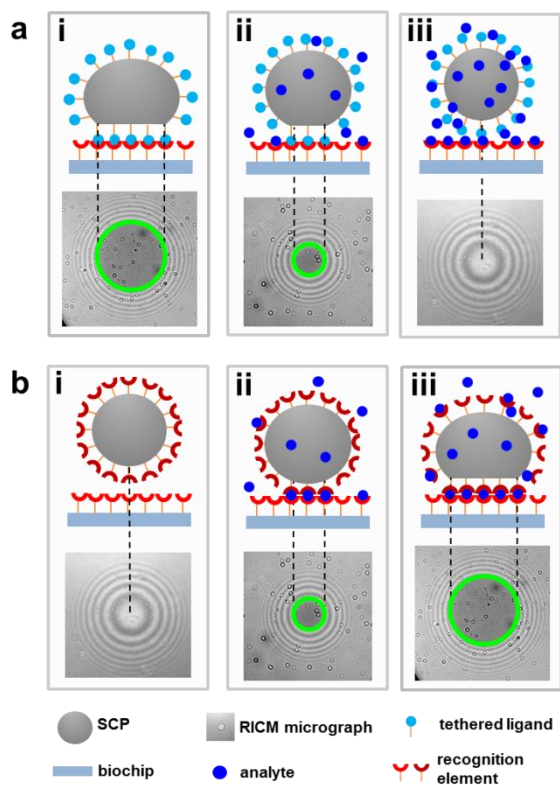
In this context of hydrogel-based biosensing approaches, Pussak et al. introduced an optomechanical biosensor for the quantification of carbohydrates using the contact mechanics of micrometer-sized elastic hydrogel particles referred to as soft colloidal probes (SCP) [13]. The interface contact mechanics of colloidal particles is well established to describe the

interaction forces between spherical particles and a spherical or planar surface. Contact mechanics models allow the interface interaction energy, the contact area and the mechanical particle deformation to relate to each other, as shown by the Johnson-Kendall-Roberts (JKR) model of elastic contact of attractive interactions, i.e. adhesion between the interface of a soft sphere and a rigid surface. Following **eq. 1**, the radius of contact area a can be related to the adhesion energy of a soft spherical probe and a hard surface W , whereby R is the radius of the SCP and E_{eff} is the effective elastic modulus of the probe ($E_{eff} = 4E / (3(1-\nu^2))$; E - Young's modulus, ν - Poisson ratio).

$$a^3 = 6\pi \frac{W}{E_{eff}} R^2 \quad (1)$$

Equipping SCP and planar surface with molecules of interest, in turn, permits to conveniently correlate the extent of interactions between the tethered moieties to the resulting contact area. So far, this approach has been adapted to measure non-specific and specific interactions in various applications ranging from adhesion between whole cells and ligands of cell surface receptors, probing interactions between biomolecules and synthetic polymers as well as to develop biosensors as the aforementioned carbohydrate sensor and for highly sensitive pM detection of glyphosate as well as estrogenic compounds [13–17]. A general description of competitive and direct binding assays employing SCPs as adhesion probes is presented in **Fig. 1**. The superior flexibility in target panel modification, multiplexing capacity, miniaturization capabilities and various adhesive contact readout technologies, i.e. on-site analysis, promise to build a platform for label-free, sensitive and selective detection of a wide range of analytes of significant importance in biomedical diagnostics and environmental monitoring in a cost- and time-efficient manner.

Fig. 1



Schematic illustration of SCP-based biosensing assays. **a** Competitive binding assay: **i** An SCP equipped with ligands adheres to a transparent biochip bearing immobilized complementary receptors and forms an extended interfacial area as a result of biospecific interactions. **ii** Analytes present in the sample block binding sites for SCP tethered ligands. As a result, the contact area between SCP and biochip is markedly diminished. **iii** At high concentrations of analytes, the presented receptors are completely occupied, and the SCP cannot adhere to the biochip anymore. **b** Bridging assay: SCP and biochip are decorated with receptors capable of binding to different domains of the analyte. **i** In the absence of analytes, no biospecific interaction between SCP and biochip is observable, and no contact area is formed. **ii** and **iii** Analytes within the sample to be analyzed cause a concentration-dependent increase in SCP-biochip interactions and contact area

At present, SCPs for the aforementioned biosensing application are typically made of polyethylene glycol (PEG), which ensures a high degree of hydration, an almost ideally elastic hydrogel material, and a density equal to the surrounding aqueous media to avoid unspecific deformation of the particles. Furthermore, the inert and repellant nature of PEG aids to prevent any adhesion that does not result from the interactions between the molecules tethered to the surface and SCP. Previously, the synthesis of SCPs was carried out in a batch precipitation polymerization process using a kosmotropic salt to force aggregation of linear PEG diacrylate forming a dispersion followed by photoradical crosslinking of the end groups [16, 18–20]. Batch synthesis by this kind of precipitation polymerization is inevitably associated with a comparatively broad distribution of particle size, a fact that complicates the analysis of the data obtained from adhesion experiments, application of alternative readout technologies, multiplexing and miniaturization. In particular, the SCP radius R has to be

recorded together with the contact radius a in the case of polydisperse particles (see **eq. 1**), consuming resources for high-resolution optical instrumentation as well as image acquisition and data evaluation. Depending on the miniaturization setup and readout technology, only particles within a certain size can be taken into account for measurements. The lower limit for interferometric and holographic readouts, respectively, used in practice is typically limited to the resolution of the optical device, and smaller particles might lead to increasingly imprecise results. On the other hand, very large particles are prone to form irregular, non-circular contact areas, implying that simple physical models like the JKR approach are no longer applicable. Moreover, sets of defined particles in a narrow range of sizes, provides new opportunities for multiplexed analysis. Lastly, the batch process of precipitation polymerization of SCPs described above results in a certain percentage of particles with micrometer-sized defects due to the inclusion of kosmotrope solution droplets within the PEG-rich phase due to vigorous shaking of the reaction mixture prior crosslinking of the macromonomers. Overall, current SCP synthesis approaches results in a significant proportion of particles that are unsuitable for high-sensitivity quantification of adhesion energy and analytes, thus hindering further extension of SCP biosensing assays into a platform technology.

To overcome these limitations, we have used droplet-based microfluidics for the highly controllable continuous production of SCPs [21–23]. Droplet-based systems are focused on creating discrete volumes using two immiscible phases by precisely generating one drop at a time. The superior control over size and composition of the dispersed droplets makes the corresponding emulsions an ideal template for generating monodisperse and functional particles in a reproducible and automated fashion. The most common strategies for producing hydrogels in microfluidic devices comprise thermal and ionic gelation as well as photopolymerization [5, 24]. Whilst each approach offers specific benefits with regard to the respective application, especially photocrosslinkable PEG-based derivatives are still the precursor material of choice for microparticle-based biosensing applications [3]. A fact that is attributed to wide possibilities of fine tuning the gel microstructure on demand, including porosity and mechanical properties, the bioinert nature of these hydrogels as well as broad commercial availability of the macromonomers in a wide range of molecular weights and geometries and relative inexpensiveness [3, 25, 26]. As a compromise, further parameters have to be taken into account, namely photoinitiator concentration, UV-radiation intensity and exposure time, which ultimately determine the degree of double bond conversion and hence mechanical and volumetric properties. Introduction of functional moieties and covalent

coupling of biomolecules is frequently carried out in a one-step procedure during particle synthesis. Although convenient, this approach usually requires the conjugation of photocrosslinkable groups to the molecules of interest and is accompanied with the risk of protein precipitation/aggregation, entrapment of biomolecules within the bulk of the hydrogel material and biomolecule degradation by free radicals, UV-exposure or contact to a hydrophobic boundary layer in the process of droplet formation [27–30].

This work describes the microfluidics-assisted synthesis of PEG microparticles and the tailoring of their properties and functionalization for SCP-based assays. For water-in-oil (W/O) emulsion formation, microfluidic flow-focusing devices were employed, and acrylamide- (ACA) based photoradical crosslinking chemistry was compared to thiol-ene addition-based hydrogel network formation. Mechanical properties were optimized and analyzed by means of reflection interference contrast microscopy (RICM) as well as colloidal probe force spectroscopy. The suitability of functionalization during synthesis and post-synthesis, both by photoradical chemistry and by the use of residual functional groups, was analyzed to improve and expand the design of the SCP assay. Biotin quantification experiments demonstrated that the advantageous features of the newly developed SCPs enabled high sensitivity of the modular assay.

2 Materials and Methods

2.1 Microfluidic preparation of SCPs

For the synthesis of PEG-ACA-based SCPs, solutions of 3.7 kDa ACA-PEG-ACA, 0.3 kDa ACA-PEG-ACA or a 1:1 mixture of 2 kDa 4-arm-PEG-ACA (starPEG-ACA) and 1 kDa ACA-PEG-COOH in a concentration of 10% (w/w) and 2% (w/w) of lithium phenyl-2,4,6-trimethylbenzoylphosphinate (LAP) in ultrapure water were prepared unless otherwise stated. A flow-focusing microfluidic chip with a channel height and nozzle width of 25 μm was connected to syringes (1750 Gastight Syringe, 500 μL , Hamilton, US) clamped in syringe pumps (Pump 11 Elite, Harvard Apparatus, US) via a polyethylene tubing (ID = 0.38 mm, OD = 1.09 mm, Smiths Medical, US). The respective PEG solution, also referred to as dispersed phase, was injected into the microfluidic device and emulsified at the junction into droplets by a continuous phase consisting of a solution of 2% (w/w) of the surfactant PicoSurf (Sphere Fluidics, UK) in HFE 7500. Flow rates of the dispersed (Q_d) and the continuous

Phase (Q_c) were individually adjusted as mentioned in the results section. Each fraction of droplet emulsion was collected in a tube, which was replaced after 30 min cycle time. The collected fractions were subsequently irradiated for 3 minutes in a UV-Crosslinker (5x 8 W, 365 nm, CL-1000L, UVP, Germany) unless otherwise stated. After adding 500 μ L of ultrapure water, the microparticles were transferred into water by washing three times with 500 μ L of a 20% (v/v) solution of 1H,1H,2H,2H-perfluoro-1-octanol (abcr, Germany) in HFE 7500 and the oil phase was discarded. Finally, the particles were collected by adding 1 mL of ultrapure water to the washed particle suspension and transferring the aqueous suspension into a 50 mL Protein low binding tube (LoBind, Eppendorf, Germany). This step was repeated six times.

To generate maleimide- (mal) thiol- (SH) based PEG SCPs, 2 kDa 4-arm-PEG-thiol (starPEG-SH) and 2 kDa 4-arm-PEG-maleimide (starPEG-mal) were dissolved separately in 1x phosphate buffered saline (PBS) to obtain solutions of either 7.5% (w/w) or 15% (w/w). The pH of the starPEG-SH solution was adjusted with 1M NaOH or 1M HCL to approximately 4.5-5.5, so that the polymerization occurred within 30 to 60 seconds after the two solutions were combined. Adjusting the pH is necessary in order to control the reaction rate, as rapid gelation increases viscosity during droplet formation, leading to polydisperse SCPs or clogging of the device. In the case of low reaction rates, competing reactions like thiol oxidation or hydrolysis of reactive groups might alter the elastic properties of the resulting SCPs.

In contrast to the PEG-ACA approach, microdroplets were formed in a PDMS-based microfluidic flow-focusing device with a nozzle width of 25 μ m and four inlets. This design allowed for the simultaneous injection of three dispersed phases starPEG-SH, starPEG-mal (syringes: Inject-F Solo 1 mL, Braun, Germany) and the same amount of 1x PBS (syringe: 1750 Gastight Syringe, 500 μ L) at a flow rate of 90 μ L h^{-1} , which led to a total starPEG-SH/starPEG-mal mass fraction of either 5% (w/w) or 10% (w/w) PEG. The continuous phase containing 2% (w/w) of the surfactant PicoSurf dissolved in HFE 7500 oil was co-injected (syringe: 1000 Gastight Syringe, 2.5 mL, Hamilton, US) at a flow rate of 800 μ L h^{-1} and SCPs were transferred directly into HFE-7500 to avoid oxidative effects. This was followed by a washing and collecting process as described for ACA-based SCPs. All solutions were injected using Pump 11 Elite pumps. Droplet formation was monitored using an Olympus IX73 inverted microscope in conjunction with a Phantom Miro C110 high speed camera (Ametek, US) in the case of ACA- as well as mal- SH-based SCP synthesis. A quantification of the SCPs was not carried out since the proportion of functional groups or the gel composition,

which changes depending on the flow rate and the type of PEG used, is more relevant for the synthesis and functionalization reactions than the number of SCPs. A protocol for PDMS-based microfluidic device fabrication is given in **SI, section 2**.

2.2 Functionalization of SCPs

Crotonic acid was grafted to SCPs made from 0.3 as well as 3.7 kDa PEG diacrylamide. Grafting of crotonic acid (Sigma Aldrich, US) was conducted as described earlier [18, 20, 31]. In short, water was exchanged by 10 mL ethanol, then 250 mg benzophenone (1.4 mmol, Sigma Aldrich, US) and 1.5 g crotonic acid (17 mmol) were added. Subsequently, the mixture was flushed with nitrogen for 30 s before irradiating with UV light for 900 s. The resulting SCP particles were then washed with ethanol and PBS three times each.

In order to introduce functional groups to SCPs, several bifunctional small molecules were coupled to unreacted residual functional moieties within the PEG network employing thiol-Michael addition. For PEG-ACA-based SCPs, the addition of the thiol-compounds 2-mercaptoethanol, 1,2-ethanedithiol, cysteamine and thioglycolic acid, all purchased from Sigma Aldrich (US), was used. Unless otherwise stated, 2.5 mmol of the respective thiol compound was dissolved in 7.5 mL 100 mM 4-(2-hydroxyethyl)-1-piperazineethanesulfonic acid (HEPES, Carl Roth, Germany)-buffer and the pH was adjusted to 7.0 using 1 M NaOH. Due to the poor solubility of 1,2-ethanedithiol in water, 2.5 mmol were dissolved in 12 mL of a mixture of HEPES-buffer and tetrahydrofuran (THF, 3.75 mL HEPES buffer, 8.75 mL THF) and the pH was adjusted to approx. 7.0 using 1 M NaOH. In the case of higher concentrations of 1,2-ethanedithiol, the amount of THF was increased. The solutions were added to 2.5 mL of a suspension containing unfunctionalized SCPs, and the reaction was allowed to proceed at room temperature for 1 h while agitating. The SCPs were subsequently centrifuged at 1840x g, and the supernatant was discarded. After several washing steps with 100 mM HEPES buffer or the aforementioned buffer-THF mixture in the case of 1,2-ethanedithiol-functionalized SCPs, the particles were resuspended and stored in 100 mM HEPES buffer (pH = 7.0).

Functionalization of SCPs bearing SH-groups was conducted employing maleimide compounds. Therefore, 2-maleimidoethylamine hydrochloride (mal-NH₂*HCl), 3-maleimidopropanoic acid (mal-COOH), both purchased from Iris Biotech (Germany), were dissolved in 100 mM HEPES buffer in a concentration of 133 μM (1.5 mL, 22.5 mg mal-COOH, 23.5 mg mal-NH₂*HCl) and the pH was adjusted to 7.0 by addition of NaOH. 1.5 mL

of a suspension containing SCPs made from 10% (w/w) starPEG-mal and starPEG-SH per condition was centrifuged at 1840x g, the supernatant was discarded, and the respective solution was added. The reaction was allowed to proceed for 1 h while agitating. Subsequently, the SCPs were centrifuged and rinsed at least three times with 100 mM HEPES buffer.

2.3 Fluorescence staining of SCPs

Success of functionalization and coupling reactions was assessed by confocal laser scanning microscopy (cLSM). For the introduction of fluorescent moieties to SCPs, fluorescein, carboxyfluorescein- and carboxytetramethylrhodamine-based dyes bearing complementary functional groups to the respective functionalization of the SCPs were used. Information about dye conjugate, the corresponding stained reactive group and manufacturer is given in table 1.

Table 1 Dye conjugates used for staining of SCPs. Corresponding abbreviations, stained functional groups and manufacturers are given

Fluorescent dye	Abbreviation	Stained group	Manufacturer
fluorescein isothiocyanate	FITC	ACA, NH ₂	Thermo Fisher Scientific, US
6-(fluorescein-5(6)-carboxamido)hexanoic acid <i>N</i> -hydroxysuccinimide ester	FAM-scm	NH ₂	Sigma Aldrich, US
5(6)-carboxytetramethylrhodamine <i>N</i> -hydroxysuccinimide ester	TAMRA-scm	NH ₂	VWR, Germany
5-(6)-carboxyfluorescein ethylenediamine	FAM-NH ₂	COOH	AAT Bioquest, US
<i>N</i> -(5-fluoresceinyl)maleimide	FAM-mal	SH	Sigma Aldrich, US
5-(6)-carboxyfluorescein thiol	FAM-SH	mal	BioActs, South Korea
biotin-4-fluorescein	FAM-btn	streptavidin	Biomol, Germany

For the preparation of staining solutions, $250 \mu\text{g mL}^{-1}$ of the respective compound were weighed and dissolved in 100 mM HEPES buffer (pH = 7.0). As an exception, FITC was dissolved in 100 mM borate buffer (pH = 9.0) and coupling of FAM-NH₂ required activation prior to coupling, as will be described later. 1 mL of SCP suspension was centrifuged, the supernatant was discarded, 1.5 mL of the staining solution was added to the pellet and the SCPs were subsequently resuspended in the reaction mixture. The reaction was allowed to proceed overnight in a rotator. The SCPs were finally centrifuged, the supernatant was discarded, and SCPs were washed several times in 100 mM HEPES buffer (pH = 7.0).

For coupling of FAM-NH₂, SCPs were activated by EDC/NHS. Therefore, 1.5 mL of a solution containing 5.75 mg EDC (37 μmol) and 8.625 mg NHS (75 μmol) in 100 mM MES buffer (pH = 5.3) was prepared and added to the SCP pellet. The SCPs were subsequently resuspended and activated for 30 min in a rotator. The activated SCPs were centrifuged and washed once with 100 mM MES buffer (pH = 5.3). Finally, 1.5 mL of a staining solution containing $250 \mu\text{g mL}^{-1}$ FAM-NH₂ was added and allowed to react overnight. Washing of the stained SCPs was conducted as described above.

A protocol for fluorescence microscopy is given in **SI, section 3**.

2.4 Homogeneity assessment of SCPs

For homogeneity assessment of SCPs, bright-field images were acquired as described in **SI section 5**, and analysis was conducted using Fiji. To compare averaged grey value standard deviations, the standard deviation of 15 linear sections within 5 particles per condition was averaged and plotted as a function of functionalization degree.

2.5 Reflection interference contrast microscopy measurements

RICM was used to examine contact areas of SCPs. For analysis, coverslips (\varnothing 32 mm, Menzel Glaeser) were clamped into a Teflon rack, covered with 2 mL of ddH₂O unless otherwise stated, and examined via RICM. The respective SCP suspension was carefully pipetted onto the glass slides, allowed to sediment for 20 min, and the SCPs were subsequently investigated. The probes and their corresponding radial profiles were imaged

using an inverted microscope (Olympus IX73, Germany). To obtain interference reflection patterns, samples were illuminated by a monochromatic 530 nm collimated LED (M530L2-C1, Thorlabs, Germany). An Olympus 60x, NA 1.35 oil-immersion objective (UPlanSApo 60x 1.35) was used. Images were captured with a monochrome CCD camera (DMK 23U274, ImagingSource, Germany) using Micro-Manager microscopy software. All datasets were recorded applying an exposure time of 50 ms and stored in tagged image file format (tiff).

2.6 Preparation of biotin-functionalized SCPs

For the studies of interaction and adhesion of biotin-functionalized SCPs on streptavidin-(SA) coated glass surfaces, SCPs made from a 10% (w/w) solution of starPEG-mal and starPEG-SH were used. 1 mL of the SCP suspension was centrifuged at 1844x g for 10 min and the supernatant was discarded. SCPs were functionalized with biotin by adding 1 mg mL⁻¹ of biotinyl-PEG₂-maleimide (Bachem, Switzerland) dissolved in 100 mM HEPES buffer (pH = 7.0) to the particles. The reaction was allowed to proceed for 1 h while agitating, followed by three washing steps.

2.7 Preparation of streptavidin-functionalized SCPs

Two different strategies were employed to functionalize SCPs with streptavidin (SA). The first strategy utilizes biotin-coated SCPs (see above) and the biomolecular recognition between biotin and SA. Therefore, 1.3 mL of a solution containing 1 mgmL⁻¹ SA (ProSpec-Tany TechnoGene, Israel) in 100 mM HEPES buffer (pH = 7.0) was prepared. 500 µL of a suspension containing biotin-functionalized SCPs was centrifuged, 300 µL of the supernatant was discarded, and the SCPs were subsequently resuspended in the SA solution. After 1 h of incubation while agitating, the SCP suspension was centrifuged again and washed at least three times with 100 mM HEPES buffer.

For coupling via sulfosuccinimidyl 4-(N-maleimidomethyl)cyclohexane-1-carboxylate (s-SMCC, Iris Biotech, Germany), 1.5 mL of a 400 nM s-SMCC solution in 100 mM HEPES buffer was prepared. Subsequently, 1.5 mg of SA were dissolved in the solution and allowed to react for 30 minutes at room temperature. Meanwhile, 500 µL of a suspension containing unfunctionalized SCPs made from 10% (w/w) 2 kDa starPEG-mal and starPEG-SH was

centrifuged, and 300 μL of the supernatant was discarded. 1.3 mL of the solution containing the activated SA was added to the SCPs and left for 1 h. Finally, the suspension was centrifuged and washed three times with 100 mM HEPES buffer.

2.8 Studies of interaction and adhesion of biotin-functionalized SCPs on streptavidin-coated glass surfaces

SA-coated coverslips were incubated with 1.5 mL of dilute biotin (sigma Aldrich, US) solutions dissolved in 100 mM HEPES buffer (pH = 7.0) in a range of 10^{-13} M to 10^{-5} M. After a period of 1 h, the surfaces were washed three times with 100 mM HEPES buffer (pH = 7.0) and clamped in a polytetrafluoroethylene (PTFE) ring for RICM measurements. The surfaces were covered with 1 mL HEPES buffer, and 200 μL of the suspension containing biotin-functionalized SCPs was added dropwise. 50 contact areas per condition were measured as described above.

2.9 Data analysis of RICM measurements

Obtained images of radial profiles resulting from the respective adhering or non-adhering SCPs were analyzed by a home-built software based on pattern matching [32]. Contact areas, particle radii as well as adhesion energies were calculated by the software.

3. Choice of materials and coupling reactions

Elasticity is a key feature of SCPs and the elastic modulus is determined by the precursor material, the solid content of the precursor material used for the synthesis, the particular architecture of the precursor molecule and the reactivity of the functional groups for cross-linking, i.e. the degree of conversion and resulting crosslinking density. As mentioned within the introduction, the lateral resolution of reflection interference contrast microscopy, which determines the accuracy with which the contact area is determined, is set by the limits of conventional optical microscopy and hence, contact areas of adhering SCPs should be larger than 1 μm in diameter [33]. Furthermore, the contact area must be spherical to assure applicability of JKR-model, whereby very soft SCPs with an elastic modulus below 10 kPa are prone to form large and irregular contact areas and high elastic moduli reduce the size of the resulting contact area, thereby decreasing the sensitivity of the assays. Consequently, elastic moduli of SCPs of 20-40 kPa, which yield contact diameters of 1 μm or more with well-defined circular areas, are demanded [34]. In addition, offsets, i.e. the formation of contact areas in the absence of adhesion, should be avoided, as unspecific deformation of SCPs decreases the sensitivity of the respective assays for geometrical reasons.

Colloidal probe assays were carried out using particles made of various materials, including silicone rubber and different hydrogels [34–36]. Silicon rubber-based beads typically suffer from hydrophobic recovery, which renders functionalization of the corresponding probes temporary, making these probes unsuitable [37, 38]. To avoid unspecific deformation and, at the same time, enable sedimentation, the probes should have a density slightly higher than the surrounding aqueous media. This can be conveniently achieved by strong hydration, making hydrogels a superior choice as a probe material. However, certain hydrogels retain water to a large extent due to the presence of charged groups. Such hydrogels are inappropriate for SCP-based sensing approaches, as the high charge density might lead to extensive unspecific adsorption phenomena and blocking of these moieties by conversion into other groups alters the hydration behavior of the material. Consequently, uncharged strongly hydrated polymers are the material of choice for the preparation of the SCP scaffold. While agarose, for example, might also be considered for this purpose, PEG offers the advantage of superior long-term stability of the prepared gels. In addition, the broad commercial availability of derivatives with different functional groups allows preparing SCP by various chemical processes and mechanisms, which facilitates tailoring of the SCP's properties.

PEG-based hydrogels can be prepared by chain-growth polymerization using vinyl-modified PEGs and a radical initiator. In addition, several strategies for preparing PEG-based hydrogels by a step-growth mechanism, leading to more homogeneous gels, were proposed and extensively exploited [39]. Chain-growth-polymerized PEG hydrogels are formed by propagation of active centers, i.e. free radicals, through unsaturated carbon-carbon bonds of the PEG macromonomers, whereas step-growth-polymerized PEG hydrogels are formed by at least two mutually reactive multifunctional macromonomers with an average macromonomer functionality greater than two [39-41]. For our studies, we used different linear as well as a star-shaped four-arm acrylamide-terminated PEGs, all of which are prepared according to the chain-growth mechanism. Low molecular weight PEGs, in this case 0.3 kDa, contribute more functional groups than high molecular weight PEGs, in this case 3.7

kDa at constant solid content. An increased number of functional groups should increase the crosslinking density of the polymer scaffold, increasing the elastic modulus of the corresponding gels. Multi-arm PEGs contribute additional crosslinking points to gel formation independently of the crosslinking reaction, which is useful in case of sluggish conversion of functional end groups. A comparison of the SCPs made from these different PEGs reveals the impact of PEG molecular weight and architecture on the mechanical properties. For step-growth-polymerized gels, two different 2 kDa four-arm PEGs were chosen. The crosslinking relies on a thiol-Michael addition. Maleimides are used as the ene component due to their superior reactivity with thiols compared to e.g. acrylamides and acrylates. The reaction rate is typically adjusted by varying pH and buffer concentration.

A second focus of this study is the functionalizability of SCPs, as this is a prerequisite for performing biosensing assays. Strategies for the introduction of groups for later coupling reactions include post-synthesis grafting of small unsaturated molecules with carboxy groups. This method allows superior control over the density of the functional groups on the SCPs and the carboxy groups without compromising the mechanical properties of the SCPs. As a drawback, several additional steps to introduce these functional groups are necessary [19]. In addition, a one-step procedure for gel formation and functionalization is probed by using molecules bearing photocrosslinkable acrylamide groups as well as carboxy groups for further coupling reactions. This approach is convenient, but the bifunctional molecules for functionalization consume potential crosslinking sites, leading to a decrease in elastic modulus, which must be compensated. As a third option, groups that were not reacted during the crosslinking reaction are tested for their usefulness as functionalization sites. Therefore, unreacted groups were functionalized with bifunctional small molecules, since these are commercially available and inexpensive with a large variety of functional groups. In this context, thiol-Michael addition was used for gels prepared by both chain-growth and step-growth mechanisms since both gels are prepared from precursors containing Michael acceptors. Thiol-Michael additions offer the advantage of high reaction rates with low cross-reactivity and that no other compounds or reagents are required for the coupling.

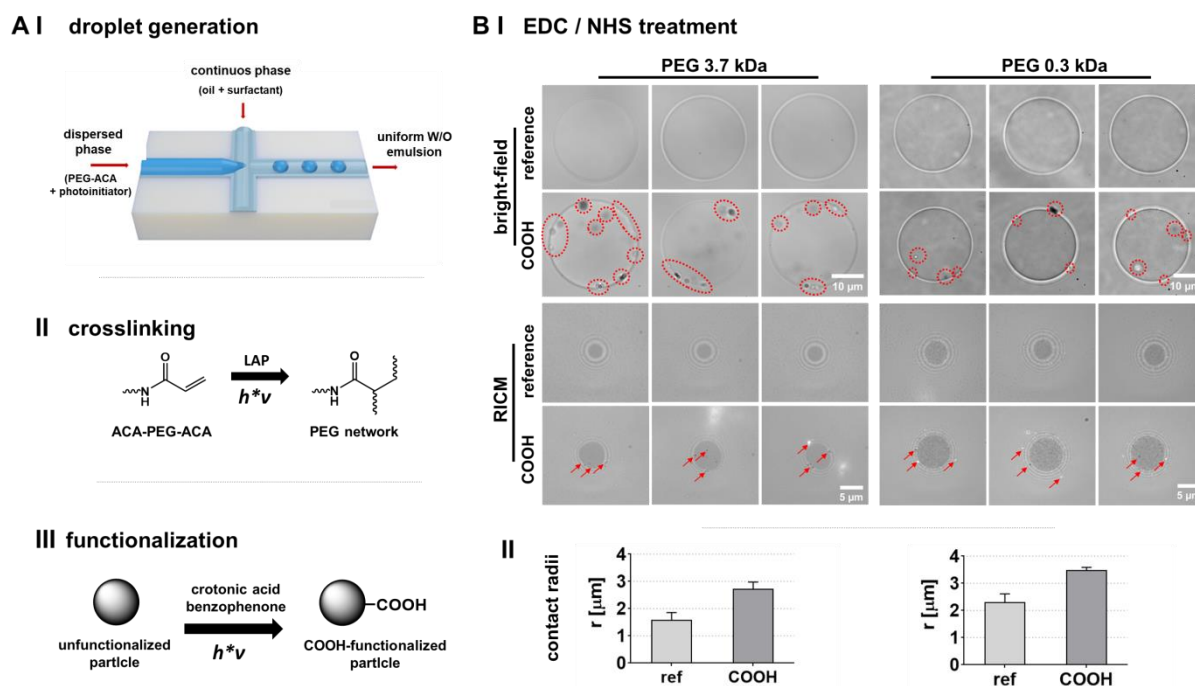
An overview of all synthesized and functionalized SPCs is provided in the SI (see **section 1, tab. S1 in the SI**).

4. Results

4.1 Microfluidic synthesis of SCPs based on photocrosslinkable PEG–ACA and functionalization during synthesis and by post-synthesis photoradical grafting

As a starting point, we probed the transferability of the original synthesis scheme to the microfluidic assisted synthesis of SCPs by employing PEG macromonomers bearing photocrosslinkable ACA end groups as precursor molecules at a concentration of 10% (w/w) [19, 20]. ACA moieties offer the benefit of enhanced stability even under harsh pH conditions when compared to acrylate groups, which are not suitable for integration of Fmoc- and Boc-protecting group strategies. In our experimental setup, we used conventional PDMS-based microfluidic devices with a flow-focusing geometry to generate uniform W/O emulsion droplets. COOH-functionalization of the synthesized probes was carried out using photoradical grafting of crotonic acid to the PEG-network after UV-crosslinking as described previously [18, 20]. An overview of the microfluidic device geometry, crosslinking chemistry and COOH-functionalization is shown in **Fig. 2 a**.

Fig. 2

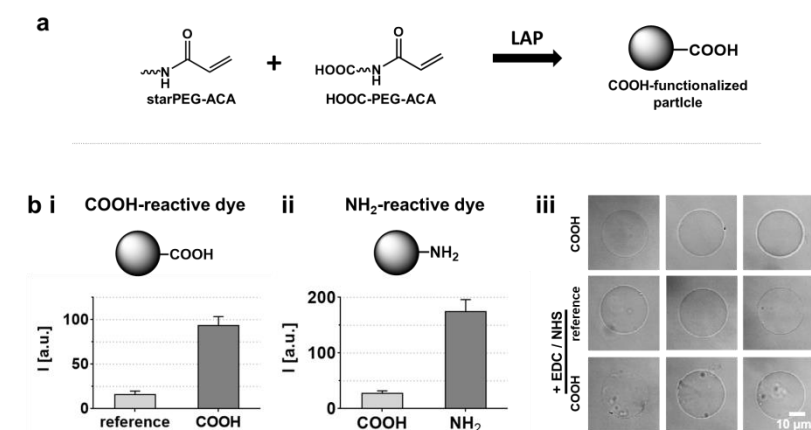


Synthesis, functionalization and characterization of SCPs made from linear PEG-ACA generated by photoradical reactions. **a i** Generation of a uniform W/O emulsion is achieved using a flow-focussing microfluidic device. The premixed dispersed phase made of an aqueous solution of PEG and a photoinitiator is emulsified into droplets by a continuous phase made of a fluorinated oil, supplemented with surfactant to prevent emulsion droplet coalescence. **ii** PEG macromonomers are crosslinked to an insoluble network by UV-initiated radical crosslinking of the ACA end groups. **iii** Post-synthesis COOH-functionalization of SCPs is conducted by UV-initiated abstraction of hydrogen through excited benzophenone from the PEG backbone and subsequent grafting of an unsaturated carbon-carbon bond of a carboxylic acid (crotonic acid). **b i** Top: Comparison of EDC/NHS-treated SCPs made from high molecular weight (3.7 kDa, $Q_d = 40 \mu\text{L h}^{-1}$, $Q_c = 200 \mu\text{L h}^{-1}$) and low molecular weight (0.3 kDa, $Q_d = 50 \mu\text{L h}^{-1}$, $Q_c = 200 \mu\text{L h}^{-1}$) unbranched ACA-PEG-ACA before and after COOH-functionalization by grafting of crotonic acid. All SCPs were treated with EDC/NHS. Upper row: Bright-field images of SCPs. Dashed circles highlight manifestations of EDC/NHS-mediated degradation. Bottom row: Corresponding RICM images. Red arrows highlight manifestations of EDC/NHS-mediated degradation. **ii** Averaged contact radii of at least 10 SCPs per condition are presented. Results are presented as mean + SD.

After synthesis and functionalization, SCPs were examined by bright-field microscopy and RICM. The analysis showed a narrow size distribution of $27 \pm 0.6 \mu\text{m}$ for particles made from 3.7 kDa PEG and $30.5 \pm 1.2 \mu\text{m}$ for particles made from 0.3 kDa PEG. Inclusions within the SCPs could not be found and only a negligible proportion of particles showed other defects like deformations of the spherical shape. Next, the SCPs were activated by active ester chemistry for the coupling of primary amine- (NH_2) containing compounds. In contrast to unfunctionalized SCPs, treatment with EDC/NHS resulted in degradation of COOH-functionalized SCPs, as shown in **Fig. 2 b i**, indicated by dashed red lines (bright-field) and red arrows (RICM). Bright-field microscopy revealed more pronounced defects for 3.7 kDa particles than for 0.3 kDa PEG, but the overall effect was observed in both cases. The impact of EDC/NHS treatment on the mechanical properties of SCPs was studied using RICM. Both COOH-functionalized SCP-types displayed irregular contact areas as well as light and dark

spots. The increase in contact radii after EDC/NHS treatment indicates a change in the SCPs mechanical properties, i.e. softening due to degradation, which disqualifies the overall synthesis and functionalization approach for the envisioned highly sensitive and accurate adhesion energy measurements (see **FIG 2 b ii**). We observed that a reduced degree of functionalization and a reduced EDC/NHS concentration mitigated particle degradation to some extent (data not shown), but the overall effect could not be avoided with this strategy.

Fig. 3



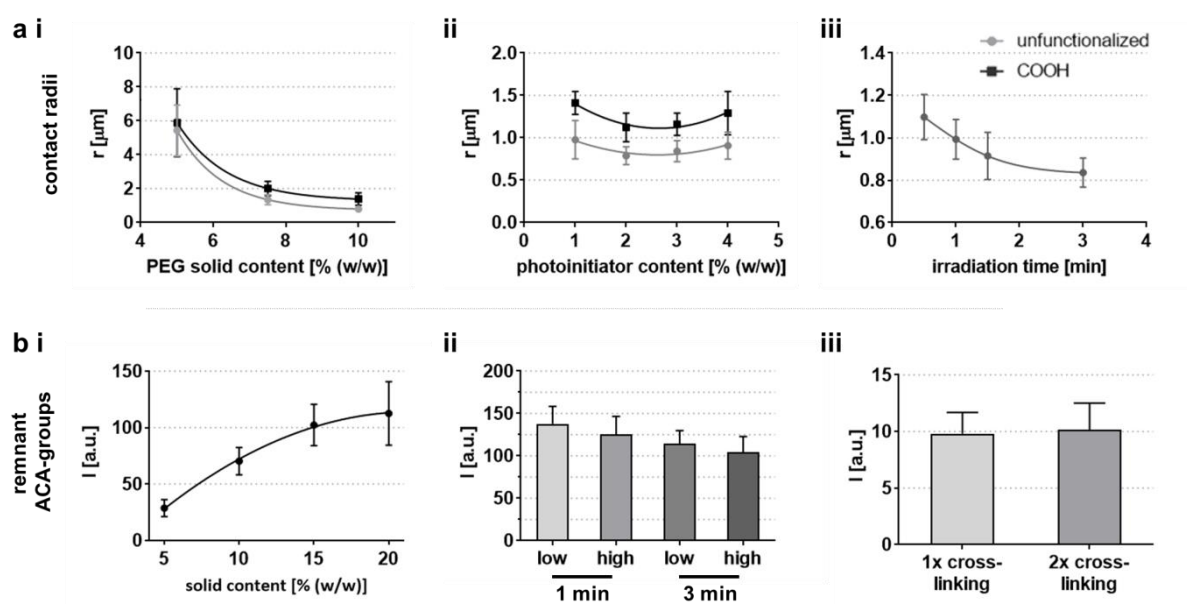
Simultaneous synthesis and COOH-functionalization of SCPs made from starPEG-ACA generated by photoradical reactions. **a** Overview of PEG macromonomers (2 kDa starPEG-ACA and 2 kDa ACA-PEG-COOH) and reaction scheme. UV-initiated crosslinking of the PEG-ACA end groups leads to covalent anchoring of the COOH-bearing PEG derivative to the polymer scaffold by the same photoradical coupling reaction used for macromonomer crosslinking. **b i** Verification of SCP-functionalization based on the comparison of fluorescence intensities via cLSM. COOH-groups of the particles were stained with COOH-reactive FAM-NH₂ by active ester chemistry (EDC/NHS) and analyzed via cLSM to verify the presence of COOH-groups. **b ii** Ethylenediamine is coupled to COOH-functionalized SCPs by active ester chemistry (EDC/NHS), stained with amine-reactive FITC and analyzed via cLSM to verify the presence of NH₂-groups after ethylenediamine functionalization. **b iii** Bright-field images of COOH-functionalized SCPs before and after treatment with EDC/NHS as well as SCPs made from starPEG-ACA (2 kDa) as a reference. Degradation of SCPs is exclusively observable in the case of COOH-functionalized SCPs treated with EDC/NHS (bottom row). 20 SCPs per condition were measured for cLSM and bright-field analysis. Results are presented as mean + SD

As an alternative approach and to investigate whether these detrimental effects arise from the post-synthesis photoradical functionalization, we tested the functionalization of SCPs during particle crosslinking (see **Fig. 3 a**). For this, starPEG-ACA with a molecular weight of 2 kDa was mixed with unbranched heterobifunctional PEG bearing an ACA- and COOH-group. 4-arm-starPEG was chosen to introduce additional crosslinks, as the linear ACA-PEG-COOH reduces crosslinking density. To validate COOH-functionalization, 5(6)-fluorescein ethylenediamine (FAM-NH₂) was coupled to SCPs as a fluorescent tag, whereby particles produced from starPEG-ACA only acted as negative control (reference). Additionally, ethylenediamine was coupled to COOH-functionalized SCPs to introduce NH₂-groups, which

were subsequently labeled with FITC acting as an amine-reactive dye. COOH-functionalized particles served as a negative control. In both cases, the fluorescence intensities were significantly increased compared to the reference SCPs, clearly demonstrating the success of the respective functionalization (**Fig. 3 b i and ii**). Lastly, applicability for active ester chemistry was probed by treatment of the particles with EDC/NHS. **Fig. 3 b iii** shows representative SCPs before and after EDC/NHS treatment, which reveal a similar degree of degradation as observed for the aforementioned types of COOH-functionalized SCPs (**Fig. 2**).

4.2 Characterization and optimization of double bond conversion and mechanical properties of SCPs based on photocrosslinkable starPEG-ACA

To overcome these obstacles, we decided to closely examine and optimize synthesis and functionalization parameters. Here, we started with an improvement of double bond conversion by adjusting solid content, photoinitiator concentration as well as irradiation time and intensity. To test the dependence of SCP contact area on the tested parameters, SCPs were applied to glass slides cleaned with isopropanol in an ultrasonic bath. These surfaces possess sufficient hydrophobicity to drive entropic adhesion of SCPs. SCPs synthesized using flow rates of $Q_d = 50 \mu\text{L h}^{-1}$ and $Q_c = 200 \mu\text{L h}^{-1}$ revealed only minor differences in diameter ($24.4 \pm 1.0 \mu\text{m}$ (5% (w/w)), $24.2 \pm 1.0 \mu\text{m}$ (7.5% (w/w)) and $22.6 \pm 0.6 \mu\text{m}$ (10% (w/w))), making RICM a suitable method to compare contact radii and indirectly particle stiffness (see **eq. 1**).

Fig. 4

Analysis and optimization of synthesis and functionalization parameters of SCPs made from 2 kDa starPEG-ACA ($Q_d = 50 \mu\text{L h}^{-1}$, $Q_c = 200 \mu\text{L h}^{-1}$). **a** The impact of synthesis parameters on the mechanical properties of SCPs was probed by contact area analysis using RICM. SCPs with a lower elastic modulus are characterized by the formation of increased contact radii. **i** Analysis of contact radii in dependence on PEG solid content at 1% (w/w) photoinitiator concentration. **ii** Contact radii in dependence on photoinitiator concentration (10% (w/w) PEG). **iii** Contact radii in dependence on UV irradiation time (10% (w/w) PEG, 2% (w/w) photoinitiator). The graphs for non-functionalized and functionalized SCPs are indicated by grey and black lines, respectively. SCPs adhered to uncoated glass surfaces. Mean contact radii of at least 50 particles per condition are shown except for SCPs made from 5% (w/w) PEG solutions. In this case, the mean contact radius of 10 SCPs is presented. Error bars indicate SD. **b** Determination of remnant ACA-groups of FITC-labeled unfunctionalized SCPs by cLSM. Fluorescence intensity increases with an increasing number of remnant ACA-groups. **i** Variation of the solid content of the PEG solutions between 5 and 20%. The number of remaining ACA-groups correlates positively with the solid content. **ii** Impact of UV intensity and irradiation time. Both correlate positively with double bond conversion. The low and high irradiation intensity represents a curing setup with five 8 W UV lamps (low) and a 250 W (high) UV lamp, respectively. **iii** Impact of a repeated crosslinking step after initial crosslinking and workup. Photoinitiator was added to an SCP suspension and irradiated. Both crosslinking steps were conducted using a curing setup with five 8 W UV lamps and an irradiation time of 3 minutes. The photoinitiator content used for all SCP syntheses depicted in **b** was 2% (w/w). At least 20 particles per condition were fluorescently labeled and measured via cLSM. Results are presented as means and error bars indicate SD

As expected, contact areas of SCPs adhering to unfunctionalized glass surfaces decreased with increasing PEG solid content, indicating higher elastic moduli for higher solid contents (**Fig. 4 a i**). It has to be noted that SCPs made from 5% (w/w) PEG solutions yielded blurred, non-circular interfacial areas and a lack of Newtonian fringes, making this type of SCP unsuitable for precise measurements. RICM images of SCPs made from 7.5 and 10% (w/w) PEG solutions showed strong contrast and circular contact areas. The particle stiffness could be further increased by using higher concentrated PEG solutions above 10% (w/w) (see **section 7, fig. S1 in the SI**). However, follow-up experiments were conducted with SCPs made from 10% (w/w) PEG solutions, as SCPs with higher elastic moduli resulted in smaller contact areas and consequently lower sensitivity in subsequent sensing applications. Additionally, higher concentrated PEG solution exhibit increased viscosity, which might lead

to non-uniform SCPs and satellite droplet formation. A slight difference between unfunctionalized and COOH-functionalized SCPs could be observed, indicating either the presence of attractive interactions between SCPs and the glass surface or negligible alterations of elastic moduli after COOH-functionalization.

Next, the effect of photoinitiator concentration on the double bond conversion of the SCPs was examined. Photoinitiator contents ranging from 1 to 4% (w/w) were tested. Increasing the concentration from 1 to 2% (w/w) resulted in smaller contact areas for both unfunctionalized and COOH-functionalized SCPs (**Fig. 4 a ii**). A further increase above 2% (w/w) resulted in larger contact radii, most likely due to chain terminations caused by the increased amount of photoinitiator radicals in higher concentrated solutions. The photoinitiator concentration for subsequent experiments was therefore set to the optimum concentration of 2% (w/w). In addition to the aforementioned synthesis parameters, the irradiation time was optimized. Freshly synthesized SCPs were UV-irradiated (254 nm) for 0.5 to 3 min, and contact radii were analyzed by RICM. As can be seen from **Fig. 4 a iii**, the SCP stiffness (i.e. the decrease in the contact area) correlates with the exposure time, with saturation being reached after 3 minutes of UV exposure.

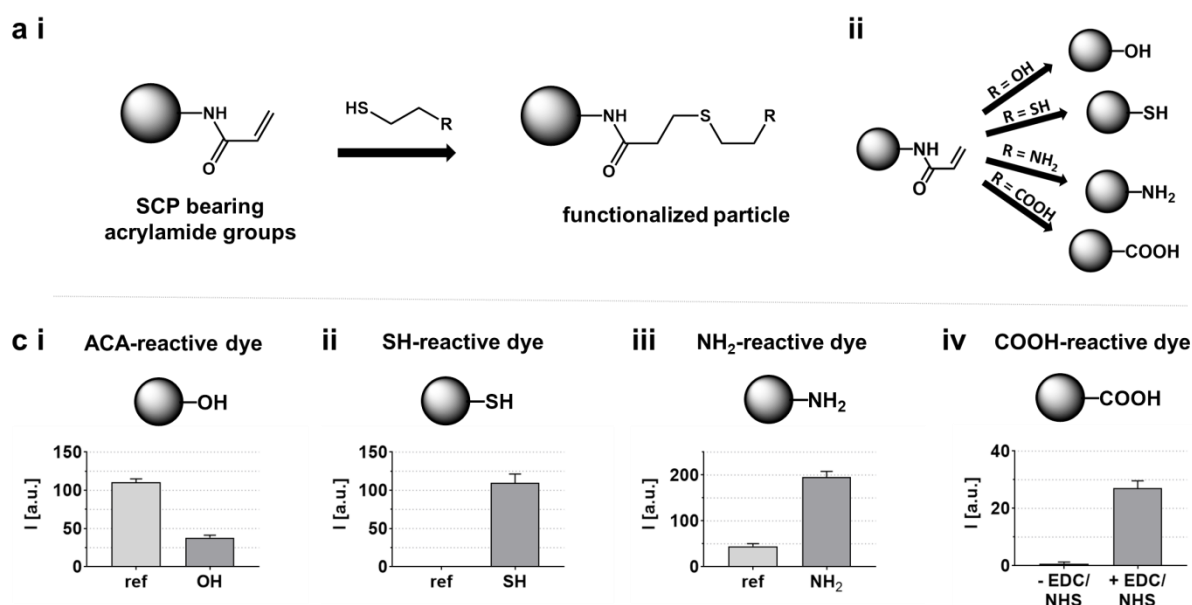
It should be noted that confinement of polymer precursor molecules at high w/w content within the comparatively small droplet volume generated by the microfluidic flow-focusing device is associated with a steric hindrance that severely limits the mobility of the reactive species during crosslinking. Hence, unreacted functional ACA-residues are most likely present in the resulting particles, as reported in previous studies [42]. We therefore exploited fluorescein isothiocyanate (FITC) for labeling these remnant groups. As can be seen from **Fig. 4 b i**, the number of available ACA-groups increased strongly with the PEG macromonomer solid content. A similar series of experiments with mixtures of linear and starPEG macromonomers did not reveal options for a comprehensive improvement of double bond conversion or a reduction of the remnant functional groups (see **section 8, fig. S2 in the SI**). The addition of highly mobile monofunctional small molecules to quench the remnant groups was not tested at this point, as this strategy is expected to excessively reduce the elastic moduli. Therefore, we investigated the impact of UV irradiation time as well as intensity on the number of remnant ACA-groups using a low ($5 \times 8 \text{ W}$, 43 mW cm^{-2}) and a high energy (250 W , 250 mW cm^{-2}) UV curing device to exclude possible consequences of oxygen inhibition due to rapid diffusion of gas into the solution. Only a minor improvement could be achieved by increasing the UV intensity, whereby the same UV irradiation time dependence could be observed for both setups (**Fig. 4 b ii**). Prolonged irradiation at high

intensity yields clumped and irregularly shaped SCPs (data not shown). Finally, to verify that the maximum double bond conversion for the 2 kDa starPEG-ACA system was achieved, we followed up with a second crosslinking step, i.e. the addition of photoinitiator to cured and fully swollen SCPs. As no difference in fluorescence intensity in comparison to the reference (1x crosslinking) could be detected, it was concluded that no further improvements regarding double bond conversion are possible (**Fig. 4 b iii**).

4.3 Functionalization of SCPs based on photocrosslinkable starPEG-ACA by thiol-Michael addition using remnant ACA-groups

After optimizing and analyzing the double bond conversion of starPEG-ACA-based SCPs, we explored strategies for quenching residual unreacted ACA-moieties and alternatively introducing functional groups that utilize ACA-groups. As possible reaction partners, we used isopropyl-isothiocyanate as an isothiocyanate derivative for addition to ACA-groups. Furthermore, hydroquinone and mequinol were exploited as radical scavengers to prevent thermally initiated radical reactions arising from ACA-groups (data not shown). Both strategies proved to be inefficient compared to the thiol-Michael addition of ethanethiol derivatives and were not considered further for follow-up experiments. In contrast, strategies for conversion of remnant ACA-groups to OH-, SH-, NH₂- as well as COOH-groups were extensively exploited as depicted in **Fig. 5**. The ethanethiol related molecules mercaptoethanol, ethanedithiol, cysteamine and thioglycolic acid served as bifunctional small molecules, whereby the SH-group, respectively one of the SH-groups in the case of ethanedithiol, was coupled to a remnant ACA-moiety and the second functional group, i.e. OH, SH, NH₂ or COOH, determines the functionality of the SCP (**Fig. 5 a i and ii**).

Fig. 5



SCP-functionalization by thiol-Michael addition. **a i** Reaction scheme: Remnant ACA-groups of SCPs serve as Michael acceptors for the thiol addition of ethanethiol derivatives to introduce diverse functional groups by coupling after synthesis of SCPs. **a ii** Overview of prepared SCP types. Conversion into OH-, SH-, NH₂- and COOH-functionalized SCPs is achieved by using mercaptoethanol, ethanedithiol, cysteamine and thioglycolic acid, respectively. **b** Verification of SCP-functionalization based on the comparison of fluorescence intensities. **i** OH-functionalization was examined by FAM-SH and the corresponding decrease of ACA-groups after mercaptoethanol-functionalization. **ii and iii** Detection of SH- and NH₂-groups by reacting the SH-group with FAM-mal and the NH₂-group with TAMRA-scm. Both dyes offer a specific reactivity for the respective functional group. **iv** COOH-groups were verified by reacting FAM-NH₂ in the absence (no reaction) and presence (reaction proceeds) of EDC/NHS. Fluorescence intensities of the labeled SCPs were assessed by cLSM. 60 particles per condition were measured. Results are presented as mean + SD

All functionalization approaches were specifically probed by fluorescence staining of SCPs and cLSM analysis. 5-(6)-carboxyfluorescein-thiol (FAM-SH) was used to verify OH-functionalization, as the introduction of OH-groups is accompanied by consumption of available ACA-groups. SH- and NH₂-functionalized SCPs were directly labeled by SH-reactive *N*-(5-fluoresceinyl)maleimide (FAM-mal) and amine-reactive 5(6)-carboxymethylrhodamine succinimidyl ester (TAMRA-scm), respectively. 5-(6)-carboxyfluorescein ethylenediamine (FAM-NH₂) was coupled to COOH-groups by pre-activation of SCPs with EDC/NHS and the same conditions were applied in the absence of EDC/NHS to obtain a negative control.

As shown in **Fig. 5 c i**, the fluorescence intensity emanating from SCP-coupled FAM-SH is significantly reduced after mercaptoethanol-functionalization, indicating the successful introduction of OH-groups. SH- as well as NH₂-functionalization, could be verified by the strong increase of fluorescence intensities for ethanedithiol- or cysteamine-functionalized SCPs in comparison to unfunctionalized SCPs (**Fig. 5 c ii and iii**). Finally, COOH-

functionalization via coupling of thioglycolic acid was examined. Only SCPs preactivated with EDC/NHS exhibit notable fluorescence, proving successful introduction of COOH-groups (**Fig. 5 c iv**).

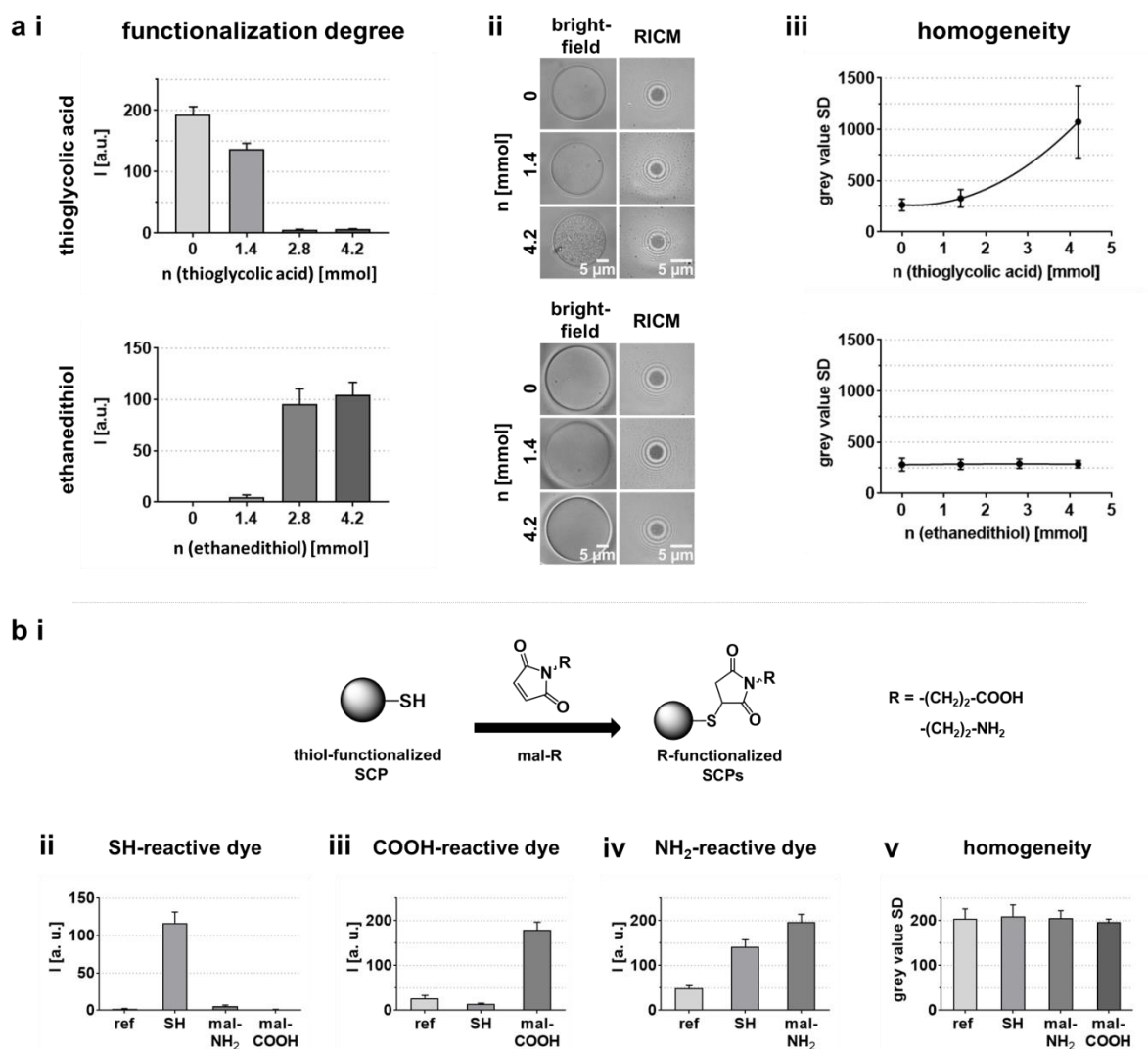
It can be concluded that the thiol-Michael addition of thiol compounds to remnant ACA-groups is a simple method for introducing distinct moieties that are not limited to the bifunctional small molecules mentioned above. It should be noted that the more commonly used PEG acrylates are stronger Michael acceptors than ACA and that the functionalization of acrylate-based hydrogels in this way should be even more efficient.

4.4 Impact of thiol-Michael addition-based conjugation on SCP characteristics

After evaluating the functionalization of starPEG-ACA-based SCPs, we examined the SCPs for possible impacts of the functionalization on homogeneity and the occurrence of degradation effects. Since the extent of degradation is likely to be related to the degree of functionalization, both characteristics were correlated for all different types of functionalized SCPs. A stepwise increase in functionalization degree was achieved by the addition of solutions containing 1.4, 2.8 or 4.2 mmol of the bifunctional molecules to 2.5 mL of the corresponding particle suspension. Functionalization was verified using FITC for ACA-staining to probe thioglycolic acid-, i.e. COOH-, and FAM-mal to probe ethanedithiol-, i.e. SH-, functionalization. As shown in **Fig. 6 a i**, the fluorescence signal of FITC-stained ACA-groups decreases with increasing amounts of mercaptoethanol coupled to SCPs and the enhancement of the signal, arising from SH-groups, correlated with the amount of ethanedithiol added to the SCPs. In both cases, saturation was achieved at 4.2 mmol. Microscopic analysis by bright-field microscopy as well as RCM imaging was used to examine defects of SCPs after functionalization. The analysis revealed structural irregularities within the SCPs and the corresponding interfaces for COOH- but not SH-functionalized SCPs (**Fig. 6 a ii**). Following the idea that these structural defects on the micrometer scale are associated with a broadening of the range of the grey values recorded, we analyzed the grey value distribution within a suitable section of one representative particle per condition for homogeneity assessment. COOH-functionalized SCPs showed a broadening of the Gaussian with increasing functionalization degree, whereas grey value distributions for all types of SH-functionalized SCPs exhibit impeccable overlap with the reference (0 mmol), thereby indicating the absence of degradation effects (see **section 9, fig. S3 in the SI**). To assure an

adequate averaging over several SCPs, the standard deviation of 15 sections was calculated and utilized as a measure of homogeneity. As depicted in **Fig. 6 a iii**, the mean values, i.e. the severity of structural defects, likewise positively correlates with the functionalization degree in the case of COOH-functionalized but not SH-functionalized SCPs.

Fig. 6



Characterization of functionalized SCPs made from 2 kDa starPEG-ACA. **a** Comparison of thioglycolic acid (COOH) and ethanedithiol (SH) functionalization. **i** Dependence of the functionalization degree on the concentration of the bifunctional ethanedithiol derivative. In the case of thioglycolic acid (COOH-) functionalization, ACA-groups were stained with FITC. Fluorescence intensity inversely correlates with the degree of functionalization due to consumption of ACA-groups. Ethanedithiol- (SH-) functionalized SCPs were stained with FAM-mal. Fluorescence intensity correlates positively with the degree of functionalization due to a progressively increasing number of SH-groups. **ii** Bright-field images and RICM micrographs of SCPs functionalized with different concentrations of ethanedithiol derivatives to detect alterations of the structure of SCPs as a result of functionalization. Structural distortions are observed in SCPs treated with thioglycolic acid. **iii** Comparison of averaged grey value standard deviations of cross sections of SCPs for quantifying the impact of functionalization on the homogeneity of the SCPs. The averaged grey value standard deviation correlates positively with the extent of structural distortions. **b** Post-functionalization of SCPs bearing SH-groups introduced by post-synthesis thiol-Michael addition. **i** Reaction scheme. A bifunctional small molecule bearing a maleimide for specific conjugation to the SH functionalized SCP converts the functionalization from maleimide to group R. In the data shown, R is either an ethylamine or a propionic acid residue, introducing NH₂ and COOH-groups, respectively. **ii-iv** Verification of SCP-functionalization based on the comparison of fluorescence intensities measured by cLSM. Verification of SH, NH₂ and COOH-functionalization is conducted using FAM-mal (SH-reactive dye (**ii**)), FAM-NH₂ + EDC/NHS (COOH-reactive dye (**iii**)) and FAM-scm (NH₂-reactive dye (**iv**)), respectively. **v** Homogeneity analysis by comparison of post-functionalized SCPs and SH- as well unmodified SCPs (reference). Averaged grey value standard deviations are constant and do not reveal an increase of structural distortions as a result of functionalization. For all cLSM-based analysis of SCPs, 60 particles per condition were measured. For homogeneity assessment by comparison of grey value SD, 5 SCPs per condition, each at 3 different regions, were measured. Results are presented as means and error bars indicate SD

A comparison of structural homogeneity between the different types of SCPs by particle grey value SD analysis is provided in the ESI (see **SI, section 9**). Increasing structural irregularities of the different types of SCPs were observed in the order SH < NH₂ < OH < COOH with additional EDC/NHS-mediated degradation encountered in the case of SH-, NH₂- and COOH-functionalized SCPs. As an alternative strategy, the possibility of coupling further compounds to SH-groups presented by ethanedithiol-functionalized SCPs was exploited using bifunctional maleimides in a similar way as described for the aforementioned thiol compounds. 2-maleimidoethylamine (mal-NH₂) and 3-maleimidopropionic acid (mal-COOH) served as prototypic compounds for this approach (**Fig. 6 b i**). Functionalization was verified by labeling the SH-groups with FAM-mal (**Fig. 6 b ii**) and NH₂-groups with FAM-scm (**Fig. 6 b iii**). COOH-groups were stained with FAM-NH₂ + EDC/NHS (**Fig. 6 b iv**). All experiments indicated successful coupling of the maleimide compounds, as can be concluded from the infinitesimal fluorescence of maleimide-functionalized, FAM-mal-stained SCPs and the increase of signal intensity of mal-NH₂ and mal-COOH-functionalized SCPs labeled with the respective specific dye. FAM-scm shows reactivity towards SH-groups, most likely due to the formation of thioester linkages, which can be removed by basic workup, i.e. at elevated pH, of the suspension. Importantly, the maleimide addition step did not affect the particle homogeneity, although the subsequent application of EDC/NHS active ester chemistry led to the same degradation as observed before (see **section 9, fig. S3 in the SI**). Similar results were obtained by introduction of SH-groups using hydrogen disulfide (H₂S) instead of ethanedithiol. H₂S-functionalized SCPs did not reveal any degradation effects either (see **section 10, fig. S4 in the SI**).

To summarize the microfluidic SCP synthesis and functionalization based on photocrosslinkable ACA-PEG macromonomers, SCP functionalization is conveniently achieved by reacting acrylamide residues within the PEG-meshwork with thiol compounds by thiol-Michael addition. However, a strong dependence between structural inhomogeneities within SCPs and the functional groups of the bifunctional molecules used for SCP functionalization was observed. These inhomogeneities were not elicited by SH-groups and the coupling reaction itself. Testing the suitability of SCPs for active ester chemistry revealed general inapplicability of EDC/NHS-mediated coupling reactions due to structural defects, independent of the chosen strategy for introducing functional groups. On the other hand, coupling of maleimide compounds to SCPs bearing SH-groups was not accompanied by further degradation or the occurrence of any distortions within the PEG network, making SH-functionalized SCPs the superior basis for the envisioned sensing system.

4.5 Microfluidic synthesis, functionalization and characterization of SCPs based on thiol-Michael addition of starPEG-SH and starPEG-mal

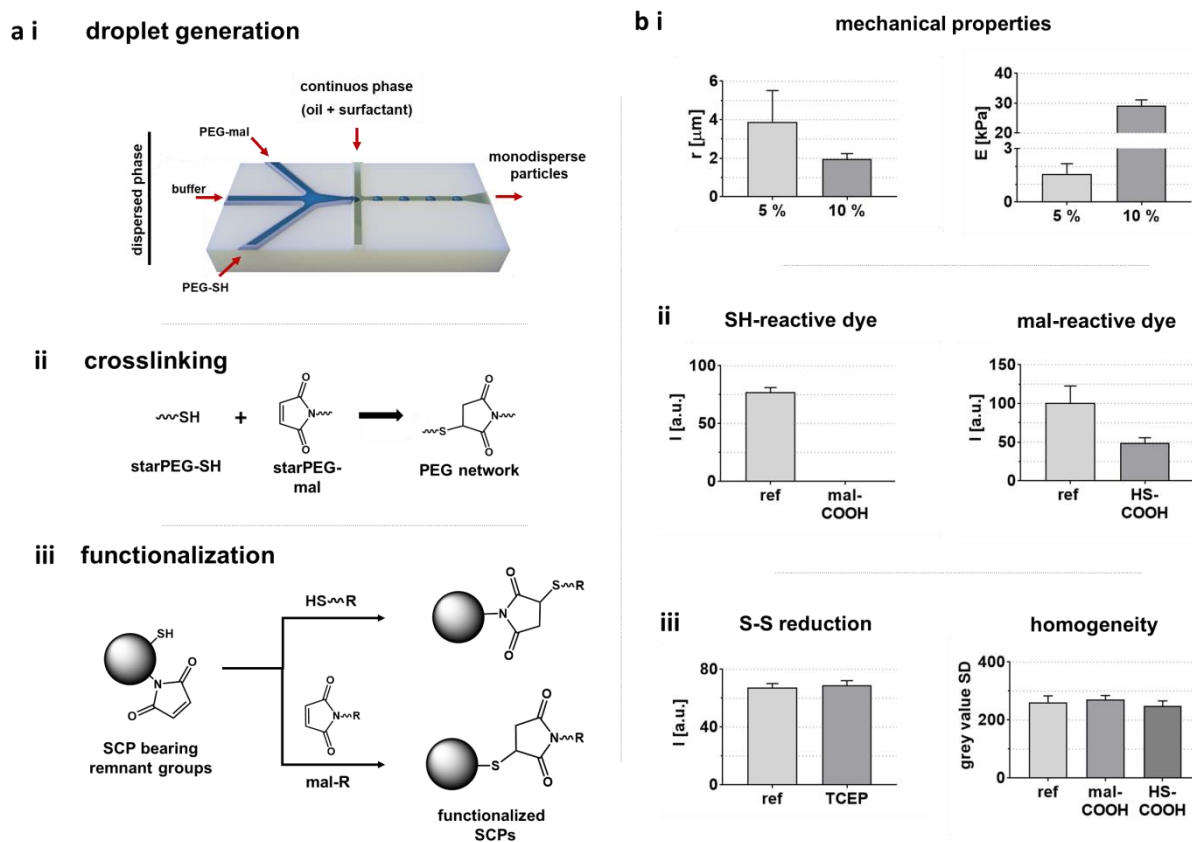
In the light of the above findings, we decided to investigate a fundamentally different particle synthesis setup using thiol-Michael addition of maleimides as acceptors to avoid multi-step post-synthesis functionalization protocols. A PDMS-based flow-focusing microfluidic device with four inlets was used to achieve on-chip crosslinking of homofunctional 2 kDa four arm starPEG maleimide (starPEG-mal) and 2 kDa four arm starPEG-thiol (starPEG-SH, **Fig. 7 a i** and **ii**). For further functionalization of the corresponding SCPs, the possibility of employing remnant SH- or mal-groups was investigated (**Fig. 7 a iii**).

Initially, the mechanical properties, i.e. elastic modulus and resulting contact area, of SCPs made from a 5% (w/w) and 10% (w/w) PEG solution (each 50% starPEG-mal and 50% starPEG-SH) was evaluated. The particles were $33.8 \pm 1.9 \mu\text{m}$ (5% (w/w)) and $30.0 \pm 0.6 \mu\text{m}$ (10% (w/w)) in diameter. It has to be noted that SCPs made from 5% (w/w) PEG solutions generally exhibited non-circular contact areas due to the low stiffness of the polymer network, which was further confirmed by AFM-nanoindentation experiments (**Fig. 7 b i**). SCPs made from 10% (w/w) starPEG solutions, on the other hand, exhibited regular contact areas of roughly $2 \mu\text{m}$ in diameter on coverslips cleaned with isopropanol in an ultrasonic bath, representing a satisfactory ratio between particle and contact radius, accompanied by an elastic modulus of nearly 30 kPa, which fits an optimal range of sensitive and robust biosensing applications of the SCP assay.

Next, the SCPs were screened for unreacted SH- and mal-moieties which could be utilized for subsequent conjugation reactions. Therefore, the SCPs were functionalized with the model compounds mal-COOH as well as thioglycolic acid (HS-COOH). The functionalized SCPs were compared to unfunctionalized reference SCPs after labeling with SH- (FAM-mal) and mal- (FAM-SH) reactive dyes. The results indicate complete conversion of SH-groups after 1 h reaction with mal-COOH. Functionalization with HS-COOH under the same conditions led to incomplete conversion (**Fig. 7 b ii**). The latter approach was therefore not further pursued. It is necessary to note that these results strongly depend on experimental details, as both thiol and maleimide are susceptible to oxidation, i.e. disulfide formation and hydrolysis of the maleimide, respectively, and both effects are heavily affected by pH and other factors [43, 44]. Maleimides in the SCP networks are most likely hydrolyzed after synthesis and 24 h storage and unspecific coupling of FAM-SH might be a result of disulfide formation, contributing to the observed fluorescence signal when using FAM-SH. Therefore, the rapid

and quantitative functionalization of SCPs by targeting remnant SH-groups was used in follow up experiments. To probe whether thiol-oxidation plays a role for storage of unfunctionalized SCPs, the particles were labeled with FAM-mal after one week of storage and compared to SCPs after the addition of the reducing agent tris(2-carboxyethyl)phosphine (TCEP). Additionally, the impact of functionalization with mal-COOH as well as HS-COOH on particle homogeneity was tested by grey value SD analysis (**Fig. 7 b iii**). As neither storage nor functionalization did affect the SCPs, we decided to proceed with the biofunctionalization of SCPs using maleimide derivatives.

Fig. 7

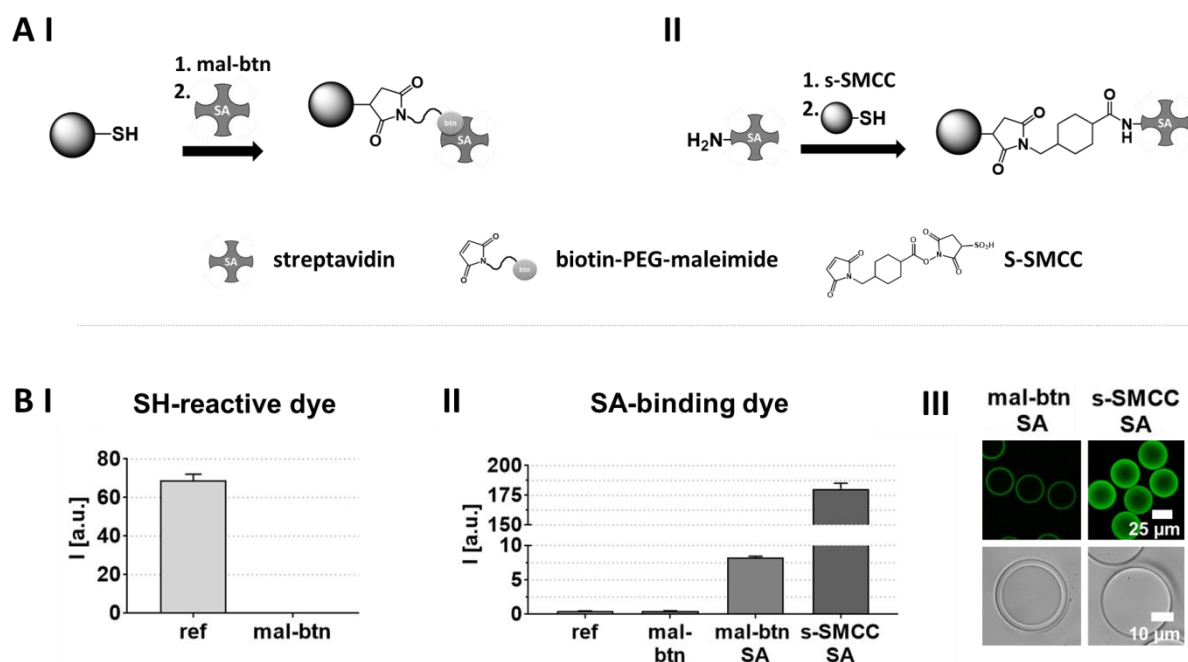


Synthesis, functionalization and characterization of SCPs made from 2 kDa starPEG-SH and 2 kDa starPEG-mal. **a i** Generation of a uniform W/O emulsion is achieved using a flow-focussing microfluidic device. starPEG-SH solution, starPEG-mal solution and PBS are co-injected into the microfluidic device and emulsified into droplets by a continuous phase made of a fluorinated oil, supplemented with a surfactant (continuous phase) to prevent emulsion droplet coalescence. **ii** Crosslinking proceeds within the droplets, and monodisperse SCPs are formed. Macromonomer crosslinking and gel formation is achieved by thiol-maleimide addition. **iii** SCPs are functionalized using remnant functional groups, which are further functionalized by thiol-maleimide addition using bifunctional small molecules with either a mal- (SH-reactive) or SH- (mal-reactive) group. **b i** Characterization of mechanical properties by RICM and AFM. Contact radius r measured via RICM and the elastic modulus E measured via AFM correlate inversely. **ii** Functionalization strategies employing maleimides and thiols probed by cLSM. FAM-mal (SH-reactive) is used for detecting remnant SH-groups. SH-groups of the SCP are blocked by reaction with mal-COOH. FAM-SH (mal-reactive) is used to detect unreacted mal-groups. mal-groups of the SCP are blocked by reaction with HS-COOH. The decrease in fluorescence intensity resulting from the conversion of either SH- or mal-groups of the SCP indicates functionalizability with maleimide and thiol compounds, respectively. **iii** Impact of disulfide reduction using TCEP as reducing agent to probe the extent of thiol oxidation after 1 week of storage as well as homogeneity assessment using cLSM and bright field microscopy. Neither extensive thiol oxidation nor impacts of the functionalization reactions on the particle homogeneity were detected. Fluorescence intensities were calculated from 60 particles per condition. For homogeneity analysis, 15 suitable sections within 5 different SCPs per condition were evaluated. Results are presented as means + SD

To investigate the suitability of this functionalization strategy for protein immobilization on the SCPs, we used streptavidin (SA) as a model-protein due to the specific detectability by labeled biotin. Additionally, the SA-coated SCPs serve as a platform for convenient binding of several molecules of interest to SCPs using the streptavidin-biotin-system. **Fig. 8 a** depicts the strategies chosen for SA-functionalization. As a first approach, biotinyl-PEG₂-maleimide

(mal-btn) was used to introduce biotin and bind tetravalent SA (**Fig. 8 a i**) where the unoccupied binding pockets served as the basis for post-functionalization. The second approach made use of a low molecular excess of sulfosuccinimidyl 4-(N-maleimidomethyl)cyclohexane-1-carboxylate (s-SMCC), presenting an activated COOH-group for SA-coupling and a mal-group for tethering the conjugate to SCPs in a subsequent step (**Fig. 8 a ii**). mal-btn-coupling was examined using FAM-mal for labeling of SH-groups, whereby a quantitative conversion of SH-groups could be achieved as shown in **Fig. 8 b i**. SA-immobilization was verified via labelling of the binding pockets with biotin-4-fluorescein (FAM-btn). Both strategies indicated efficient coupling of SA to SCPs but the resulting labeling degree turned out to be several orders of magnitude higher utilizing s-SMCC (**Fig. 8 b ii**). The appearance of both types of SCPs also differed profoundly. The mal-btn-functionalization strategy led to SCPs labeled exclusively in the fringe area and bright-field imaging revealed the formation of a ring-shaped structure in the SA-functionalized region (**Fig. 8 b iii**). Additionally, crosslinking between SCPs was observed. On the other hand, s-SMCC-SA conjugates are capable of penetrating into the SCPs and such functionalized SCPs did not show any structural alterations, formation of ring-shaped structures or SCP aggregates.

Fig. 8



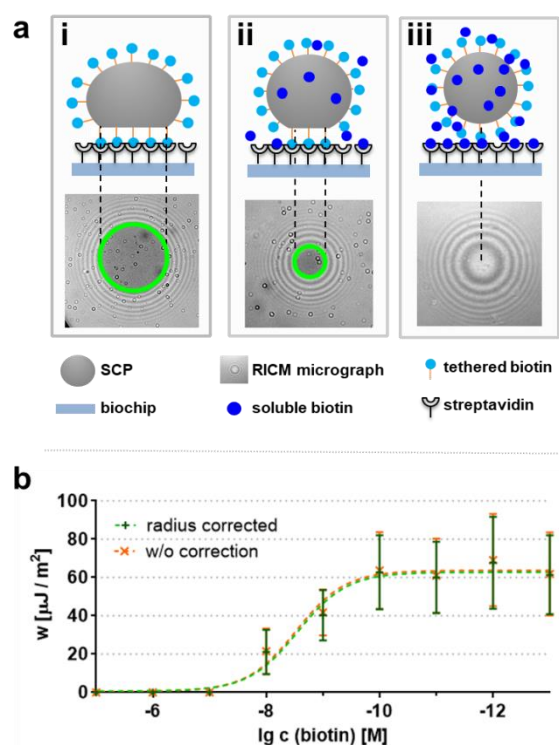
Biofunctionalization of SCPs made from 2 kDa starPEG-SH and 2 kDa starPEG-mal with streptavidin (SA). **a** Overview of functionalization strategies. **i** Biotinyl-PEG₂-maleimide (mal-btn) is coupled to SCPs bearing SH-groups using thiol-maleimide addition. Subsequently, SA is tethered to the biotin-functionalized SCPs using affinity binding. Tetravalency of SA assures the presence of unoccupied binding pockets of the immobilized protein. **ii** Sulfo succinimidyl 4-(N-maleimidomethyl)cyclohexane-1-carboxylate (s-SMCC) is coupled to an NH₂-group of SA for introducing mal-groups in a first step. In a second step, the mal-functionalized SA is added to a suspension of SCPs bearing SH-groups, and immobilized on the SCPs using thiol-maleimide addition. **b i** Proof of mal-btn-coupling using FAM-mal labeling and cLSM analysis. SH-groups are quantitatively converted, resulting in weakly fluorescent SCPs. **ii** SA-immobilization was probed using affinity binding of biotin-4-fluorescein (FAM-btn) to SA decorated SCPs and cLSM analysis. Strong fluorescence is exclusively detectable for SA functionalized SCPs, with SA immobilization using s-SMCC yielding the highest fluorescence intensity and therefore highest SA density. **iii** Micrographs showing the appearance of SA-functionalized SCPs were recorded by cLSM (top) and bright-field microscopy (bottom). Annular structures are formed in the case of the mal-btn functionalization strategy, while no such effect is observed for the s-SMCC functionalization strategy. Please note that only cross-sections in close proximity to the SCP-glass surface interface were measured to obtain fluorescence intensities in these homogeneously labeled regions. Fluorescence intensities were calculated from 60 particles per condition. Results are presented as means +SD

4.6 Proof of suitability of SCPs based on thiol-Michael addition for the sensitive quantification of analytes

Finally, we employed the streptavidin-biotin system as a model system to prove the suitability of the newly developed SCPs for biosensing approaches. Additionally, we probed their applicability for assays, without the necessity of determining the individual size of each particle for precise analyte concentration measurements. The latter point is of particular interest as the possibility of directly relating the analyte concentration to the contact areas makes the RICM-based reconstruction of height profiles of adhering SCPs redundant. Height reconstruction is necessary to calculate SCP radii as well as adhesion energies (see **eq. 1**). It requires resources for high-resolution optical instrumentation, image acquisition and data evaluation, which hinders the development of inexpensive miniaturized on-site analysis devices.

The experimental setup and results are depicted in **Fig. 9**. Biochips covalently coated with SA were prepared by reacting an anhydride-functionalized glass slide with the NH_2 -groups of SA (see **section 11, fig. S5 in the SI**). Tetravalency of SA ensures the presence of sufficient available binding sites for biotin. For binding assays, the biochips were incubated with soluble biotin in a concentration range from 10^{-13} to 10^{-5} M and biotin-functionalized SCPs were added so that a concentration-dependent differential adhesion between biochip and SCPs should be observable as schematically illustrated in **Fig. 9 a**. For this experiment SCPs based on thiol-Michael addition of starPEG-SH and starPEG-mal were used due to their simple and efficient biofunctionalization with biotiny-PEG-maleimide. Since no precise quantification of the SCPs was required for these experiments, SCPs were added to the SA-coated biochips so that no overlap was observed.

Fig. 9



Results of SCP-based biotin quantification using SCPs functionalized with s-SMCC conjugated SA. **a** Assay principle: **i** An SCP equipped with biotin adheres to a transparent biochip bearing immobilized SA and forms an extended interfacial area as a result of biospecific interactions. **ii** Soluble biotin blocks binding sites for particle tethered biotin. As a result, the contact area and adhesion energy between SCP and biochip decreases. **iii** At high concentrations of soluble biotin, the presented binding sites are completely occupied and the SCP cannot adhere to the biochip anymore. Immobilized SA molecules are depicted as monomers for better overview. **b** Comparison of biotin concentration dependent adhesion energies of SCPs. Adhesion energies were calculated on the basis of individual particle radii (green, radius corrected) and an averaged particle radius (orange, w/o radius correction). 60 particles per concentration were measured. The averaged SCP radius was calculated from 600 SCPs and is 14.9 μm . Results are presented as means \pm SD

In this verification experiment, we compared adhesion energies calculated based on an averaged particle radius (w/o radius correction) to adhesion energies calculated from individual particle radii (radius corrected) (**Fig. 9 b**). Our results indicate sensitivity in the range between 10^{-7} and 10^{-10} M and measurements employing averaged contact radii are almost identical with the adhesion energies calculated from individual particle radii. Maximum deviations between data points of the same concentration are less than 0.1% and can therefore be regarded negligible for routine measurements. The data demonstrate the straightforward application of monodisperse PEG-based SCPs developed within this study to measure analyte concentration with high sensitivity based on prior knowledge of SCP size, without the necessity of individual determination of SCP radii.

5. Conclusions

In this work, we presented the design, characterization and optimization of SCPs fabricated by droplet-based microfluidics employing PDMS-based flow-focusing devices. Two crosslinking approaches, namely photocrosslinking of ACA-functionalized PEG as well as thiol-Michael addition of SH- and mal-modified PEGs were tested, both of which yielded highly monodisperse and homogeneous SCPs. The mechanical properties had to be adjusted to meet the requirements of the SCP assay, whereby SCPs made from 2 kDa starPEG-SH and 2 kDa starPEG-mal exhibit an ideal elastic modulus of 30 kPa. In the case of photocrosslinkable PEG-ACA, additional parameters, including photoinitiator concentration, UV exposure time, intensity, etc., had to be optimized to tailor the SCPs mechanical properties. Both SCP types exhibit sufficient unreacted functional groups for convenient post-synthesis conjugation of the SCPs through thiol-Michael addition, allowing avoiding harsh chemistries like photoradical grafting for the introduction of functional groups. A particular strength of the system is the flexibility regarding the possibilities for introducing several functional groups, moieties and biomolecules. In this context, especially SCPs fabricated via thiol-maleimide Michael addition proved to be well-suited, as maleimides can be specifically and efficiently coupled to the unreacted SH-groups in a one-step procedure. Finally, we could demonstrate that highly sensitive quantification of biomolecules is feasible and that our monodisperse and conveniently chemically modifiable SCPs eliminate the need to determine individual radii based on interference patterns, which will greatly facilitate the translation of the SCP technique.

On the other hand, it should be noted that direct coupling of compounds with amino groups to carboxy-functionalized SCPs using active ester chemistry is not possible without degrading the SCPs and altering the mechanical properties. Consequently, amine compounds must be conjugated with linkers bearing a carboxy and maleimide group prior to SCP coupling to prevent degradation. Compared to solution phase methods for SCP synthesis, it can be criticized that the scalability of this method is usually limited to parallelization and that organic solvents and relatively expensive instrumentation are required [45].

Acknowledgement

The authors thank Max J. Männel (Leibniz IPF Dresden) for supporting microfluidic device fabrication. T. P. acknowledge the support by a grant from EFRE and Free State of Saxony (SAB, Grant No. 100346488) within the collaborative research project '*Glyphosate trace analysis in aqueous systems and food by holographic in-place analytics*' (GlyHo) together with Technische Universität Dresden (Germany) and industrial partners Umex GmbH (Dresden, Germany), IfU GmbH Privates Institut für Umweltanalysen (Lichtenau, Germany) and Anvajo GmbH (Dresden, Germany). J. T. receives funding from the European Research Council (ERC) under the European Union's Horizon 2020 research and innovation program (Grant agreement no. 852065) and support from the Dresden Center for Intelligent Materials (DCIM) by the Free State of Saxony and TU Dresden. T. P. and C. W. acknowledge the support from Deutsche Forschungsgemeinschaft (DFG, Grant Nos. SFB-TRR67 / A10 and B10).

References

1. Caló E, Khutoryanskiy VV (2015) Biomedical applications of hydrogels: A review of patents and commercial products. *European polymer journal* 65:252–267. doi: 10.1016/j.eurpolymj.2014.11.024
2. Bahram M, Mohseni N, Moghtader M (2016) An Introduction to Hydrogels and Some Recent Applications. In: Majee SB (ed) *Emerging Concepts in Analysis and Applications of Hydrogels*. InTech
3. Le Goff GC, Srinivas RL, Hill WA, Doyle PS (2015) Hydrogel microparticles for biosensing. *European polymer journal* 72:386–412. doi: 10.1016/j.eurpolymj.2015.02.022
4. Andrade J (1989) Hydrogels in medicine and pharmacy. *Journal of Controlled Release* 10:225. doi: 10.1016/0168-3659(89)90067-9
5. Peppas NA, Hilt JZ, Khademhosseini A, Langer R (2006) Hydrogels in Biology and Medicine: From Molecular Principles to Bionanotechnology. *Adv. Mater.* 18:1345–1360. doi: 10.1002/adma.200501612
6. Peppas N (2000) Hydrogels in pharmaceutical formulations. *European Journal of Pharmaceutics and Biopharmaceutics* 50:27–46. doi: 10.1016/s0939-6411(00)00090-4
7. Miyata T, Uragami T, Nakamae K (2002) Biomolecule-sensitive hydrogels. *Advanced Drug Delivery Reviews* 54:79–98. doi: 10.1016/S0169-409X(01)00241-1
8. Shang J, Yan J, Zhang Z, Huang X, Maturavongsadit P, Song B, Jia Y, Ma T, Li D, Xu K, Wang Q, Lin Q (2016) A hydrogel-based glucose affinity microsensor. *Sensors and actuators. B, Chemical* 237:992–998. doi: 10.1016/j.snb.2016.03.146
9. Zhang C, Losego MD, Braun PV (2013) Hydrogel-Based Glucose Sensors: Effects of Phenylboronic Acid Chemical Structure on Response. *Chem. Mater.* 25:3239–3250. doi: 10.1021/cm401738p
10. Wustoni S, Savva A, Sun R, Bihar E, Inal S (2019) Enzyme-Free Detection of Glucose with a Hybrid Conductive Gel Electrode. *Adv. Mater. Interfaces* 6:1800928. doi: 10.1002/admi.201800928
11. Yetisen AK, Jiang N, Fallahi A, Montelongo Y, Ruiz-Esparza GU, Tamayol A, Zhang YS, Mahmood I, Yang S-A, Kim KS, Butt H, Khademhosseini A, Yun S-H (2017) Glucose-Sensitive Hydrogel Optical Fibers Functionalized with Phenylboronic Acid. *Adv. Mater.* 29. doi: 10.1002/adma.201606380
12. Wu M, Zhang Y, Liu Q, Huang H, Wang X, Shi Z, Li Y, Liu S, Xue L, Lei Y (2019) A smart hydrogel system for visual detection of glucose. *Biosensors & bioelectronics* 142:111547. doi: 10.1016/j.bios.2019.111547
13. Pussak D, Ponader D, Mosca S, Ruiz SV, Hartmann L, Schmidt S (2013) Mechanical carbohydrate sensors based on soft hydrogel particles. *Angewandte Chemie (International ed. in English)* 52:6084–6087. doi: 10.1002/anie.201300469
14. Martin S, Wang H, Hartmann L, Pompe T, Schmidt S (2015) Quantification of protein-materials interaction by soft colloidal probe spectroscopy. *Physical chemistry chemical physics PCCP* 17:3014–3018. doi: 10.1039/C4CP05484A

15. Martin S, Wang H, Rathke T, Anderegg U, Möller S, Schnabelrauch M, Pompe T, Schmidt S (2016) Polymer hydrogel particles as biocompatible AFM probes to study CD44/hyaluronic acid interactions on cells. *Polymer* 102:342–349. doi: 10.1016/j.polymer.2016.02.019
16. Rettke D, Döring J, Martin S, Venus T, Estrela-Lopis I, Schmidt S, Ostermann K, Pompe T (2020) Picomolar glyphosate sensitivity of an optical particle-based sensor utilizing biomimetic interaction principles. *Biosensors & bioelectronics* 165:112262. doi: 10.1016/j.bios.2020.112262
17. Rettke D, Seufert F, Döring J, Ostermann K, Wilms D, Schmidt S, Pompe T (2021) Biomimetic estrogen sensor based on soft colloidal probes. *Biosensors & bioelectronics* 192:113506. doi: 10.1016/j.bios.2021.113506
18. Pussak D, Behra M, Schmidt S, Hartmann L (2012) Synthesis and functionalization of poly(ethylene glycol) microparticles as soft colloidal probes for adhesion energy measurements. *Soft Matter* 8:1664–1672. doi: 10.1039/C2SM06911C
19. Schmidt S, Wang H, Pussak D, Mosca S, Hartmann L (2015) Probing multivalency in ligand-receptor-mediated adhesion of soft, biomimetic interfaces. *Beilstein journal of organic chemistry* 11:720–729. doi: 10.3762/bjoc.11.82
20. Wang H, Jacobi F, Waschke J, Hartmann L, Löwen H, Schmidt S (2017) Elastic Modulus Dependence on the Specific Adhesion of Hydrogels. *Adv. Funct. Mater.* 27:1702040. doi: 10.1002/adfm.201702040
21. Seiffert S, Thiele J (2020) *Microfluidics*. De Gruyter. doi: 10.1515/9783110487701
22. Guo MT, Rotem A, Heyman JA, Weitz DA (2012) Droplet microfluidics for high-throughput biological assays. *Lab on a chip* 12:2146–2155. doi: 10.1039/C2LC21147E
23. Whitesides GM (2006) The origins and the future of microfluidics. *Nature* 442:368–373. doi: 10.1038/nature05058
24. Moreira A, Carneiro J, Campos JBLM, Miranda JM (2021) Production of hydrogel microparticles in microfluidic devices: a review. *Microfluid Nanofluid* 25. doi: 10.1007/s10404-020-02413-8
25. Roh YH, Lee HJ, Bong KW (2019) Microfluidic Fabrication of Encoded Hydrogel Microparticles for Application in Multiplex Immunoassay. *BioChip J* 13:64–81. doi: 10.1007/s13206-019-3104-z
26. Pinelli F, Magagnin L, Rossi F (2020) Progress in hydrogels for sensing applications: a review. *Materials Today Chemistry* 17:100317. doi: 10.1016/j.mtchem.2020.100317
27. Lee AG, Beebe DJ, Palecek SP (2012) Quantification of kinase activity in cell lysates via photopatterned macroporous poly(ethylene glycol) hydrogel arrays in microfluidic channels. *Biomedical microdevices* 14:247–257. doi: 10.1007/s10544-011-9602-y
28. Lee HJ, Roh YH, Kim HU, Kim SM, Bong KW (2018) Multiplexed immunoassay using post-synthesis functionalized hydrogel microparticles. *Lab on a chip* 19:111–119. doi: 10.1039/C8LC01160E
29. Appleyard DC, Chapin SC, Doyle PS (2011) Multiplexed protein quantification with barcoded hydrogel microparticles. *Analytical chemistry* 83:193–199. doi: 10.1021/ac1022343

30. Mozziconacci O, Kerwin BA, Schöneich C (2010) Exposure of a monoclonal antibody, IgG1, to UV-light leads to protein dithiohemiacetal and thioether cross-links: a role for thiyl radicals? *Chemical research in toxicology* 23:1310–1312. doi: 10.1021/tx100193b
31. Strzelczyk AK, Wang H, Lindhorst A, Waschke J, Pompe T, Kropf C, Luneau B, Schmidt S (2017) Hydrogel Microparticles as Sensors for Specific Adhesion: Case Studies on Antibody Detection and Soil Release Polymers. *Gels* (Basel, Switzerland) 3. doi: 10.3390/gels3030031
32. Waschke J, Pompe T, Rettke D, Schmidt S, Hlawitschka M (2019) Radial profile detection of multiple spherical particles in contact with interacting surfaces. *PloS one* 14:e0214815. doi: 10.1371/journal.pone.0214815
33. Limozin L, Sengupta K (2009) Quantitative reflection interference contrast microscopy (RICM) in soft matter and cell adhesion. *Chemphyschem a European journal of chemical physics and physical chemistry* 10:2752–2768. doi: 10.1002/cphc.200900601
34. Pussak D, Behra M, Schmidt S, Hartmann L (2012) Synthesis and functionalization of poly(ethylene glycol) microparticles as soft colloidal probes for adhesion energy measurements. *Soft Matter* 8:1664–1672. doi: 10.1039/c2sm06911c
35. Buzio R, Bosca A, Krol S, Marchetto D, Valeri S, Valbusa U (2007) Deformation and adhesion of elastomer poly(dimethylsiloxane) colloidal AFM probes. *Langmuir the ACS journal of surfaces and colloids* 23:9293–9302. doi: 10.1021/la700941c
36. Erath J, Schmidt S, Fery A (2010) Characterization of adhesion phenomena and contact of surfaces by soft colloidal probe AFM. *Soft Matter* 6:1432. doi: 10.1039/B923540J
37. Fritz JL, Owen MJ (1995) Hydrophobic Recovery of Plasma-Treated Polydimethylsiloxane. *The Journal of Adhesion* 54:33–45. doi: 10.1080/00218469508014379
38. Williams RL, Wilson DJ, Rhodes NP (2004) Stability of plasma-treated silicone rubber and its influence on the interfacial aspects of blood compatibility. *Biomaterials* 25:4659–4673. doi: 10.1016/j.biomaterials.2003.12.010
39. Gao Y, Peng K, Mitragotri S (2021) Covalently Crosslinked Hydrogels via Step-Growth Reactions: Crosslinking Chemistries, Polymers, and Clinical Impact. *Advanced materials* (Deerfield Beach, Fla.) 33:e2006362. doi: 10.1002/adma.202006362
40. Lin C-C, Anseth KS (2009) PEG hydrogels for the controlled release of biomolecules in regenerative medicine. *Pharmaceutical research* 26:631–643. doi: 10.1007/s11095-008-9801-2
41. Lee S, Tong X, Yang F (2016) Effects of the poly(ethylene glycol) hydrogel crosslinking mechanism on protein release. *Biomaterials science* 4:405–411. doi: 10.1039/c5bm00256g
42. Barnes SE, Cygan ZT, Yates JK, Beers KL, Amis EJ (2006) Raman spectroscopic monitoring of droplet polymerization in a microfluidic device. *The Analyst* 131:1027–1033. doi: 10.1039/b603693g
43. Fontaine SD, Reid R, Robinson L, Ashley GW, Santi DV (2015) Long-term stabilization of maleimide-thiol conjugates. *Bioconjugate chemistry* 26:145–152. doi: 10.1021/bc5005262
44. Kirchhof S, Strasser A, Wittmann H-J, Messmann V, Hammer N, Goepferich AM, Brandl FP (2015) New insights into the cross-linking and degradation mechanism of Diels-Alder hydrogels. *Journal of materials chemistry. B* 3:449–457. doi: 10.1039/C4TB01680G

45. Jeong H-H, Issadore D, Lee D (2016) Recent developments in scale-up of microfluidic emulsion generation via parallelization. *Korean J. Chem. Eng.* 33:1757–1766. doi: 10.1007/s11814-016-0041-6

1 Supplemental Information

Microfluidics-assisted synthesis and functionalization of monodisperse colloidal hydrogel particles for optomechanical biosensors based on reflection interference contrast microscopy

David Rettke¹, Christian Danneberg¹, Talika Alina Neuendorf², Sebastian Kühn³, Jens Friedrichs³, Nicolas Hauck², Carsten Werner³, Julian Thiele^{2,4}, Tilo Pompe^{1,3}

1) Institute of Biochemistry, Leipzig University, Johannisallee 21 – 23, 04103 Leipzig, Germany

2) Leibniz-Institut für Polymerforschung Dresden e.V., Hohe Strasse 6, 01069 Dresden, Germany

3) Leibniz-Institut für Polymerforschung Dresden e.V., Max Bergmann Center of Biomaterials, Hohe Strasse 6, 01069 Dresden, Germany

4) Dresden Center for Intelligent Materials (DCIM), Technische Universität Dresden, 01069 Dresden, Germany.

* Corresponding Author:

Institute of Biochemistry, Leipzig University, Johannisallee 21 – 23, 04103 Leipzig, Germany

E-mail: tilo.pompe@uni-leipzig.de

1. Summary of synthesized and functionalized SCPs

Table S1: Summary of synthesized and functionalized SCPs. Corresponding functionalization method, molecule used for functionalization and the reference are given.

SCP synthesis method	Precursor molecules (PEG)	Functionalization	Functionalization method	Compound for functionalization	Section / figure
Photoradical	0.3 kDa linear PEG-diacrylamide	-	-	-	section 3, fig. 2
		COOH	photoradical grafting	crotonic acid	section 3, fig. 2
	3.7 kDa linear PEG-diacrylamide	-	-	-	section 3, fig. 2
		COOH	photoradical grafting	crotonic acid	section 3, fig. 2
	2 kDa four-arm starPEG acrylamide	-	-	-	section 3.1, fig. 2 / section 3.2, fig. 4
		COOH	photoradical grafting during particle synthesis	crotonic acid	section 3.1, fig. 2
		I, COOH II, NH ₂	I, during particle synthesis (COOH) II, active ester (NH ₂)	I, 2kDa linear acrylamide-PEG-COOH II, ethylenediamine	section 3.1, fig. 3
		OH	thiol-Michael addition	mercaptoethanol	section 3.3, fig. 5
		NH ₂		cysteamine	section 3.3, fig. 5
		COOH		thioglycolic acid	section 3.3, fig. 5
		SH		ethanedithiol	section 3.3, fig. 5
		I, SH II, NH ₂	thiol-Michael addition (both steps)	I, ethanedithiol II, maleimidoethylamine	section 3.4, fig. 6
I, SH II, NH ₂		I, ethanedithiol II, maleimidopropanoic acid		section 3.4, fig. 6	
Thiol-Michael addition		2 kDa four-arm starPEG maleimide + 2 kDa four-arm starPEG thiol	X	thiol-Michael addition	-
	NH ₂		maleimidoethylamine		section 3.5, fig. 7
	COOH		maleimidopropanoic acid		section 3.5, fig. 7
	biotin	biotinyl-PEG ₂ -maleimide	section 3.5, fig. 8		
	I, biotin II, streptavidin	I, thiol-Michael addition II, affinity binding	I,biotinyl-PEG ₂ -maleimide II, streptavidin	section 3.5, fig. 8	
	streptavidin	thiol-Michael addition	SMCC conjugated streptavidin	section 3.5, fig. 8	

2. Microfluidic device fabrication

A combination of photo and soft lithography was used for the preparation of poly(dimethylsiloxane) (PDMS)-based flow-focusing microfluidic devices. Silicon wafers containing a defined microstructure with a channel height of 10 and 25 μm , serving as a negative master, were prepared as follows: First, a negative photoresist (SU-8 25, Microchem. Co., Westborough, MA, US) was spin-coated onto a 3-inch silicon wafer (Siegert Wafer, Aachen, Germany). Patterning of the silicon wafer with the desired microchannel structure was achieved by UV-illumination of the photoresist through a printed photomask using a mask aligner (MJB3, Süss MicroTec, Garching, Germany). Subsequent removal of non-illuminated photoresist by washing with a developer solution (mr-Dev 600, Micro Resist Technology, Berlin, Germany) yielded the desired microchannel structure with defined height and width. After cleaning with filtered isopropanol, a degassed solution of PDMS base and crosslinker (DOWSILTM 184 Silicone Elastomer Base, Dow, US) in a ratio of 10:1 was poured onto the silicon wafer, repeating the degassing step once for 30 minutes before curing at 65 °C for 2 h. The device was cut out with a scalpel, and access ports for tubing (1 mm) were punched into the device with a biopsy needle (\varnothing 1 mm, pfm medical). The microfluidic device was then assembled by bonding the PDMS replica to a cleanroom-cleaned glass slide (Schott Nexterion, Germany), treated with oxygen plasma in a low-pressure plasma chamber (PDC-002, Harrick Plasma, US) immediately before bonding. PDMS replica and glass slides form stable Si-O-Si bonds when brought into contact after plasma treatment. Finally, the microfluidic channels were treated with 1% (w/w) tridecafluoro-1,1,2,2-tetrahydrooctyl-trichlorosilane (abcr, Germany) in a fluorinated oil (HFE 7500, 3M, US) at room temperature for 1 h and rinsed with HFE 7500 in order to provide a hydrophobic surface for ideal flow conditions.

3. Fluorescence microscopy of SCPs

Successful functionalization was assessed employing confocal laser scanning microscopy (cLSM, LSM700, Zeiss, Germany). Therefore, untreated coverslips (\varnothing 32 mm, Menzel Glaeser, Thermo Fisher Scientific, US) were adhered to a sticky-slide 16 well (Grace Biolabs, US), and each surface was covered with 200 μ L of 100 mM HEPES buffer (pH = 7.0). 50 μ L of the respective SCP suspension was carefully pipetted into the wells, allowed to sediment for 20 min, and the particles were subsequently investigated. With the exception of TAMRA-scm-stained SCPs, all stained samples were excited using a 488 nm solid-state laser. TAMRA-scm was excited using a 555 nm solid-state laser. Stained SCPs were imaged using a C-Apochromat water immersion objective with a 40x magnification and a numerical aperture of 1.2 (C-Apochromat 40x/1.20 W Korr, Zeiss, Germany). Areas of 320 x 320 μ m (512 x 512 pixels, 1.60 pixels μ m⁻¹) were recorded, whereby the z-position of the imaged x-y-plane was individually adjusted to avoid the recording of areas with incomplete staining and gradients from SCP surface to center, respectively. To analyze the fluorescence intensities of the SCPs, the mean grey value of each particle was calculated based on the fluorescence intensity within the corresponding x-y plane using Fiji [1]. Only SCPs located within the central 160 x 160 μ m region of each image were analyzed. Unless otherwise stated, 60 SCPs per condition were analyzed.

4. 1-ethyl-3-(3-dimethylaminopropyl)carbodiimide (EDC)/N-hydroxysuccinimide (NHS) treatment of SCPs

To assess whether SCPs are suitable for coupling reactions employing active ester chemistry, the COOH-groups were activated using EDC (Carbolution Chemicals, Germany) and NHS (Sigma Aldrich, US). First, 1.5 mL of the respective particle suspension was centrifuged at 1840x g, and the supernatant was discarded. Next, 1.5 mL of a solution containing 5.75 mg EDC (37 μ mol) and 8.625 mg NHS (75 μ mol) in 100 mM 2-(N-morpholino)ethanesulfonic acid buffer (MES, Carl Roth, Germany) buffer (pH = 5.3) was prepared and added to the respective SCP pellet. The SCPs were subsequently resuspended and activated for 1 h in a rotator. Finally, the SCPs were centrifuged and washed several times with 100 mM HEPES buffer.

5. Bright-field microscopy

SCPs were analyzed using bright-field microscopy to determine whether any defects occurred in the course of synthesis, functionalization, conjugation or activation by active ester chemistry. For imaging, an inverted microscope with an integrated halogen lamp was used (Olympus IX73, Germany). The microscope was equipped with a 60x, NA (numerical aperture) 1.35 oil-immersion objective (UPlanSApo 60x 1.35 oil, Olympus, Germany) and 108.5 x 81.34 μm patches (1600 x 1200 pixel) were imaged using Micro-Manager software [2, 3].

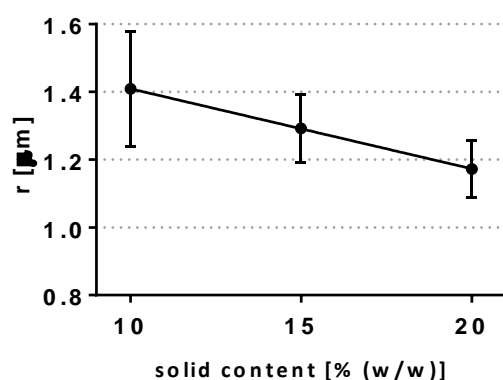
6. Determination of elastic modulus

The Young's modulus of functionalized SCPs was determined by atomic force microscopy (AFM) - based indentation measurements using a NanoWizard IV AFM (JPK instruments, Germany) mounted on an inverted optical microscope (Axio Observer, Zeiss, Germany). Tipless cantilever (PNP-TR-TL-Au, Nanoworld, Switzerland, nominal spring constant $k = 0.08 \text{ N m}^{-1}$), equipped with a silica bead (diameter: 10 μm , Kisker, Germany) were used for indentation measurements. Cantilever were calibrated by the thermal noise method before each experiment [4]. For indentation measurements, the silica indenter was aligned over the center of individual SCPs and force-distance curves were acquired with an approach velocity of 5 $\mu\text{m/s}$ and a contact force of 2 nN. The Young's modulus of the SCPs was extracted from approach force-distance curves using the Hertz model for spherical indenter and applying a double-contact correction considering an additional deformation derived from the counter pressure at the bottom side of the bead during indentation.

7. Impact of PEG solid content on contact radii of SCPs based on photocrosslinkable starPEG-acrylamides

For synthesis of SCPs made from 2 kDa 4-arm-starPEG-acrylamide (starPEG-ACA), 10, 15 and 20% (w/w) PEG solutions were prepared and lithium phenyl-2,4,6-trimethylbenzoylphosphinate (LAP) was added in a concentration of 2% (w/w). Generation of droplets, synthesis of SCPs and workup was performed as described in **section 2.1**.

Fig. S1



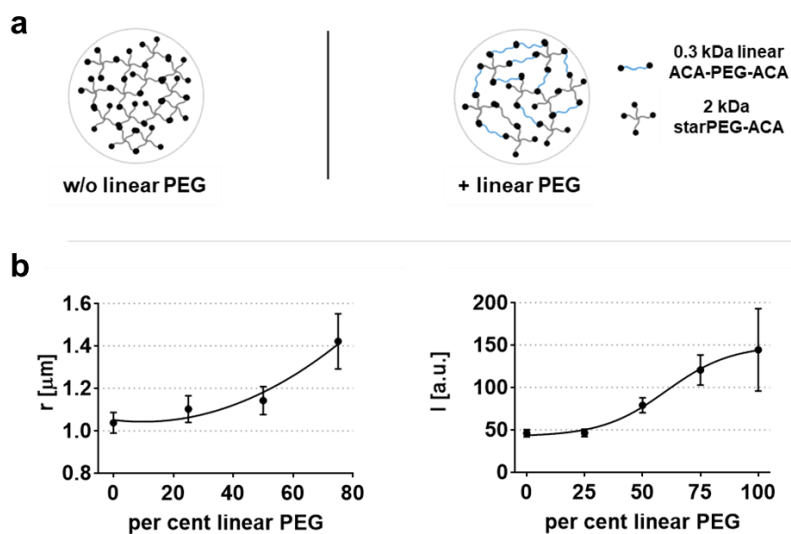
Analysis of contact radii of SCPs made from 10, 15 and 20% (w/w) solutions of 2 kDa starPEG-ACA. SCPs adhered to uncoated glass surfaces and were evaluated using RICM. Mean contact radii of at least 50 particles per condition are shown. Error bars indicate SD

The radius of contact and the modulus of elasticity of SCPs are important parameters that influence the performance of the sensor and allow adjusting the working range and sensitivity of the sensor. Hence, the influence of 2 kDa starPEG-ACA solid content on contact radii of the SCPs was investigated (see **Fig. S1**). By increasing the PEG solid content, the contact radii decreased without affecting the radius of the SCPs, which indicates increasing elastic moduli with increasing PEG solid contents. SCPs made from PEG solutions containing more than 20% (w/w) PEG were not investigated, as solutions containing 10% (w/w) PEG proved to yield the most suitable SCPs for our purpose.

8. Microfluidic preparation and characterization of SCPs made from mixed linear and star-shaped PEGs

For the synthesis of SCPs made from mixtures of 0.3 kDa acrylamide-PEG-acrylamide (ACA-PEG-ACA) and 2 kDa starPEG-ACA, 10% (w/w) PEG (total PEG concentration) solutions containing different ratios of ACA-PEG-ACA and starPEG-ACA in ultrapure water were prepared, and LAP was added in a concentration of 2% (w/w). Generation of droplets, synthesis of SCPs and workup was performed as described in **section 2.1**.

Fig. S2



Analysis and optimization of synthesis parameters of SCPs made from mixed PEG system containing 2 kDa starPEG-ACA and 0.3 kDa linear ACA-PEG-ACA. **a** Schematic representation of the optimization strategy based on a mixed PEG system with different percentages of 0.3 kDa linear ACA-PEG-ACA (blue) and 2 kDa starPEG-ACA (black). Left: SCP made from 2 kDa starPEG-ACA. Right: SCP made from 2 kDa starPEG-ACA plus 0.3 kDa linear ACA-PEG-ACA. **b** Contact radii and fluorescence intensities of SCPs in dependence of the proportion of 0.3 kDa linear PEG (10% (w/w) total PEG solid content). Left: Contact radii of SCPs adhering to uncoated, cleaned glass surfaces. Right: Fluorescence intensities of FITC-stained SCPs measured by cLSM. Results are presented as means and error bars indicate SD

In addition to the optimization of the synthesis parameters of SCPs made from 2 kDa starPEG-ACA, the impact of the addition of 0.3 kDa linear ACA-PEG-ACA on double bond conversion was assessed. Therefore, mixtures with a total solid content of 10% (w/w) PEG were prepared as precursor solutions. Low molecular weight (0.3 kDa) linear starPEG exhibits higher diffusivity than its starPEG counterpart, which is likely to be associated with improved conversion rates of acrylamide- (ACA) groups. With two ACA-groups present on the 0.3 kDa linear PEG, the

molecule has two possible residues that can each form two radicals for crosslinking, whereby the same mass of 0.3 kDa ACA-PEG-ACA has roughly three times more ACA-groups than 2kDa starPEG-ACA.

However, increasing the percentage of linear ACA-PEG-ACA did not lead to more strongly crosslinked particles and the contact areas increase with increasing proportions of the linear ACA-PEG-ACA, indicating lower elastic moduli (**Fig. S2 b**). Fluorescence intensities of the FITC-labeled SCPs serve as a measure of remnant ACA-groups, i.e. ACA-groups not involved in the crosslinking reaction. As can be seen from **Fig S2 b**, fluorescence intensities positively correlate with the amount of linear ACA-PEG-ACA added. SCPs made exclusively from ACA-PEG-ACA exhibit three times the fluorescence intensity compared to SCPs made exclusively from starPEG-ACA. None of the results suggests any improvement of SCP-crosslinking. Mixed linear and star-shaped PEG systems were therefore not taken into further consideration.

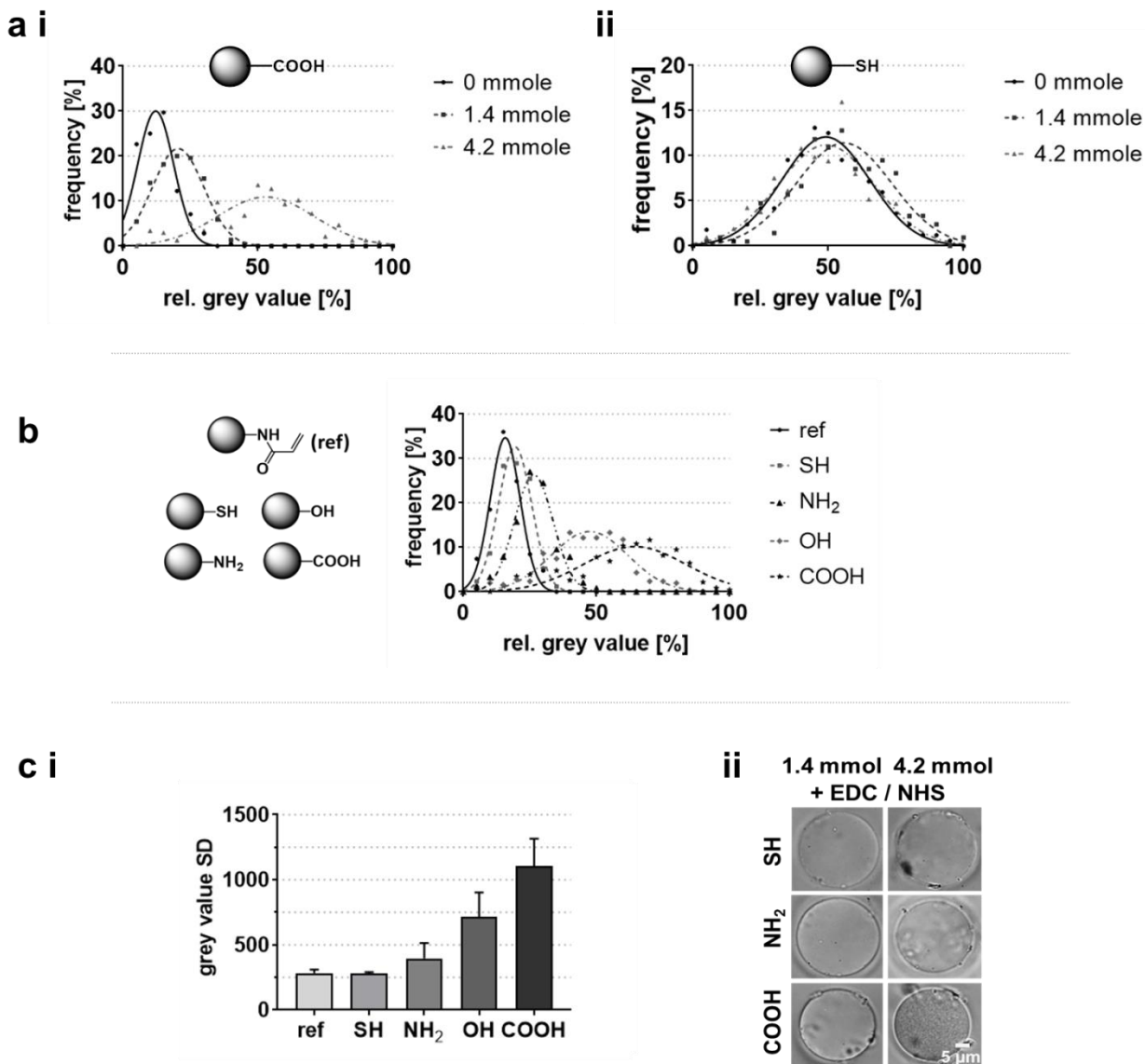
9. Single particle homogeneity assessment of functionalized SCPs based on photocrosslinkable 2 kDa starPEG-ACA

SCPs were synthesized as described in **section 2.1**. Solutions containing 10% (w/w) 2 kDa starPEG-ACA and 2% (w/w) LAP were used.

For homogeneity assessment of SCPs, bright-field images were acquired as described in **SI section 4** and analysis was conducted using Fiji Is Just ImageJ software. For single particle analysis of homogeneity, a linear section within one particle per condition was examined. Therefore, a grey value profile was plotted, and the minimum value obtained from each condition was regarded as background and subtracted from all values obtained within the respective condition. The resulting maximum value within a test series (several conditions) was defined as 100% grey value intensity and the scale was divided into 5% quantiles. The frequency distribution of the values within the quantiles was plotted and fitted using Gaussian distribution. Curve fitting was conducted using GraphPad Prism (GraphPad Software, US).

To compare averaged grey value standard deviations, the standard deviation of 15 linear sections within 5 particles per condition was averaged and plotted as a function of functionalization degree.

Fig. S3



Characterization of functionalized SCPs made from 2 kDa starPEG-ACA by grey value analysis. **a** Single particle analysis of grey value distribution of unfunctionalized (0 mmol) SCPs and SCPs functionalized with 1.4 or 4.2 mmol of thioglycolic acid (**i**) and ethanedithiol (**ii**). **b** Single particle analysis of grey value distribution of all types of SCPs functionalized with 4.2 mmol of the respective thiol compound. SCPs were functionalized with ethanedithiol (SH), cysteamine (NH₂), mercaptoethanol (OH) and thioglycolic acid (COOH). **c** Comparison of averaged grey value standard deviations of all types of SCPs (**i**) and representative bright field images of SCPs suffering from degradation caused by EDC/NHS activation at low (1.4 mmole) and quantitative (4.2 mmole) functionalization (**ii**). For analysis of averaged grey value standard deviations, 5 SCPs per condition, each at 3 different regions, were measured. Results are presented as means and error bars indicate SD

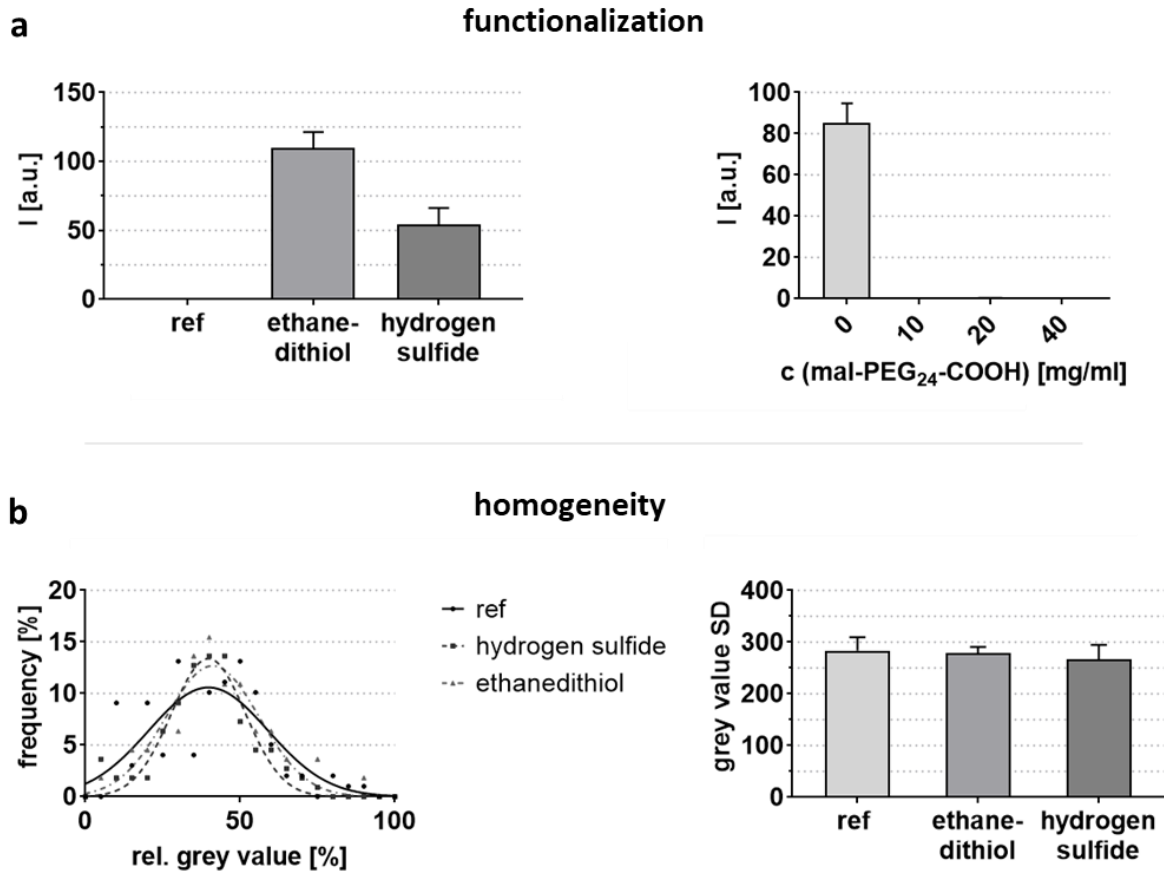
10. Thiol-functionalization and characterization of SCPs based on photocrosslinkable 2 kDa starPEG-ACA using hydrogen sulfide

SCPs were synthesized as described in **section 2.1**. Solutions containing 10% (w/w) 2 kDa starPEG-ACA and 2% (w/w) LAP were used. Thiol- (SH) functionalization of SCPs employing ethanedithiol was conducted as described in **section 2.2**.

As an alternative approach for introducing SH-groups, hydrogen sulfide (H₂S) was coupled to unreacted residual ACA-moieties within the PEG network employing thiol-Michael addition. 5 mL of the SCP suspension was centrifuged at 1850x g, the supernatant was discarded, and the SCPs were subsequently resuspended in 5 mL HEPES buffer. 5 mL of a 0.8 M H₂S solution in THF (Sigma Aldrich, US) were mixed with 10 mL HEPES buffer and the pH was adjusted to 7.0. After combining the SCP suspension and H₂S-solution, the reaction was allowed to proceed for 1 h while agitating. Subsequently, the suspension was centrifuged, the supernatant was discarded, and the SCPs were washed five times with HEPES buffer. Functionalization of H₂S-functionalized SCPs bearing SH-groups was conducted employing maleimide (mal) compounds. Therefore, alpha-maleimido-24(ethylene glycol)-omega-propionic acid (mal-PEG₂₄-COOH, Iris Biotech, Germany) was dissolved in 100 mM HEPES buffer in a concentration of 10, 20 and 30 mg mL⁻¹, and the pH was adjusted to 7.0 by adding of NaOH. The suspension containing SH-functionalized SCPs was split into 1.5 mL fractions, centrifuged at 1840x g, the supernatant was discarded, and 1.5 mL of the respective solution was added to the SCP pellet. The reaction was allowed to proceed for 1 h while agitating. Subsequently, the SCPs were centrifuged and rinsed at least three times with 100 mM HEPES buffer.

The SCPs were labeled with *N*-(5-fluoresceinyl)maleimide (FAM-mal) as described in **section 2.3**. Homogeneity assessment was conducted as described above (**SI section 10**) and in **section 2.4**.

Fig. S4



Characterization of SH-functionalized SCPs made from 2 kDa starPEG-ACA by cLSM and particle grey value analysis. **a** Comparison of fluorescence intensities of FAM-mal-stained SCPs by means of cLSM. Left: Comparison of SCPs functionalized with ethanedithiol to SCPs functionalized with hydrogen sulfide. Unfunctionalized SCPs served as a reference. Right: mal-PEG₂₄-COOH was coupled to H₂S-functionalized SCPs. Concentration dependent conversion of SH-groups was probed by FAM-mal labeling of residual SH-groups. **b** Homogeneity assessment of unfunctionalized SCPs and SCPs functionalized with ethanedithiol or hydrogen sulfide by grey value analysis. Left: Single particle analysis of grey value distributions. Right: Comparison of averaged grey value standard deviations. For all fluorescence-based analysis of SCPs, 60 particles per condition were measured. For homogeneity assessment by comparison of grey value SD, 5 SCPs per condition, each at 3 different regions, were measured. Results are presented as means and error bars indicate SD

Fig. S4 provides a comparison of SCPs based on 2 kDa starPEG-ACA functionalized with ethanedithiol and hydrogen sulfide. Both strategies yield SH-functionalized SCPs. The efficiency of SH-group introduction was probed using FAM-mal for SH-staining and cLSM for fluorescence intensity measurements of the labeled SCPs. Ethanedithiol-functionalized SCPs exhibit roughly twice the fluorescence intensity of H₂S-functionalized SCPs, indicating a higher functionalization degree (**Fig. S4 a**, left). It has to be noted that functionalization employing

ethanedithiol was conducted with 1.25-fold the amount of substance compared to H₂S-functionalization. To verify SH-functionalization, mal-PEG₂₄-COOH was coupled to SCPs functionalized with hydrogen sulfide and residual SH-groups were labeled with FAM-mal. Quantitative conversion of SH-groups was achieved by the addition of a 10 mg mal-PEG₂₄-COOH solution per 1 mL of the SCP suspension, as can be seen from **Fig. S4 a** (right).

The effect of both SH-functionalization approaches on particle homogeneity was assessed by single particle analysis of grey value distribution. The grey value distributions for both types of SH-functionalized SCPs exhibit impeccable overlap with the reference (unfunctionalized SCP), thereby indicating the absence of degradation effects (**Fig. S4 b** left). To assure an adequate averaging over several SCPs, the standard deviation of 15 sections was calculated and utilized as a measure of homogeneity. As depicted in **Fig. S4 b** (right), none of the functionalized SCPs exhibit significant differences in grey value standard deviation compared to the reference, verifying the absence of degradation effects.

11. Preparation of streptavidin-coated glass surfaces

For the preparation of biochip surfaces, glass coverslips (Menzel Glaeser, Ø 32 mm, Thermo Fisher Scientific, US) were pre-cleaned in ultrapure water and ethanol for 30 min each. A chemical cleaning process was performed subsequently in a mixture of ultrapure water, 25% (v/v) NH₃ aqueous solution (Merck, Germany) and 35% (v/v) H₂O₂ (Grüssing, Germany) in a ratio of 5:1:1 for 10 min at 64 °C. After rinsing twice with ultrapure water, the coverslips were dried in a nitrogen stream. The coverslips were then silanized with 3-aminopropyl)triethoxysilane (APTES, 0.51% (v/v), Sigma Aldrich, US) dissolved in isopropanol with 1.1% (v/v) ultrapure water for 10 min with continuous stirring, washed twice with isopropanol and dried again in a nitrogen stream. Annealing of the silanized coverslips was carried out in an oven at 120 °C for 1 h.

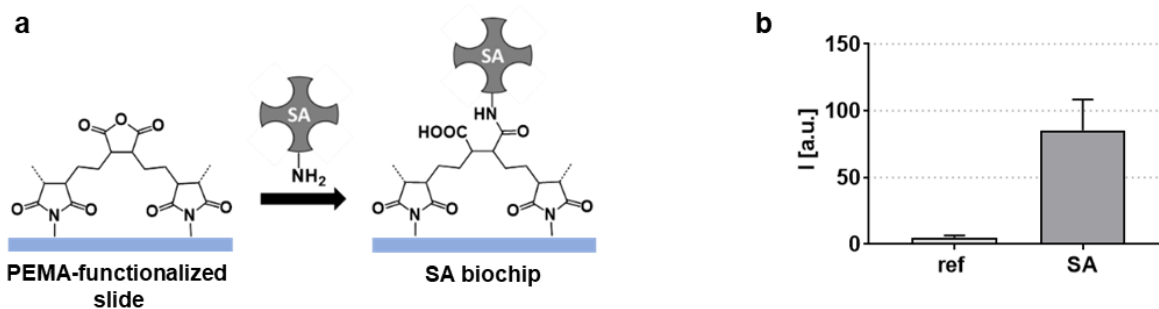
To coat the silanized glass surfaces with poly(ethylene-alt-maleic anhydride) copolymer (PEMA, average Mw = 100,000 – 500,000 g mol⁻¹, Sigma Aldrich, US), 100 µL of a solution of 0.1% (w/v) PEMA dissolved in a 1:2 acetone-THF mixture were centrally pipetted on the coverslips. A spin coating process was used to produce a thin and evenly distributed layer of PEMA. Immediately after the polymer solution was pipetted onto the glass surface, the coverslip was slowly rotated for 1 s so that the liquid could homogeneously cover the surface. This first

acceleration step was followed by a maximum rotation step of 3000 rpm for 30 s. In order to stabilize the linkage between the silanized glass surface and PEMA, the coverslips were then annealed at 120 °C for 2 h, as described above. Excess polymer was removed by leaving the coverslips in acetone for 15 min, followed by washing each sample three times with acetone before drying them in a nitrogen stream.

To produce streptavidin- (SA) coated glass surfaces, freshly annealed PEMA-coated glass slides presenting amine reactive anhydrides were covered with 1.5 mL of a 1 mg mL⁻¹ SA-solution in 100 mM HEPES buffer, pH = 7.0. After 60 min incubation at room temperature, the surfaces were washed several times with 100 mM HEPES buffer, pH = 7.0 for further use to carry out interaction studies between biotin-functionalized SCPs and SA-coated surfaces.

The success of functionalization and coupling reactions was assessed by cLSM. For the introduction of fluorescent moieties, biotin-4-fluorescein (FAM-btn), which specifically binds to SA, was used. 250 µg mL⁻¹ of FAM-btn was weighed and dissolved in 100 mM HEPES buffer (pH = 7.0). 2 mL of the staining solution was pipetted onto the coated coverslips and the reaction was allowed to proceed overnight. Finally, the supernatant was discarded, and the coverslips were washed several times in 100 mM HEPES buffer (pH = 7.0).

Fig. S5



SA-coating of coverslips **a** Illustration of immobilization of SA using a PEMA-coated surface. PEMA bears carboxylic anhydrides, capable of forming amide bonds with the amino groups of SA. **b** Verification of SA-immobilization by cLSM. FAM-btn-labeled PEMA- and SA-coated surfaces were compared. 15 patches on 3 coverslips per condition were measured. Results are presented as means and error bars indicate SD

Fig. S5 illustrates the covalent immobilization of SA on PEMA-coated transparent coverslips. The carboxylic anhydride residues form a stable amide bond upon reaction with NH_2 -groups of SA. The tetrameric structure of SA ensures the presence of accessible binding sites for biotin.

SA-immobilization was verified by means of cLSM. Therefore, PEMA-coated surfaces (reference) as well as SA-coated surfaces were stained using FAM-btn. Strong fluorescence was observed in the case of SA-coated surfaces, whereas the reference surfaces showed neglectable fluorescence intensities, thereby indicating successful immobilization of SA.

References

1. Schneider CA, Rasband WS, Eliceiri KW (2012) NIH Image to ImageJ: 25 years of image analysis. *Nature methods* 9:671–675. doi: 10.1038/nmeth.2089
2. Edelstein A, Amodaj N, Hoover K, Vale R, Stuurman N (2010) Computer control of microscopes using μ Manager. *Current protocols in molecular biology* Chapter 14:Unit14.20. doi: 10.1002/0471142727.mb1420s92
3. Edelstein AD, Tsuchida MA, Amodaj N, Pinkard H, Vale RD, Stuurman N (2014) Advanced methods of microscope control using μ Manager software. *Journal of biological methods* 1. doi: 10.14440/jbm.2014.36
4. Hutter JL, Bechhoefer J (1993) Calibration of atomic-force microscope tips. *Review of Scientific Instruments* 64:1868–1873. doi: 10.1063/1.1143970

Chapter III

-

Conclusions & Outlook

Summary

In this work, the use of Soft Colloidal Probe- (SCP) based sensing approaches for the detection of environmentally concerning analytes and aspects for the improvement of this platform were presented. In particular, the methods developed use biomimetic recognition strategies to achieve a selective recognition of the analytes or compound classes of interest, and the acceleration of data processing and the establishment of a reliable procedure for the reproducible synthesis of monodisperse SCPs with tunable properties contribute to the commercialization of this technology. In this chapter, I will summarize the approaches that have been developed to specifically detect glyphosate and estrogenic compounds and the improvements of data processing as well as SCPs.

i, Development and validation of a specific and sensitive biomolecular recognition strategy for a typical contaminant of water resources and its integration into the SCP-based sensing methodology

Pollution of various water bodies, groundwater and drinking water poses a serious threat to the environment and public health. Possible impurities include nitrogen and phosphorus compounds, various salts, bleaching agents, pesticides, metals and other substances. Glyphosate, as a virtually ubiquitous pesticide, has attracted considerable attention because of its potentially underestimated health effects.

Publication I describes the development of a colorimetric rapid test for glyphosate. As a distinction to other colorimetric assays for glyphosate detection, the target enzyme of glyphosate, 5-enolpyruvylshikimate-3-phosphate synthase (EPSPs), is used for molecular recognition of glyphosate and signal amplification. Malachite green was used for quantification of the substrate turnover by formation of a colored complex in the presence of inorganic phosphate generated during the catalyzed reaction. A convenient immobilization strategy of EPSPs on glass and plastics based on adsorptive binding of hydrophobins to these surfaces was developed. A detection limit for glyphosate of 50 nM was determined, and cross-reactivity with structurally related compounds was low, as expected due to the specificity of the molecular interaction. Superior selectivity and convincing practicability have been demonstrated. One limitation, however, is the comparatively high detection limit, which is insufficient for most applications and may require pre-concentration of samples. Inorganic phosphate in the sample also interferes with the assay.

Next, the transferability of the molecular recognition between EPSPs and glyphosate to an affinity-based SCP assay was probed, as described in **publication II**. Previous studies suggested that the binding properties of SCPs can be adjusted by varying the elastic modulus, ligand density, and other parameters (Pussak et al. 2013; Wang et al. 2017). For the detection of glyphosate using the EPSPs, glyphosate was coupled to SCPs via different linkers and in different orientations to investigate the effects on the detection limit in competitive binding assays. These functionalizations were validated using confocal laser scanning microscopy (cLSM) as well as confocal Raman microscopy (cRM). EPSPs-hydrophobin fusion proteins were immobilized on glass slides, and the resulting biochips were examined for surface

roughness and coarse aggregates using atomic force microscopy, and were optimized to ensure suitability for the SCP-based assay. Glyphosate in aqueous solution could be detected at picomolar concentrations corresponding to the limit value for German drinking water. The disadvantages of this method are the narrow operating range of 10^{-11} to 10^{-8} M and the special laboratory equipment required for reflection interference contrast microscopy (RICM).

ii, Transfer of the SCP-based sensing concept to other substance classes relevant to health and environment

Since the interaction partners used for molecular recognition can be varied depending on the analyte to be detected, the SCP assay offers many conceivable applications. In the context of anthropogenic environmental pollution, estrogenic and anti-estrogenic compounds are of particular concern because these compounds are known to affect hormone balance at even the lowest, i.e., sub-picomolar, concentrations and are omnipresent.

Publication III addresses the adaptation of the SCP assay in order to provide a platform for the rapid detection of these numerous estrogenic and antiestrogenic compounds. Estrogen sulfotransferase (SULT1E1) was selected as recognition element for these compounds because its substrate specificity largely overlaps with that of estrogen receptors. In addition, SULT1E1 is able to bind certain structures that do not bind to estrogen receptors but influence estrogen balance. For site-specific immobilization of SULT1E1, glass slides were functionalized with chelators that allow for complexing nickel (II) ions to bind hexahistidine-tagged SULT1E1. The resulting surfaces were tested for homogeneity using RICM and cLSM and optimized for SCP studies, with particular emphasis on avoiding the formation of coarse sediments. SCPs were functionalized with estrogen and estrogen conjugates, capable of binding to SULT1E1, using reductive amination and active-ester chemistry. In a final proof-of-concept study, it was demonstrated that the detection of natural and semisynthetic estrogens is possible by employing the SCP approach and that the molecular recognition of these compounds by SULT1E1 provides excellent specificity, as no cross-reactivity with representative androgens and progestogens was observed. However, it should be noted that additional validation experiments are required for this method, as predicted no-effect concentrations for environmental contaminants such as ethinylestradiol are in the femtomolar range and it has not been determined whether appropriate detection limits are feasible using SCP assays. In addition, while a broad substrate specificity can generally be considered advantageous as it allows detecting many contaminants with a single measurement, the varying affinity of these compounds for the SULT1E1 may necessitate the use of additional recognition elements and multiplexed analysis.

iii, Optimization of the SCP-based assay. Improving overall assay performance, shorten analysis time and enhancing modularity

Steady progress in improving the SCP assay is contributing to the commercialization of this technology. In this work, ways to improve throughput by automated image analysis of adherent SCPs were investigated. In addition, a novel method for synthesizing SCPs with narrow size distribution was developed in conjunction with various functionalization strategies to improve throughput as well as modularity of the assay.

Publication IV describes a method to automatically evaluate the adhesion energies of a large set of SCPs interacting with the chip surface. The corresponding radial profiles are automatically localized and the contact radius as well as the particle radius is extracted from the interference patterns, and the adhesion energy is calculated. For fast analysis of the image, the search space within each image is narrowed down by grey-value gradient analysis and exclusion of areas with non-zero gradients. Based on the theory of Raedler and Sackmann, theoretical sample interferograms reflecting the dependence of the profile on the SCP size, deformation, and distance from the surface are generated and compared with the profiles in the preselected areas (Raedler and Sackmann 1992). This template matching algorithm identifies the best fitting sample profile based on the correlation between image and sample profile. From the matching sample profile, the contact area and particle radius as well as the corresponding adhesion energy are extracted. To speed up the computationally intensive process of pattern matching, GPU-based parallel computing is used instead of CPU-based computations. This software-based analysis tool massively increases the throughput of image analysis.

In addition to advances in data analysis, throughput and efficiency of the assay can be improved in several ways, such as at the level of molecular recognition and signal transduction. The latter is based on the interplay between the deformation of the SCP and the quantification of the deformation by an optical readout. The sensor setups for the detection of glyphosate and estrogenic compounds described in publication II and III were developed using polydisperse SCPs with a diameter of 20 to 100 μm . Height reconstruction of the adherent SCP is required to calculate the radius of the respective SCP. The correlation between SCP size, deformation and distance from the surface significantly increases the required number of sample profiles for a reasonable match between image and sample profile. Monodisperse SCPs are therefore highly desirable because they reduce the time and resources required for image analysis. Furthermore, the ability to produce SCPs with a discrete size enables multiplexed analysis with a single readout operation by barcoding based on the size of the SCPs.

To produce monodisperse SCPs, microfluidic droplet generators were used. These allow the generation of highly reproducible SCPs with adjustable size, as described in **publication V**. Uniform water-in-oil emulsions were formed using a flow-focusing geometry and the PEG-macromonomers were crosslinked in the droplets by either photoradical chemistry or thiol-Michael addition, with both strategies resulting in highly monodisperse particles. The respective networks were weakly crosslinked, as evidenced by their mechanical properties and the incomplete turnover of the functional groups of the

macromonomers. The mechanical properties were optimized for applications in the context of SCP-based sensing approaches by adjusting the solid content of PEG, the architecture of the PEG molecules and the concentration of the photoinitiator in the case of photoradical crosslinking. Furthermore, SCPs prepared by droplet generators were found to be susceptible to active ester-mediated decomposition. Therefore, carboxy functionalization of SCPs is not applicable as a basis for further coupling reactions, regardless of the strategy used to introduce the carboxy-groups. To overcome this obstacle, thiol-Michael additions to unreacted functional groups within the PEG networks were used to introduce functional groups, and no effect of this coupling reaction on the structure of the polymer networks of the SCPs was observed. In particular, the coupling of maleimide derivatives to unreacted thiol groups proved to be a very simple and efficient method to functionalize the SCPs. In a final test, these SCPs were successfully evaluated for their applicability in biosensor systems by quantifying biotin using the biotin-streptavidin system.

Conclusions

In this thesis, the development of biosensors for low molecular weight anthropogenic analytes based on the SCP methodology is described. Glyphosate served as a prototypical, potentially threatening, and widespread compound in need of more extensive monitoring. Here, it was demonstrated that I) Molecular recognition between glyphosate and its target enzyme EPSPs can be exploited for biosensing and leads to superior specificity for glyphosate over structurally related compounds without the need for derivatization or pretreatment of the analyte. II) Integration of this highly specific detection strategy in the SCP assay is possible, and the detection limit can be fine-tuned by adjusting the linker type and coupling position of glyphosate. III) The recognition and SCP-based detection strategy can be readily applied to other classes of compounds, as demonstrated by the detection of estrogens and xenoestrogens using SULT1E1 as the natural target of these compounds and estrogen-decorated SCPs. Therefore, this sensing method can be transferred to many other environmentally and diagnostically relevant compounds and substance classes.

Nevertheless, it should be noted that additional efforts are required for a translation into commercially available assays and devices. The performance of the assay in real-sample testing needs to be evaluated, the working range may need to be extended, and the reproducibility under different conditions and sample compositions needs to be determined.

The second focus of the work was to improve the performance of the SCP-method. This was achieved by developing high-throughput analysis software that automatically evaluates the adhesion energies of a large number of SCPs. Furthermore, microfluidics was used to fabricate monodisperse SCPs with adjustable size and mechanical properties to meet the requirements of highly sensitive adhesion energy measurements. Active ester-based functionalization strategies were found to be unsuitable for SCPs produced in this manner, but the thiol-maleimide-Michael addition using residual functional groups

serves as a simple, rapid, and modular strategy for functionalizing these SCPs. Other issues that need to be addressed to improve the method and develop a competitive approach to on-site analysis include an accelerated and automated readout, and miniaturization of the assay, readout, and data processing. These improvements help to create a handy, easy-to-use and cost-effective instrument.

Outlook

The methods described here for detecting anthropogenic pollution are promising examples of the power and utility of SCP-based biosensors. An expansion of the toolbox for more modular assays, that allow rapid response to different market needs, is a key to the future success of SCP-based sensing approaches. This can be achieved by integrating different detection elements and appropriate immobilization strategies to detect a broad range of chemically diverse analytes. An amplification mechanism that allows the measurement range and detection limit to be adjusted is also highly valuable, as these parameters are highly dependent on the occurrence and threshold values of the respective analyte. In addition to this aspect, an advanced readout technology, which must be portable, automated, simple, and cost-effective, is essential for commercialization, and the use of multiplexing approaches to determine multiple analytes by one measurement would increase throughput and reduce costs of operation.

In preliminary studies not listed in the publications section, various strategies have been developed for the detection of analytes such as lipopolysaccharides (LPS), drugs, inflammatory markers, and disease-related nucleic acids. In this context, both LPS and peptides specifically recognizing the lipid component of LPS were successfully coupled to either SCPs or immobilized on glass supports using active ester chemistry or the streptavidin-biotin system. LPS testing is of enormous economic importance, as every intravenously administered drug must be tested for LPS to prevent sepsis. The gold standard for LPS testing still relies on the use of blood derived from an endangered species. Biological membrane preparations enriched in transmembrane proteins that specifically function as drug targets have been successfully immobilized on glass supports by formation of solid-supported lipid bilayers and polymer-cushioned lipid bilayers. The embedded G-protein-coupled receptors are the most important class of drug targets. In addition, immobilized protein A was successfully used for site-specific immobilization of antibodies on glass supports by binding the Fc region, and antibodies labeled with biotin were bound to SCPs or the biochip surface using streptavidin. This system can be used for the detection of inflammatory markers via sandwich assays and immobilized protein A and SCPs functionalized with the antigen recognized by the antibody can be used for simple antibody detection in a diagnostic scenario as well. Also, biochips and SCPs for immobilizing γ -PNA-oligomers via thiol-maleimide coupling for the detection of microRNA via bridging assays were prepared. MicroRNAs are very promising diagnostic markers and PNA-based probes reduce non-specific hybridization, stabilize native nucleic acids and increase melting temperature, which, in this case, would be in the range of room temperature for native nucleic acids.

In further preliminary tests, the possibility of creating sets of SCPs with a defined size was investigated. By adjusting the flow rates of the dispersed phase, three sets of SCPs of defined size could be prepared, with the important feature that each set can be distinguished from each other, i.e., there is no overlap and sufficient spacing of size distributions between the sets. This opens new possibilities for multiplexing, as each SCP set can be individually functionalized for the detection of a specific analyte. The chip surface can be decorated with different detection elements to allow for quantifying different analytes with a single readout based on SCP size barcoding. Apart from this multiplexing approach, adjusting the size and elastic modulus of the SCPs allows the detection limit and working range to be tailored to the particular analytical scenario.

Signal amplification can be achieved, for example, by the use of mixed systems. Nanometer-sized objects do not interfere with the SCP readout and can function as specifically recognized delivery vehicles for the release of large amounts of, e.g., bridging nucleic acids. The bridging nucleic acids bind to the surface due a partially complementary sequence and the SCP bearing another partially complementary nucleic acid binds to the chip surface.

In this thesis, RICM was used as a readout technology for quantifying the adhesion energy of SCPs interacting with the underlying surface. Although convenient for laboratory use, miniaturization capabilities are limited, and especially when the individual size of each SCP needs to be determined, specialized optical instruments consisting of many components are required. However, the conceivable readout technology for the SCP assay is not limited to RICM, and other optical readout devices based on holography are currently being tested, for which a portable device already exists. Furthermore, other technologies such as surface plasmon resonance, fiber optics, impedimetric readouts and many others are also suitable for SCP assays.

References

- Acha, V., Andrews, T., Huang, Q., Sardar, D.K., Hornsby, P.J., 2010. Tissue-Based Biosensors, in: Zourob, M. (Ed.), *Recognition Receptors in Biosensors*. Springer New York, New York, NY, pp. 365–381.
- Ahmad, Z.A., Yeap, S.K., Ali, A.M., Ho, W.Y., Alitheen, N.B.M., Hamid, M., 2012. *Clinical and Developmental Immunology* 2012, 980250.
- Ahmadi, A., Kabiri, S., Omidfar, K., 2020. *IEEE Sensors Journal*, 20 (16), 8912–8921.
- Ahmed, E.M., 2015. *Journal of advanced research* 6 (2), 105–121.
- Akbar, R., Robert, P.A., Pavlović, M., Jeliazkov, J.R., Snapkov, I., Slabodkin, A., Weber, C.R., Scheffer, L., Miho, E., Haff, I.H., Haug, D.T.T., Lund-Johansen, F., Safonova, Y., Sandve, G.K., Greiff, V., 2021. *Cell Reports* 34 (11), 108856.
- Alfonso-Prieto, M., Navarini, L., Carloni, P., 2019. *Frontiers in Molecular Biosciences* 6, 29.
- Arshady, R., 1992. *Colloid and Polymer Science* 270 (8), 717–732.
- Bae, Y.C., Lambert, S.M., Soane, D.S., Prausnitz, J.M., 1991. *Macromolecules* 24 (15), 4403–4407.
- Bailey, F.E., Callard, R.W., 1959. *Journal of Applied Polymer Science* 1 (1), 56–62.
- Balamurugan, S., Obubuafo, A., Soper, S.A., Spivak, D.A., 2008. *Analytical and Bioanalytical Chemistry* 390 (4), 1009–1021.
- Begum, R., Hiroatsu Matsuura, a., 1997. *Faraday Transactions* 93 (21), 3839–3848.
- Bhalla, N., Jolly, P., Formisano, N., Estrela, P., 2016. *Essays in Biochemistry* 60 (1), 1–8.
- Blandamer, M.J., Fox, M.F., Powell, E., Stafford, J.W., 1969. *Makromolekulare Chemie* 124 (1), 222–231.
- Blumenthal, D.K., Stull, J.T., 1982. *Biochemistry* 21 (10), 2386–2391.
- Bosco, F., Capolongo, A., Ruggeri, B., 2002. *Bioremediation Journal* 6 (1), 65–76.
- Branca, C., Magazù, S., Migliardo, F., Romeo, G., 2003. *Journal of Molecular Liquids* 103–104, 181–185.
- Briones, C., Moreno, M., 2012. *Analytical and Bioanalytical Chemistry* 402 (10), 3071–3089.
- Bugg, T., 2008. *Introduction to Enzyme and Coenzyme Chemistry*, 2. ed. Blackwell Publ, Oxford.
- Butt, H.-J., 1991. *Biophysical Journal* 60 (6), 1438–1444.
- Caldwell, D.J., Mastrocco, F., Anderson, P.D., Långe, R., Sumpter, J.P., 2012. *Environmental Toxicology and Chemistry* 31 (6), 1396–1406.
- Caló, E., Khutoryanskiy, V.V., 2015. *European Polymer Journal* 65, 252–267.
- Castellana, E.T., Cremer, P.S., 2006. *Surface Science Reports* 61 (10), 429–444.
- Chambers, J.P., Arulanandam, B.P., Matta, L.L., Weis, A., Valdes, J.J., 2008. *Current Issues in Molecular Biology* 10 (1-2), 1–12.
- Chiu, M.L., Goulet, D.R., Teplyakov, A., Gilliland, G.L., 2019. *Antibodies* 8 (4), 55.
- Choi, J., Seong, T.W., Jeun, M., Lee, K.H., 2017. *Advanced Healthcare Materials* 6 (20).
- Clark, L.C., Lyons, C., 1962. *Annals of the New York Academy of Sciences* 102, 29–45.
- Contreras-Naranjo, J.C., Ugaz, V.M., 2013. *Nature Communications* 4 (1), 1919.
- Crapnell, R.D., Dempsey-Hibbert, N.C., Peeters, M., Tridente, A., Banks, C.E., 2020. *Talanta Open* 2, 100018.

da Silva, E.T.S.G., Souto, D.E.P., Barragan, J.T.C., de F. Giarola, J., de Moraes, A.C.M., Kubota, L.T., 2017. *ChemElectroChem* 4 (4), 778–794.

Ducker, W.A., Senden, T.J., Pashley, R.M., 1991. *Nature* 353 (6341), 239–241.

Duša, F., Chen, W., Witos, J., Rantamäki, A.H., King, A.W.T., Sklavounos, E., Roth, M., Wiedmer, S.K., 2020. *Biochimica et Biophysica Acta - Biomembranes* 1862 (2), 183115.

Elbert, D.L., 2011. *Acta Biomaterialia* 7 (1), 31–56.

Ensing, B., Tiwari, A., Tros, M., Hunger, J., Domingos, S.R., Pérez, C., Smits, G., Bonn, M., Bonn, D., Woutersen, S., 2019. *Nature Communications* 10 (1), 2893.

Erath, J., Schmidt, S., Fery, A., 2010. *Soft Matter* 6 (7), 1432.

European Commission. Joint Research Centre, 2018. Review of the 1st Watch List Under the Water Framework Directive and Recommendations for the 2nd Watch List. Publications Office of the European Union, Luxembourg.

Féger, J., Gil-Falgon, S., Lamaze, C., 1994. *Cellular and Molecular Biology* 40 (8), 1039–1061.

Fischer, L., Strzelczyk, A.K., Wedler, N., Kropf, C., Schmidt, S., Hartmann, L., 2020. *Chemical Science* 11 (36), 9919–9924.

Flake, M.M., Nguyen, P.K., Scott, R.A., Vandiver, L.R., Willits, R.K., Elbert, D.L., 2011. *Biomacromolecules* 12 (3), 844–850.

Franssen, O., Hennink, W.E., 1998. *International Journal of Pharmaceutics* 168 (1), 1–7.

Friedman, M., Nordberg, E., Höidén-Guthenberg, I., Brismar, H., Adams, G.P., Nilsson, F.Y., Carlsson, J., Ståhl, S., 2007. *Protein Engineering, Design and Selection* 20 (4), 189–199.

Fritz, J.L., Owen, M.J., 1995. *The Journal of Adhesion* 54 (1-4), 33–45.

Gao, M., Gao, Y., Chen, G., Huang, X., Xu, X., Lv, J., Wang, J., Xu, D., Liu, G., 2020. *Frontiers in Chemistry* 8, 616326.

Gao, S., Guisán, J.M., Rocha-Martin, J., 2021. *Analytica Chimica Acta*, 338907 (in press).

Gao, Y., Peng, K., Mitragotri, S., 2021. *Advanced Materials* 33 (25), e2006362.

Gaudin, V., 2017. *Biosensors & Bioelectronics* 90, 363–377.

Gaudin, V., 2019. Receptor-based electrochemical biosensors for the detection of contaminants in food products, in Ensafi, A.A. (Ed.): *Electrochemical Biosensors*. Elsevier, Amsterdam, pp. 307–365.

Glaubitx, M., Medvedev, N., Pussak, D., Hartmann, L., Schmidt, S., Helm, C.A., Delcea, M., 2014. *Soft Matter* 10 (35), 6732–6741.

Glazier, D.A., Liao, J., Roberts, B.L., Li, X., Yang, K., Stevens, C.M., Tang, W., 2020. *Bioconjugate Chemistry* 31 (5), 1213–1233.

Gombotz, W.R., Wang, G.H., Horbett, T.A., Hoffman, A.S., 1991. *Journal of Biomedical Materials Research* 25 (12), 1547–1562.

Görrn, P., Wagner, S., 2010. *Journal of Applied Physics* 108 (9), 93522.

Grand View Research, 2021. *Biosensors Market Size | Global Industry Report 2021-2028*. Grand View Research, San Francisco.

Groff, K., Brown, J., Clippinger, A.J., 2015. *Biotechnology advances* 33 (8), 1787–1798.

Guo, M.T., Rotem, A., Heyman, J.A., Weitz, D.A., 2012. *Lab on a Chip* 12 (12), 2146–2155.

Heida, T., Neubauer, J.W., Seuss, M., Hauck, N., Thiele, J., Fery, A., 2017. *Macromolecular Chemistry and Physics* 218 (2), 1600418.

Hennig, S., Rödel, G., Ostermann, K., 2016. *Sensors* 16 (5).

Hoffmann, R.M., Coumbe, B.G.T., Josephs, D.H., Mele, S., Ilieva, K.M., Cheung, A., Tutt, A.N., Spicer, J.F., Thurston, D.E., Crescioli, S., Karagiannis, S.N., 2018. *Oncoimmunology* 7 (3), e1395127.

Hossain, S.M.Z., Mansour, N., 2019. *Arab Journal of Basic and Applied Sciences* 26 (1), 502–518.

Huang, L., Nishinari, K., 2001. *Journal of Polymer Science Part B: Polymer Physics* 39 (5), 496–506.

Jeon, S., Andrade, J., 1991. *Journal of Colloid and Interface Science* 142 (1), 159–166.

Jeon, S., Lee, J., Andrade, J., Gennes, P. de, 1991. *Journal of Colloid and Interface Science* 142 (1), 149–158.

Jeong, H.-H., Issadore, D., Lee, D., 2016. *Korean Journal of Chemical Engineering* 33 (6), 1757–1766.

Jesionowski, T., Zdarta, J., Krajewska, B., 2014. *Adsorption* 20 (5-6), 801–821.

Johnson, K.L., Kendall, K., Roberts, A.D., 1971. *Proceedings of the Royal Society A: Mathematical, Physical and Engineering Sciences* 324 (1558), 301–313.

Jonkheijm, P., Weinrich, D., Schröder, H., Niemeyer, C.M., Waldmann, H., 2008. *Angewandte Chemie International Edition* 120 (50), 9762–9792.

Juska, V.B., Pemble, M.E., 2020. *Sensors* 20 (21).

Justino, C.I.L., Duarte, A.C., Rocha-Santos, T.A.P., 2017. *Sensors* 17 (12).

Kalecki, J., Iskierko, Z., Cieplak, M., Sharma, P.S., 2020. *ACS Sensors* 5 (12), 3710–3720.

Karkare, S., Bhatnagar, D., 2006. *Applied microbiology and biotechnology* 71 (5), 575–586.

Kihm, K.D., 2011. Reflection Interference Contrast Microscopy (RICM), in: Kihm, K.D. (Ed.), *Near-Field Characterization of Micro/Nano-Scaled Fluid Flows*. Springer Berlin Heidelberg, Berlin, Heidelberg, pp. 119–130.

Kim, J., Park, H., Jung, D., Kim, S., 2003. *Analytical Biochemistry* 313 (1), 41–45.

Kingshott, P., Griesser, H.J., 1999. *Current Opinion in Solid State and Materials Science* 4 (4), 403–412.

Kivirand, K., Kagan, M., Rinken, T., 2015. Biosensors for the detection of antibiotic residues in milk, in: Rinken, T. (Ed.), *Biosensors - Micro and Nanoscale Applications*. InTech, London, pp. 425–456.

Korotkaya, E., 2014. *Foods and Raw Materials* 2 (2), 161–171.

Lakhin, A.V., Tarantul, V.Z., Gening, L.V., 2013. *Acta Naturae* 5 (4), 34–43.

Lee, S., Tong, X., Yang, F., 2016. *Biomaterials Science* 4 (3), 405–411.

Leobandung, W., Ichikawa, H., Fukumori, Y., Peppas, N.A., 2002. *Journal of Controlled Release* 80 (1-3), 357–363.

Li, C., Karadeniz, H., Canavar, E., Erdem, A., 2012. *Electrochimica Acta* 82, 137–142.

Li, J., Kao, W.J., 2003. *Biomacromolecules* 4 (4), 1055–1067.

Limozin, L., Sengupta, K., 2009. *ChemPhysChem* 10 (16), 2752–2768.

Lin, C.-C., Anseth, K.S., 2009. *Pharmaceutical Research* 26 (3), 631–643.

Liszewski, K., 2015. *Genetic Engineering & Biotechnology News* 35 (7), 16-18, 21.

Liu, R., Li, Z., Huang, Z., Li, K., Lv, Y., 2019. *Trends in Analytical Chemistry* 118, 123–137.

Liu, Y., Yu, J., 2016. *Microchimica Acta* 183 (1), 1–19.

Llanos, G.R., Sefton, M.V., 1993. *Journal of Biomaterials Science. Polymer edition* 4 (4), 381–400.

Mark, A., Helfricht, N., Rauh, A., Karg, M., Papastavrou, G., 2019. *Small* 15 (43), e1902976.

Marques, M.E., Mansur, A.A., Mansur, H.S., 2013. *Applied Surface Science* 275, 347–360.

Marsden, C.J., Eckersley, S., Hebditch, M., Kvist, A.J., Milner, R., Mitchell, D., Warwicker, J., Marley, A.E., 2014. *Journal of Biomolecular Screening* 19 (6), 829–838.

Martin, S., Wang, H., Hartmann, L., Pompe, T., Schmidt, S., 2015. *Physical Chemistry Chemical Physics* 17 (5), 3014–3018.

Martin, S., Wang, H., Rathke, T., Anderegg, U., Möller, S., Schnabelrauch, M., Pompe, T., Schmidt, S., 2016. *Polymer* 102, 342–349.

Maxfield, J., Shepherd, I.W., 1975. *Polymer* 16 (7), 505–509.

Mehrotra, P., 2016. *Journal of Oral Biology and Craniofacial Research* 6 (2), 153–159.

Messing, R.A., 1975. *Journal of Non-Crystalline Solids* 19, 277–283.

Milstein, C., 1999. *Bioessays* 21 (11), 966–973.

Mohamad, N.R., Marzuki, N.H.C., Buang, N.A., Huyop, F., Wahab, R.A., 2015. *Biotechnology & Biotechnological Equipment* 29 (2), 205–220.

Monzel, C., Fenz, S.F., Merkel, R., Sengupta, K., 2009. *ChemPhysChem* 10 (16), 2828–2838.

Morales, M.A., Halpern, J.M., 2018. *Bioconjugate Chemistry* 29 (10), 3231–3239.

Moreira, A., Carneiro, J., Campos, J.B.L.M., Miranda, J.M., 2021. *Microfluidics and Nanofluidics* 25 (2).

Muir, T.W., Dawson, P.E., Kent, S.B., 1997. Protein synthesis by chemical ligation of unprotected peptides in aqueous solution, in Fields, G.B. (Ed.): *Solid-Phase Peptide Synthesis Vol. 289*. Elsevier, Amsterdam, pp. 266–298.

Muir, T.W., Sondhi, D., Cole, P.A., 1998. *Proceedings of the National Academy of Sciences of the United States of America* 95 (12), 6705–6710.

Murata, M., Nakayama, M., Irie, H., Yakabe, K., Fukuma, K., Katayama, Y., Maeda, M., 2001. *Analytical Science* 17 (3), 387–390.

Myung, D., Koh, W., Ko, J., Hu, Y., Carrasco, M., Noolandi, J., Ta, C.N., Frank, C.W., 2007. *Polymer* 48 (18), 5376–5387.

Nadal, M., Prekovic, S., Gallastegui, N., Helsen, C., Abella, M., Zielinska, K., Gay, M., Vilaseca, M., Taulès, M., Houtsmuller, A.B., van Royen, M.E., Claessens, F., Fuentes-Prior, P., Estébanez-Perpiñá, E., 2017. *Nature Communications* 8 (1), 14388.

Naresh, V., Lee, N., 2021. *Sensors* 21 (4) 1109.

Nichols, M.D., Scott, E.A., Elbert, D.L., 2009. *Biomaterials* 30 (29), 5283–5291.

Nolan, C.M., Reyes, C.D., Debord, J.D., García, A.J., Lyon, L.A., 2005. *Biomacromolecules* 6 (4), 2032–2039.

Omidfar, K., Ahmadi, A., Syedmoradi, L., Khoshfetrat, S.M., Larijani, B., 2020. *Journal of Diabetes and Metabolic Disorders*, 1–5.

Oue, S., Okamoto, A., Yano, T., Kagamiyama, H., 1999. *Journal of Biological Chemistry* 274 (4), 2344–2349.

Parcekani, J., Hashemzadeh, H., Allahverdi, A., Siampour, H., Abbasian, S., Moshaii, A., Naderi-Manesh, H., 2021. *Sensing and Bio-Sensing Research* 34, 100449.

Pardeshi, S., Singh, S.K., 2016. *RSC Advances* 6 (28), 23525–23536.

Park, J.-W., Park, Y.J., Jun, C.-H., 2011. *Chemical Communications* 47 (17), 4860–4871.

Plamper, F.A., Richtering, W., 2017. *Accounts of Chemical Research* 50 (2), 131–140.

Pussak, D., Behra, M., Schmidt, S., Hartmann, L., 2012. *Soft Matter* 8 (5), 1664–1672.

Pussak, D., Ponader, D., Mosca, S., Ruiz, S.V., Hartmann, L., Schmidt, S., 2013. *Angewandte Chemie International Edition* 52 (23), 6084–6087.

Puthenkalam, R., Hieckel, M., Simeone, X., Suwattanasophon, C., Feldbauer, R.V., Ecker, G.F., Ernst, M., 2016. *Frontiers in Molecular Neuroscience* 9, 44.

Raedler, J., Sackmann, E., 1992. *Langmuir* 8 (3), 848–853.

Renneberg, R., Pfeiffer, D., Lisdat, F., Wilson, G., Wollenberger, U., Ligler, F., Turner, A.P.F., 2008. *Frieder Scheller and the Short History of Biosensors*, in: Renneberg, R., Lisdat, F. (Eds.), *Biosensing for the 21st Century*, Springer Berlin Heidelberg, Berlin, Heidelberg, pp. 1–18.

Rusmini, F., Zhong, Z., Feijen, J., 2007. *Biomacromolecules* 8 (6), 1775–1789.

Saunders, B.R., Vincent, B., 1999. *Advances in Colloid and Interface Science* 80 (1), 1–25.

Saxena, S., Hansen, C.E., Lyon, L.A., 2014. *Accounts of Chemical Research* 47 (8), 2426–2434.

Scheper, T., 1992. *Journal of Industrial Microbiology* 9 (3-4), 163–172.

Schmidt, S., Wang, H., Pussak, D., Mosca, S., Hartmann, L., 2015. *Beilstein Journal of Organic Chemistry* 11, 720–729.

Schneider, M.H., Tran, Y., Tabeling, P., 2011. *Langmuir* 27 (3), 1232–1240.

Seiffert, S., Thiele, J., 2019. *Microfluidics*. De Gruyter, Berlin.

Serfling, R., Coin, I., 2016. *Methods in Enzymology* 580, 89–107.

Sevenler, D., Trueb, J., Ünlü, M.S., 2019. *Proceedings of the National Academy of Sciences of the United States of America* 116 (10), 4129–4134.

Sharma, S., Byrne, H., O’Kennedy, R.J., 2016. *Essays in Biochemistry* 60 (1), 9–18.

Shen, M., Rusling, J., Dixit, C.K., 2017. *Methods* 116, 95–111.

Slomkowski, S., Alemán, J.V., Gilbert, R.G., Hess, M., Horie, K., Jones, R.G., Kubisa, P., Meisel, I., Mormann, W., Penczek, S., Stepto, R.F.T., 2011. *Pure and Applied Chemistry* 83 (12), 2229–2259.

Strzelczyk, A.K., Wang, H., Lindhorst, A., Waschke, J., Pompe, T., Kropf, C., Luneau, B., Schmidt, S., 2017. *Gels* 3 (3), 31.

Stuart, J.K., Hlady, V., 1999. *Biophysical Journal* 76 (1), 500–508.

Suh, J.-S., Kim, H.-S., Kim, T.-J., 2021. *Sensors and Actuators B: Chemical* 334, 129663.

Suzuki, D., Horigome, K., Kureha, T., Matsui, S., Watanabe, T., 2017. *Polymer Journal* 49 (10), 695–702.

Tibbitt, M.W., Kloxin, A.M., Sawicki, L., Anseth, K.S., 2013. *Macromolecules* 46 (7).

Tóth, A., Bertóti, I., Blazsó, M., Bánhegyi, G., Bogнар, A., Szaplóniczay, P., 1994. *Journal of Applied Polymer Science*. 52 (9), 1293–1307.

Tse Sum Bui, B., Haupt, K., 2010. *Analytical and Bioanalytical Chemistry* 398 (6), 2481–2492.

Turner, A.P.F., 2013. *Chemical Society Reviews* 42 (8), 3184–3196.

- Vasapollo, G., Del Sole, R., Mergola, L., Lazzoi, M.R., Scardino, A., Scorrano, S., Mele, G., 2011. *International Journal of Molecular Sciences* 12 (9), 5908–5945.
- Verma, S., Eckstein, F., 1998. *Annual Review of Biochemistry* 67, 99–134.
- Wackerlig, J., Schirhagl, R., 2016. *Analytical Chemistry* 88 (1), 250–261.
- Wada, R., Fujimoto, K., Kato, M., 2014. *The Journal of Physical Chemistry. B* 118 (42), 12223–12231.
- Wahab, S.A., Harada, T., Matsubara, T., Aida, M., 2006. *The Journal of Physical Chemistry. A* 110 (3), 1052–1059.
- Wang, H., Jacobi, F., Waschke, J., Hartmann, L., Löwen, H., Schmidt, S., 2017. *Advanced Functional Materials* 27 (41), 1702040.
- Wang, J., 2008. *Chemical reviews* 108 (2), 814–825.
- Wang, J., Wang, R., Gu, Y., Sourakov, A., Olsen, B.D., Johnson, J.A., 2019. *Chemical Science* 10 (20), 5332–5337.
- Wu, C.-S.C., Chen, G., 1989. *Analytical Biochemistry* 177 (1), 178–182.
- Young, C.L., Britton, Z.T., Robinson, A.S., 2012. *Biotechnology Journal* 7 (5), 620–634.
- Yu, Y., Chau, Y., 2015. *Biomacromolecules* 16 (1), 56–65.
- Yuan, H.G., Kalfas, G., Ray, W.H., 1991. *Journal of Macromolecular Science, Part C: Polymer Reviews* 31 (2-3), 215–299.
- Zhang, H., 2013. *European Polymer Journal* 49 (3), 579–600.
- Zhou, W., Huang, P.-J.J., Ding, J., Liu, J., 2014. *The Analyst* 139 (11), 2627–2640.
- Zhu, J., 2010. *Biomaterials* 31 (17), 4639–4656.
- Zhu, M., Lerum, M.Z., Chen, W., 2012. *Langmuir* 28 (1), 416–423.

Appendix

Zusammenfassung

Im Rahmen dieser Arbeit wurden *Soft Colloidal Probe*- (SCP) basierte Sensoransätze für den Nachweis von umweltrelevanten Analyten sowie Ansätze für die Verbesserung dieser Sensorplattform entwickelt. Die entsprechenden Methoden nutzen insbesondere biomimetische Strategien um eine selektive Erkennung der betreffenden Verbindung bzw. Verbindungsklasse zu ermöglichen. Des Weiteren leistet die Verbesserung der Datenverarbeitung sowie der Qualität und Eigenschaften der SCPs einen Beitrag zur Kommerzialisierung dieser Technologie. Speziell befasst sich die Arbeit mit der Entwicklung von Sensoransätzen für den spezifischen, SCP-basierten Nachweis von Glyphosat und Verbindungen mit östrogenartiger Wirkung sowie der schnelleren Datenverarbeitung durch die Anwendung von *Pattern-Matching* Algorithmen und mit der Herstellung monodisperser Partikel mittels mikrofluidischer Synthese für Anwendungen im Bereich der Biosensorik. Daher ergaben sich für die Arbeit die nachfolgenden Ziele:

i, Entwicklung und Validierung einer spezifischen biomolekularen Erkennungsstrategie für eine typische Verunreinigung von Wasserressourcen und Integration in die SCP-basierte Sensormethode

Die Verschmutzung verschiedener Oberflächengewässer, des Grundwassers und des Trinkwassers stellt eine ernstzunehmende Gefahr für die Umwelt und die öffentliche Gesundheit dar. Zu den möglichen Verunreinigungen gehören Stickstoff- und Phosphorverbindungen, verschiedene Salze, Bleichmittel, Pestizide, Metalle und andere Stoffe. Glyphosat ist ein praktisch allgegenwärtiges Pestizid, welches aufgrund seiner möglicherweise unterschätzten gesundheitlichen Risiken große Aufmerksamkeit auf sich gezogen hat.

Veröffentlichung I beschreibt die Entwicklung eines kolorimetrischen Schnelltests für Glyphosat. Im Unterschied zu anderen kolorimetrischen Tests zum Nachweis von Glyphosat wird das Target-Enzym von Glyphosat, die 5-Enolpyruvylshikimat-3-Phosphat-Synthase (EPSPs), zur molekularen Erkennung sowie zur Signalverstärkung verwendet. Malachitgrün dient der Quantifizierung des Substratumsatzes mittels Bildung eines farbigen Komplexes in Gegenwart von anorganischem Phosphat, das sich im Zuge der katalysierten Reaktion bildet. Die im Rahmen der Arbeit entwickelte Strategie für die Immobilisierung der EPSPs auf Gläsern und Kunststoffen beruht auf der adsorptiven Bindung von Hydrophobinen an diese Oberflächen. Es konnte nachgewiesen werden, dass die immobilisierte EPSPs Glyphosat bindet, wobei eine Nachweisgrenze von 50 nM bestimmt wurde. Die Kreuzreaktivität mit strukturell verwandten Verbindungen fiel, aufgrund der Spezifität der molekularen Wechselwirkung, erwartungsgemäß vernachlässigbar aus. Neben der sehr guten Selektivität zeichnet sich der Assay durch einfache Handhabung und gute Reproduzierbarkeit aus. Als Einschränkung ist jedoch die vergleichsweise hohe Nachweisgrenze, die für die meisten Anwendungen unzureichend ist und möglicherweise zusätzliche Extraktionsschritte der Proben erfordert, zu nennen. Anorganisches Phosphat in der Probe stört den Nachweis ebenfalls.

In **Veröffentlichung II** wurde die Nutzung der molekularen Erkennung zwischen EPSPs und Glyphosat in einem Affinitäts-basierten SCP-Assay untersucht. Frühere Studien ergaben, dass die Bindungseigenschaften der SCPs mittels Variation des Elastizitätsmoduls, der Ligandendichte und anderer Parameter beeinflusst und angepasst werden können. Für die Detektion von Glyphosat mittels der EPSPs, wurde Glyphosat über verschiedene Linker und in verschiedenen Orientierungen an SCPs gekoppelt, um die Auswirkungen auf die Nachweisgrenze im Rahmen kompetitiver Bindungsassays zu untersuchen. Die Funktionalisierungsschritte wurden mittels konfokaler Laser-Scanning-Mikroskopie (cLSM) und konfokaler Raman-Mikroskopie (cRM) validiert. EPSPs-Hydrophobin-Fusionsproteine wurden auf Glasobjektträgern immobilisiert, und die resultierenden Biochips wurden mit Hilfe rasterkraftmikroskopischer Untersuchungen auf Oberflächenrauigkeit sowie grobe Aggregate geprüft und optimiert, um die Eignung für SCP-basierte Assays sicherzustellen. In wässrigen Lösungen konnte Glyphosat in einer pikomolaren Konzentration nachgewiesen werden, welche dem in Deutschland geltenden Grenzwert für Trinkwasser entspricht. Die Nachteile dieser Methode sind der enge Arbeitsbereich von 10^{-11} bis 10^{-8} M und die für Reflexionsinterferenzkontrastmikroskopie (RICM) erforderliche spezielle Laborausrüstung.

ii, Übertragung des SCP-basierten Sensorkonzepts auf andere gesundheits- und umweltrelevante Stoffklassen

Da die zur molekularen Erkennung verwendeten Interaktionspartner je nach nachzuweisendem Analyten variiert werden können, bietet der SCP-Assay vielseitige Einsatzmöglichkeiten. Im Zusammenhang mit der anthropogenen Umweltverschmutzung sind Verbindungen mit östrogenen und antiöstrogenen Wirkung von besonderem Interesse, da diese Stoffe bekanntermaßen schon in geringsten Konzentrationen den Hormonhaushalt beeinflussen und gleichzeitig nahezu omnipräsent sind.

Veröffentlichung III befasst sich mit der Entwicklung eines SCP-Assays für den schnellen Nachweis der zahlreichen Verbindungen mit östrogenen und antiöstrogenen Wirkung. Die Östrogen-Sulfotransferase (SULT1E1) wurde als Erkennungselement für diese Verbindungen ausgewählt, da sich ihre Substratspezifität weitgehend mit der von Östrogenrezeptoren überschneidet. Darüber hinaus ist die SULT1E1 in der Lage bestimmte Strukturen zu binden, die nicht mit Östrogenrezeptoren interagieren, jedoch den Östrogenhaushalt beeinflussen. Für die ortsspezifische Immobilisierung der SULT1E1 wurden Glasobjektträger mit Chelatoren funktionalisiert, die eine Komplexierung von Nickel(II)-Ionen ermöglichen, was wiederum die spezifische Bindung Hexahistidin-markierter SULT1E1 erlaubt. Die resultierenden Oberflächen wurden mittels RICM und cLSM auf ihre Homogenität geprüft und für SCP-Assays optimiert, wobei besonderer Wert auf die Vermeidung grober Sedimente und Aggregate gelegt wurde. Die SCPs wurden durch reduktive Aminierung sowie Aktivesterchemie mit Östrogen und Östrogenkonjugaten funktionalisiert, die in der Lage sind, mit dem aktiven Zentrum der SULT1E1 zu interagieren. In einer abschließenden *Proof-of-Concept*-Studie wurde gezeigt, dass der Nachweis

natürlicher und semisynthetischer Östrogene mit SCP-basierten Methoden möglich ist. Aus der vernachlässigbaren Kreuzreaktivität mit repräsentativen Androgenen und Progestogenen lässt sich dabei eine ausgezeichnete Spezifität der molekularen Erkennung östrogenartiger Verbindungen durch die SULT1E1 ableiten. Es ist jedoch anzumerken, dass zusätzliche Validierungsexperimente für diese Methode erforderlich sind, da sich die *Predicted No-Effect*-Konzentrationen für Umweltkontaminanten wie Ethinylestradiol im femtomolaren Bereich bewegen und nicht ermittelt wurde, ob mittels SCP-Assay entsprechende Nachweisgrenzen realisierbar sind. Darüber hinaus kann eine breite Substratspezifität zwar generell als vorteilhaft angesehen werden, da sie den Nachweis vieler Verbindungen mit einer einzigen Messung ermöglicht, allerdings kann die unterschiedliche Affinität dieser Verbindungen für die SULT1E1 die Nutzung zusätzlicher Erkennungselemente und Multiplex-Analysen erforderlich machen.

iii, Optimierung des SCP-basierten Assays. Verbesserung der Effizienz des Assays, Verkürzung der Analysezeit und Erweiterung der Modularität

Stetige Fortschritte bei der Verbesserung des SCP-Assays tragen zur Kommerzialisierung des SCP-Assays bei. In dieser Arbeit wurden Möglichkeiten zur Verbesserung des Durchsatzes durch die automatisierte Bildanalyse adhärerender SCPs untersucht. Darüber hinaus wurde eine neuartige Methode zur Synthese von SCPs mit enger Größenverteilung in Verbindung mit verschiedenen Funktionalisierungsstrategien zur Verbesserung des Durchsatzes sowie der Modularität des Assays entwickelt.

Veröffentlichung IV beschreibt eine Methode zur automatischen Bestimmung der Adhäsionsenergie einer großen Anzahl von mit Chipoberflächen interagierenden SCPs. Die entsprechenden radialen Profile werden dabei automatisch lokalisiert und der Kontaktradius sowie der Partikelradius werden zur Berechnung der Adhäsionsenergie aus den Interferenzmustern extrahiert. Für die schnelle Analyse des jeweiligen Bildes wird der Suchraum für radiale Profile mittels Grauwertgradientenanalyse und Ausschluss von Bereichen mit Nicht-Null-Gradienten eingegrenzt. Anschließend werden Musterinterferogramme, welche die Abhängigkeit des Profils von der SCP-Größe, der Verformung und dem Abstand von der Oberfläche widerspiegeln, erzeugt und mit den Profilen in vorgewählten Bereichen verglichen. Der *Template-Matching*-Algorithmus identifiziert das am besten passende Musterprofil auf Grundlage der Korrelation zwischen detektiertem und Musterprofil. Aus dem passenden Musterprofil werden die Kontaktfläche und der Partikelradius sowie die zugehörige Adhäsionsenergie extrahiert. Um den rechenintensiven Prozess des Musterabgleichs zu beschleunigen, wird GPU-basiertes paralleles Rechnen anstelle von CPU-basierten Berechnungen verwendet. Mittels dieses softwarebasierten Analysetools konnte der Durchsatz bei der Bildanalyse massiv erhöht werden.

Zusätzlich zu den Fortschritten bei der Datenanalyse können Durchsatz und Effizienz des Assays auf verschiedene Weise verbessert werden, so zum Beispiel auf der Ebene der molekularen Erkennung und der Signaltransduktion. Letztere basiert auf dem Zusammenspiel zwischen der Verformung des SCP und

der Quantifizierung dieser Verformung durch einen optischen Readout. Die in den Veröffentlichungen II und III beschriebenen Sensoransätze zum Nachweis von Glyphosat und Verbindungen mit östrogenen Wirkung wurden unter Verwendung polydisperser SCPs mit einem Durchmesser von 20 bis 100 μm entwickelt. Die Höhenrekonstruktion der adhärenen SCPs ist dabei erforderlich um den Radius des jeweiligen SCP zu berechnen. Die Korrelation zwischen SCP-Größe, Verformung und Abstand von der Oberfläche erhöht wiederum die Anzahl der erforderlichen Musterprofile für eine angemessene Übereinstimmung zwischen detektiertem und Musterprofil erheblich. Monodisperse SCPs sind daher höchst wünschenswert, da sie den Zeit- und Ressourcenaufwand für die Bildanalyse verringern. Die Fähigkeit SCPs mit einer diskreten Größe herzustellen, ermöglicht darüber hinaus eine Multiplex-Analyse mit einem einzigen Auslesevorgang durch Kodierung auf Grundlage der Größe der SCPs.

Zur Herstellung monodisperser SCPs wurden mikrofluidische Tröpfchengeneratoren eingesetzt. Diese erlauben es hochgradig reproduzierbare SCPs mit einstellbarer Größe zu erzeugen, wie in **Veröffentlichung V** beschrieben. Wasser-in-Öl-Emulsionen wurden unter Verwendung einer strömungsfokussierenden Geometrie gebildet und die PEG-Makromonomere wurden in den gebildeten Tröpfchen entweder photoradikalisch oder via Thiol-Michael-Addition vernetzt, wobei beide Strategien zu hochgradig monodispersen Partikeln führten. Die Vernetzung der jeweiligen Netzwerke war nur schwach ausgeprägt, was mittels der Untersuchung der mechanischen Eigenschaften der SCPs und des Umsatzes der funktionellen Gruppen der Makromonomere festgestellt wurde. Die mechanischen Eigenschaften wurden für Anwendungen im Rahmen SCP-basierter Sensoransätze optimiert, indem der Feststoffgehalt an PEG, die Architektur der PEG-Moleküle und die Konzentration des Photoinitiators im Falle photoradikalischer Vernetzung angepasst wurden. Des Weiteren erwiesen sich die mittels von Tröpfchengenerator präparierten SCPs als anfällig gegenüber Aktivester-vermittelter Zersetzung. Eine Carboxy-Funktionalisierung der SCPs ist daher, unabhängig von der Strategie zur Einführung der Carboxy-Gruppen, als Grundlage für weitere Kopplungsreaktionen ungeeignet. Daher wurden Thiol-Michael-Additionen an nicht umgesetzte funktionelle Gruppen innerhalb der PEG-Netzwerke zur Funktionalisierung verwendet, wobei kein Einfluss dieser Kopplungsreaktion auf die Struktur der Polymernetzwerke der SCP beobachtet wurde. Insbesondere die Kopplung von Maleimid-Derivaten an nicht umgesetzte Thiol-Gruppen erwies sich als eine sehr einfache und effiziente Methode zur Funktionalisierung der SCPs. In einer abschließenden Untersuchung wurden diese SCPs erfolgreich auf ihre Anwendbarkeit in Biosensorsystemen durch die Quantifizierung von Biotin unter Verwendung des Biotin-Streptavidin-Systems untersucht.

Im Rahmen dieser Arbeit konnten sowohl Biosensoren für niedermolekulare Verbindungen mit großer Umwelt- und gesundheitlicher Relevanz auf Grundlage des SCP-basierten Sensoransatzes entwickelt, als auch die SCP-Methodik verbessert werden. Dabei konnte dieses Sensorprinzip für die Detektion verschiedener Substanzklassen genutzt und somit die breite Anwendbarkeit aufgezeigt werden. Des Weiteren wurden biomimetische Erkennungsstrategien für eine hochspezifische Detektion der jeweiligen Analyten genutzt. Der Arbeitsbereich und die Nachweisgrenze des Assays erwiesen sich als einstellbar,

sodass praxisrelevante Messbereiche erzielt werden konnten. Die Verbesserung der SCP-Methodik beinhaltet die beschleunigte Datenauswertung durch die Software-gestützte Analyse der radialen Profile adhärerender SCPs. Mittels mikrofluidischer Tröpfchengeneratoren konnten darüber hinaus monodisperse SCPs mit maßgeschneiderten mechanischen Eigenschaften hergestellt werden. Diese SCPs ermöglichen eine schnellere und einfachere Analyse der Adhäsionsenergien und sind gleichzeitig modular modifizierbar, was die Kopplung verschiedenster funktioneller Gruppen und Moleküle an die SCPs für weitere Sensoranwendungen erlaubt.

Publikationen

- [I] Döring, J., **Rettke, D.**, Rödel, G., Pompe, T., Ostermann, K., 2019. Surface functionalization by hydrophobin-EPSPS fusion protein allows for the fast and simple detection of glyphosate. *Biosensors* 9, 104.
- [II] **Rettke, D.**, Döring, J., Martin, S., Venus, T., Estrela-Lopis, I., Schmidt, S., Ostermann, K., Pompe, T., 2020. Picomolar glyphosate sensitivity of an optical particle-based sensor utilizing biomimetic interaction principles. *Biosensors & bioelectronics* 165, 112262.
- [III] **Rettke, D.**, Seufert, F., Döring, J., Ostermann, K., Wilms, D., Schmidt, S., Pompe, T., 2021. Biomimetic estrogen sensor based on soft colloidal probes. *Biosensors & bioelectronics* 192, 113506.
- [IV] Waschke, J., Pompe, T., **Rettke, D.**, Schmidt, S., Hlawitschka, M., 2019. Radial profile detection of multiple spherical particles in contact with interacting surfaces. *PloS one* 14 (4), e0214815.
- [V] **Rettke, D.**, Danneberg, C., Neuendorf, T.A., Kühn, S., Friedrichs, J., Hauck, N., Thiele, J., Werner, C., Pompe, T. Microfluidics-assisted synthesis and functionalization of monodisperse colloidal hydrogel particles for optomechanical biosensors. (eingereicht).

Patente

- [I] Verfahren zur Detektion von Analyten auf Basis immobilisierter Proteine, DE102018130133A1.
- [II] Method, surface, particle, and kit for the detection of analytes in samples, PCT/EP2019/081614
- [III] Method for the detection of hormonally active compounds, kit and their use, PCT/EP2021/051033
- [IV] Method and kit for the detection of toxins and pathogens (PCT Anmeldung eingereicht)

Curriculum vitae

David Rettke

Address Paunsdorfer Str. 3, 04316 Leipzig
E-Mail d.rettke0@gmx.de
Telephone +49 176 39885595

Personal Information

Nationality German
Date of birth September 3, 1986
Place of birth Annaberg-Buchholz, Germany

Education

Since 02/2017 Doctoral candidate
Biophysical Chemistry, Institute of Biochemistry
Universität Leipzig, Leipzig, Germany

Since 06/2016 Master of Science in Chemistry
Technische Universität Dresden, Dresden, Germany
Thesis: *“Solid-phase synthesis of fluorogenic thrombin-cleavable hydrogel crosslinkers to study the degradation behavior of thrombin-sensitive Star PEG-heparin hydrogels”*

Since 08/2012 Bachelor of Science in Chemistry
Hochschule Zittau-Görlitz, Zittau, Germany
Thesis: *“Directed immobilization of stem cell factor (SCF) on biohybrid hydrogels and interaction studies between SCF and heparin”*

Since 06/2005 Abitur
St. Annen-Gymnasium Annaberg, Annaberg-Buchholz, Germany

Work Experience

Since 01/2017 Research associate
Biophysical Chemistry, Institute of Biochemistry
Universität Leipzig, Leipzig, Germany

List of publications

- [1] **Rettke, D.**, Danneberg, C., Neuendorf, T.A., Kühn, S., Friedrichs, J., Hauck, N., Thiele, J., Werner, C., Pompe, T. Microfluidics-assisted synthesis and functionalization of monodisperse colloidal hydrogel particles for optomechanical biosensor. (submitted).
- [2] **Rettke, D.**, Seufert, F., Döring, J., Ostermann, K., Wilms, D., Schmidt, S., Pompe, T., 2021. Biomimetic estrogen sensor based on soft colloidal probes. *Biosensors & bioelectronics* 192, 113506.
- [3] **Rettke, D.**, Döring, J., Martin, S., Venus, T., Estrela-Lopis, I., Schmidt, S., Ostermann, K., Pompe, T., 2020. Picomolar glyphosate sensitivity of an optical particle-based sensor utilizing biomimetic interaction principles. *Biosensors & bioelectronics* 165, 112262.
- [4] Döring, J., **Rettke, D.**, Rödel, G., Pompe, T., Ostermann, K., 2019. Surface functionalization by hydrophobin-EPSPS fusion protein allows for the fast and simple detection of glyphosate. *Biosensors* 9, 104.
- [5] Waschke, J., Pompe, T., **Rettke, D.**, Schmidt, S., Hlawitschka, M., 2019. Radial profile detection of multiple spherical particles in contact with interacting surfaces. *PLoS one* 14 (4), e0214815.

List of patents

- [1] Verfahren zur Detektion von Analyten auf Basis immobilisierter Proteine, DE102018130133A1.
- [2] Method, surface, particle, and kit for the detection of analytes in samples, PCT/EP2019/081614
- [3] Method for the detection of hormonally active compounds, kit and their use, PCT/EP2021/051033
- [4] Method and kit for the detection of toxins and pathogens (PCT application submitted)

List of oral presentations

- [1] Ultrasensitive particle-based detection of glyphosate and other small molecules using an interferometric readout and biomimetic interaction principles
31st Anniversary World Congress on Biosensors, July 26 - 29 2021, online
- [2] A biomimetic approach for an optical glyphosate sensor with picomolar sensitivity.
SPIE Optics + Optoelectronics, April 1 - 4 2019, Prague, Czech Republic
- [3] Hydrogel Microparticles for Biosensing.
Annual Conference of the Leipzig School of Natural Sciences – Building with Molecules and Nano-objects, March 18 - 19 2019, Leipzig, Germany
- [4] Hydrogel Microparticles for Biosensing
Biotechnology and Biomedicine Doctoral Colloquium, November 8 2017, Leipzig, Germany

List of poster presentations

- [1]** A biomimetic approach for an optical glyphosate sensor with picomolar sensitivity
6th International Conference on Bio-Sensing Technology, June 16 - 19, Kuala Lumpur, Malaysia
- [2]** A soft colloidal probe-based biomimetic tool to directly quantify pesticide residues by optical readout
28th Anniversary World Congress on Biosensors, June 12 - 15 2018, Miami, United States
- [3]** A soft colloidal probe-based biomimetic tool to directly quantify pesticide residues by optical readout
Eurotrode XIV, March 25 - 28 2018, Naples, Italy
- [4]** Hydrogel Microparticles for Biosensing
Annual Conference of the Leipzig School of Natural Sciences – Building with Molecules and Nano-objects, March 19 - 20 2018, Leipzig, Germany
- [5]** Ein biomimetisches Tool auf Basis weicher kolloidaler Sonden zur direkten Quantifizierung von Pestizidrückständen mittels optischer Auslesung
13. Dresdner Sensorsymposium, December 4 - 6 2017, Dresden, Germany

Acknowledgements

Firstly, I thank my supervisor Prof. Tilo Pompe for guidance, support and encouragement.

I especially thank all the bachelor, master, and research assistant students who helped me in the lab: Aline Patzschke, Kay Huber, Florian Seufert, Cornelia Clemens, Christian Danneberg, Nataly Föst, Konstantin Danis, Matthias Portius and Clara Gebhardt.

In addition, I would also like to thank everyone in the Biophysical Chemistry Group for their encouragement, especially Steve Martin and Christian Danneberg for an uncomplicated and fruitful collaboration, Tina König and Manuela Miessler for their assistance and the well-organized labs, Petra Zamzow and Susanne Vogt for assistance with the numerous paperwork, and Katja Franke, Michael Ansoerge, Andreas Müller, Christina Müller, Jiranuwat Sapudom, Franziska Ullm, Cornelia Clemens, Veronika and Phillip Riedl, and Max Quaas for constructive discussions.

I also thank our collaborators Julia Döring and Kai Ostermann (Genetics, TU Dresden), Jun. Prof. Stephan Schmidt (Colloidal Bioadhesion, HHU Düsseldorf), Johannes Waschke and Prof. Mario Hlawitschka (Computer graphics, HTKW Leipzig), Tom Venus and Irina Estrela-Lopis (Medical physics and biophysics, Uni Leipzig) as well as Max Männel and Julian Thiele (IPF Dresden).

Finally, I thank my family and friends for their great support and motivation to pursue my work.

Selbstständigkeitserklärung

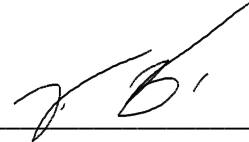
Hiermit erkläre ich, dass ich die vorliegende Arbeit selbständig und ohne unzulässige Hilfe oder Benutzung anderer als der angegebenen Hilfsmittel angefertigt habe.

Ich versichere, dass Dritte von mir weder unmittelbar noch mittelbar geldwerte Leistungen für Arbeiten erhalten haben, die im Zusammenhang mit dem Inhalt der vorgelegten Dissertation stehen, und dass die vorgelegte Arbeit weder im Inland noch im Ausland in gleicher oder ähnlicher Form einer anderen Prüfungsbehörde zum Zwecke einer Promotion oder eines anderen Prüfungsverfahrens vorgelegt wurde.

Alles aus anderen Quellen und von anderen Personen übernommene Material, das in der Arbeit verwendet wurde oder auf das direkt Bezug genommen wird, wurde als solches kenntlich gemacht. Insbesondere wurden alle Personen genannt, die direkt an der Entstehung der vorliegenden Arbeit beteiligt waren.

Leipzig, 22.04.2022

Ort, Datum



David Rettke

Nachweis über Anteile der Co-Autoren:

Titel: **Surface functionalization by hydrophobin-EPSPS fusion protein allows for the fast and simple detection of glyphosate**

Journal: Biosensors

Autoren: Julia Döring, David Rettke, Gerhard Rödel, Tilo Pompe, Kai Ostermann

Anteil Julia Döring:

- Projektidee
- Konzeption
- Methodik
- Formale Analyse
- Durchführung der Experimente
- Validierung
- Ausarbeitung des Originalentwurfs der Publikation
- Schreiben der Publikation
- Visualisierung

Anteil David Rettke:

- Validierung
- Überprüfung und Überarbeitung der Publikation

Anteil Gerhard Rödel:

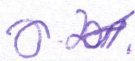
- Bereitstellung von Ressourcen
- Validierung
- Überprüfung und Überarbeitung der Publikation

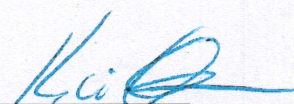
Anteil Tilo Pompe:

- Validierung
- Überprüfung und Überarbeitung der Publikation

Anteil Kai Ostermann:

- Projektidee
- Konzeption
- Bereitstellung von Ressourcen
- Methodik
- Validierung
- Überprüfung und Überarbeitung der Publikation
- Projektbetreuung
- Fördermittelakquise


David Rettke

20.10.4 
Kai Ostermann

Nachweis über Anteile der Co-Autoren:

Titel: Picomolar glyphosate sensitivity of an optical particle-based sensor utilizing biomimetic interaction principles
Journal: Biosensors and Bioelectronics
Autoren: David Rettke, Julia Döring, Steve Martin, Tom Venus, Irina Estrela-Lopis, Stephan Schmidt, Kai Ostermann, Tilo Pompe

Anteil David Rettke:

- Methodik
- Durchführung der Experimente (Biochip-Präparation, SCP-Funktionalisierung, Analyse Beschichtung und Funktionalisierung, SCP-Assay)
- Formale Analyse
- Visualisierung
- Ausarbeitung des Originalentwurfs der Publikation

Anteil Julia Döring:

- Bereitstellung von Ressourcen (Hydrophobine und Fusionsproteine)
- Überprüfung und Überarbeitung der Publikation

Anteil Steve Martin:

- Durchführung der Experimente (Biochip-Präparation, SCP-Funktionalisierung)
- Formale Analyse

Anteil Tom Venus:

- Durchführung der Experimente (Analyse der SCP-Funktionalisierung)
- Formale Analyse

Anteil Irina Estrela-Lopis:

- Formale Analyse
- Überprüfung und Überarbeitung der Publikation

Anteil Stephan Schmidt:

- Bereitstellung von Ressourcen (SCP-Präparation)
- Überprüfung und Überarbeitung der Publikation

Anteil Kai Ostermann:

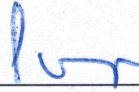
- Projektidee
- Konzeption
- Überprüfung und Überarbeitung der Publikation
- Fördermittelakquise

Anteil Tilo Pompe:

- Projektidee
- Konzeption
- Ausarbeitung des Originalentwurfs der Publikation
- Fördermittelakquise



David Rettke



Tilo Pompe

Nachweis über Anteile der Co-Autoren:

Titel: Biomimetic estrogen sensor based on soft colloidal probes
Journal: Biosensors and Bioelectronics
Autoren: David Rettke, Florian Seufert, Julia Döring, Kai Ostermann, Dimitri Wilms, Stephan Schmidt, Tilo Pompe

Anteil David Rettke:

- Projektidee
- Konzeption
- Methodik
- Durchführung der Experimente (SCP-Funktionalisierung, Biochip-Präparation, SCP-Assay)
- Formale Analyse
- Visualisierung
- Ausarbeitung des Originalentwurfs der Publikation
- Projektbetreuung

Anteil Florian Seufert:

- Durchführung der Experimente (SCP-Funktionalisierung, Biochip-Präparation, SCP-Assay)
- Validierung
- Formale Analyse
- Überprüfung und Überarbeitung der Publikation

Anteil Julia Döring:

- Formale Analyse
- Überprüfung und Überarbeitung der Publikation

Anteil Kai Ostermann:

- Überprüfung und Überarbeitung der Publikation
- Fördermittelakquise

Anteil Dimitri Wilms:

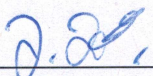
- Bereitstellung von Ressourcen
- Formale Analyse

Anteil Stephan Schmidt:

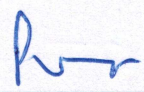
- Methodik
- Bereitstellung von Ressourcen
- Überprüfung und Überarbeitung der Publikation

Anteil Tilo Pompe:

- Methodik
- Überprüfung und Überarbeitung der Publikation
- Projektbetreuung
- Fördermittelakquise



David Rettke



Tilo Pompe

Nachweis über Anteile der Co-Autoren:

Titel: Radial profile detection of multiple spherical particles in contact with interacting surfaces
Journal: Plos One
Autoren: Johannes Waschke, Tilo Pompe, David Rettke, Stephan Schmidt, Mario Hlawitschka

Anteil Johannes Waschke:

- Methodik
- Software
- Ausarbeitung des Originalentwurfs der Publikation
- Schreiben der Publikation

Anteil Tilo Pompe:

- Methodik
- Datenerstellung
- Betreuung
- Projektverwaltung
- Überprüfung und Überarbeitung der Publikation

Anteil David Rettke:

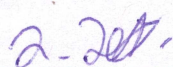
- Datenerstellung
- Überprüfung und Überarbeitung der Publikation

Anteil Stephan Schmidt:

- Betreuung
- Projektverwaltung
- Überprüfung und Überarbeitung der Publikation

Anteil Mario Hlawitschka:

- Betreuung
- Überprüfung und Überarbeitung der Publikation



David Rettke



Mario Hlawitschka

Nachweis über Anteile der Co-Autoren:

Titel: Microfluidics-assisted synthesis and functionalization of monodisperse colloidal hydrogel particles for optomechanical biosensors based on reflection interference contrast microscopy

Journal: *submitted*

Autoren: David Rettke, Christian Danneberg, Talika Alina Neuendorf, Sebastian Kühn, Jens Friedrichs, Nicolas Hauck, Carsten Werner, Julian Thiele, Tilo Pompe

Anteil David Rettke:

- Konzeption
- Methodik
- Durchführung der Experimente (SCP-Synthese, SCP-Funktionalisierung, Analyse der Eigenschaften, Beschichtung und Funktionalisierung)
- Formale Analyse
- Ausarbeitung des Originalentwurfs der Publikation
- Projektbetreuung

Anteil Christian Danneberg:

- Methodik
- Durchführung der Experimente (SCP-Synthese, SCP-Funktionalisierung, Analyse der Eigenschaften, Beschichtung und Funktionalisierung, SCP-Assay)
- Formale Analyse
- Ausarbeitung des Originalentwurfs der Publikation

Anteil Talika Alina Neuendorf:

- Methodik
- Überprüfung und Überarbeitung der Publikation

Anteil Sebastian Kühn:

- Methodik
- Überprüfung und Überarbeitung der Publikation

Anteil Jens Friedrichs:

- Methodik
- Durchführung der Experimente (Analyse der Eigenschaften der SCPs)
- Formale Analyse
- Überprüfung und Überarbeitung der Publikation

Anteil Nicolas Hauck:

- Methodik

Anteil Carsten Werner:

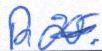
- Bereitstellung von Ressourcen
- Überprüfung und Überarbeitung der Publikation
- Projektbetreuung
- Fördermittelakquise

Anteil Julian Thiele:

- Konzeption
- Methodik
- Bereitstellung von Ressourcen
- Überprüfung und Überarbeitung der Publikation
- Projektbetreuung
- Fördermittelakquise

Anteil Tilo Pompe:

- Konzeption
- Überprüfung und Überarbeitung der Publikation
- Bereitstellung von Ressourcen
- Projektbetreuung
- Fördermittelakquise



David Rettke



Tilo Pompe